UNIVERSITÄT
BERN

Graduate School for Cellular and Biomedical Sciences

University of Bern

The Challenges of Measuring Membrane Protein Function in Giant Unilamellar Vesicles

PhD Thesis submitted by

Nicolas Dolder

from **Schangnau, BE**

for the degree of

PhD in Biochemistry and Molecular Biology

Supervisor
Prof. Dr. Christoph von Ballmoos
Department of Chemistry, Biochemistry and Pharmaceutical Sciences
Faculty of Science of the University of Bern

Co-advisor
Prof. Dr. Christine Peinelt
Institute of Biochemistry and Molecular Medicine
Faculty of Medicine of the University of Bern

Accepted by the Faculty of Medicine, the Faculty of Science and the Vetsuisse Faculty of the University of Bern at the request of the Graduate School for Cellular and Biomedical Sciences

Bern, Dean of the Faculty of Medicine

Bern, Dean of the Faculty of Science

Bern, Dean of the Vetsuisse Faculty Bern

“I got my hands up shaking just to let you know

That you've got a higher power

Got me singing every second, dancing every hour

Oh yeah, you've got a higher power

And you're really someone I wanna know (oh oh)”

Lyrics Higher Power, Coldplay, 2021

Acknowledgment

Here I am, rock you like a hurricane. With this work, which you are about to read, it feels like a great era is coming to an end. When I started writing this PhD thesis, it has been 7 years that I have known the von Ballmoos group and I will finish my PhD studies almost exactly 7 years after I started with my bachelor thesis in Christoph's lab. The first time I got to know the group was of course in the second biochemistry practical course where we expressed and purified ATP synthase and performed coreconstitution experiments using SNARE-mediated fusion. In a department dominated by RNA, the work in Christoph's lab on membrane proteins with the goal to create a synthetic respiratory chain seemed very creative and diverse and immediately fascinated me. It was also clear from the practical that the lab was rather new in the department and only starting out, which meant that there was still a lot of room to establish new things and help to build and shape the lab, which was very intriguing to me. We should of course not forget the people in the group which made a very good first impression, especially Christoph which struck me as a young, good-looking scientist with great motivation, a nice work attitude and a really good relationship with the students that he supervised, all qualities which should make for an amazing boss. After almost 7 years in the lab, I can certainly say that this was indeed the case. Before I go on to thank you and all the people that have accompanied me on this journey, I would like to make a brief resumé and give the reader an impression why this time has been so amazing.

As already mentioned, my journey started officially during my Bachelor Thesis where I worked on the purification of SNARE proteins and got to know the OG CvB (Christoph von Ballmoos) gang. It was evident from the bowling events and the atmosphere in the lab that the CvBs knew how to have a good time both on and off work all the while researching a great topic. Thus, it was clear to me that I wanted to spend more time in this group and so I joined again for my Master Thesis project, which was about establishing an *in vitro* transcription assay to study an antibiotics sensor. During this time, we had some nice parties besides the scientific endeavors, like Christmas Fonclette (Fondue and Raclette at the same time), a wine tasting excursion and even a sledging trip. During my Master I learned how to be a scientist thanks to the great supervision in the lab, but unfortunately, I had to take a small break and just one weekend after handing in my written thesis, I headed off to military school to learn how to protect the country as an NBC corporal. However, I came back even more hungry for science, and I still felt that my work in the CvB group was not done yet. Thus, I asked if I could come back for a PhD and luckily, as you may guess by looking at this thesis, I was allowed to come back to work on yet another cool project. This time my stay in the group would be a bit longer which means there were also many more opportunities for cool events, parties (I also got to be the DJ for the biochemistry Christmas party), Fonclettes, group hikes and more. At least, as long as it was allowed. The Covid-19 pandemic did change many things and

put the brakes on many fun activities. Despite all the struggles, the spirit in the lab stayed high which I always appreciated.

Thank you, Christoph, for letting me stay for such a long time in your group and allowing me to come back again and again to work on many cool and interesting projects. You were a great boss, mentor, co-worker, friend, sometimes also competitor when it came to bowling or other lab games. I am grateful for the freedom that you have given me in my project to let me explore and take a deep dive into the world of GUVs. During all this time, you were always there when I needed guidance, both scientifically and non-scientifically. I admire your drive and the good spirit that you bring to the lab, all while balancing the difficult job of a professor with the (hopefully not as difficult) job of being a family father at home. Even during hard times or when you were annoyed by some students, you always managed to make some jokes which meant there was rarely any day in the lab without at least some laughter.

I also had two amazing supervisors that showed me the necessary skills during my Bachelor's and Master's degree. First, I would like to thank my Bachelor supervisor Dr. Olivier Biner. At first, it was a bit difficult to understand you because of the "Walliserdütsch" but I not only got to learn a new "language", you also showed me how to be a dedicated, motivated and cheerful scientist and throughout my time in the lab, you were always helpful and gave me very good advice, also on topics outside of work. I would also like to thank Dr. Linda Näsvik Öjemyr which supervised me during my Master Thesis. As a Postdoc in the lab, you were very experienced and knowledgeable and thus could help me out whenever I needed it. You also let me work and do many things on my own, which I highly appreciated and has made me an independent researcher, giving me the tools for starting a PhD. I also want to thank all my study colleagues that were on this journey through the Bachelor and Master with me, especially Yannic Müller who was my dancing and singing partner during the Bachelor Thesis. Next of course are the members of the OG CvB gang. First, Dr. Thomas Schick who has started the project that I took over during my PhD. Not only did you lay the groundwork for my journey into the GUV universe, you were also a great and fun person in the lab responsible for many good stories, either by organizing events or by other means ;). Thanks to you I was also at my first Ice hockey game (Cee Bee!). Dr. Axel Meyrat, I am glad you were there to participate in my role-playing shenanigans and accepted and joined in on my sometimes a bit weird antics. Dr. Andrea Amati, although you were quite the tough guy as a bouncer for Bierhübeli, you also had a very big heart and I knew that if I would encounter some hard times, you would always be there to help out. You also knew many short-cuts and how to make experiments more efficient and could thus show me many tips and tricks. Dr. Simone Graf, it was really nice to have another geek in the lab with a great spirit and a party-loving nature. It was great to discuss science with you as well as other topics like Marvel and Disney movies and you were always up for some dancing at parties. I especially want to also thank Sabina Deutschmann. Although at first you struck me as a rather quiet person, I got

to know you a bit better during our time at the conference in Bonn and the unforgettable ride back in the overcrowded, delayed train learning about strange Swiss German words. You also became my office neighbor where we shared many laughs together. Despite your reserved nature, I believe you have been the heart of the group, supervising and teaching many students and technicians and making sure that we do not run out of consumables.

During my time in the group there have of course been quite a few people in and out of the lab. Sarah Krummenacher, Martin Schori, Tobias Blatter, Aymar Ganguin, Meike Wieser, Sandra Schär, Eveline Jäger, and all the others, thank you for contributing to the great atmosphere. Some people that joined during my time managed to stick around and form a new generation of CvB's. Philipp Müller, you have joined me on this quest to make GUVs the new membrane protein characterization platform. I was really glad to have someone with me on the struggles and to get another opinion on experiments. You were also a great motivator for many fun events like culture night and card games. Roman Mahler, whenever I wanted to discuss the newest Marvel or Star Wars episode, I knew that I could come to you. I was also amazed by your craftiness, and you contributed to many great PhD hats and other gadgets in the lab. I am thankful for the nice conversations we had. Lukas Rimle, you are a fun person and very talented scientist. You always had an open ear to listen to my experiment failures and were always willing to give some good advice. I am sure that with all of you PhD students, the lab will be in good hands in the future. Dr. Abbas Abou Hamdan, it was great to have some more cultural diversity in the group and you introduced us to many Lebanese goodies and were also a good office neighbor. Thanks also to Leticia Herran Villalain that brought some Spanish flavor into the lab.

At this point I want to also highlight the current (and a bit less current) Master and Bachelor students, some of which I supervised and some of which have returned for their PhD studies. Stephan Berger, you have been a great student to me and with your bachelor thesis, you have done a major contribution to this work. You were not only a good student but also a very good friend. With you I could talk almost about anything and make some jokes I probably could not do with other people. Your motivation and dedication were above many other students and despite a lot of struggles, you never gave up. Micha Marti, you were my second Master student and although the start of the project was a bit difficult, you also finally joined the GUV world. I really admire your calm nature and all the while, you are also great to talk to. I could also count on you to join me for Pizza or Mannan, when others decided to eat more healthy alternatives. Linus Hopf, you were only here for a few weeks as a German exchange student, but I appreciated your free spirit and your ability to just take things as they would come. Stefan "Stoni" Moning, with you we had another Party Animal in the group and it was always a pleasure to talk to you and discuss things. You were always cheerful and an amazing person as well. Ana Nikolov, you not only taught us some Serbian words, you were also a great dance partner for our weekly dance breaks and

someone with a creative mind. It was always fun to talk to you and sometimes explore the weirdness of my dreams. Yannick Bärtschi, you were another very dedicated and highly motivated student and talking to you was always a pleasure. Also, thanks to Sofia Hutter and Nik Lüpold for being great bachelor students, and Ana-Marija Stanic and Stefan Täuber that joined us recently for their Master Thesis.

Finally, I want to thank all my family and friends without whom I probably would not have managed to stay a sane human person on this journey. First, my second family which is the Möngö group as we like to call it. Starting with some very dear friends I have made in Highschool, Lucas, Sää, Raphi, our group established itself during our university time with Küse, Mari, Mü, Irina and Sasha joining as well. Some of you are currently also doing a PhD and I wish you the best of luck for your project and studies and hope that you will not feel too stressed when writing your thesis in one or two years. I know I can always rely on you, and you have given me many great memories, from amazing holidays to cool events and activities to the regular Friday evening beer. I also want to thank my best friend Eric Ulrich, which I also know since more than 10 years, with whom I have also spent many great holidays and evenings and could talk about almost anything. Even though we lived a bit further apart, I appreciated every moment that we could share together, and I wish you the best of luck as well with your PhD that you just started.

Save the best for last. Thanks to my real family which has always been there for me and supported me throughout this journey. Thanks to my godparents for the great support along the way. Thanks to my brother for introducing me to the world of science with subtle presents and through his work as a chemistry PhD student and now chemistry teacher. Thanks to my sister for fostering my more creative side by helping out in movie projects and introducing me to dancing and my love of music. Thanks to the partners and children of my siblings for all the help, great advice and all the good time we shared. Thanks to my mother which has always been there for me and has given me the great care I needed while allowing me to express myself however I wanted. Thank you for making me the man I am today and for all the love and knowledge you have given me.

Of course, there are many more people that have shared moments with me and contributed to my story which I can not all name here. I just want to thank everybody that I have met and which shaped my life, and with this, I wish you a good time and a lot of endurance reading the culmination of my work as a PhD student.

Abstract

Giant unilamellar vesicles (GUVs) are a desired membrane-mimetic system for the study of many membrane-related phenomena, the function of MPs and the creation of synthetic cells. These micrometer sized vesicles are similar in size to bacteria and eukaryotic cells, and thus mimic these organisms more closely in terms of surface and volume. The size allows the integration of complex systems and entire metabolic processes such as transcription and translation, as well as the investigation of individual vesicles using light microscopy techniques, potentially cutting the costs of purified MPs needed to perform experiments by a factor of 100 compared to bulk methods. This makes them a very attractive system to investigate MPs, for example to test and develop novel drugs, and to create a bottom-up synthetic cell. However, lipids do not spontaneously assemble into cell-sized vesicles which has prompted the development of several different techniques for GUV formation. For the same reason, these vesicles are more fragile towards the use of detergents, which complicates MP reconstitution. To harness the power of light microscopy measurements, GUVs have to be immobilized to enable real-time observation over several minutes to hours. Lastly, the success of measuring MP function in a GUV also depends on the choice of detection system.

In previous work in our lab, GUV electroformation on indium-tin-oxide (ITO) coated glass slides and reconstitution of MPs using charge-mediated fusion of oppositely charged vesicles was established. GUVs were immobilized using a streptavidin-biotin system to enable measurement of MP function. One of the disadvantages of GUV electroformation on ITO coated glass slides is the poor compatibility with high ionic solution, which could result in low protein activities due to formation at non-physiological conditions. One of the aims of this project was to establish GUV formation under physiologically relevant conditions to allow formation in buffer compositions optimal for MP function. We thus compared previously established electroformation on ITO coated glass slides with electroformation on platinum (Pt) wires and the more recently developed polymer assisted swelling using PVA. We observed that both Pt wire and PVA formation produced GUVs using various buffer compositions and that polymer assisted swelling produced a high yield of GUVs without much optimization, showing the potential and versatility of this method. Interestingly, we discovered that the immobilization was affected by the buffer composition, and that strong adhesion can lead to leakage and loss of encapsulated cargo, especially in PVA GUVs. This is an important finding as MPs are frequently followed using encapsulated fluorescent dyes, showing that immobilization conditions have to be tuned according to the buffer composition to provide sufficient immobilization while preventing too much cargo loss. Protons play an important role in many cellular processes, they are involved in many transmembrane transport reactions as well as in the production of ATP by the ATP synthase. Thus, GUVs should be able to maintain a proton gradient. Our measurements suggest that this is indeed the case also in immobilized vesicles that have not leaked

encapsulated fluorophores. We further presented a simple strategy that could be used to estimate the protein concentration in GUVs after charge-mediated reconstitution by fusion of GUVs with small vesicles containing labeled lipids and labeled MP. We could show that GUVs with more lipid-coupled dye signal also showed more MP-coupled dye signal, which could simplify the quantification of MPs in GUVs after fusion by following lipid-coupled dye incorporation without the need for MP labeling. However, this strategy is not able to distinguish between simple adhesion or hemifusion of small vesicles and full fusion, which would be required for functional reconstitution of a MP. However, the same is true for simply following labeled MP signal, meaning that potentially other methods such as content mixing assays would be needed to get a better idea on the amount of functionally reconstituted MP.

Finally, knowledge gained from the characterization of GUVs was applied for the reconstitution and measurement of cytochrome *c* oxidase from *Rhodobacter sphaeroides* using carboxyfluorescein and pyranine (HPTS). The former produced only weak and unclear signals and was prone to fast bleaching. Using ratiometric dyes such as HPTS, pH calibration can be performed, where the observed ratios should be independent of dye concentration and bleaching. This proved to be challenging in GUVs, as the vesicles size seemed to have an effect on the observed HPTS ratio. Despite that, cytochrome *c* oxidase measurements using HPTS yielded better results and by characterization of vesicle shape and measurement of lipid-coupled dye signal introduced via fusion, a correlation between the proton translocation and the relative amount of MP per vesicle could be observed, showing that thorough characterization of the GUVs can help to relate vesicle activities. Nonetheless, the different sizes of the vesicles were a considerable challenge for data analysis. We thus plan to use monodisperse GUVs produced by microfluidic techniques in collaboration with members of the deMello group form the ETH Zürich and we could show that these GUVs are fusogenic and can be potentially used to measure proton translocation.

In a second project, we used bifunctional DNA duplexes to establish a new tool for the measurement of MP function. By linking pH-sensitive dyes via DNA oligomers to cholesterol moieties, fluorescent probes can be anchored to the lipid membrane, allowing more efficient encapsulation compared to soluble dyes which could safe costs using precious probes. Addition of DNase I allows fast and simple removal of probes facing the liposome exterior, which are exposed to the buffered solution and thus do not contribute to the measurement of proton translocation in or out of the vesicle, a common problem with lipid-coupled probes. Incorporation of bifunctional DNA into GUVs was slightly more challenging. Depending on the GUV formation method, as well as lipid and buffer composition, differences in the degree of incorporation into the membrane were observed, ranging from no membrane localization to complete incorporation. Formation further seemed to be negatively affected by the probe. Thus, further optimization of the probe might be needed to enable measurement of MP function in GUVs.

Table of Contents

1. Introduction

In this thesis, we will take a dive into the world of giant unilamellar vesicles (GUVs), a micrometer sized model membrane system which serves as a tool for *in vitro* studies of various membrane related processes, such as lipid domain formation, membrane fusion and fission, cell division and membrane protein (MP) function. The latter is of special interest in this work, as MPs enable many key functions of the cellular membrane, such as taking up nutrients and sensing changes in the environment, lipid biogenesis, energy metabolism, regulating the structure and dynamics of the membrane, nerve signaling and establishment of cell-to-cell contacts.[1] MPs are crucial for the survival of a cell, and about 20 - 30 % of the protein coding genes of various organisms are estimated to encode for MPs.[2] Aberrant expression or activity of those proteins is related to many diseases, such as neurodegenerative disorders, diabetes and certain cancers.[3–6] As these proteins are often accessible on the cellular surface, they are also considered desirable drug targets and it is estimated that currently, about 50 - 60 % of developed drugs target MPs.[7] Thus, characterization and the study of the function of these proteins is crucial for a better understanding how they are involved in a disease and for the development of new drugs and treatment methods. *In vitro* systems are of high value in such studies as they drastically reduce the complexity of the biological system and the chance of observing off-target effects. The development and improvement of model membrane systems such as GUVs is a major aspect of current MP research, as they enable the study of these proteins in their natural environment.

The introduction into this topic will be split into two main sections. In the first section, our recent review *"Current Problems and Future Avenues in Proteoliposome Research"*[8] will serve as a general introduction into the field of MP research using proteoliposome based systems. It will introduce some of the main aspects relevant for the *in vitro* study of MPs, such as reconstitution into model membrane systems, MP orientation and the detection of MP function using fluorescent dyes. While the main focus of the review is on smaller, nanometer-sized vesicles, the final section presents a small overview on recent advances using GUVs for the investigation of MP function, especially studying the interplay between different cellular components. Many of the concepts introduced for small vesicles also apply to their giant counterparts, which will be explored in more detail in the second section of the introduction. This part will take a closer look at the formation of giant vesicles and the required steps to transform them into a tool for the investigation of MP function, such as MP reconstitution into GUVs and immobilization for the observation of single vesicles using microscopic techniques.

1.1. Current Problems and Future Avenues in Proteoliposome Research

Title: Current Problems and Future Avenues in Proteoliposome Research

Journal: Biochemical Society Transactions

Status: Published, July 2020

Authors: Andrea Amati, Simone Graf, Sabina Deutschmann, Nicolas Dolder and Christoph von Ballmoos

Contribution: All authors contributed to the writing and editing of the manuscript; Nicolas wrote the first draft of sections *Rational Design of Fluorescent Dyes to Follow Enzyme Function* and *Towards a Synthetic Cell*; Christoph and Nicolas designed, and all authors revised figures.

Abstract

Membrane proteins (MPs) are the gatekeepers between different biological compartments separated by lipid bilayers. Being receptors, channels, transporters, or primary pumps, they fulfill a wide variety of cellular functions and their importance is reflected in the increasing number of drugs that target membrane proteins. Functional studies of MPs within a native cellular context, however, is difficult due to the innate complexity of the densely packed membranes. Over the past decades, detergent-based extraction and purification of MPs and their reconstitution into lipid mimetic systems has been a very powerful tool to simplify the experimental system. In this review, we focus on proteoliposomes that have become an indispensable experimental system for enzymes with a vectorial function, including many of the here described energy transducing MPs. We first address long standing questions on the difficulty of successful reconstitution and controlled orientation of MPs into liposomes. A special emphasis is given on coreconstitution of several MPs into the same bilayer. Second, we discuss recent progress in the development of fluorescent dyes that offer sensitive detection with high temporal resolution. Finally, we briefly cover the use of giant unilamellar vesicles for the investigation of complex enzymatic cascades, a very promising experimental tool considering our increasing knowledge of the interplay of different cellular components.

Introduction

Lipid membranes are found in all living cells and provide several vital functions. Not only do they protect the organism from a potentially hostile environment, but they also allow chemical compartmentalization, e.g. reducing and oxidizing conditions in bacterial cytoplasm and periplasm, respectively. In eukaryotes, cellular organelles such as mitochondria, endoplasmic reticulum or endosomes are also surrounded by membranes. The chemical scaffold of these membranes is a bilayer of lipid molecules, that hosts small hydrophobic components such as vitamins, quinones, and pigments, as well as very large and complex membrane proteins (MP). The mass percentage of proteins in natural membranes varies between 25 % in the myelin sheath to 75 % in energy transducing membranes such as the mitochondrial inner membrane.[9–11] This complexity makes the direct investigation of MP function in native membranes difficult. To circumvent this problem, MPs are purified and reinserted into membrane mimetic systems, such as protein wrapped lipid patches (nanodiscs), (supported) planar lipid bilayers or lipid vesicles.[12] Here, we focus on the use of small to giant unilamellar vesicles (diameter ranging from 30 nm to 50 µm), called liposomes, to study MPs with vectorial functions. Bordered by a single lipid bilayer, liposomes form spontaneously from dried lipids resuspended in aqueous solution.

The advent of proteoliposome studies is tightly coupled to the experimental verification of the chemiosmotic theory brought forward by Peter Mitchell in 1961.[13,14] This hypothesis led to a controversy amongst research groups across continents that lasted for decades.[15] A crucial experiment, positively stimulating the debate, was the coreconstitution of purple membrane *Halobacterium salinarum* (i.e. essentially 2D-crystallized bacteriorhodopsin) and the F_1F_0 ATP synthase from mitochondria, showing ATP synthesis upon illumination, as described by Racker and Stoeckenius[16] along with other coreconstitutions.[17–19] It was the simplicity of these experiments which stood out and manifested the connection between an electrochemical gradient and ATP synthesis. The use of purified components inserted into an empty lipid bilayer ensured that no unknown factors had to be considered during the interpretation of results. Racker's method was readily picked up by many researchers to advance the mechanistic understanding of various MPs. A comprehensive overview of numerous pioneering experiments is given by Etemadi.[20]

In general, proteins embedded in liposomes can be investigated employing the same techniques that are also used to study enzymes in solution, such as UV/VIS and fluorescence spectroscopy. Nevertheless, the signal-to-noise ratio of optical measurements is typically decreased in proteoliposomes due to light scattering. Importantly, proteoliposomes also allow for electrometric techniques to follow charge movements across the membranes, as initially developed by Drachev *et al.*[21,22] for light-inducible reactions and recently adapted by Fendler and colleagues[23,24] for slower reactions that require mixing

techniques (SSM electrophysiology). Proteoliposomes can also be immobilized onto many different kinds of support further increasing their experimental value.[25]

Besides examining transmembrane transport, liposomes have been used to investigate other membrane related biological phenomena, especially membrane fusion events. Fusion of lipid bilayers is vital during virus entry into their host cells, for instance, where it is either triggered by direct virus-membrane interaction or it is receptor-mediated. Liposome studies have successfully been used to investigate virus-target cell interactions and potential inhibitors,[26] mechanistic studies of virus-membrane fusion,[27–30] or interaction of viral protein, receptor and antibodies in HIV.[31] Furthermore, proteoliposomes have been used for NMR based structure determination of MPs, wherein the membrane ensures proper protein folding due to the near-native environment.[32–34] Finally, liposomes have been long-known as promising drug delivery systems for both hydrophobic and hydrophilic drugs alike,[35–40] which is a very active field of research.

In this short review, we will highlight three different aspects of current proteoliposome research. In the first, main part, we will focus on the use of liposomes for the investigation of MPs, many of them being ion-translocating enzymes involved in cellular bioenergetics. As our knowledge of the interplay of cellular components vastly expanded in the last years, experimental setups of more complex systems are of increasing interest. This also involves the coreconstitution of several MPs in desired orientations into the same liposomal membrane. However, robust protocols to measure or guide orientation of reconstituted proteins or to coreconstitute MPs into the same membrane are still in development. We discuss current problems during reconstitution of MPs and their joining into more complex systems. In the second part, we will discuss recent progress in the development of fluorescent dyes that are suitable for proteoliposome studies. Using orthogonal chemistry and different linker techniques, such dyes can be tailored to meet specific requirements, ensuring high sensitivity and temporal resolution. Finally, we briefly describe the use of giant vesicles in the bottom-up construction of synthetic cells, highlighting recent projects, in which an impressive complexity of experimental systems was achieved.

Membrane Protein Reconstitution in a Nutshell

In the seminal experiment of Racker and Stoeckenius described above, native purple bacteria were mixed with cholate-extracted mitochondrial particles (containing enriched F_1F_0 ATP synthase) with asolectin lipids that had been sonicated and solubilized by the bile salt sodium cholate. This mixture was then dialyzed to remove excess detergent allowing the formation of proteoliposomes capable of light-driven ATP synthesis.[16] Almost 50 years later, close variants of this very method are still powerful protocols to reconstitute MPs. Over the years, several other approaches to functionally reconstitute purified MPs into liposomes were developed. Some employ organic solvents, or mechanical means such as sonication, freeze-thawing, or French-press.[41,42] However, the most common methods are based on the use of detergents discussed in the next paragraphs. For an overview of different reconstitution techniques consider the pioneering reviews[41] and[20], for more recent perspectives refer to[12,43–45].

Generally, the process of detergent-mediated reconstitution can be divided into two main steps. First, a purified and detergent-solubilized MP is mixed with lipids. Second, the detergent is removed from the mixture, leading to the incorporation of the MP into liposomes. In the first step, the lipids are added to the solubilized MP either as fully solubilized mixed detergent-lipid micelles, or as preformed, detergent-destabilized vesicles. Detergent removal in the second step is achieved by various methods based on the critical micelle concentration (CMC) of the employed detergent.[41] For small sized micelles (< 25 kDa, high CMC; e.g. sodium cholate, octyl glucoside), rapid dilution, dialysis with an appropriately sized membrane or size exclusion chromatography can be used. For detergents forming large micelles (typically very low CMC), adsorption to polystyrene beads or complex formation with various cyclodextrins is used.[45–48] Especially the use of cyclodextrins holds promise as different ring sizes are available that offer some specificity for certain detergents,[46] e.g. allowing the selective removal of one detergent from a detergent mixture. While the exact mechanism of reconstitution by detergent removal is still not fully understood,[44,49] there is agreement that at a critical detergent concentration (which depends on a variety of factors), solubilized MPs cannot be kept in a soluble state any further and either precipitate or spontaneously integrate into the present phospholipid membrane.[12,44] The efficiency of the reconstitution process (fraction of the solubilized MP that incorporates into liposomes) depends on various factors, as e.g. the MP of interest itself, the type of detergent used, the initial detergent concentration, the composition of the lipid membrane, the choice of buffer and ionic strength and importantly, the method and rate of detergent removal.[41,44]

A special role is assigned to the lipid composition in proteoliposomes. Critical aspects for a good lipid mixture are easy liposome formation, preservation of enzyme activity and tightness of the liposomes towards leakage of protons or other ions. For many MPs, a (rather crude) lecithin (phosphatidylcholine (PC)) extract of soybean has been successfully applied. In this extract, next to PC,

phosphatidylethanolamine (PE), and the negative lipid phosphatidyl inositol (PI) are the other main components. Although both PC and PI are not found in bacteria, the extract has been successfully used for many prokaryotic MPs. In addition, natural extracts from bacteria, e.g. from *Escherichia coli* or mixtures from synthetic lipids are used. Tsai and Miller[50] have convincingly shown that mixtures of synthetic lipids are much tighter towards proton leakage compared to a polar extract of *E. coli* lipids. Although being outside of the scope of this review, it is noteworthy that the correct lipid composition can have a direct impact on the protein activity as briefly described in the following few examples. Non-bilayer lipids such as PE were shown to stimulate the activity of secondary transporters (e.g. Lyp1 of *Saccheromyces cerevisiae)*.[51] Furthermore, the headgroups of lipids, especially of anionic lipids, are responsible for the topology and the regulation of conformational dynamics of transporters by interacting with the transport proteins.[52–56] The importance of negatively charged lipids, especially cardiolipin, for the activity and stability of bacterial and mitochondrial respiratory (super)complexes has also been described.[57–59]

The impact of lipids on the reconstitution process has been studied for some proteins, e.g. Na^+/K^+-ATPase.[60–64] De Lima Santos *et al*.[60] proposed that the lipids surrounding the MP, as well as the physical state of the lipid environment as e.g. its fluidity, have a stabilizing effect on MPs. Longer saturated fatty acyl chains decreased membrane fluidity leading to activity loss of the MP. Thus, phospholipid mixtures that contribute to membrane fluidity (higher fractions of short-chain or unsaturated fatty acyl chains) can reduce activity loss.[60,61,63,65] Further excellent studies, in which many of these parameters have been described, were published for bacteriorhodopsin and ATP synthase by Paternostre and colleagues, as well as for LacS by Knol and colleagues (see Table 1 and references therein as well as Lichtenberg *et al.*).[66] These studies show that the lipid composition can affect both the reconstitution yield and the orientation of the protein in the membrane (see below). A final complication is the natural asymmetry of lipid composition in the two leaflets of the bilayer as observed in eukaryotes and prokaryotes[67–69] and first protocols for the generation of asymmetric liposomes have been described.[70,71]

Table 1: Non-exhaustive list of different studies with a focus on coreconstitution of MPs or orientation of MPs. For the latter, studies are further distinguished between simply investigating orientation under one or several different conditions and actively influencing orientation by different means. Studies are grouped according to the investigated MP and the origin of the MP and the studied parameter is indicated. A short summary of the study is provided in the comments row.

Membrane Protein	Organism	Study	Comments	References
aa$_3$CcO	*Rhodobacter sphaeroides*	Coreconstitution	Coreconstitution of aa$_3$*CcO* with F_1F_0 ATP synthase (*E. coli*) or spinach ATP synthase.	[72]
		Investigating orientation	70 - 80 % CcO was found with soluble domain of subunit II carrying the cytochrome *c*-binding site towards the outside of the liposomes. Functional unidirectionality can be imposed over orientation of the MP in the liposomal membrane by providing cytochrome *c* and electrons only on one side of the membrane.	[73]
	Paracoccus denitrificans	Influencing orientation	MP was immobilized on Ni-NTA-functionalized silica nanoparticles for orientated encapsulation into liposomes (bead on outside of proteoliposome).	[74,75]
ArcD2	*Lactococcus lactis*	Coreconstitution	Coreconstitution with OpuA and soluble proteins ArcA, B and C (*L. lactis*)	[76]
bacteriorhodopsin	*Halobacterium salinarum*	Coreconstitution	Coreconstitution with ATP synthase from bovine heart mitochondria.	[16]
		Investigating orientation	Only slight preference for inside-out was detected.	[77]
			Orientation in proteoliposomes was shown to depend on lipid composition of the liposomes, pH value, ionic strength, & membrane curvature (in order of decreasing influence on orientation).	[78]
Ca^{2+}-P-ATPase	rabbit sarcoplasmic reticulum	Investigating orientation	Unidirectional orientation with 80 % - 100 % of the cytoplasmic domain facing outwards was observed, depending on the rate of detergent removal	[79]
cytochrome *bo$_3$* ubiquinol oxidase	*E. coli*	Coreconstitution	coreconstitution of *bo$_3$* oxidase with F_1F_0 ATP synthase (*E. coli*) via charge-mediated fusion of liposomes to GUVs	[80,81]
			coreconstitution of *bo$_3$* oxidase with F_1F_0 ATP synthase (*E. coli*) or spinach ATP synthase	[72]

Membrane Protein	Organism	Study	Comments	References
			coreconstitution of *bo₃* oxidase with F_1F_0 ATP synthase (*E. coli*) via SNARE-mediated fusion	[82]
		Investigating orientation	72 - 77 % to pump protons out of liposomes	[83,84]
			Unidirectional orientation is reported using a reconstitution method based on Rigaud *et al.*[41] However, no biochemical proof of unidirectionality is provided.	[85]
cytochrome *b*-563/*c*-554 (Q*bc*)	*Synechococcus 6716*	Coreconstitution	Coreconstitution with H^+-ATP synthase from *Synechococcus 6716.*	[86]
F_1F_0 ATP synthase	*E. coli*	Coreconstitution	Refer to cytochrome *bo₃* ubiquinol oxidase. Further coreconstitutions with Na^+/H^+ antiporters (*Thermus thermophilus* NapA and human NHA2), rat VGLUT2 as well as mitochondrial complex I from *Bos Taurus* together with alternative oxidase from *Trypanosoma brucei brucei*.	[87–90]
		Investigating orientation	> 97 % of F_1 facing outwards was shown.	[91]
LacS	*Streptococcus thermophilus*	Investigating orientation	Different detergents & detergent concentrations were evaluated as well as different rates of detergent removal. Unidirectional inside-out orientation is reported for reconstitution with Triton X-100 and random orientation for reconstitution with n-Dodecyl β-D-maltoside.	[92,93]
large-conductance calcium- and voltage-activated potassium channel (BK)	*Homo sapiens*	Investigating orientation	70 % inside-out orientation of MP is reported.	[94]
mechanosensitive channel of small conductance (MscS)	*Bacterial* (no further statement made)	Investigating orientation	Unidirectional incorporation is reported based solely on electrophysiological results; no physical evidence is provided. Two ion channel reconstitution methods based on dehydration/rehydration of liposomes in presence of MP were tested.	[95]
Na^+/K^+-P-ATPase	*Electrophorus electricus* or *Squalus acanthias*	Investigating orientation	Functional unidirectionality was imposed over orientation of MP in membrane by selective inhibition of one of the two orientation	[96,97]

Membrane Protein	Organism	Study	Comments	References
			populations with ouabain (exterior) or vanadate ions (interior).	
	dark red outer medulla of kidney of adult New Zealand white rabbits	Investigating orientation	Different protein-to-lipid ratios, different phospholipids and methods of detergent removal were investigated.	[60]
proteorhodopsin	uncultured Gammaproteobacterium EBAC31A08	Coreconstitution	Coreconstitution with *Spinacia oleracea* PSII and *Bacillus pseudofirmus* ATP synthase	[98]
		Influencing orientation	Interaction of MP with the surface of the liposomes was shown to dictate orientation. The surface charge of liposomes was modulated to prearrange orientation.	[99,100]
			MP was immobilized on Ni-NTA-functionalized silicate beads for orientated reconstitution (bead on outside of proteoliposome).	[101]
			Fusion domains were reported to guide the orientated insertion of proteorhodopsin into liposomes.	[102]
various (Ca^{2+}-P-ATPase, H^+-F-ATPase, LacS)	various	Investigating orientation	More uniform orientation of MPs was observed in the reconstituted liposomal bilayer when reconstituted into preformed, detergent-destabilized liposomes.	[93,103–106]
voltage-dependent K^+ channel (K_VAP)	*Aeropyrum pernix*	Influencing orientation	Ni-NTA-functionalized beads were used as membrane organization centers during bilayer reconstitution (bead in proteoliposome; bSUM).	[107]
YidC	*Escherichia Coli*	Coreconstitution	Coreconstitution with LacY and SecYEG as a fusion construct	[108,109]

In contrast with natural membranes, proteoliposomes contain much fewer proteins (< 5 % of lipid weight), as higher amounts of protein often negatively affect the reconstitution process. An interesting approach to tackle this problem is the GreCon method, in which the solubilized protein is placed onto a sucrose density gradient with increasing concentrations of cyclodextrin and detergent destabilized liposomes. During centrifugation, the detergent is gradually replaced by lipids, yielding liposomes with very high protein content, even triggering 2D-cristallization.[110] In the density gradient, proteoliposomes and empty liposomes migrate differently and are visible as opaque bands allowing their facile separation. Such proteoliposomes have been successfully used for electron tomography imaging using large membrane complexes,[111] but have not yet been tested for transport measurements.

In recent years, peptides mimicking the properties of nanodiscs,[112] i.e. embedding the MP in small lipid bilayer discs surrounded by a scaffold protein, have been described.[113–115] While these have the advantage over traditional nanodiscs that their size can be modulated by varying the peptide to lipid ratio, they share the common drawback that they cannot be used to extract protein from native membranes, making the prior use of detergent necessary. A MP extraction method not requiring any detergent is based on the use of styrene maleic acid (SMA) lipid particles (SMALPs), which has been successfully employed to purify[116,117] and also functionally reconstitute MPs into lipid bilayers.[118–122] Recent examples are the purification and reconstitution of cytochrome *c* oxidase from *Saccharomyces cerevisiae*[121] and of a plant sodium/proton antiporter.[122] Although not without downside (the solubilization properties of SMAs are pH-dependent),[123] these novel molecules are valuable gadgets in the toolbox of MP biochemists.

The Problem of Protein Orientation

In cells, insertion of MPs in membranes is thought to happen co-translationally and the final orientation of the protein is fixed during insertion and remains static (see [124] for a recent discussion on the topic). Unfortunately, this is not the case during MP reconstitution into liposomes as no translational machinery or chaperones are present that help to insert MPs into the liposomal bilayer.[78,125]

The relative orientation of the inserted MP strongly affects functional studies. As liposomes typically contain many copies of the MP in a random orientation, hundreds of different proteoliposome populations are formed during a single reconstitution process, causing a strong heterogeneity in the experimental system (see Figure 1B). In some cases, functional unidirectionality can be imposed over random orientation of the MPs by using substrates which are unable to penetrate the membrane (e.g. ATP, NADH, cytochrome *c*), but in others, the substrate binding site is located in the hydrophobic part of the membrane and, hence, both populations are stimulated (e.g. quinone-coupled enzymes). Alternatively, membrane-impermeable inhibitors can be used, which selectively inhibit one enzyme population.[106] In a worst-case scenario, the reconstitution method yields unidirectional insertion, but in

the non-preferred orientation (e.g. substrate binding site on the inside), complicating functional experiments. The orientation of MPs is not only important for primary ion pumps but has to be considered as well for secondary transport proteins. While these can often catalyze transport of their substrates in both directions, the affinities for the substrate might be different on either side of the membrane, a situation that severely complicates the quantitative interpretation of experimental results. The difficulties imposed by uncontrolled orientation are even more pronounced if the coupled activity of two or more MPs coreconstituted in the same liposomal membrane is investigated (see Table 1).

The orientation of reconstituted MPs is difficult to predict and even harder to influence, and it seems to be essentially unique for each protein and specific set of reconstitution technique.[44] Over the past decades, however, several studies have accumulated knowledge on protein orientation (see Table 1). Many reports describe the use of bacteriorhodopsin or proteorhodopsin, which are good models for monomeric MPs with no soluble domain, but inadequate as models for large multi-subunit MPs or MPs harboring large soluble domains. A prerequisite for the investigation of MP orientation in liposomal membranes is a reliable assay to determine the ratio of the two possible populations. If feasible, orientation can be assessed via a functional assay that is able to discriminate the relative contribution of both populations. As an example, the orientation of respiratory complex I in liposomes can be determined by measuring NADH:hexaammineruthenium oxidoreductase activity that can be spectroscopically followed at 340 nm. If NADH, which is membrane-impermeable, is added to liposomes, only the population with the NADH binding site oriented towards the outside will contribute to the activity. Upon solubilization of the proteoliposomes with detergent, all complex I molecules will contribute to the activity. Setting both activities in relation allows for estimation of the orientation of complex I in the liposomes.[126] However, care has to be taken in such approaches, as detergents often affect turnover activities of enzymes. Furthermore, if the measured activity is independent of the presence of the membrane, non-incorporated enzyme also contributes to the activity. A different method that has been used to determine orientation of proteo-/bacteriorhodopsin, is the use of proteases which will only digest MP domains accessible from the outside of the liposomes due to their inability to cross the lipid bilayer. The cleavage pattern can then be analyzed by SDS-PAGE, Western blot or mass spectrometry.[100,127,128] However, this cannot be considered as a general approach, since cleavage patterns are expected to become increasingly complex with larger proteins, and proteolysis might be incomplete. A special case is the F_1F_0 ATP synthase, in which those hydrophilic F_1 headgroups that are located on the outside of the liposomes can be specifically stripped off using defined buffer conditions.[91] Yet another approach, often used for secondary antiporters, is based on the selective labelling of cysteine residues from the outside by a membrane impermeable thiol-reactive compound. This is followed by complete labelling with membrane permeable biotin-maleimide that can later be

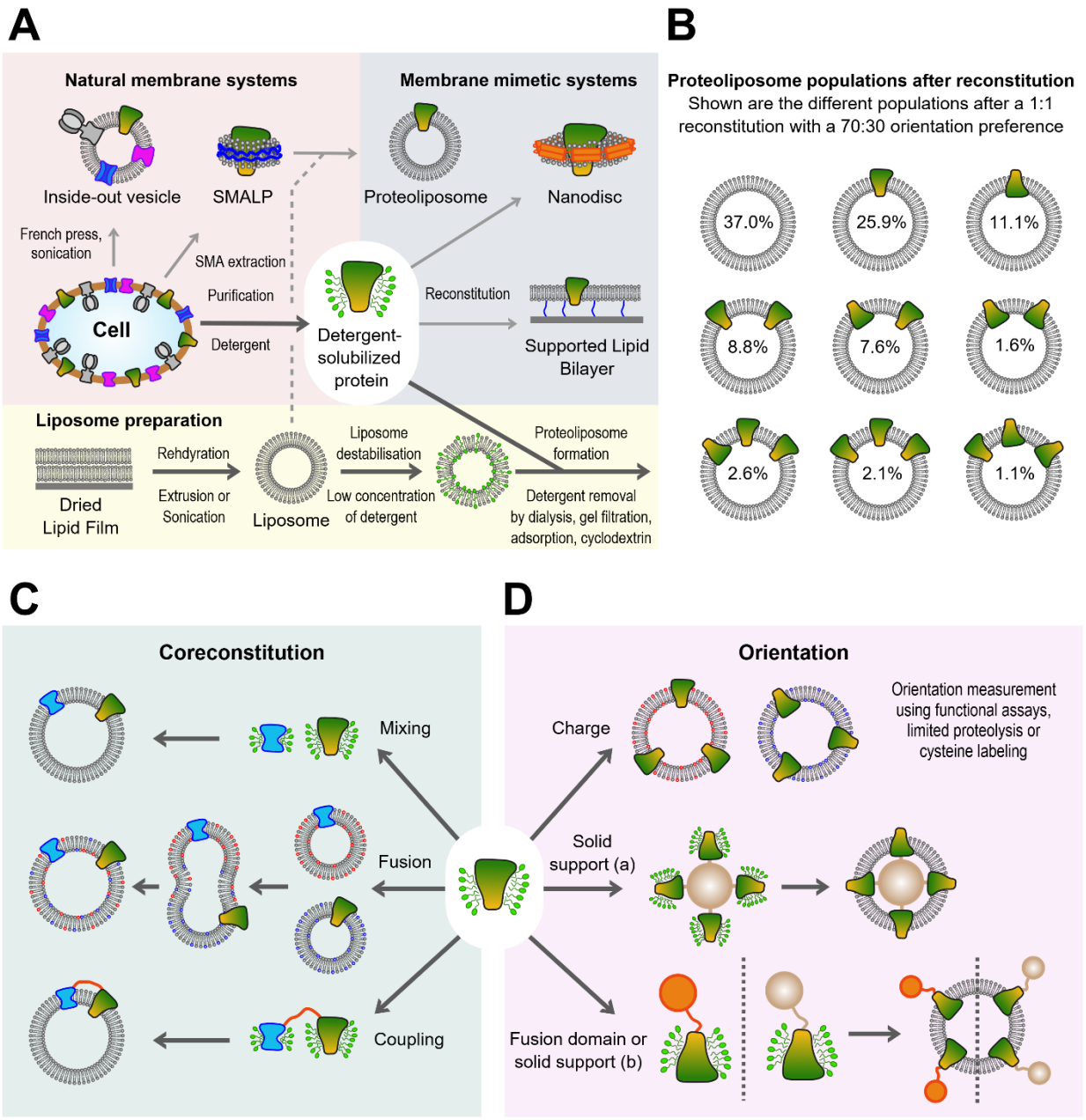

Figure 1: The ins and outs of membrane protein reconstitution. A) The general procedure for the formation of proteoliposomes is shown as well as a few alternative approaches for the *in vitro* study of membrane protein (MP) function. In a first step, MPs are extracted and purified from the native cell environment using detergents. In parallel, liposomes are formed by rehydration of a dried lipid film and subsequent extrusion or sonication of the vesicles. These liposomes are partially solubilized by the addition of detergents and mixed with the detergent-solubilized MP to form proteoliposomes after removal of the detergent by a variety of methods. Detergent-free extraction of MPs from the cell can be achieved by generating inside-out vesicles[129] or using styrene-maleic acid (SMA) copolymers to generate SMALPs. The latter can be used for the detergent-free reconstitution of MPs into liposomes.[116–122] If a closed compartment is not needed, detergent-solubilized MPs can also be reconstituted into planer supported lipid bilayers or nanodiscs.[12] B) The calculated distribution of proteoliposome populations after reconstitution with a 1:1 liposome to protein stoichiometry and a 70 % green-side out preference in orientation. Values were calculated assuming a Poisson distribution for reconstitution and a binomial distribution for orientation. Only populations > 1 % are shown. C) Coreconstitution of more than one membrane protein. Shown are coreconstitutions by a combined incubation of both MPs with liposomes, via fusion of different proteoliposome populations (e.g. charge-mediated fusion, red lipids = negatively charged, blue lipids = positively charged),[80,81] or via covalent/transient coupling of the MPs prior to reconstitution.[130] D)

Methods for the guided orientation during reconstitutions. Shown are examples of charge-controlled insertion,[99,100] by coupling the MP to a solid support (a) that will be encapsulated by the liposome[107] or by attaching a fusion domain[102] or coupling to a solid support (b)[74,75] that will be excluded from the vesicle interior.

detected by Western-blot analysis.[93,131,132] Further attempts to determine orientation of MPs reconstituted into liposomes can be found in Table 1.

Over the years, it has been found that numerous parameters can affect enzyme orientation during reconstitution. De Lima Santos *et al.*[60] report that at a slow detergent removal rate, liposome formation precedes protein incorporation into liposomes (leading to a more unidirectional incorporation of the MP), while liposome formation and protein incorporation happen simultaneously with fast detergent removal (resulting in a random orientation of MPs). Knol *et al.*[93] found a similar behavior for LacS, including further differences depending on the detergent used for reconstitution. If unidirectional orientation is not desirable, repetitive freeze/thaw cycles were shown to randomize orientation.[47]

In general, experiments have shown that orientation seems to be more uniform when the MPs are reconstituted into preformed, partially detergent-solubilized liposomes.[49,104,105,133] A rationale behind this observation is that the most hydrophilic domain will be least efficient in crossing the bilayer, and the protein will insert with its most hydrophobic side first.[49] However, experiments with cytochrome *c* oxidases show that the hydrophilic extramembraneous cytochrome *c*-binding domain (~ 25 kDa) of subunit II is not sufficient to promote more asymmetry than a 70:30 ratio.[73] F_1F_0 ATP synthase, on the other hand, with its soluble 350 kDa F_1 headgroup, has been reported to incorporate > 95 % with its head piece towards the outside with a similar reconstitution protocol.[91] In proteins such as bR and pR, where no large soluble domain is present, the interaction of the surface charge of the proteins and liposomes seems to play a role.[99,100] Tunuguntla *et al.* hold the asymmetry of charge distribution of pR, i.e. an overall positive charge at the C-terminus and a negative charge at the N-terminus, responsible for the lipid-charge dependent orientation of pR in liposomes. Through the use of either positively or negatively charged lipids in their liposomes, the N- or the C-terminus could be attracted towards the liposomal membrane, respectively, promoting a unidirectional orientation of pR.[100]

In one of the very few attempts to actively influence orientation, Ritzmann *et al.*[102] recently showed that fusion domains can guide orientated insertion of pR into liposomes. By genetic engineering, GFP and mCherry were added to the C-terminus or to the N-terminus as fusion domains, respectively. The resulting fusion proteins pumped protons across the liposomal membrane in opposite directions upon reconstitution. This elegant method is unique in the sense that both orientations can be chosen by attaching a fusion domain on either end of the protein and is a promising approach for small proteins with no soluble domain. Whether the addition of a GFP is sufficient to orient larger MPs remains to be determined. Other approaches for guided orientation employed Ni-NTA-functionalized beads to

immobilize His-tagged MPs prior to reconstitution,[74,75,107] a method also used to form planar bilayers for AFM studies.[134,135] The liposomal membrane was formed *de novo* between the immobilized MPs either around the bead-support,[107] or the beads were suggested to force unidirectional orientation because they were too big to be incorporated into the newly formed liposomes.[74,75] However, a more thorough characterization of these methods, e.g. regarding membrane leakiness, is required. Taken together, despite identification of several parameters that influence orientation of a MP in liposomes, there is still no general method to reconstitute MPs independently of all these parameters. The rather unpredictable effect of the lipid composition on the yield and on the orientation displays a major problem, as the effect of different lipid compositions on protein activity is a frequent aspect of research. A general method for guided orientation of MPs independent of the lipid composition is highly desirable. Approaches, in which orientation is guided by steric constraints might display a promising tool that has to be further developed in the future.[74,75,102,107] Robust and easy to implement methods for the quantitative determination of incorporation yield and relative protein orientation are required to compare established and develop new reconstitution protocols, e.g. only a small subset of detergents have been used in reconstitution.

Coreconstitution of Membrane Proteins

The incorporation of different MPs into the same liposomal membrane is called coreconstitution and is desirable for several reasons. The small interior volume of liposomes leads to quick accumulation or depletion of the transported substrate, which does not allow for long steady-state measurements and thus complicates quantitative interpretation of the data. For instance, if a membrane potential is required for the transport process, often a potassium/valinomycin diffusion potential is used that quickly exhausts due to the rapid change of the internal K^+ concentration. Furthermore, as our understanding of biological processes increases, the interplay of different proteins at the molecular level becomes an important field of research. An impressive example of cooperating enzymes are the members of the respiratory chain which have been shown to form different supercomplexes in mitochondria.[136,137] Functional measurements comparing kinetics and efficiencies between individual complexes or multiple complexes arranged in a supercomplex are necessary to understand the functional relevance of such supramolecular arrangements.[138,139]

There are relatively few reports on the coreconstitution of more than one type of MP in the same liposomal membrane. Most work has been published on the coreconstitution of ATP synthase together with proton pumps such as bacteriorhodopsin, cytochrome bo_3 ubiquinol oxidase and cytochrome *c* oxidase, which energize the liposomal membrane with an electrochemical potential. Such systems have been recently extended by the addition of peripheral MPs. Biner *et al.*[89] added trypanosomal alternative oxidase to proteoliposomes containing coreconstituted ATP synthase from *E. coli* and mitochondrial complex I to generate a minimal respiratory chain. Furthermore, ATP synthase has been used as a

constant generator of proton motive force for several proton dependent secondary transporters, such as Na^+/H^+ antiporter[87,90] and glutamate transporter.[88] An alternative way to regenerate ATP from ADP and phosphate was recently shown in a synthetic metabolic network consisting of coreconstituted ArcD and OpuA as well as soluble proteins ArcA, B and C entrapped in the vesicle lumen. In this complex network, ArcA – D couple the breakdown of arginine to the regeneration of ATP which is then used by OpuA for glycine betaine transport which regulates the internal osmotic balance of the vesicles.[76] Non-transport related processes can also be studied by coreconstitution such as the chaperone activity of the MP YidC on the folding of LacY.[108] Further examples of coreconstitutions are given in Table 1. In all these examples, both types of integral MPs have been reconstituted in parallel. However, given the individual requirements of every MP for optimal reconstitution and orientation, it has to be assumed that these coreconstitutions were far from being optimal.[16,72,86]

One way to resolve this problem is to split the coreconstitution into two steps. First, either protein of interest is reconstituted under optimal conditions individually, followed by fusion of the two populations. Successful functional coreconstitution of two MPs by fusion was first reported using a minimal SNARE machinery that fused liposome populations containing either F_1F_0 ATP synthase or bo_3 oxidase.[82] The same enzymes have also been successfully coreconstituted using fusion of oppositely charged proteoliposome populations.[80,81] However, the latter method requires the use of non-natural positively charged lipids, limiting the free choice of the lipid composition. Alternative techniques which have been used for "pure" liposome fusion are coiled-coil forming peptides[140] as well as complementary DNA strands.[141,142] However these methods have not yet been tested with MP containing liposomes.[143]

From the above considerations on orientation and coreconstitution experiments, it is obvious that the relative number of MPs reconstituted (stoichiometry) and the distribution of orientation of these MPs is of high importance for quantitative interpretations. Given the various parameters influencing reconstitution efficiency and orientation, this seems an almost insuperable obstacle. A ray of hope was provided by Raschle *et al.* with a method that ensures a 1:1 reconstitution stoichiometry of MPs. Using maleimide chemistry, complementary DNA molecules were attached to a unique cysteine of individual VDAC populations.[130] Upon DNA hybridization, the two populations form a stable complex that can be purified and reconstituted. This technique should be applicable to any MP and using DNA linkers of appropriate lengths might not only ensure the correct stoichiometry, but also correct relative orientation of the reconstituted proteins. Alternatively, proteins can be genetically linked by creating a fusion construct that can be cleaved via proteases, as was used in the coreconstitution of SecYEG and YidC in a 1:1 stoichiometry.[109]

Rational Design of Fluorescent Dyes to Follow Enzyme Function

As mentioned in the introduction, many different methods have been successfully used to follow chemical reactions in proteoliposomes, ranging from fast techniques such as absorption spectroscopy or electrometry, over luminescence (ATP detection) to slow methods such as micro electrodes, NMR, or uptake/release of isotope labeled substrates.[144–147] Probably the best combination of high sensitivity and high temporal resolution is found in fluorescent dyes which are able to detect a variety of reactions such as the change of proton or other ion concentrations or the presence of a membrane potential. Some of these dyes are membrane impermeable and have to be entrapped inside the liposomes (and the nonincorporated dye has to be removed) while others can be added from the outside, where they typically interact with the membrane. These latter, hydrophobic dyes are mainly used for the detection of proton gradients (e.g. ACMA, acridine orange)[72,148–151] or membrane potentials (e.g. oxonol VI, TMRE, VoltageFluors)[152–156] and do not directly report the translocated substrates.

In the following, we focus on membrane-anchored fluorescent probes that offer several advantages over entrapped dyes. A prototype of such a lipid anchored dye is obtained by the reaction of an amine-reactive carboxyfluorescein derivative with PE, first reported in 1984 by Thelen *et al*.[157] Such lipophilic probes have been mostly used *in vivo*[158–163] or to characterize different membrane properties.[164] Recently, Kemmer *et al.* have coupled the ratiometric pH-sensitive dyes pHrodo or SNARF to PE, which in contrast to fluorescein increase fluorescence upon acidification. Notably, they found a significant increase of the apparent pK_a of the lipid-coupled dyes in comparison to their soluble counterparts, an effect that is likely related to the close proximity of the dye to the membrane.[165,166] To avoid this pK_a shift, a linker can be introduced between the fluorophore and the lipophilic moiety.[159]

The main advantage of membrane-anchored sensors compared to soluble dyes is their efficient incorporation into the liposomes. The lipid moiety of the former ensures stable and efficient integration into the lipid bilayer which reduces the amount of potentially costly dyes that have to be used, as entrapment of freely soluble dye is an inherently inefficient procedure.[167–172] Even more importantly, membrane-anchored dyes do not leak from the membrane, a problem often encountered with soluble dyes containing carboxylic acids. On the other side, an obvious drawback of lipid-coupled dyes is that they are randomly distributed in both leaflets and selective removal or quenching is impossible or connected to the use of harsh chemicals that are often incompatible with delicate MPs and their catalytic activities.[173] We have recently solved this limitation by using a DNA double strand between the lipophilic anchor (cholesterol) and fluorescent moiety. Incorporation efficiency of the dye was shown to be > 90 %, and the outer dye is conveniently removed by a short incubation of the liposomes with DNase I and an ultracentrifugation step. In addition, the use of a DNA linker suppressed the undesired pK_a shift, previously observed with dyes directly coupled to a lipid. The simple chemistry involved makes this

method attractive for many different sensors and the use of DNA hybridization technology ensures a high versatility.[174] In addition to these simple examples, more advanced membrane-anchored sensors rely on structural changes of environmentally sensitive DNA motifs, such as the pH-sensitive i-Motif,[175,176] G-quadruplexes,[163,177,178] aptamers,[160] DNAzymes,[179] nanotweezers,[180,181] and nano-switches.[182] In these, the structural changes are transformed into a fluorescent read-out by attaching fluorescence quencher or FRET pairs to the DNA, in order to detect protons, metal ions and even small solutes such as ATP. Although mostly used *in vivo* so far, such complex sensors could also be useful for liposomal studies.

The development of new fluorescent dyes that are photostable as well as progress in the sensitivity of microscope cameras has further stimulated the field of single-molecule techniques. Here, instead of observing the readout of an ensemble of a large number of molecules, single enzymes are monitored by fluorescence microscopy which allows to classify them into populations with different enzymatic behaviors. While such techniques have been around for many years for soluble enzymes and MPs in detergent solution,[84,183–185] their application with proteoliposomes is very limited so far. It is however thanks to single molecule experiments with soluble and liposome embedded F_1F_0 ATP synthase that we have such a detailed picture of the F_1 binding change mechanism.[186] Apart from the ATP synthase, the groups of Jeuken and Stamou have performed single molecule proton pumping measurements with the quinol oxidase of *E. coli*[84] and the plasmamembrane P-type ATPase,[187] in which the pH change within the lumen of small unilamellar vesicles (SUVs) was followed by fluorescent pH sensors. Surprisingly, in both systems they have observed long phases of enzymatic inactivity or even passive proton leakage through the protein and have attributed their findings to a sensitive enzyme regulation by the local environment (but see Berg *et al.* for a different finding).[83] In case of the bo_3 oxidase, Jeuken and colleagues combined single protein/liposome studies with electrochemical measurements by tethering the proteoliposome to a gold electrode. By applying a voltage to the electrode, electrons were directly donated via lipid embedded ubiquinone to the bo_3 enzyme.[84]

The challenges of fluorescent detection is to find a probe with all desired properties, such as high incorporation into vesicles, resistance to bleaching, specificity for the substrate/product, and high signal-to-noise ratio. Rational design of fluorescent dyes using click-chemistry in combination with biomolecules such as DNA allow for optimization of these properties leading to improved probes for the investigation of enzyme function in proteoliposomes.

Towards a Synthetic Cell

In the last section, we would like to briefly touch the potential of giant unilamellar vesicles (GUVs) to study MP function. In contrast with “classical” liposomes, GUVs are much larger in size (1 – 100 µm) and can directly be observed by light microscopic techniques.[188] On the downside, GUVs are less robust and

their preparation is less straightforward (see [189–198] for literature on GUV formation). Compared with SUVs, GUVs have a vastly increased surface and inner volume that allows for the encapsulation of entire protein machineries, small vesicles or even whole bacteria, in order to mimic increasingly complex functions of living cells.[199] Already in 2004, Noireaux and Libchaber[200] demonstrated the successful *in vitro* transcription and translation (IVTT) of GFP within GUVs, and recently similar systems were used to produce MPs directly inside GUVs, with either spontaneous[201] or assisted insertion[202] into the membrane. Very few examples describe the use of GUVs as replacement for SUVs in traditional vectorial transport experiments with MPs. A reason for this lack of transport experiments is the less than straightforward insertion of MPs into the fragile GUV membrane which is an ongoing field of research.[80,81,188,203] Levy and colleagues[204] showed successful detergent-mediated (using very small amounts of detergent) incorporation of bacteriorhodopsin which acidified the GUV lumen upon illumination and was followed by the pH-sensitive dye pyranine. Biner *et al.* applied charged-mediated fusion to insert up to three different MPs reconstituted in positively charged SUV into a negatively charged GUV membrane.[119] Hansen *et al.*[205] finally reconstituted glucose transporter GLUT1 into GUVs using hydrogel assisted swelling. Passive uptake of glucose into the GUV lumen was detected with a glucose oxidase coupled fluorescence system that was entrapped during GUV formation.

Given their size, GUVs are also of interest in the research on synthetic or artificial cells.[203,206,207] A recent example is the light-induced energization of IVTT in GUVs after entrapment of SUVs containing bacteriorhodopsin and ATP synthase,[208] mimicking a cellular organelle. Lee *et al.* used photosystem II (PSII) and proteorhodopsin coreconstituted with ATP synthase in SUVs that can individually be stimulated by red and green light, respectively. PSII generates a pH gradient by oxidation of water on the inside of the vesicles and pR dissipates the gradient by outward proton pumping. These liposomes were entrapped in GUVs and, depending on the used light, ATP synthesis is either stimulated or abolished.[98]

Another impressive example to use GUVs as a cell-mimicking system was demonstrated by Ces and colleagues by creating a non-natural signal cascade. Passive calcium influx into the GUV lumen via α-hemolysin activates phospholipase A2 that triggered liposome embedded mechanosensitive channels. The successful signal cascade was demonstrated by the release of calcein from the liposomes which can be detected as a fluorescence increase.[209] Finally, Chen *et al.* demonstrated the bottom-up synthesis of pancreatic beta cells using GUVs. The uptake of glucose via the glucose transporter GLUT2 into the GUV lumen triggered a cascade that mediated controlled insulin release by fusion of insulin containing vesicles with the GUV membrane. Most impressively, the system was able to discriminate between normal and hyperglycemic glucose concentrations.[210]

As mentioned above, GUVs are not very stable and have also been shown to be susceptible for leakage.[211,212] Cell-sized vesicles produced from synthetic block copolymers, so called polymersomes[213] or hybrids thereof with liposomes are improved in this regard[206,214] and have successfully been used to mimic compartmentalization of the eukaryotic cell[215] or to achieve spatial separation of otherwise incompatible multienzyme synthesis reactions.[216,217] However, initial experiments on polymersome embedded MPs have shown that enzymatic activity was decreased compared with pure lipid vesicles.[218,219] Nevertheless, proton pumping by bo_3 oxidase was recently demonstrated in hybrid polymer-lipid GUVs.[220] Some of these examples discussed above are depicted in Figure 2, see legend for further details.

These cell-mimetic applications greatly demonstrate the potential of giant vesicles. Importantly, a wise choice of detection method is crucial that allows high temporal resolution combined with sufficient sensitivity. To this end, photostable fluorophores are required to minimize bleaching during observation of single vesicles. To allow for prolonged observation and addition of substrates, vesicles have to be immobilized, which might have adverse effects on membrane properties such as the tightness of the membrane. Recently, experiments using microfluidics have shown formation and entrapment of GUVs in a nano-factory on a chip,[221,222] which in the future might allow to create automated systems. However, many of the current approaches (single molecule measurements, microfluidics) require technical expertise and specialized equipment which limits the use of the techniques in other labs. In the future, robust methods with a broad application and high reproducibility are critical for the success of GUVs in the field of MP research. Equivalently important is a detailed description of the data treatment. As microscopy experiments produce a large amount of data, user-friendly yet powerful analytical software is a necessary support during data analysis.

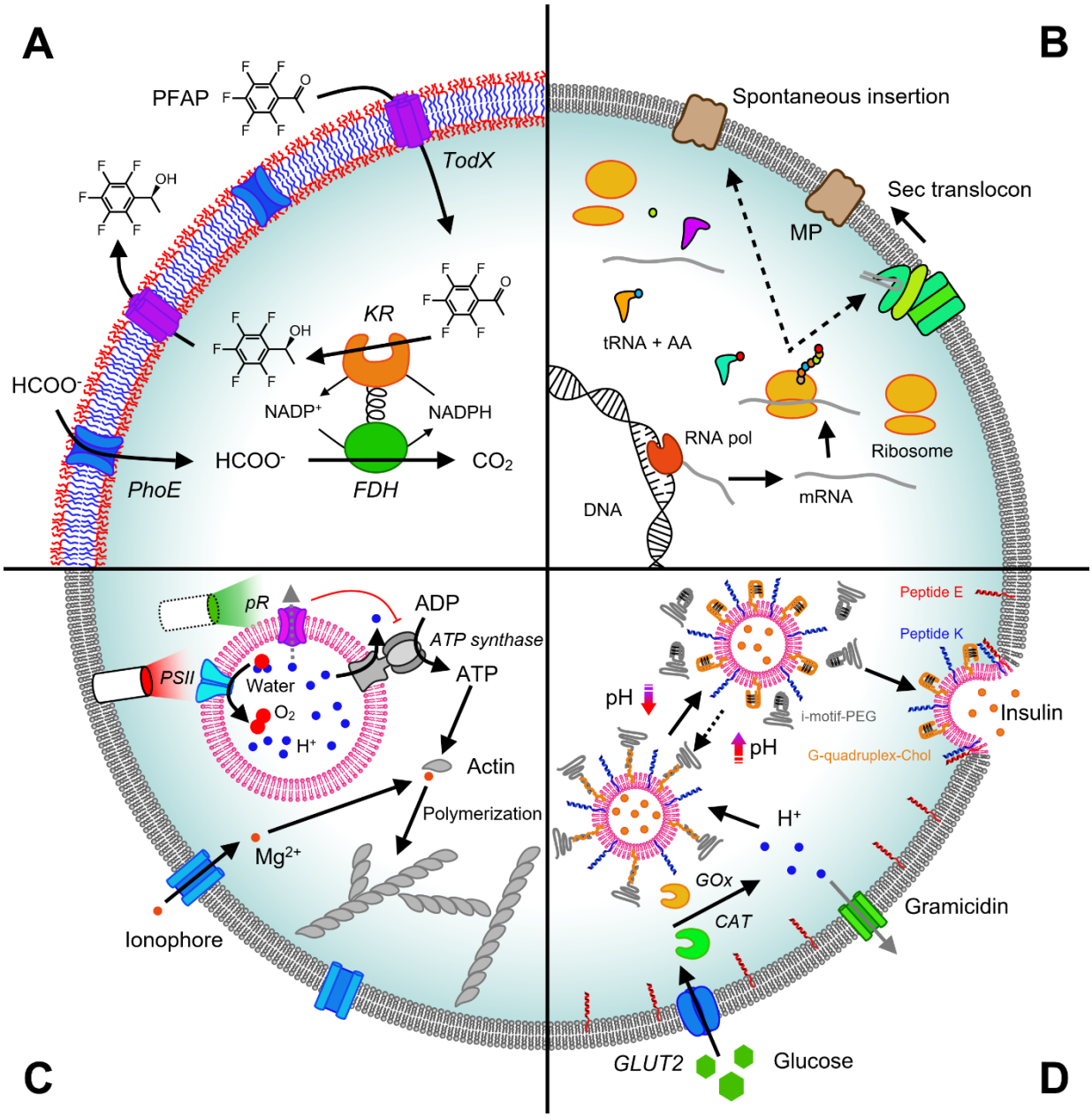

Figure 2: Applications of membrane proteins (MPs) in giant unilamellar vesicles (GUVs) and polymersomes. A) MPs embedded in a polymersome membrane enables import and export of substrates and products from a synthetic reaction cell. In that cell, pentafluoracetophenon (PFAP) is transformed to (S)-pentafluorophenyl ethanol ((S)-PFE) by ketoreductase (KR) inside of polymersomes with NADPH as cofactor. NADPH is regenerated by formate dehydrogenase (FDH) which is fused to KR. As PFAP, (S)-PFE and formate do not readily diffuse across the polymersome membrane, the selective channel protein TodX and the outer membrane pore PhoE were reconstituted in the membrane to alleviate the mass transport limitations.[217] B) Membrane protein synthesis in GUVs by *in vitro* transcription and translation. Relevant components shown for these processes are DNA, RNA polymerase (RNA pol), the produced mRNA, ribosomes, tRNAs and amino acids (AA). After translation, the synthesized MP inserts either spontaneously[201] into the vesicle membrane, or requires the Sec translocon for correct insertion.[202] C) Regulated ATP synthesis promoting actin polymerization in synthetic organelles. The membrane proteins F_1F_0 ATP synthase, photosystem II (PSII) and proteorhodopsin (pR) are coreconstituted in SUVs that are entrapped in GUVs. Red light stimulates PSII leading to oxidation of water and thus acidification of the SUV interior. Acidification leads to a proton gradient across the SUV membrane energizing ATP synthesis in the GUV lumen that is used to polymerize actin. On the other hand, green light stimulates proton export from the SUV lumen by proteorhodopsin, abolishing the proton gradient. Consequently, synthesis of ATP is stopped and

actin polymerization is interrupted.[98] D) Design of minimal pancreatic beta cell. The glucose transporter GLUT2 is reconstituted into the membrane of GUVs containing SUVs with encapsulated insulin. After uptake by GLUT2, glucose is oxidized by glucose oxidase (GOx) and catalase (CAT), leading to an acidification of the GUV lumen. This pH drop leads to the dehybridization of DNA double strand anchored to the SUV outer membrane by the formation of a pH-sensitive motif, exposing the fusogenic peptide K on the outer SUV membrane. This allows fusion of the SUV with the GUV membrane via peptide E/K interaction, leading to the release of the encapsulated insulin. Gramicidin present in the GUV membrane modulates the pH response and allows to discern between normal and hyperglycemic conditions.[210] Figures 2A-D are adapted from the respective publications.

Perspective Section

(i) Importance of the field: Proteoliposome research continues to be an indispensable tool for the mechanistic understanding of MPs. With the advent of structure determination by cryo electron microscopy, functional measurements are becoming the rate-limiting step.

(ii) Current thinking: Development of improved methods for the precise orientation and coreconstitution of MPs into membranes are required. This is especially relevant for the bottom-up construction of artificial cells. Using fluorescent dyes with precisely tailored properties will ensure high sensitivity and temporal resolution.

(iii) Future directions: Microscopy based measuring techniques applied on liposomes will further minimize the required amount of MPs, enabling the investigation of eukaryotic enzymes. The use of microfluidics for the generation and manipulation of GUVs might allow a higher level of control in lab-on-a-chip type experiments.

Acknowledgements

We thank the members of the group for helpful discussions.

Funding

Research in the author's lab is funded by the Swiss National Science Foundation (grant No. 176154).

Competing Interests

The authors declare that there are no competing interests associated with the manuscript.

1.2. Giant Unilamellar Vesicles – the Future of Membrane Protein Research?

As outlined in the previous section, GUVs have become increasingly popular in the field of MP research, especially in the creation of complex multi-component systems towards the bottom-up creation of synthetic cells. However, GUVs have rarely been used for the detailed characterization of a MP, which is still done mainly in SUVs. In this next section, the key steps and requirements for successful measurement of MP function in GUVs will be introduced in more detail. Briefly, the first step involves the formation of GUVs, using either simple or complex synthetic lipid mixtures or natural lipid extracts and physiological buffers in order to preserve enzyme activity. Secondly, MPs need to be incorporated into the GUV membrane, which is either achieved directly during formation or into preformed GUVs, e.g. using detergent-mediated approaches similar to what has been described for SUVs in the previous section. Thirdly, a suitable detection system is needed to follow the function of the MP in the GUV, such as fluorescent dyes or enzyme cascades that lead to a fluorescent read-out as demonstrated in some of the examples given in the previous section. The detection system might need to be encapsulated in the giant vesicle during formation. Further, to measure protein function in real-time, vesicles need to be continuously followed, which is often achieved by immobilization of GUVs using a variety of techniques. This immobilization, however should not compromise the membrane integrity, i.e. the tightness of the GUV towards protons or other ions is important if vectorial transport of such solutes is to be measured.

1.2.1. Formation of GUVs

Dried lipids spontaneously assemble into vesicles upon rehydration with aqueous media. This spontaneous self-assembly occurs due to the amphiphilic nature of the lipids and is thermodynamically driven by hydrophobic interactions and van der Waals forces between the hydrocarbon tails, as well as electrostatic interactions and hydrogen bonding between the polar hydrophilic headgroups of the lipids and surrounding water.[223] The structures into which these molecules assemble further reduce the need for oriented water molecules and thus increase the entropy of the system.[224] These structures depend mostly on the shape of the lipid, roughly determined by the area-ratio of the headgroup compared to the hydrocarbon tail (Figure 3). A relatively large headgroup results in a positive curvature leading to a shape like an inverted cone. This results in the formation of so-called micelles, spherical structures where all hydrocarbon tails are in contact with each other, while water molecules are excluded from the inside. Lipids with a similar area for both hydrocarbon tails and headgroup assume a more cylindrical shape, which leads to the formation of lamellar phases, lipid bilayers where the hydrophobic tails of each leaflet are pointing towards each other while the headgroups are pointing outward towards the water molecules. These bilayers can assemble into vesicles, where an aqueous solution is encapsulated and separated from the surrounding solution. Lipids with a relatively small headgroup have a negative

curvature leading to a cone shape which can result in the formation of hexagonal and even cubic phases. These can be viewed as inverted micelles, with headgroups pointing inwards, often assembling into larger structures. Those lipids are further able to transition between the lamellar and hexagonal phase, depending on the temperature, sometimes involving the cubic phase as an intermediate step. The fatty acid composition can further determine which phase is favoured (Figure 3A).[225]

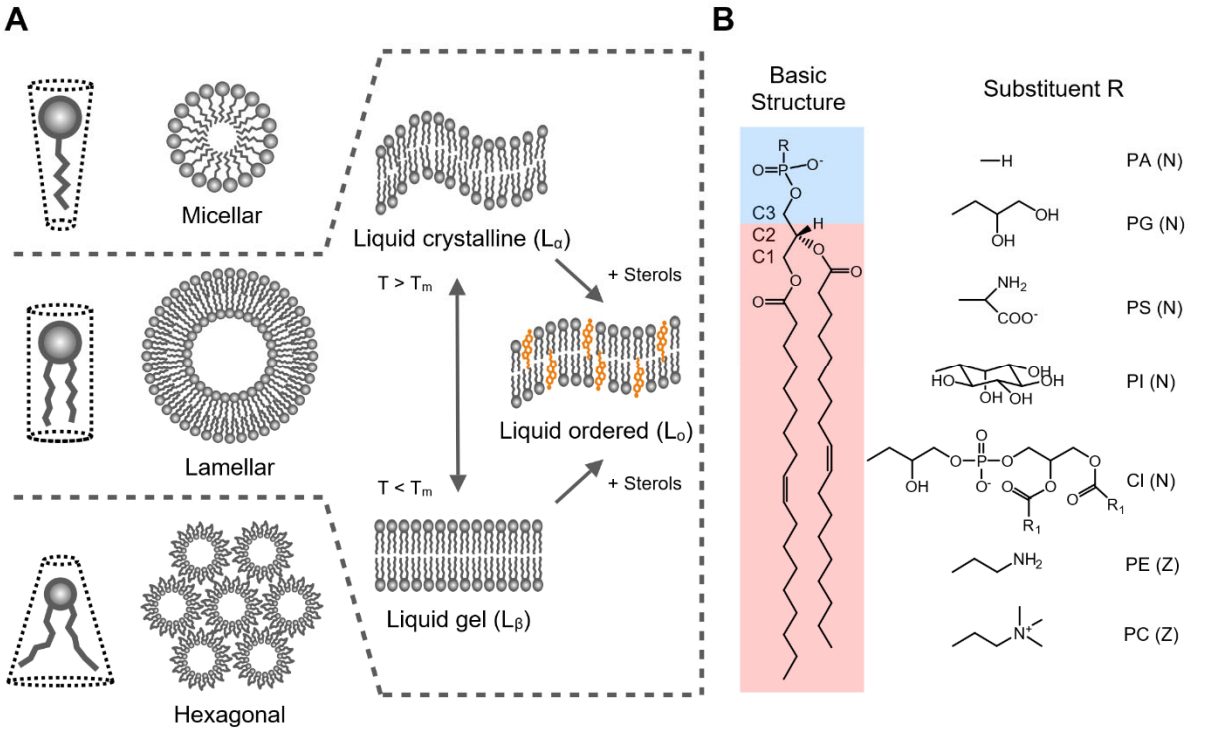

Figure 3: Lipid structure and membrane phases. A) Schematic representation of different lipids and membrane phases. Lipids with large headgroups and small tails have the shape of an inverted cone, leading to a micellar membrane phase. Lipids with small headgroups and large tails have the shape of a cone, leading to a hexagonal phase. Lipids with a similar tail and headgroup area have a cylindrical shape leading to a lamellar membrane phase. At temperatures below the transition temperature ($T < T_m$), the membrane is organized in a liquid gel phase (L_β), while it is in the liquid crystalline phase (L_α) or liquid disordered phase above the transition temperature ($T > T_m$). Addition of sterols (orange) leads to the formation of the liquid ordered phase (L_o). B) Basic structure of a double unsaturated lipid (Δ9-cis-1,2-dioleoyl-sn-glycerophospholipid) and substituents for R. The hydrophobic hydrocarbon tails are highlighted in red and the hydrophilic headgroup in blue. Anionic lipids are indicated with (N) and zwitterionic lipids with (Z). Substituents are phosphatidic Acid (PA), phosphatidylglycerol (PG), phosphatidylserine (PS), phosphatidylinositol (PI), cardiolipin (Cl) with R_1 denoting hydrocarbon tails, phosphatidylethanolamine (PE) and phosphatidylcholine (PC).

Natural membranes are composed of many different types of lipids that vary in their headgroup and the degree of saturation. Glycerophospholipids, or in short phospholipids, are the most important lipids for biological membranes and are composed of two fatty acyl chains linked to a glycerol molecule via ester linkages at the C1 and C2 atom, while a hydrophilic headgroup is attached to C3 via a phosphodiester bond.[226,227] The fatty acyl chains can vary in length and number of C-atoms and can be saturated or unsaturated, meaning that they contain either no, or one to several double bonds, respectively. While

saturated chains are in an extended conformation, the introduction of double bonds in the cis-configuration leads to the formation of kinks which can result in branched and bulky hydrocarbon tails.[227] Cellular membranes further have a physiologically relevant asymmetric distribution of charged lipids.[228,229] The charge of a lipid is determined by the headgroup. Phosphatidic Acid (PA) is the simplest form, where no additional moiety is present on the phosphate group. As the name suggests, this lipid is acidic and thus has a net negative charge. Phosphatidylserine (PS), phosphatidylinositol (PI) and phosphatidylglycerol (PG) are also lipids that carry a net negative charge at physiological pH, while phosphatidylcholine (PC) as well as phosphatidylethanolamine (PE) behave as zwitterions, carrying both a negative and a positive charge, resulting in a net neutral charge. A special case is cardiolipin, which is formed by two phosphatidic acid molecules that are joined by a glycerol molecule via phosphodiester bonds. Due to the two phosphate groups, cardiolipin carries two negative charges (Figure 3B).[227]

For biological membranes, the lamellar phase is the most relevant, although it is possible that other phases are transiently present as well.[230] Three main lamellar phases can be distinguished, and their occurrence depends on the temperature, acyl-chain, and membrane composition. At low temperatures, many lipids tend to adopt the gel phase (L_β), a quasi-solid state with restricted movement of the lipids in the membrane. Elevated temperatures give rise to the liquid crystalline phase (L_α), in which there is unhindered translational and rotational diffusion of the lipids.[230,231] The temperature at which the transition from the L_β to the L_α occurs is called the main transition temperature (T_m). The third phase is called the liquid ordered (L_o) phase and is formed in the presence of sterols in the membrane. It is characterized by a high degree of order in the acyl-chains similar to the L_β phase while maintaining a high lateral diffusion as in the L_α phase (Figure 3A). The discovery of the L_o phase formed the basis for the "lipid raft" hypothesis, the co-existence of different phases in cellular membranes.[230,232–234] The phase behaviour of the lipid bilayer is also an important parameter for GUV formation, as most methods require membranes which are in a fluid state. It is also important to note that a bilayer itself does not assemble into a vesicle of a given size. Thus, methods for the formation of micrometre-sized vesicles essentially guide the bilayer to adopt the shape of a GUV.[235] Reeves and Dowben (1969) were the first to control the spontaneous swelling conditions to obtain micrometre-sized vesicles.[236] Since then, many different approaches have been established for GUV formation (Figure 4). They can be separated into two main categories. The film hydration methods are based on the rehydration of dried or nearly dried lipid deposits on solid surfaces or hydrogels. This leads to the formation of small vesicle buds which grow to giant vesicles by bud coalescence. Thus, factors that influence the density of buds on the surface or the kinetics of vesicle merging might impact the yield and size distribution of GUVs.[237,238] The second category can be termed solvent displacement methods and involves the formation of aqueous droplets, usually in lipid-solvent mixtures. These droplets, which serve as the basis for GUV formation, can be

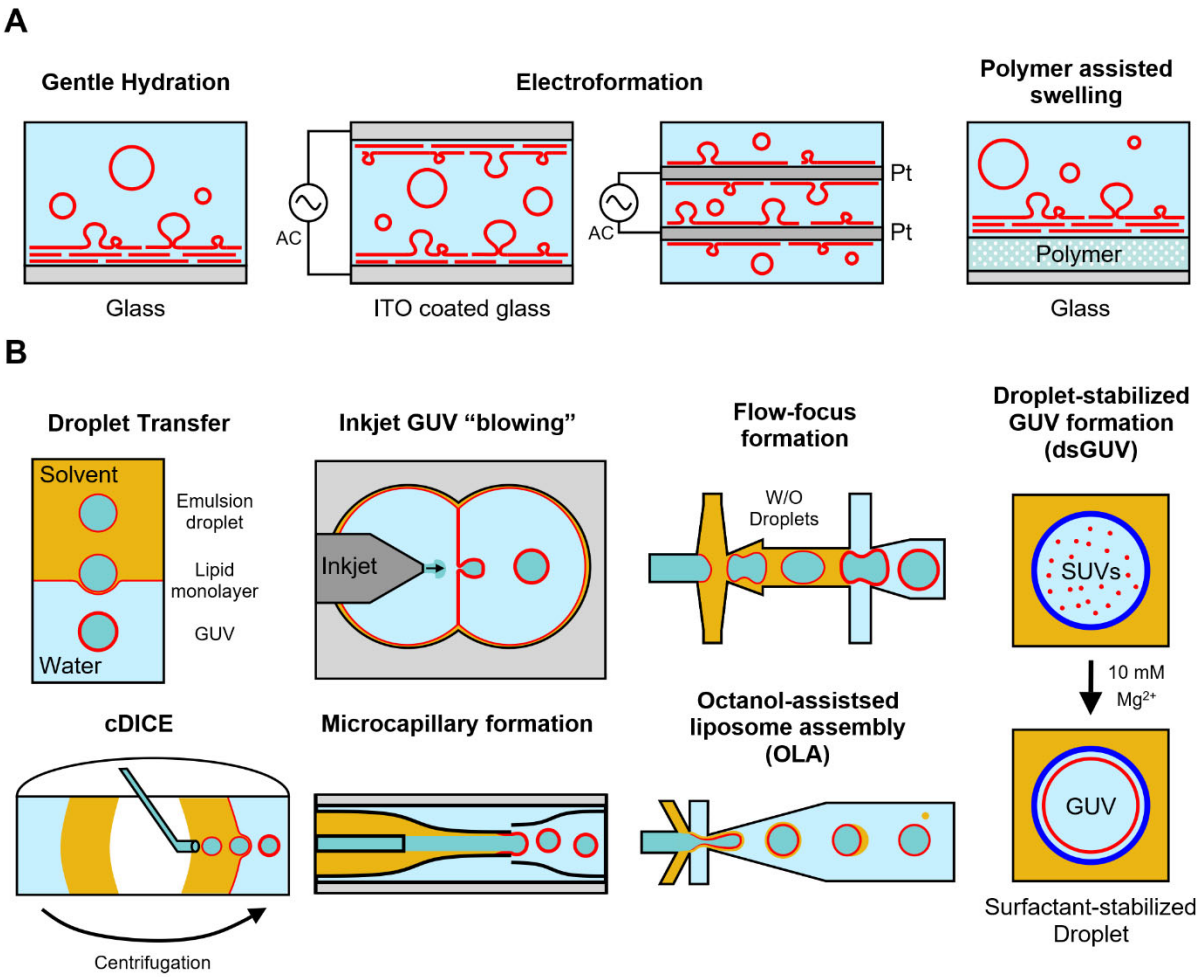

Figure 4: Schematic overview of GUV formation methods. Aqueous solutions are depicted in blue, apolar solvents (e.g. octanol, oil) in yellow, lipids in red and surfactants in dark blue. A) Solvent-free film hydration methods. For gentle hydration, lipids are deposited on glass and swelled overnight to several days without perturbations. For electroformation, lipids are deposited on indium-tin-oxide (ITO) coated glass slides or Platinum (Pt) wires and swelled in presence of an alternating-current-(AC)-electric field. For polymer assisted swelling, lipids are deposited on a polymer which promotes formation by its hydration.[194] B) Solvent displacement methods. Lipid-stabilized emulsions pass through a lipid monolayer at the solvent-water interface in the droplet transfer method.[189] Continuous droplet interface crossing encapsulation (cDICE) is achieved using a rotating disk with horizontal aqueous and solvent layers. Droplets are added using a capillary and pass through the layers due to centrifugation.[281] Inkjet GUV "blowing" involves the formation of a planar lipid bilayer by contacting two water droplets surrounded by an organic solvent. The inkjet nozzle is used to "blow" GUVs out of the bilayer (similar to soap bubble blowing).[292] In microcapillary formation, an inner aqueous solution is flowed into a solvent-lipid mixture flow, leading to bulging at the end of a tapered capillary. An outer aqueous flow into the outlet capillary leads to tear-off of the vesicles.[194] The flow-focus formation uses a microfluidic double cross-junction design for GUV production, with sequential formation of the single water-in-oil (W/O) and double (W/O/W) emulsion.[239,274] Octanol-assisted liposome assembly (OLA) uses a six-way junction, with the production of the double emulsion in one step and subsequent de-wetting of the membrane by separation of an octanol-pocket.[193] GUVs are formed inside of surfactant stabilized droplets by charge-mediated fusion in the droplet-stabilized GUV (dsGUV) formation method.[199]

generated using bulk emulsification methods or microfluidic approaches. The method of droplet formation heavily influences the yield and size of GUVs obtained.[198,239] In the following sections, a brief

overview over the different and most popular methods will be given. More detailed descriptions and further reading can be found in published reviews[191,196,240–244] as well as in *"The Giant Vesicle Book".*[235]

Film Hydration Methods

The film hydration methods (Figure 4A) are in essence based on the approach by Reeves and Dowben,[236] often termed "gentle hydration method", and involve the deposition of lipids on a solid substrate, followed by complete or partial drying of the lipid film, after which it is rehydrated using non-electrolyte aqueous solutions. The deposition can be made from lipids dissolved in organic solvents, as was shown by Reeves and Dowben using chloroform-methanol,[236] or using SUVs as demonstrated later, which additionally offers the benefit of incorporating MPs into GUVs by using proteo-SUVs and creating giant vesicles of complex lipid mixtures.[245–247] The gentle hydration method, although very mild and simple to perform, has some disadvantages. The formation requires a lot of time (several hours to days), GUV distribution is typically very heterogenous with many of the produced vesicles being multilamellar or containing other defects, and formation using physiological buffers can be challenging.[196,235,248,249] Several improvements of this method have been made over the years, such as the incorporation of charged lipids and sugars to improve formation in physiological buffers.[249] More variations on this method are given in Chapter 1.2 of *"The Giant Vesicle Book".*[235]

In order to improve yield and reduced the time of the formation process, Angelova and Dimitrov deposited the lipids on a charged surface and applied an electric field, first using direct current[250] and later using an alternating current.[251] Many solid substrates, mainly indium-tin-oxide (ITO) coated glass or Platinum (Pt) wires have been used,[194,196,235,250,251] but also other materials such as gold,[252] titanium[253] or stainless steel have been reported as well.[195,254] The choice of substrate as well as the frequency and voltage of the current offers a large amount of adjustability, which has enabled the electroformation of GUVs in physiological buffers[194,255–257] or using cationic lipids,[258] and further offers some control on the size of the formed GUVs.[259,260] However, this also means that there is not a single protocol for the efficient formation of GUVs under many different conditions, rather the parameters need to be optimized for every setup to get the desired amount and size of GUVs under various conditions. For example, it has been demonstrated that Pt wires might be more suitable for the electroformation of giant vesicles under physiological conditions at small electrode distances.[257] The application of an electric field has been shown to affect the formation of GUVs from charged lipids, resulting in the formation of vesicles with asymmetric lipid distributions.[261] While this could be desirable for some applications, as natural membranes are also asymmetric, other applications might require even distribution of the lipids across both leaflets. Further, electric fields might lead to lipid oxidation as an undesirable side effect.[262] Despite these issues, electroformation has established itself as one of the most popular GUV formation methods as it is a fast and impurity-free approach to obtain GUVs.[196]

A more recent GUV formation method, polymer assisted swelling, omits the use of an electric field and offers both the simplicity of the gentle hydration method and the high yield and short time of the electroformation approach. Here, the lipids are not deposited on a solid substrate but rather on a polymer-based gel or material that improves the influx of buffers from below the lipid film. This method was first demonstrated by Horger *et al*. (2009) using agarose as substrate, and GUVs with charged lipids and in physiological buffer conditions were formed.[263] However, it was quickly discovered that agarose was not an ideal substrate, as it was frequently incorporated inside the GUVs.[264] An improvement of the method was published by Weinberger *et al.* (2013) with the use of polyvinyl alcohol (PVA) as substrate.[265] No PVA could be detected in the GUVs using fluorescence,[265] but it was later reported that PVA GUVs displayed altered physicochemical membrane properties due to trace amounts of PVA in the medium and in the GUV membrane.[266] Despite that, PVA assisted swelling showed once again the potential of this method, as it was able to produce sufficient GUVs with a variety of charged lipids and under various buffer conditions without the need to change parameters of the formation.[194] Using other materials as deposit layer might help to overcome alteration of the membrane properties by avoiding the contamination of the lipid bilayer with trace amounts of polymer. Subramaniam and colleagues showed that cellulose (in other words paper) and diverse fabrics such as cotton, silk, polyester and others can be used for GUV formation.[197,238,267,268] Using paper further allows cheap and simple scale-up of formation, as demonstrated by the preparation of giant vesicles in a baking tray format.[238] Polyacrylamide was recently shown to improve the unilamellarity of the GUVs[269] and cross-linked dextran(ethylene-glycol) offers some control over the vesicle size by changing the degree of cross-linking.[270,271] The influence of the hydrogel morphology and charge on GUV formation was also demonstrated using cross-linked poly-(methacrylic acid-co-ethylene glycol diacrylate)[272] or cellulose-based substrates.[238] By micropatterning of a surface and coating with poly(N-isopropylacrylamide), it was even possible to generate monodisperse GUVs of different sizes.[273] All of these approaches show the potential of polymer assisted swelling, as it is as simple as the gentle hydration method and does not require specialized equipment as needed for electroformation. It is easily scalable and produces a sufficient quantity of GUVs in a short amount of time (30 – 60 min) with various lipid compositions and buffer conditions. The main drawback is the possible alteration of the membrane properties due to polymer incorporation, which has been shown for agarose and PVA but not sufficiently investigated for other materials.

Solvent Displacement Methods

The film hydration methods have two general limitations. Owing to the procedure, these methods have a low encapsulation efficiency as the vesicles are formed in the same solution which they encapsulate.[189,191,199,274] The second limitation is the formation of vesicles with a specific transbilayer asymmetry, which is an important property of biological membranes, as the formation process relies on

the self-assembly of the lipids.[275] Methods to exchange lipids in the outer leaflet of the GUV membrane using spontaneous lipid transfer from vesicles or via methyl-beta cyclodextrins have been described,[276–278] but they do not offer full control over the exact composition of each leaflet. Both of those limitations were overcome by the so-called droplet-transfer method demonstrated by Pautot *et al.* (2003),[189,275] where the two monolayers of the bilayer are formed independently (Figure 4B). The first step is the creation of a stable water-in-oil emulsion in an oil-lipid mixture, whereby the lipid molecules form a monolayer surrounding the water droplets (inner solution). This emulsion is then added to a second oil-lipid mixture that has been layered on top of an aqueous solution (outer solution), whereby a monolayer has been formed at the interface between the oil and aqueous phases. As the water droplets are heavier than the oil, they will sediment towards the bottom and acquire the second monolayer by passing the interface, resulting in the formation of GUVs. The sedimentation can be enhanced using centrifugation[189] or by the use of sugar solutions with different densities.[279] This method offers a high encapsulation efficiency as the inner solution differs from the outer solution during formation.[189] By choosing different lipids for the emulsion and the formation of the water-oil interface, asymmetric vesicles can be constructed.[275] One can also vary the method of emulsification (for example shaking, vortexing, sonication) which might affect the efficiency of GUV formation[198] and different nonpolar organic solvents might be used as the oil phase, see chapter 1.3 of *"The Giant Vesicle Book"* for some examples.[235] The effect of several other parameters on formation such as centrifugal force, inner solution volume, temperature and pH were recently investigated by Robinson and colleagues.[280] An interesting variation of the classical droplet-transfer method is the continuous droplet interface crossing encapsulation (cDICE), where the droplet transfer takes place horizontally instead of vertically and droplets are generated using a capillary rather than by bulk emulsification (Figure 4B). Centrifugal forces are used to enable the horizontal droplet transfer.[281,282]

GUVs formed by the droplet-transfer method are still polydisperse in nature. Microfluidic devices can help to produce monodisperse droplets. The generation of GUVs using glass-microcapillary devices was reported by Weitz and colleagues in 2008 where water-oil-water double emulsions were created with subsequent evaporation of the oil to form GUVs.[283] This method was later improved to minimize possible remnants of oil trapped in the GUV membrane (Figure 4B).[240,284] Ota *et al.* (2009) used microfluidic devices consisting of T-junctions to produce monodisperse vesicles[285] while Matosevic and Pagel (2011) used multiphase flow and a triangular post guiding the transfer of droplets into the aqueous phase.[286] The latter authors later adapted the two-step assembly of the individual monolayers to create asymmetric and even multilamellar GUVs by trapping of aqueous droplets and passing several different oil-lipid mixtures and aqueous solutions over the droplets.[192] Another approach by Teh *et al.* (2011) relied on flow focusing of water droplets in oleic acid/lipid mixtures to create a double emulsion followed by solvent extraction using ethanol. This method further allowed the creation of monodisperse

GUVs of different sizes (20 – 120 µm) using a single device by controlling the relative fluid flow rates for droplet generation (Figure 4B).[274]

A major concern of many of these methods is the long incubation time (several hours) needed to remove the oil or solvent from the lipid membrane and the possibility of remnants after removal, which questions the biocompatibility of these vesicles. To tackle these issues, Dekker and colleagues proposed the octanol-assisted liposome assembly (OLA) approach (Figure 4B).[193] In this method, a double emulsion is created at a six-way junction using octanol as a solvent. The octanol then forms a pocket which can be efficiently removed in a short amount of time from the GUVs, thus potentially creating solvent-free vesicles. The lateral diffusion of lipids of OLA generated vesicles was recently compared to electroformed GUVs and no significant difference was found.[287] It was also shown that vesicles from binary lipid mixtures could be formed.[287] A variation on this technique showed that separation of the octanol pocket from the GUV could also be performed off-chip.[288] Octanol as solvent was also recently used by Robinson and colleagues[239] to adapt the flow focusing based approach initially presented by Teh *et al*. (2011).[274] Using this modification allowed elimination of surfactants as well as the solvent extraction step required in previous versions of this approach[274,289,290] and enabled the creation of GUVs from only water, lipid and octanol as ingredients (Figure 4B). Thickening agents like PVA or glycerol that are used in many other approaches were also not required in this new technique.[239]

The methods presented so far are all based on lipid-oil or lipid-solvent mixtures which serve as the basis for GUV formation. While they offer great encapsulation efficiency and the potential to create monodisperse vesicles and GUVs with transbilayer asymmetry, the creation of GUVs with lipids poorly soluble in those solvents might be challenging. This limitation can be overcome by "blowing" GUVs out of a planar lipid bilayer which is formed by contacting two water droplets surrounded by an organic solvent (Figure 4B).[190,291–294] By supplying the lipids in the form of SUVs, which then fuse into a continuous monolayer at the oil-water interface, a planar lipid bilayer that incorporates lipids poorly soluble in organic solvents can be formed and used for the formation of GUVs.[292] To create the microfluidic jets to "blow" the GUVs, glass capillary nozzles,[190] inkjet nozzles,[291,292] or acoustic jetting[294] might be used. Another method that also uses SUVs as the basis for GUV formation is the recently published droplet-stabilized GUV (dsGUV) formation method (Figure 4B).[199,295,296] SUVs are fused inside of polymer-surfactant-stabilized water-in-oil droplets and fusion is mediated by the charge of the lipids and the surfactant.[296] Droplets can either be generated using microfluidic approaches[295,296] or by bulk emulsification methods.[199] Free-standing GUVs can be formed by disruption of the surfactant layer and release of the vesicles into aqueous media.[199] In essence, this approach is similar to the formation of supported lipid bilayers with the difference that the support is not a solid surface but the fluid interface

of the polymer-surfactant-stabilized droplet. For further reading on this approach, refer to chapter 30 of *"The Giant Vesicle Book".*[235]

Choosing the Right Method

A first challenge for a researcher who wants to use GUVs to investigate MP function is choosing the right formation method out of the plethora of available approaches, as they each have their own strengths and limitations. The choice depends on the requirements on the GUVs and their order of importance. Most of the methods support the formation of GUVs under physiological conditions, although the gentle hydration method and electroformation approaches do need adjustment and optimization to achieve sufficient formation. If contamination in the membrane or the media are a great concern, then film hydration methods are preferably used, although polymer assisted swelling should be treated with caution as depending on the material, contaminations might also occur. The solvent displacement methods are the right choice if a high encapsulation efficiency is required. Microfluidic approaches are necessary if the GUVs should have a narrow size distribution, although micropatterned polymer surfaces might be used as well. Bulk droplet transfer and dsGUV formation as well as polymer assisted swelling and gentle hydration are the simplest in terms of materials and expertise required, although the latter is rather time-consuming. Lastly, the quality of GUVs (unilamellarity, free of defects) might also vary depending on the method. In the end, the choice might also depend on the method to be used for the incorporation of the MP into the GUV, as some reconstitution methods are specific to certain GUV formation techniques. In the following section, we will present the most common approaches to achieve MP reconstitution in GUVs.

1.2.2. Reconstitution of Membrane Proteins in GUVs

The second key step for MP measurement in GUVs is the functional reconstitution of the protein of interest into the giant vesicle membrane. We will focus on methods for the reconstitution of integral MPs which are embedded in the membrane, spanning the hydrophobic core of the lipid bilayer. These proteins are amphipathic, with hydrophilic parts protruding out of the membrane while apolar amino acids dominate in the regions located on the inside of the lipid bilayer. Two structural motifs enable MP insertion in the membrane, namely α-helices and β-sheets. While the latter must assemble into a rigid β-barrel to allow insertion, α-helices can span the membranes by themselves and thus, proteins might be integrated by a single or multiple α-helices. Unlike β-barrels, α-helices offer considerable flexibility in the membrane and atomic structures of MPs show that they can arrange also in a non-perpendicular way.[297] It is thus not surprising that they are more frequently found in MPs,[298] as flexibility might be an important factor for the controlled transport of solutes across the membrane, one important biological function of MPs. Further, we will focus on the reconstitution of purified MPs. There are other methods

for the formation of giant vesicles containing MPs, such as for example *in vitro* transcription-translation[201,299,300] or giant plasma membrane vesicles (GPMVs),[301,302] which will not be presented here.

The detergent-mediated reconstitution of MPs into small or large vesicles was presented in chapter 1.1 *"Current Problems and Future Avenues in Proteoliposome Research"*. In GUVs, this process is not as straight-forward. While small vesicles can also be reassembled after complete solubilization and detergent removal, this is not the case for GUVs since the guiding forces that promote formation of these micrometer-sized vesicles are not present anymore. Several different strategies have thus emerged over the past two decades to circumvent these difficulties.[188,191,303] Similar to GUV formation, these methods can be separated into two different categories. Methods that involve a partial drying step of the MP will be categorized as *Dehydration-Rehydration reconstitutions* and those where the protein is only added during or after formation of the GUV without a drying step as *non-drying reconstitutions*. The vesicles resulting from these processes will be referred to as proteo-GUVs.

Dehydration-Rehydration Reconstitution

The formation of proteo-GUVs by the controlled dehydration of proteins and lipids was demonstrated as early as the 1980s (Darszon *et al.*, Vaz *et al.*, Keller *et al.*).[245,246,304] Darszon *et al.* (1980) dissolved proteins in solvent-lipid mixtures (hexane or ether) to form GUVs by the gentle rehydration method.[304] This was later adapted for electroformation on ITO coated glass slides by Manneville and colleagues using diethyl ether as solvent, reporting functional incorporation of the MP bacteriorhodopsin isolated as purple membranes from *H. salinarium*. The protein was mixed in solvent with egg phosphatidyl-choline and the lipid-protein mixture was dried on ITO coated glass for subsequent GUV formation.[305,306] A different approach was taken by Vaz and colleagues, using proteoliposomes as deposit to form a lipid-protein film on glass, with subsequent proteo-GUV formation by the gentle hydration method.[245,246] This omits dissolving the protein in organic solvents that might be potentially harmful for MP activity. The partial dehydration of proteoliposomes was later also adapted for electroformation by Girard *et al.* (2004), showing activity of both bacteriorhodopsin and sarcoplasmic reticulum Ca^{2+}-ATPase (SERCA) using fluorescent pH and calcium sensors.[307] To obtain proteo-GUVs at more physiological salt concentrations, platinum wires are frequently used instead of ITO coated glass slides.[308–310]

One of the most crucial aspects of the Dehydration-Rehydration reconstitution is the drying step, as already highlighted by Girard *et al.* (2004). They observed drastic reduction in MP activity by complete dehydration under high vacuum.[307] On the other hand, sufficient drying is necessary as the proteoliposomes need to fuse, forming a membrane patch that enables GUV formation.[309,311,312] Different strategies for drying of the proteoliposomes while preserving protein activity have thus emerged. The drying step can be performed under controlled humidity, using vapor pressure of a saturated salt solution in a desiccator for 2 hours up to overnight.[307,313,314] A detailed protocol is given

by Collins *et al.* (2013), according to which a minimum of 30 % humidity is required.[314] A different approach uses stabilizing agents such as sugars (e.g. sucrose, sorbitol, trehalose)[308,311,312,314,315] or ethylene glycol[312,315] to reduce activity loss during the drying step. Low amounts of stabilizing agent might be sufficient while high concentrations might impede GUV formation, as shown for example with sucrose.[311] The drying conditions can further vary, from 30 min at room temperature and ambient pressure[308] to overnight at 4 °C under vacuum in a desiccator.[312] For some MPs, short drying under vacuum (30 min to 1 hour) might even be possible without the need for stabilizing agents.[310,316–318]

Although electroformation seems to be the standard method nowadays for the Dehydration-Rehydration reconstitution, polymer assisted swelling has been used as well in recent years. First, a slightly different approach was taken by Hansen and colleagues, where monomeric glucose transporter was directly embedded into molten agarose. The agarose was then partially dehydrated using a nitrogen gas stream until the gel appeared dry. Lipids were then added, dried using nitrogen gas and after rehydration with aqueous buffer, GUVs containing the transporter were obtained.[205,319] The agarose retains a considerable amount of water when heated, protecting the protein from denaturing.[319] However, an important consideration is the temperature at which the agarose is still molten, as this might impede the function of heat-sensitive MPs. Partial drying of proteoliposomes on agarose was first demonstrated by Horger *et al.* (2015) and Garten *et al.* (2015) and was also more recently used to reconstitute a sigma 1 receptor.[309,320,321] Garten *et al.* (2015) further compared the reconstitution of KvAP using agarose assisted swelling and electroformation on platinum wires. A more homogenous protein distribution was obtained in the giant vesicles formed by agarose assisted swelling, although with a slightly lower yield.[309] However , agarose is not an attractive substrate for polymer assisted swelling as discussed earlier due to its incorporation into the GUVs. Garten *et al.* (2015) initially reported that reconstitution with PVA assisted swelling was not successful,[309] but more recent reports show functional reconstitution of ABC transporters and integrins into proteo-GUVs by dehydration/rehydration of proteo-SUVs on PVA.[322,323] Lactose permease from *E. coli* was also recently reconstituted by this method on cross-linked dextran(ethylene-glycol) hydrogels.[324] There are many more substrates that have so far not been investigated and hold the potential for the facile production of proteo-GUVs in high yields and free of impurities.

Non-Drying Reconstitution

To avoid the crucial dehydration step, which might lead to a loss of enzyme activity, strategies for the reconstitution of MPs into GUVs after or during formation of the vesicles have been developed. There are essentially two main approaches, although some special variations have been established for certain solvent-displacement GUV formation techniques. The first approach is based on the detergent-mediated reconstitution know from small vesicles that has been adapted for the use with GUVs, first in 2008 by

Kreir and co-workers for electrophysiological studies of outer membrane porin F,[325] and later in a seminal paper by Dezi *et al.* (2013) where MP activity of various proteins was directly measured in GUVs using fluorescent reporters.[204] Similar to reconstitution in small or large vesicles, detergent and MPs can be added to preformed GUVs,[325] although detergent amount has to be carefully evaluated to prevent rupture of the vesicles. Alternatively, GUV formation can be performed in the presence of detergent, whereby MPs are added during or after formation.[204,326] Subsequent detergent removal results in the formation of proteo-GUVs and is usually achieved using polystyrene BioBeads. Various detergents have been used, such as octyl glucoside (OG),[325] n-Dodecyl-β-D-Maltopyranoside (DDM),[327–329] n-dodecyl-β-D-thiomaltopyranoside (DOTM),[204] n-octylpolyoxyethylen (Octyl-POE),[330–335] to name a few. It is worth noting that many publications using the detergent-mediated reconstitution primarily performed electrophysiological studies of MPs (Table 2). In those studies, the GUVs are often used as intermediates for the formation of planar or supported lipid bilayers[334,336,337] or for the extraction of membrane patches using micropipettes.[308,334,335] Only few publications show MP activity in intact vesicles using fluorescent reporters, as for example Dezi *et al.* (2013)[204] and more recently Almendro-Vedia *et al.* (2017).[326] The latter authors measured F_1F_0 ATP synthase activity in GUVs using pyranine, rhodamine 123 and membrane shape fluctuations.[326] The need to precisely control the detergent amount and the concern of incomplete detergent removal, which might increase the leakiness of the membrane, could be potential reasons to choose other methods for MP reconstitution in GUVs if activity is to be followed in intact vesicles.

Kahya *et al.* (2001) were the first to show that vesicle fusion could be used to incorporate MPs into GUVs. Bacteriorhodopsin was first reconstituted into small vesicles containing fusogenic peptides, which induce fusion when anchored to cationic lipids in the membrane of preformed GUVs.[188,338] Fusion of proteo-SUVs with GUVs has some potential benefits over other reconstitution approaches. As already discussed in chapter 1.1., fusion allows for the coreconstitution of multiple MPs which have been individually reconstituted under optimal conditions beforehand. Further, the orientation of MPs is expected to be preserved during fusion. Methods for controlling the orientation during reconstitution in small or large vesicles are currently developed as presented in chapter 1.1. This would allow the formation of proteo-GUVs with well-defined MP orientation, which might be challenging using the Dehydration-Rehydration reconstitution or the detergent-mediated approach described above.[188] Apart from fusogenic peptides, other strategies have been employed to reconstitute MPs via vesicle fusion. Tsumoto and colleagues incorporated MPs into recombinant baculovirus particles which can be fused to GUVs.[339–341] Spontaneous fusion was also reported either by adding proteoliposomes to a concentrated GUV solution and incubation overnight at 4 °C,[342,343] or by adding proteoliposomes to the formation buffer during electroformation.[344] MP reconstitution into GUVs can further be achieved using GUV "blowing"[292,345] and dsGUV formation methods,[199,295] where the formation of GUVs themselves is

based on SUV fusion. More recently, charge-mediated fusion has been employed by our group and others, using small charged proteoliposomes which are fused to oppositely charged GUVs.[80,81,346,347] Proteins with a charged surface might be used to substitute one of the charged lipid species, as demonstrated by Bian *et al.* (2016) where SUVs containing the negatively charged SERCA were fused to positively charged GUVs.[348] The SNARE machinery as well as protein- or DNA-based mimics thereof have been used for fusion of SUVs and GUVs[210,310,349] but have not been used to incorporate other MPs to the best of our knowledge.

MP research is moving towards more complex systems to understand the interplay between several proteins, as presented in our review in chapter 1.1., where correct MP orientation is relevant to ensure correct interactions between several proteins and their substrates. Most methods for the reconstitution of MPs into GUVs have not focused on the issue of orientation. However, using the droplet-transfer method, it has been shown that orientation of a MP can be controlled to some extent, as the protein can be added either to the inner or outer aqueous solution which are separately formed in this technique, resulting in a change of orientation direction.[350,351] This strategy could be applicable to all GUV formation methods, where the inner and aqueous solution are separately controlled. In the same sense, orientation of MP was demonstrated using the GUV "blowing" method by addition of proteo-SUVs to different sides of the planar bilayer.[292] A further strategy to influence MP orientation during reconstitution might be the integration of the translation machinery as well as proteins necessary for insertion of the MP into the membrane, as depicted in Figure 2 in chapter 1.1., essentially mimicking the cellular pathway that leads to incorporation of MPs with correct orientation. This method, however, requires the reconstitution of the complete transcription and translation machinery. Further, it potentially only allows for one orientation, limiting the accessibility of the protein for activity measurements or the investigation of potential drugs if the preferred orientation is not obtained.

A brief overview over some MPs that have been reconstituted up to now is given by Table 2. It focuses primarily on MPs where activities were measured rather than for example simple receptor-ligand binding, and thus, many of the proteins are transporters or pores. MPs are separated according to the measurement strategy, real-time single vesicle fluorescence measurements, electrophysiological studies and bulk or non-fluorescent measurements, as well as the reconstitution method. It can be seen that the Dehydration-Rehydration reconstitution has been preferred over other methods for single-vesicle fluorescence measurements, while as mentioned before, detergent-mediated reconstitution dominates for electrophysiological studies. The fusion approach is less frequently used, likely as it requires addition of fusogenic compounds or lipids with a non-natural positive charge if specific fusion should be achieved. However, in terms of coreconstitution of multiple proteins with a desired orientation, this strategy would be preferred.

Table 2: Non-exhaustive list of MP measurements in GUVs. Not included are studies on protein-protein interactions, phase partitioning or protein diffusion in GUVs. Studies are grouped according to the protein activity measurement performed, the reconstitution method used, and proteins are listed in alphabetical order in each group. The square brackets indicate whether a protein is inserted into the membrane via α-helices [α] or as a β-barrel [β], while the origin of the protein, if reported, is indicated in the round brackets. A brief description of the activity measurement is given. For electrophysiological studies, only the type of patch clamp experiment (Port-a-Patch or patch pipette) is indicated.

Measurement type	Reconstitution	Membrane protein	Activity detection	Reference
Real-time single vesicle fluorescence measurement	Dehydration-Rehydration Electroformation	Bacteriorhodopsin [α] (*H. salinarium*)	Light-activated inward proton translocation detected with HPTS Proton pumping (bulk) detected with 9-aminoacridine	[307]
		Ca^{2+}-P-ATPase [α] (Rabbit sarcoplasmic reticulum)	Ca^{2+}-import detected with Fluo-5N ATPase activity detected by enzyme-coupled NADH oxidation measured with absorbance (bulk)	
		F_1F_0 ATP synthase [α] (*E. coli*)	Outward proton translocation induced by a membrane potential formed with valinomycin and potassium detected with HPTS Membrane potential detected with Rhodamine 123 Protein activity detected by membrane shape fluctuations	[326]
		FhuA [β] (*E. coli*)	DNA injection through FhuA by T5 Phage detected using the DNA stain Yo-Pro I and ionic currents of patched membranes	[352]
		Photosystem II [α] (Spinach) Proteorhodopsin [α] (γ proteobacterium)	Light-activated proton translocation detected by photocurrents using patch clamping as well as by calculation of the intravesicular pH using ratiometric SNARF-1	[98]
	Dehydration-Rehydration Polymer assisted swelling	ABCB1 [α] (*H. sapiens*)	ATP-dependent import of fluorescent Rhodamine 123	[320]
		GLUT1 [α] (*Rattus norvegicus*)	Glucose import detected by enzyme-coupled conversion of Amplex Red (non-fluorescent) to resorufin (fluorescent) via glucose oxidase and horse radish peroxidase	[205]
		TAPL [α] (*H. sapiens*)	Protein mediated import or export of a carboxyfluorescein-labeled peptide	[323]

Measurement type	Reconstitution	Membrane protein	Activity detection	Reference
Real-time single vesicle fluorescence measurement	Dehydration-Rehydration Polymer assisted swelling	TmrAB [α] (*T. thermophilus*)	Protein mediated import or export of a carboxyfluorescein-labeled peptide	[323]
	Fusion	5-HT3A [α] (*H. sapiens*)	5-HT induced calcium import into 3D free standing lipid bilayers detected using Fluo-4	[347]
		Bacteriorhodopsin [α] (*H. salinarium*)	Inward proton translocation detected using HPTS	[338]
		Ca^{2+}-P-ATPase [α] (Rabbit sarcoplasmic reticulum)	Ca^{2+}-import detected with Fluo-5N	[348]
	Detergent-mediated	Bacteriorhodopsin [α] (*H. salinarium*)	Light-activated inward proton translocation detected with HPTS	[204]
		BmrC/BmrD [α] (*B. subtilis*)	ATP-dependent ethidium bromide import, fluoresces upon binding to encapsulated DNA	
		FhuA [β] (*E. coli*)	DNA injection through FhuA by T5 Phage detected using the DNA stain Yo-Pro I	
		F_1F_0 ATP synthase [α] (*E. coli*)	Same as F_1F_0 ATP synthase above	[326]
		Photosynthetic reaction center[α] (*R. sphaeroides*)	Light-induced intravesicular alkalinization detected using HPTS Measurement of the charge recombination reaction by absorbance at 865 nm (bulk)	[351]
Electrophysiology	Dehydration-Rehydration Electroformation	Connexin 26 [α] (*H. sapiens*)	Port-a-Patch (NanION)	[353]
		Connexin 43 [α] (Mouse)	Port-a-Patch (NanION)	[344]
		KvAP [α] (*A. pernix*)	Patch pipette	[308,309]
		MscL [α] (Various bacteria)	Patch pipette	[354–356]
		SsTRIC [α] (*S. solfataricus*)	Patch pipette	[357]
		TRPV1 [α] (Mammalian)	Patch pipette	[314]

Measurement type	Reconstitution	Membrane protein	Activity detection	Reference
Electrophysiology	Dehydration-Rehydration Polymer assisted swelling	KvAP [α] (*A. pernix*)	Patch pipette	[309]
	Dehydration-Rehydration Gentle Hydration	MscL [α] (*M. tuberculosis*)	Patch pipette	[358]
	Fusion	F_1F_0 ATP synthase [α] (porcine mitochondria)	Patch pipette	[343]
		VDAC [β] (*H. sapiens*)	Patch pipette	[342]
	Detergent-mediated	AgTRPA1 [α] (Mosquito)	Port-a-Patch (NanION)	[336]
		Connexin 26 [α] (*H. sapiens*)	Port-a-Patch (NanION)	[353]
		Connexin 43 [α] (Mouse)	Port-a-Patch (NanION)	[344]
		HbI-1 [α] (*H. sapiens*)	Port-a-Patch (NanION)	[359]
		KCNQ1 [α] (Mammalian)	Port-a-Patch (NanION)	[360]
		LmrA [α] (*L. lactis*)	Port-a-Patch (NanION)	[361]
		MscL/MscS [α] (*E. coli*)	Patch pipette	[327]
		OmpC [β] (*E. coli*)	Port-a-Patch (NanION)	[330,334]
		OmpF [β] (*E. coli*)	Port-a-Patch (NanION) and patch pipette	[221,325,330,331,334,335,362]
		PfKch1 & PfKch2 [α] (*P. falciparum*)	Port-a-Patch (NanION)	[363]
		TREK-2 [α] (*H. sapiens*)	Port-a-Patch (NanION)	[337]
		TRIC [α] (*C. elegans*)	Patch pipette	[364]

Measurement type	Reconstitution	Membrane protein	Activity detection	Reference
Electrophysiology	Detergent-mediated	VDAC [β] (*H. sapiens*)	Port-a-Patch (NanION)	[362]
		vGAAP [α] (Camelpox virus)	Port-a-Patch (NanION)	[359]
Bulk, non-continuous, or non-fluorescent measurement	Dehydration-Rehydration Electroformation	Bacteriorhodopsin [α] (*H. salinarium*)	Light-induced changes in membrane shape fluctuations due to proton translocation measured by micropipette aspiration of GUVs	[305,306]
		Carboxypeptidase yscY fused to transmembrane domain-GFP [α] (*S. cerevisiae*)	Shape changes induced by exogenous lipid addition due to lipid flipping, and trypan blue quenching of BODIPY-labeled lipids	[365]
		SNARE [α] (Mammalian)	Fusion-induced lipid mixing using rhodamine- and NBD-labeled lipids, Cryo-EM image analysis of SUVs fused to GUVs, docking of ^{3}H-DPPC labeled SUVs to GUVs, FRAP of hemifused GUVs	[310,366–369]
	Fusion	*bo*$_3$ oxidase / F_1F_0 ATP synthase [α] (*E. coli*)	ATP production of enzymes coreconstituted by fusion detected using luciferin-luciferase assay	[80,81,346]
		F_1F_0 ATP synthase [α] (*E. coli*)	ATP production detected by luciferin-luciferase assay	[295]
	Detergent-mediated	CopA [α] (*E. coli*)	ATP hydrolysis activity detected by ^{1}H-NMR Copper uptake detected with inductively coupled plasma – mass spectrometry at different reaction time points	[328]

1.2.3. Immobilization of GUVs

The last steps required for measuring MP function in GUVs using microscopic techniques involve the choice of a suitable detection method as well as the immobilization of GUVs to continuously follow activity in single vesicles. In our review *"Current Problems and Future Avenues in Proteoliposome Research"* presented in chapter 1.1., potential detection systems have been discussed as well as their requirements to perform real-time measurements in single vesicles. In this section, we will therefore focus on the immobilization of GUVs. Several different strategies have emerged over the past couple of decades to immobilize intact vesicles. These can be categorized into two types. Immobilization based on chemical interactions is achieved either unspecifically using Van der Waals or electrostatic forces[370–373] or specifically by ligand-receptor pairs, such as complementary DNA-strands, Histidine and Tris-NTA, or biotin and avidin and analogues thereof (Figure 5A).[370,372,374–377] Physical entrapment is achieved using gel-like matrices (Figure 5B)[282,378–380] or porous substrates,[381] micropipettes,[382] magnetic[383] or electric fields[384,385] as well as optical[386] or physical traps such as barrier structures in microfluidic devices (Figure 5C).[373,387–389] For reviews on immobilization methods, refer to Robinson[244,373] and Christensen & Stamou.[370] An important aspect to consider when immobilizing GUVs for the measurement of MP function are the kinetics of the catalyzed reaction. Proteins with fast kinetics might require a rapid addition of substrate or exchange of solution, which might be hindered or slowed down in case of entrapment of vesicles in a gel-like matrix. Some microfluidic approaches have been presented that offer fast solution exchanges on well isolated vesicles.[388,390] Other simpler microfluidic trap designs might be more limited in flow rates, where GUVs might show morphological changes or be removed from the traps at high flow rates, leading to solution exchange times of several seconds.[389,391] However, microfluidic approaches all require sophisticated equipment and considerable expertise for operation of the devices which might not be accessible to every lab. This makes simple surface-adhesion-based approaches still an attractive alternative.

The biotin-avidin interaction has become one of the most popular methods for giant vesicle immobilization due to its ease of use and high specificity and affinity ($K_d \sim 10^{-15}$ M).[372,392] It typically involves coating of a surface with avidin or one of its analogues, and functionalization of the membrane using biotinylated lipids or alternatively, biotinylated polyethylene glycol-cholesterol which can be inserted into the membrane after vesicle formation.[376] Avidin and its analogues typically form tetrameric structures that can bind up to four biotin molecules. Various approaches are used for surface coating with avidin, either by directly adding the receptor to the surface[393,394] or by first coating the surface with biotinylated BSA (bBSA) which then binds to avidin.[376] Spatial separation of vesicles might be achieved by micropatterning of the surface using bBSA.[375,376] To increase protein adsorption, a pretreatment of the surface using APTES solution can be performed, e.g. for direct coating using only streptavidin

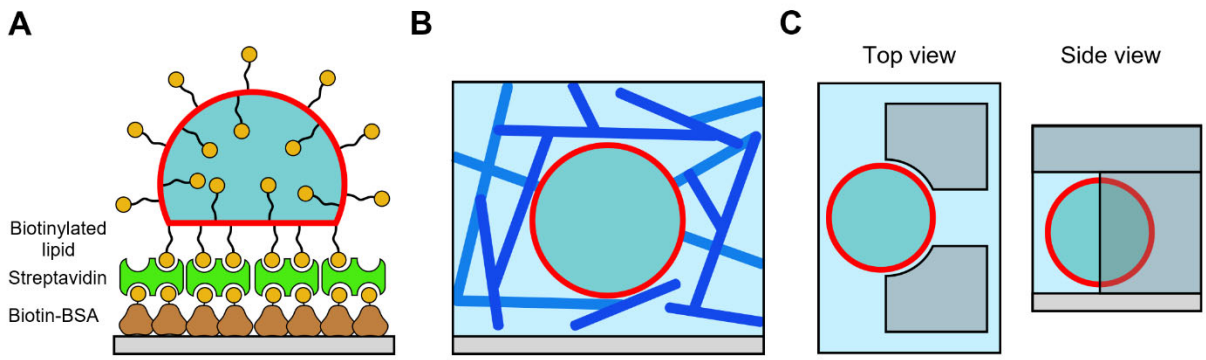

Figure 5: Schematic representation of different GUV immobilization strategies. A) Immobilization using the biotin-streptavidin system. Biotinylated lipids attach to streptavidin (green) which is bound to the surface via biotin-BSA.[375] B) Immobilization using a gel-like matrix (dark blue).[380] C) Immobilization using a microfluidic trap depicted in top and side view.[388]

without bBSA.[394] Additionally, immobilization might be influenced by the choice of biotin-linker or avidin analogue.[372,392,395,396] Further parameters that play a role in ligand-mediated adhesion of GUVs are for example receptor and ligand concentrations, vesicle radius and electrostatic forces.[370,397–400]

Adhesion of vesicles to a planar surface, either by unspecific adsorption or specific receptor/ligand-mediated interactions, results in the formation of a spherical adhesion patch.[372,377,401] This requires the deformation of the vesicle from the free-floating spherical to the attached shape which takes place by spreading of the membrane on the surface in the contact area.[394,402] The deformation of the vesicle depends on the bending rigidity of the membrane which is in competition with the adhesive strength describing the membrane-surface interaction. Thus, vesicle adhesion is favored if either the adhesive strength is sufficiently large or the bending rigidity sufficiently small.[235] The formation of the adhesion patch has been shown to lead to an increase in membrane tension, which could be exploited in previous studies to for example increase the fusion efficiency of membranes or to measure the function of a protein domain involved in endocytosis.[377,403] However, increased tension in the membrane might lead to the formation of pores and thus, GUVs might be more prone to leakage, or ultimately even rupture,[397,401,404] all of which would be detrimental to the measurement of MPs using light microscopic techniques, as for example encapsulated detection systems like fluorescent dyes or enzymes would be lost or transported substrates could immediately leak back out of vesicles. A large vesicle deformation due to strong adhesion also leads to a decrease in the volume inside the vesicles which might take place by water permeation or through the formation of pores.[401] Careful control of adhesion thus seems to be important to guarantee sufficient immobilization while at the same time preserving the tightness of the GUV membrane. For the biotin-avidin system, such control was demonstrated by modulation of the adhesion patch size and thereby the tension of the vesicle.[377] This was achieved by varying the concentration of magnesium chloride in the medium. The magnesium ions are suggested to promote the interaction of the lipid headgroups with the biotin-avidin functionalized glass surface and possibly

influencing the interaction of the biotinylated lipids with the avidin itself, both of which lead to increased vesicle adhesion.[377] A similar behavior might be observed for other ions as well, as they were shown to promote the formation of supported planar lipid bilayers which requires vesicle adhesion and rupture on the surface.[398] These ions might increase the adhesive strength, i.e. the membrane-surface interaction, by bridging, screening or charge compensating effects both on the surface and on the vesicles.[398] Further, ions have been shown to affect the bending rigidity of the membrane[405–407] which in turn could contribute to stronger adhesion if the rigidity is decreased, but effects depend on the membrane composition.[407] Thus, ions affect several parameters which can influence the adhesive properties of the GUVs.

2. Aims of the Thesis

The aim of the main project was to optimize GUVs as a tool for the study of MP function *in vitro* using light microscopy. GUVs exhibit several benefits over small liposomes like reduced curvature stress, increased inner volume and a 100-fold reduced protein amount required to perform single vesicle experiments compared to bulk measurements in cuvettes. The groundwork for this project was laid by Dr. Thomas Schick who established GUV electroformation on ITO coated glass slides and handling of GUVs after formation, and Dr. Olivier Biner, with whom Dr. Schick developed a method for the mild reconstitution of MPs in GUVs using charge-mediated fusion of oppositely charged liposomes.[80] Initial experiments to detect MP function in GUVs were performed using *E. coli* F_1F_0 ATP synthase and the sodium/hydrogen antiporter NapA from *T. Thermophilus*. In these, GUVs showed different behaviors which made analysis of the data non-trivial, and further highlighted the importance of following a sufficient number of vesicles. Further, quantitative comparison of membrane protein activity signals in GUVs, also to experiments in SUVs, was challenging and suffered from poor reproducibility. One of our main questions was therefore, how to perform MP measurements in GUVs to obtain data which can be compared to experiments done using SUVs. Although GUVs present a fast-growing field and new methods for the formation and for incorporation of MPs are constantly developed, publications showing convincing measurements of MP function in GUVs using real-time light microscopic methods are scarce and often only show average and standard deviations of signals of very few or an unknown number of analyzed GUVs.[98,205,309,347] Establishing methods to form GUVs under physiologically relevant conditions and which are tight towards proton leakage is an important aspect to reach our long term goal, the establishment of a synthetic respiratory chain from purified components. To create such a synthetic respiratory chain, coreconstitution and orientation of MPs is also required, which are tackled by other members of the group. Importantly, the production of GUVs as well as the imaging methodology should yield a sufficient number of vesicles (20 – 100) to allow meaningful statistical analysis of the data. To obtain MP activities which are comparable to measurements in SUVs, characterization of the GUVs in terms of shape and protein content will be required, which may be aided by automated analysis methods. To reduce some of the complexity, GUVs with a monodisperse size distribution could be produced using microfluidic formation methods as recently published.[193] Finally, we wanted to validate our efforts by reconstitution of a proton translocating enzyme in GUVs and reproducibly measure its activity.

The aim of the side project was to extend the tools for measuring MP activity in liposomes by developing a method which efficiently uses fluorophores for the detection of substrates such as protons. These fluorophores can be costly and encapsulation in vesicles is often inefficient. Lipid-coupled dyes are improved in this regard, as they are fully incorporated into the membrane, but simple removal from the

vesicle exterior is not possible as the lipid-coupled probe is randomly distributed in both membrane leaflets. This problem could be circumvented by introducing a cleavable linker between the fluorophore and a membrane anchoring moiety. The ease of oligonucleotide synthesis and modification makes DNA an ideal candidate for such a spacer and would allow simple enzymatic cleavage, and lipophilic oligonucleotides have already been used to sense the extracellular pH of living cells.[159,180] We thus wanted to investigate whether such probes could be used efficiently in synthetic vesicles to detect the function of multisubunit MPs, with the ultimate goal to use them for experiments in GUVs.

3. Results

This chapter presents an overview over the results obtained during this PhD thesis. It is divided into two main chapters. In chapter 3.1., the challenges of establishing GUVs as a tool for membrane protein characterization will be presented. In chapter 3.2., a bifunctional DNA duplex will be presented as a novel tool for the measurement of membrane protein function in liposomes.

3.1. The Challenges of Measuring Membrane Protein Function in GUVs

3.1.1. Experimental Platform for the Functional Investigation of Membrane Proteins in Giant Unilamellar Vesicles

Title: Experimental Platform for the Functional Investigation of Membrane Proteins in Giant Unilamellar Vesicles

Journal: Nature Communications

Status: Submitted, Pre-print available on bioRxiv.org December 2022

Authors: Nicolas Dolder, Philipp Müller, Christoph von Ballmoos

Contribution: Christoph von Ballmoos (CvB) supervised the study; Design of experiments was a shared effort of CvB, Nicolas Dolder and Philipp Müller; Nicolas Dolder and Philipp Müller performed the experiments and analyzed data together, with Nicolas Dolder focusing on PVA GUVs and Philipp on electroformed GUVs; CvB, Nicolas Dolder and Philipp Müller wrote the manuscript and made manuscript revisions.

Abstract

Giant unilamellar vesicles (GUVs) are micrometer-sized model membrane systems that can be viewed directly under the microscope. They serve as scaffolds for the bottom-up creation of synthetic cells, targeted drug delivery and have been used in many *in vitro* studies of membrane related phenomena. GUVs are also of interest for the functional investigation of membrane proteins that carry out many key cellular functions. A major hurdle to a wider application of GUVs in this field is the diversity of existing protocols that are optimized for individual proteins. Here, we compare PVA assisted and electroformation techniques for GUV formation under physiologically relevant conditions, and analyze the effect of immobilization on vesicle structure and membrane tightness towards small substrates and protons. There, differences in terms of yield, size, and leakage of GUVs produced by PVA assisted swelling and electroformation were found, dependent on salt and buffer composition. Using fusion of oppositely charged membranes to reconstitute a model membrane protein, we find that empty vesicles and proteoliposomes show similar fusion behavior, which allows for a rapid estimation of protein incorporation using fluorescent lipids.

Introduction

Giant unilamellar vesicles (GUVs) are micrometer sized (1- 100 µm) model membrane systems serving for *in vitro* studies of various lipid membrane related processes, such as membrane fusion and fission, cell division or lipid domain formation.[235] GUVs are also considered as scaffolds for the bottom-up creation of synthetic cells[8,203,408] and the targeted delivery of drugs.[409] Another, much less explored application of GUVs is the investigation of membrane proteins (MPs) that are responsible for many cellular key functions, such as nutrient uptake, signal transduction, energy metabolism and regulation of the structure and dynamics of the membrane.[1] In humans, altered expression or activity of MPs is related to many diseases, such as neurodegenerative disorders, diabetes and certain cancers.[3–6] Being accessible on the cellular surface, MPs are considered excellent drug targets.[7] A profound understanding of the enzyme mechanism and a robust platform to investigate mechanism and potential drug targets are key to the successful development of new treatment methods. With their size close to eukaryotic cells that reduces curvature stress compared to small vesicles, GUVs are an attractive platform for MP analysis. Since measurements are possible on a single vesicle level, much less protein is required, opening this field also to poorly expressing human proteins.

In our laboratory, we investigate the molecular mechanism of different membrane proteins, especially solute transporters, and members of the respiratory chain from bacteria and eukaryotes.[72,410,411] As others, we were attracted by the unique possibility of GUVs to follow the function of our proteins of interest, often including the transport of substrates as small as protons, directly under the microscope. The first functional reconstitution of a membrane protein into GUVs has been described already twenty years ago, but until today only around a dozen publications demonstrate convincing light microscopic measurements with such transporters.[98,204,351,205,220,307,323,326,338,347,348] Although these publications impressively show the potential of the methods, applications beyond proof-of principle are rare. To understand the difficulty of these experiments, we have dissected them into the substeps (i) formation, (ii) immobilization and proton leakage, and (iii) protein reconstitution.

(i) Vesicles should be produced in a suitable size range and yield that a sufficient number of free-standing GUVs can be identified as unilamellar vesicles in the field of view of the microscope. Very large vesicles are further undesirable due to concerns with stability and tightness of the membrane. A diameter of 5 – 20 µm is considered to be well suited for our applications, allowing for a number > 20 vesicles in the 40x-field of view and compatible with the size range of many eukaryotic cells. Formation should further take place under physiologically relevant conditions, including relatively high salt and buffer concentrations that stabilize MPs and are used to generate electric Nernst potentials. Generally, solvent free methods would be preferred as traces thereof in the membrane (e.g. within the hydrophobic part of the bilayer) affects

membrane thickness and is likely to negatively affect MP function. Details on various GUV formation methods have been described elsewhere.[191,196,242,244]

(ii) Immobilization of GUVs on the microscopy slide is a pre-requisite for the long-term observation of single vesicles to follow the function of MPs inside a GUV. Immobilization has been achieved using various strategies, both physical[373,378,387–389] and non-specific[370–373] or specific chemical interactions.[370] Due to its high specificity and affinity ($K_d \sim 10^{-15}$ M), the biotin-avidin interaction has become a popular immobilization strategy.[372,392] However, it has been shown that strong vesicle adhesion forms a spherical cap on the surface[401] that can lead to an increase in membrane tension and formation of pores, making GUVs prone to leakage, or ultimately even leading to rupture of the vesicles.[397,401,404] Such leakage is detrimental for measuring metabolic transporters and especially respiratory enzymes, or if the membrane should be able to hold a membrane potential or proton gradient. In general, relatively little data is available regarding the tightness of the GUV membrane towards certain substrates,[211,212] especially small ones such as protons.[220]

(iii) Functional reconstitution of the MP into the GUV membrane is critical for all downstream applications. Several methods including detergent-mediated reconstitution, rehydration of partially dehydrated SUVs or fusion of SUVs to GUVs have been exploited for MP reconstitution in GUVs.[188] We and others have recently used charge-mediated fusion to introduce MPs into GUVs.[80,81,346] This reconstitution strategy is a mild approach that transfers one or more MPs from SUVs containing positively charged lipids (reconstituted with traditional methods) to GUVs containing negatively charged lipids,[80,81] preserving the protein orientation. This fusion strategy is not without concerns, and its limitation are discussed later.

Here, using polymer assisted swelling[194,263,265,269] and electroformation[250] methods, we compare the produced GUVs on vesicle properties important for investigating MPs in GUVs as outlined above. We compare the ability of these formation methods to produce a high number of vesicles with diameters between 5 – 20 µm under physiologically relevant conditions and characterize whether immobilization using the biotin-streptavidin system was affected by the presence of salt. Vesicle leakage is analyzed using influx measurements of the hydrophilic dye pyranine (HPTS). GUVs that did not show HPTS leakage were further analyzed using a proton efflux assay to assess the ability of GUVs to maintain a pH gradient. As a last step, we used fluorescently labeled cytochrome *bo₃* ubiquinol oxidase as a model protein to monitor incorporation via charge mediated fusion.

Results

GUV formation

The best-known method for GUV formation is based on electroformation, in which hydration of dried lipids is aided by an oscillating electrical field with different frequencies and voltages. More recently, polymer assisted swelling was reported as a simpler and versatile alternative and a variety of polymers have been used as substrate.[194,197,263,265,269,270] Especially, production of GUVs with various lipid and buffer compositions was possible without the need for optimizing the method.[194,263,265,269] This is in contrast to electroformation where protocols typically must be adapted, i.e. to form GUVs in buffers containing physiological salt concentrations[194,255–257] or using cationic lipids.[258] This makes polymer assisted swelling a desirable method for the investigation of MPs as variation of the lipid and buffer composition are common requirements to obtain optimal enzyme activity or to investigate lipid effects. Among the different substrates used, polyvinyl alcohol (PVA) has established itself as a go-to material due to its wide accessibility and ease of use. In the following, we have thus focused on the use of PVA and compared GUV properties important for MP investigation for vesicles produced by PVA assisted swelling and electroformation. As lipid composition, we chose 70 % DOPC and 30 % DOPG, yielding a lipid bilayer that is negatively charged, comparable to bacterial or mitochondrial membranes. However, other lipid compositions should work analogously.

First, GUV formation was compared in the absence or presence of up to 100 mM monovalent salts (sodium and potassium chloride) and 10 mM divalent salt (calcium chloride), which we consider the upper limit of physiological concentrations needed for MP investigation (Figure 6). As most vesicles formed were unilamellar by eye, this property was ignored and only yield and size distribution of GUVs formed by the different methods were analyzed. Using 20 µg lipid as starting material, GUV formation by PVA assisted swelling and electroformation, either using platinum (Pt) wires or indium-tin-oxide (ITO) coated glass slides were compared (see Experimental Procedures and Figure S1 for sequence protocols and chamber designs). As MPs are usually investigated in free-standing vesicles, yield and size distribution were characterized for carefully detached GUVs transferred from the formation chamber to 8 well chambered microscopy slides. Our focus was the number of GUVs with diameters between 5 and 20 µm that we considered suitable for our purposes (see above). GUV formations were considered as not successful if < 10 GUVs in the desired size range were observed per field of view under the same experimental formation conditions. In the following, we considered 1.5 x 10^5 GUVs per ml in the requested size range as sufficient. The number is based on the observation that loading of 100 µL vesicle suspension should lead to at least 20 GUVs per field of view.

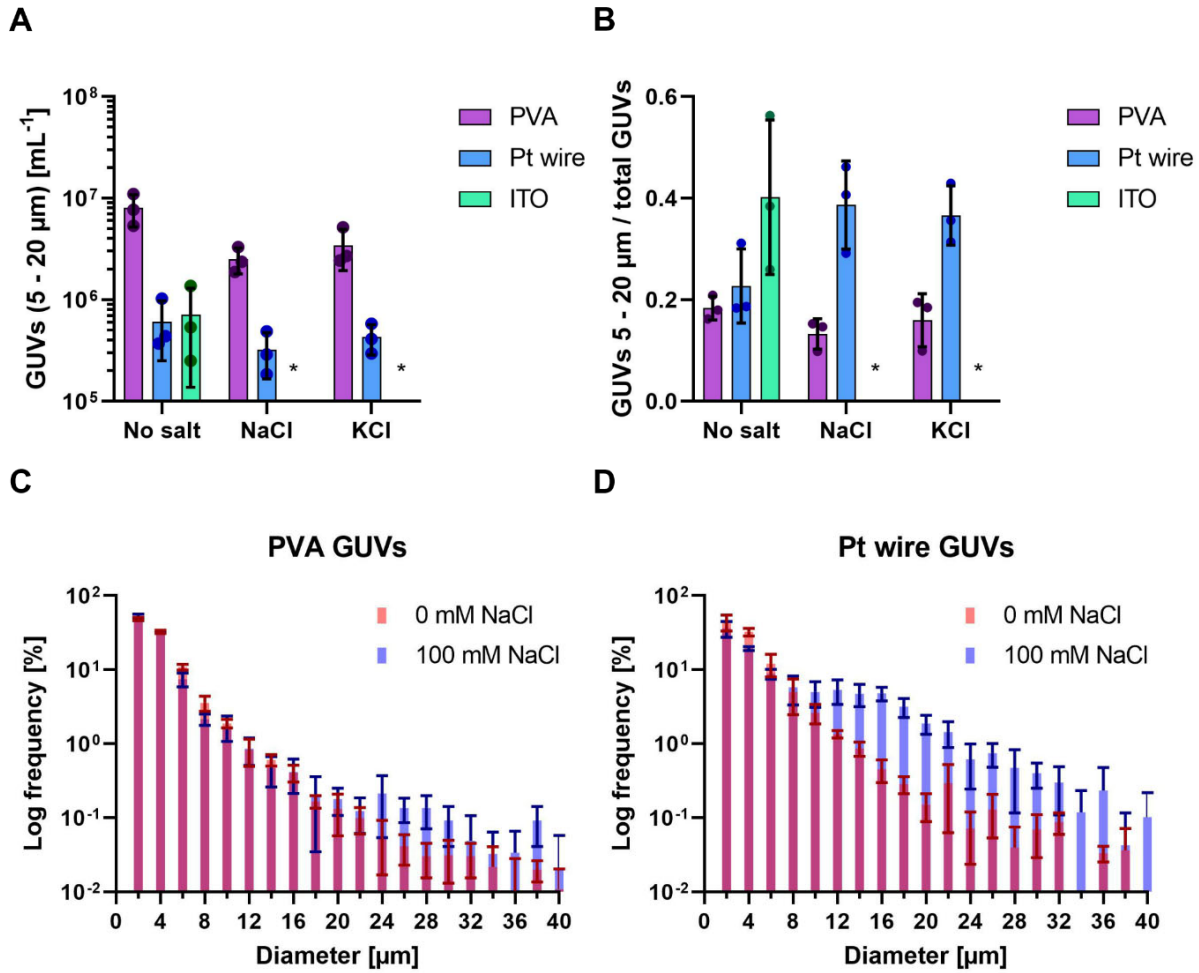

Figure 6: Characterization of GUV electroformation and PVA assisted swelling. For each condition, size and concentration of GUVs was obtained from sampling of 9 positions in each well, conducted in three independent experiments and analyzed as previously published.238 GUV formations that produced an insufficient number of vesicles (< 10 GUVs in the requested size range per 40x field of view) are marked by an asterisk. The height of the bar indicates the average with individual values from the experiments shown as dots. Error bars indicate the standard deviation. A) Concentration of GUVs with diameters of 5 – 20 µm in solution after removal from the formation chamber. B) Formation quality assessed by calculating the fraction of GUVs in the desired diameter range compared to the total amount of GUVs counted. C-D) Histograms of PVA formation and Pt wire formation in the presence or absence of 100 mM NaCl. Diameters were obtained from 780 – 6480 GUVs depending on the formation. The width of the bins is 2 µm and the graph is cut off at 40 µm. Frequencies are displayed on a logarithmic scale as larger vesicles have smaller frequencies. C) Histograms of GUVs prepared by PVA formation. D) Histograms of GUVs prepared by Pt wire electroformation.

In the absence of salt, high concentrations (> 7 x 10^5 ml^{-1}) of GUVs were obtained for all three tested formation methods. In the presence of 100 mM monovalent salts NaCl or KCl, however, only formation via PVA assisted swelling and Pt wire formation was satisfactory. Insufficient GUV concentrations were also obtained for 10 mM calcium chloride for all three formations (Figure S2). In all conditions, PVA assisted swelling yielded the largest number of GUVs in the desired size range. In the absence of salt, ~ 8 x 10^6 GUVs (5 – 20 µm) per 1 mL formation solution (Figure 6A) were obtained, while yields decreased 2 to 3-fold in presence of 100 mM monovalent salt. Roughly, the number of GUVs obtained

from both electroformation methods at 0 mM salt was about 10 times smaller than that for PVA, yielding still sufficiently high concentrations for downstream applications. Interestingly, the impact of 100 mM salt addition was less pronounced using Pt wire formation compared to the PVA method. To assess how well each formation method is suited to obtain GUVs in the desired size range, the fraction of GUVs formed with diameters of 5 - 20 µm relative to the total number was calculated (Figure 6B). The smallest fractions (< 20 %) were obtained for all three PVA formations, indicating a high number of small vesicles, while large fractions (~ 40 %) were obtained for Pt wire formation in the presence of 100 mM monovalent salt and ITO formation in absence of salt. Finally, histograms (bin size = 2 µm) of the size distribution for PVA GUVs and Pt wire GUVs with and without NaCl were calculated (Figure 6C and D) as well as the lipid yield and average diameter (Table S1), which are presented in more detail in the supplementary information. In the absence of salt, PVA and Pt wire GUVs showed a similar size distribution, while a larger frequency of GUVs > 10 µm was obtained for ITO formation (Figure S3). Interestingly, an increased frequency of larger GUVs (> 10 µm) is observed for Pt wire formation in the presence of NaCl compared to no salt, while PVA formation was barely affected, except for a slight increase for GUVs > 20 µm. Both NaCl and KCl behaved similarly in either PVA or Pt wire formation (Figure S4).

GUV immobilization

Typically, spectroscopic assays for MPs reconstituted in SUVs last from a few seconds to at least several minutes. Often, at one or more timepoints, substrates or other chemicals are added to start the reaction or otherwise influence it. It is therefore indispensable to immobilize GUVs to observe them in the same field of view over a prolonged time. Here, we focus on the well-known interaction between biotin and streptavidin that is frequently used as an immobilization system, in which biotinylated lipids in the GUV membrane interact with the streptavidin coated surface of a microscopy slide. The system allows to fine-tune the degree of immobilization by varying the concentration of either biotinylated lipids or streptavidin. We anticipate that also the ionic strength of the surrounding buffer might influence the immobilization behavior of GUVs. To standardize the immobilization condition in different microscopy slides, we calculated the streptavidin amount per area of slide surface in contact with the streptavidin solution, and the value was termed “streptavidin density” in [ng mm^{-2}]and is used from now on. In the next series of experiments, GUVs produced via the PVA and Pt wire method were immobilized using two different streptavidin densities, both in the presence and absence of 100 mM NaCl. As shown in Figure 7, a spherical adhesion cap was observed for both formation methods at high streptavidin density, and the presence of NaCl promoted the formation of adhesion caps at low streptavidin density. No caps were observed without streptavidin (Figure S5A) in either condition. Since cap sizes within one condition were rather heterogenous (Figure S5B), quantification of immobilization was not straightforward. Using commercial channel slides, we therefore developed a flow-based assay that greatly facilitated

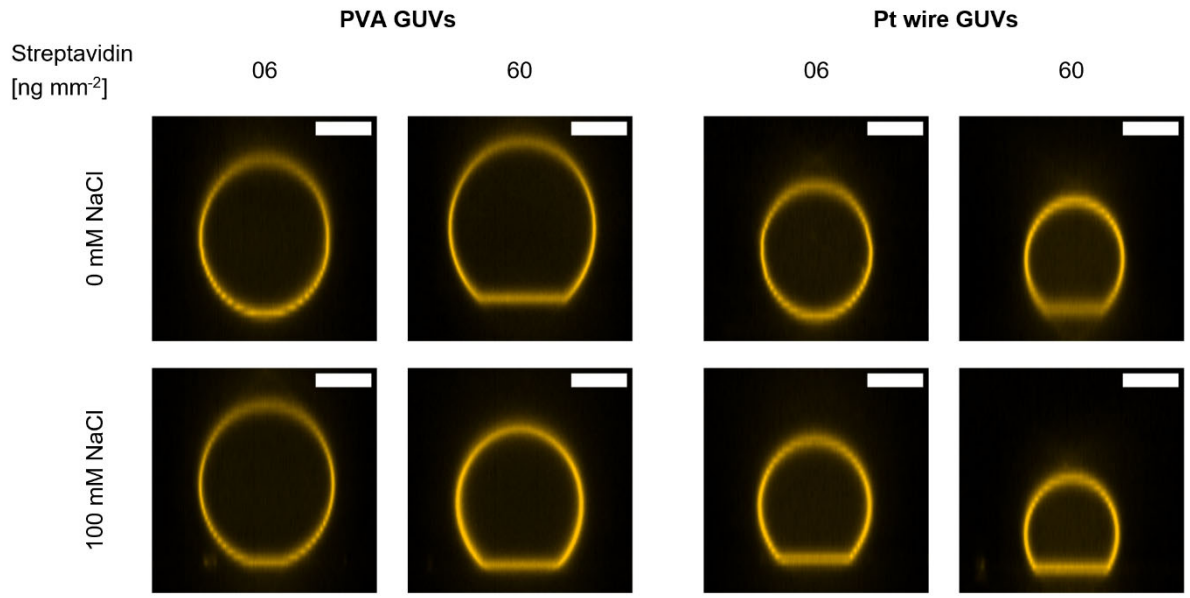

Figure 7: Formation of spherical adhesion cap at low and high streptavidin density. PVA and Pt wire GUVs in the presence and absence of 100 mM NaCl were immobilized at different streptavidin densities and confocal Z-stacks were recorded. Side-views of representative GUVs from each condition are shown. Spherical caps are observed for all conditions at high streptavidin densities while low densities show no or few caps in the absence of NaCl. The scale bar is 10 µm.

quantification of the immobilization behavior (Figure 8A). Since PVA and Pt wire GUVs showed comparable immobilization in 8 well chambered slides (Figure 7), only PVA GUVs were used in flow experiments due to the higher concentration after formation.

In this assay, PVA formed GUVs were immobilized at different streptavidin densities in presence and absence of 100 mM NaCl. First, all GUVs in the field of view were counted, before a constant flow of 5 µl s^{-1} was applied and the number of GUVs which withstood the flow were counted to determine the immobilization percentage. The general trend of the 8 well slide experiments was also observed in the flow-based immobilization assay. Without streptavidin, no immobilization was observed and at high streptavidin density almost all observed GUVs were fully immobilized in presence as well as in absence of NaCl (Figure 8C). However, GUVs immobilized at 6 ng mm^{-2} streptavidin in absence of NaCl showed almost no immobilization, whereas GUVs immobilized at the same streptavidin density but in presence of NaCl where immobilized almost to 100 %. This indicates that immobilization using the biotin-streptavidin system is highly salt sensitive.

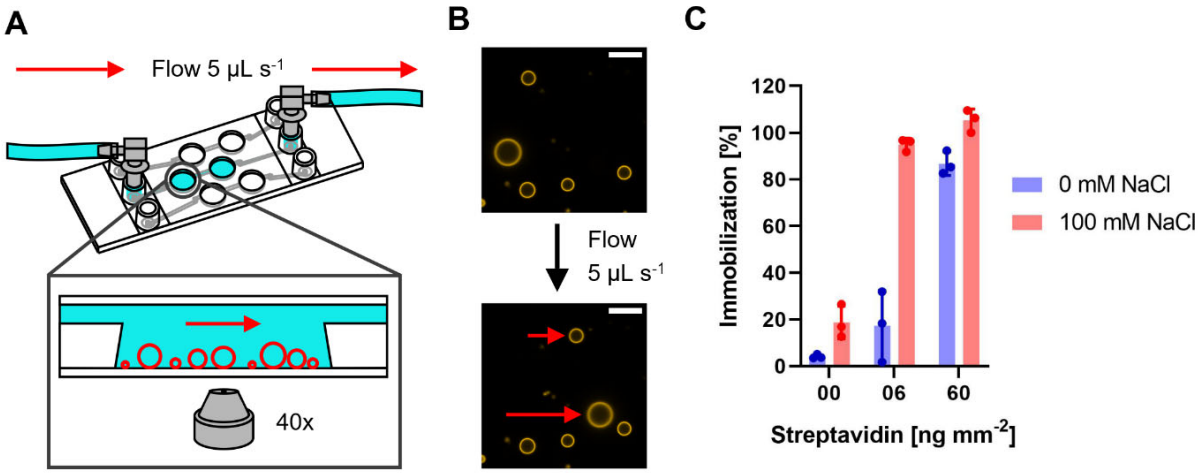

Figure 8: Immobilization assay using channel slides and PVA GUVs. A) Schematic representation of the channel slide setup with a blow-up depicting the immobilized GUVs (red circles) in the well of the channel. B) Example of immobilized GUVs under flow. Top image depicts GUVs before and bottom image during application of flow. Non-immobilized GUVs are indicated by the red arrows. The scale bar is 10 µm. C) Percentage of immobilized PVA GUVs in the presence or absence of 100 mM NaCl at different streptavidin densities assessed by comparing the number of immobilized GUVs and the number of GUVs before application of flow. Data from three independent experiments are shown. 40 – 120 GUVs were counted for analysis. The height of the bar indicates the average percentage of immobilization with individual values from the experiments shown as dots. Error bars indicate the standard deviation.

HPTS and proton leakage

To observe whether strong adhesion at high streptavidin densities affects the integrity of immobilized GUVs, we performed a dye permeation assay using HPTS. Empty GUVs were allowed to immobilize in the presence of HPTS on the outside and dye leakage into vesicles was monitored. At low streptavidin concentrations, almost no leakage was observed, while the fraction of leaky GUV increased with increasing streptavidin concentration, but never exceed 35 % (Figure S6 and S8). In addition, slight differences were observed for PVA and Pt wire GUVs. For PVA GUVs, the optimal streptavidin density was found to be between 6 and 30 ng mm^{-2} and PVA GUVs in the presence of salt remained leaky after immobilization (Figure S7 and S8). The results are discussed in more detail in the Supplementary information. HPTS has a molecular weight of 524 g/mol, making it much larger than many biological substrates of interest. Protons, the smallest biological unit, are of special interest in our research with respiratory enzymes and we therefore extended our leakiness tests with GUVs to protons using a gramicidin assay (Figure 9). Here, GUVs containing the ratiometric proton sensitive fluorophore

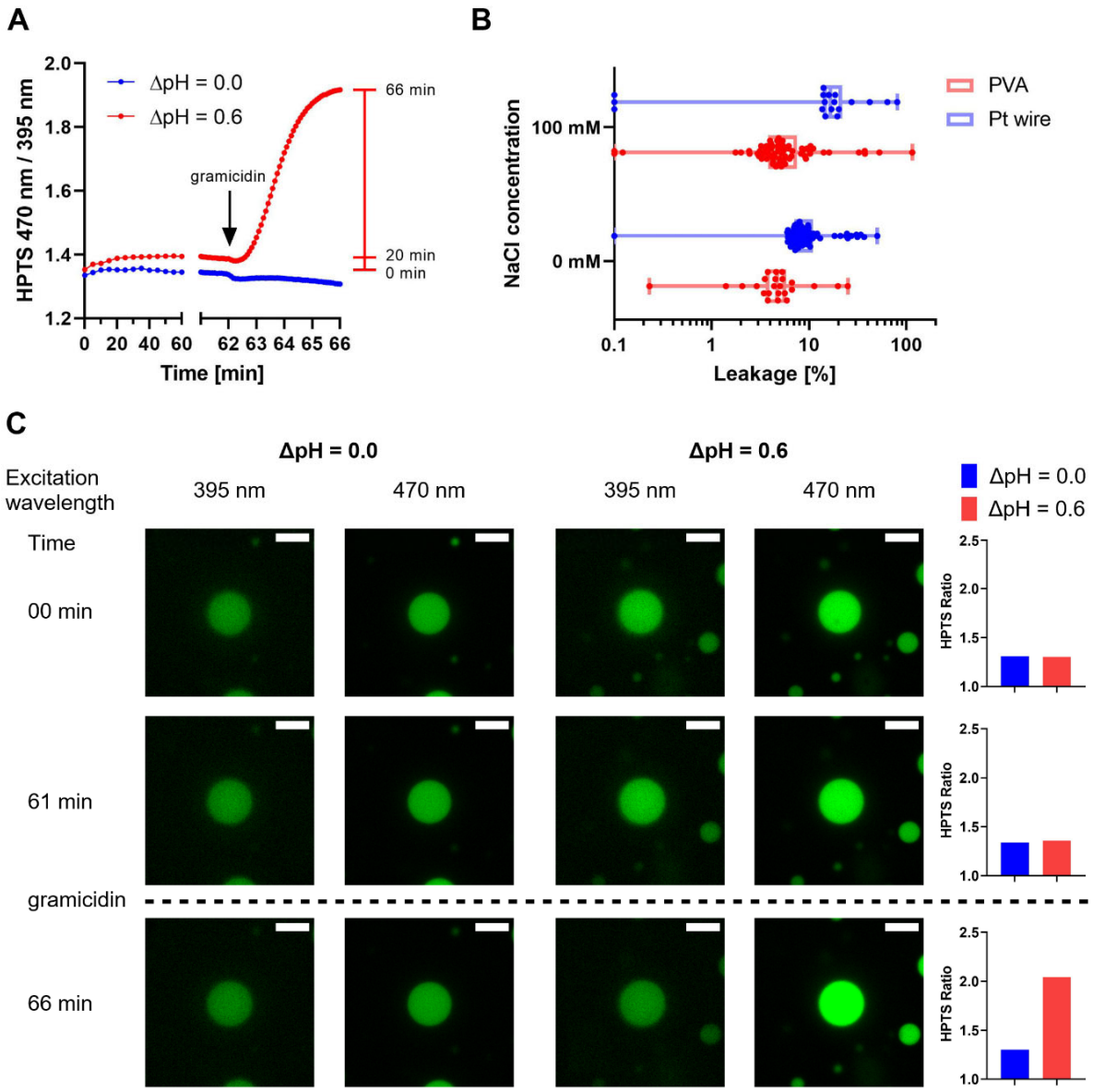

Figure 9: Proton leakage of immobilized PVA and Pt wire GUVs in the presence or absence of 100 mM NaCl. Analysis was limited to GUVs with diameters of 5 – 20 µm in the focal plane. Data are taken from a single time series for each condition. A) Average HPTS ratio of PVA GUVs with 100 mM NaCl subjected to a pH gradient of 0.0 and 0.6 over time (pH inside = 7.4, pH outside = 8.0). After 62 min, gramicidin was added to equilibrate the inner and outer pH, leading to an efflux of protons and an increase in HPTS ratio if a pH gradient is applied while no change is observed without pH gradient. The red bar indicates the time points used to assess the percentage of leakage. B) Box plot showing the percentage of leakage of PVA (red) and Pt wire GUVs (blue) with individual GUVs indicated as dots. Proton leakage was calculated by dividing the increase of the HPTS ratio after 20 min by the total increase from 0 min to 66 min (after addition of gramicidin). 20 – 70 GUVs per field of view were considered for analysis. C) Confocal microscopy images of an exemplary PVA GUV with 100 mM NaCl from the measurement with or without a pH gradient shown in (A). The two HPTS channels (green) are shown at different time points during the experiment. GUVs are shown at the start (00 min), after 1 h incubation before (61 min) and after (66 min) the addition of gramicidin. On the right, the HTPS ratio of the GUVs depicted on the left were calculated. The scale bar is 10 µm. All images were processed identically.

HPTS,[412–414] which reports pH changes in the GUV lumen, are subjected to a proton gradient. Ratiometric dyes are attractive, as bleaching effects are suppressed and with HPTS, an increase of the pH in the GUV lumen leads to an increase in the ratio of the two signals. To limit the amount of buffering molecules, we used MOPS-KOH buffer instead of MOPS-BTP. Surprisingly, PVA GUVs prepared in 5 mM MOPS-KOH in the absence of salt showed insufficient immobilization even at high streptavidin densities (Figure S9), but immobilization was possible using 10 mM MOPS-KOH and 10 ng mm^{-2} streptavidin. To detect proton leakage, GUVs containing HPTS were prepared at pH 7.4, immobilized and washed with buffer at pH 8.0, leading to a gradient of 0.6 (inside acidic). The HPTS signal was monitored for 60 min before the pH gradient was equilibrated by the addition of the protonophore gramicidin, leading to an alkalinization of the GUV lumen and an increase in HPTS ratio (Figure S10). No change in signal was observed after gramicidin addition in the absence of a pH gradient (Figure 9A and C, Figure S10E and F).

Experiments with MPs are likely to last less than one hour. Thus, we analyzed only the increase in HPTS ratio in the first 20 min and compared them to the total increase after addition of gramicidin (Figure 9A). Few GUVs showed a decrease in HPTS ratio in the first 20 min and were excluded from the analysis. Decreasing signals might be observed in GUVs with HPTS leakage before or during incubation or due to microscope drift. With the remaining GUVs, the percentage of the increase after 20 min was calculated, assuming a total pH equilibration after gramicidin addition (Figure 9B). Most GUVs that were analyzed showed very little increase after 20 min. In those, proton leakage of less than 20 % in the first 20 min was generally observed, indicating that the vesicles are sufficiently tight towards proton efflux if HPTS has not leaked. A slightly lower percentage of leaky GUVs was found in the PVA than in the Pt-wire preparation, and no influence of salt was observed in either of the preparations. A more detailed discussion of the data is found in the supplementary information.

Membrane protein reconstitution

The overall negative surface charge of lipid composition of PC:PG (7:3) not only reflects conditions found in biological membranes, but is also compatible with fusion of oppositely charged proteo-SUVs.[80,81,346] Here, every MP can be individually reconstituted into SUVs containing positively charged lipids under optimal conditions and possibly with a desired orientation. If these SUVs are mixed with negatively charged GUVs, membrane fusion occurs and the orientation of the membrane protein is conserved.[80] This modular approach is ideally suited for the bottom-up construction of artificial cells that contain a variety of membrane proteins that have non-compatible reconstitution procedures. The reconstitution yield can be directly monitored, if the membrane protein is fluorescently labeled itself. However, this is not always feasible (impaired activity after labeling, low amount of protein, no suitable labeling chemistry). We therefore hypothesized that protein reconstitution can be correlated with fusion efficiency (which can be followed by fluorescent lipids). We were also interested to see if fusion of

oppositely charged vesicles is dependent on the salt concentration, a topic that has been discussed with some controversy in the literature.[80,81,390] To tackle the latter question, we thus investigated charge mediated fusion using protein free SUVs containing a lipid-coupled dye with unlabeled GUVs in presence and absence of salt. With this approach, fusion was quantified by the amount of lipid-coupled dye found in the previously unlabeled GUV membrane. If experiments were performed directly under the microscope using immobilized GUVs, rapid fusion is observed (Supplementary movie S1) with positively charged SUVs while no fusion was observed with neutral SUVs (Figure S11A). GUVs were fusogenic both in presence and absence of salt, although a smaller fluorescence increase in the GUV membrane was observed in the presence of salt (Figure 10A and S11B). However, the signal distribution in the raw data was rather heterogenous and we were not convinced of a significant influence of salt on the fusion process (Figure S12 and S13A). To eliminate effects of immobilization and mixing or pipetting artefacts during addition under the microscope, we repeated the experiments by mixing SUVs and non-immobilized GUVs in an Eppendorf tube (Figure S13B and S14). While PVA GUVs still show a slightly decreased fusion behavior in presence of salt, the same trend was not observed with PT wire GUVs (Figure S13B). The difference in observed fusion behavior of Pt-wire GUVs either immobilized on slides or in solution is not straightforward to explain. Additions to immobilized GUVs are performed with utmost care and mixing and diffusion of added chemicals are likely to differ from experiment to experiment. A detailed description is given in the supplementary information. Nevertheless, GUVs appeared fusogenic under all conditions. Next, we investigated fusion of proteoliposomes containing rhodamine-labeled lipids and DY-647P1-labelled *bo₃* oxidase in the absence of salt with PVA GUVs that showed a slightly higher fusion yield in the previous experiment (Figure 10B and C and Figure S15). Prior to fusion, proteoliposomes (protein and lipid labeled) and empty liposomes (only lipid labeled) were mixed in different ratios (3/0, 2/1, 1/2 and 0/3) to simulate the insertion of different amounts of enzymes. As depicted in Figure 10B, a linear correlation between *bo₃* oxidase signal and lipid-coupled dye was observed in the different experiments. This is a strong indication that empty SUVs and enzyme containing vesicles have the same fusion properties and that the intensity of lipid-coupled dye correlates with the intensity of labeled *bo₃* oxidase and can be used to estimate the relative amount of enzyme reconstituted.

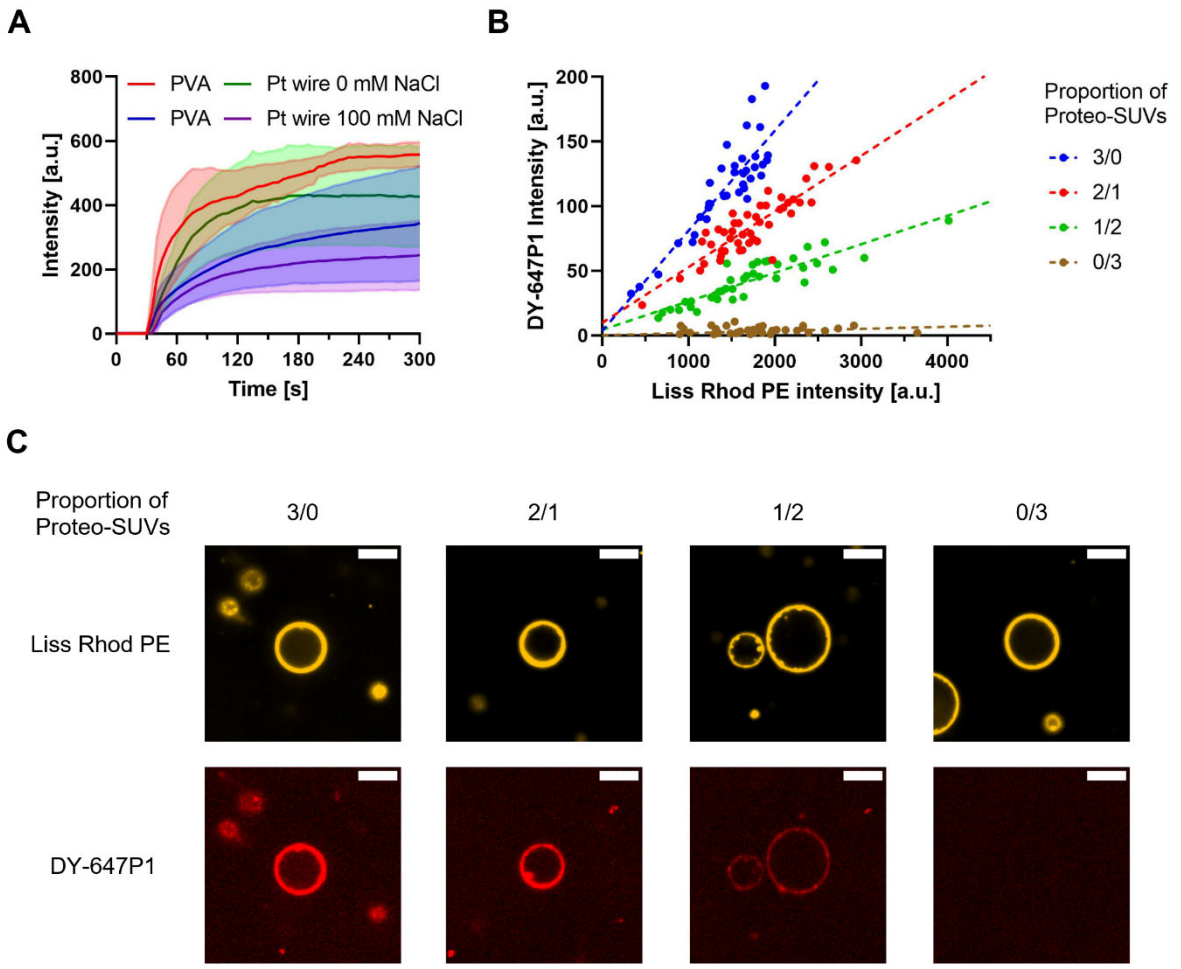

Figure 10: Charge mediated fusion of positively charged SUVs with negatively charged GUVs. Fusion was performed in an 8 well chambered slide with addition of SUVs to immobilized GUVs. Only GUVs with diameters of 5 – 20 µm in the focal plane were analyzed. A) Fusion of GUVs with empty SUVs (final concentration 10 µg mL^{-1}) followed in real time. SUVs were added to the well after 30 s after which an increase of Liss Rhod PE signal in the GUV membrane was observed. Traces represent the mean (solid line) and standard deviation (transparent area above and below the trace) of the average intensity increase of 10 – 50 GUVs from 4 experiments. B) Fusion of PVA GUVs at 0 mM NaCl with empty SUVs and proteo-SUVs (final concentration 40 µg mL^{-1}) containing DY-647P1-labeled cytochrome *bo*$_3$ ubiquinol oxidase. Empty and proteo-SUVs were mixed at different ratios with proteo-SUV proportions of 3/0, 2/1, 1/2 and 0/3. The DY-647P1 intensity is compared to the Liss Rhod PE intensity 150 s after addition of SUVs. A similar distribution of Liss Rhod PE intensities is observed in all fusion reactions as both empty and proteo-SUVs contain Liss Rhod PE. The DY-647P1 shows a linear dependency to the Liss Rhod signal with a decreasing slope as the proportion of proteo-SUVs decreases. Values of individual GUVs from one experiment are shown (30 – 50 GUVs) as dots and the linear regression is represented as a dotted line. C) Confocal microscopy images of representative GUVs from fusion with different proteo-SUV proportions shown in (B). For each GUV, the Liss Rhod PE and DY-647P1 channel are depicted. The scale bar is 10 µm. All images from each channel were processed identically.

Discussion

GUVs are attractive model systems for a variety of biological questions, including the investigation of membrane proteins. Except for a few examples, however, these investigations stayed at the level of proof-of-principle. In our lab, we are investigating different membrane proteins with substrates as small as proton or sodium ions, requiring robust and tight vesicles, also in the presence of physiological salt concentrations. As additions of substrates during the measurements are required, GUVs need to be immobilized to be monitored over a prolonged time. Reconstitution yield of membrane proteins into GUVs should be predictable to compare activities from single GUVs allowing to divide them into subpopulations. All these factors are highly important if GUVs should serve as a versatile and powerful model system to functionally characterize a MP beyond binding studies and serving as a spherical container.

Here, we compared the popular electroformation method with the more recently developed polymer assisted swelling for GUV formation in the presence of mono and -divalent ions. For electroformation, either Pt wires or ITO coated glass slides were used. All three methods yielded GUVs using buffer without salt with polymer assisted swelling producing the highest concentration and yield of GUVs. PVA assisted swelling and electroformation have been compared in the literature[194,238,309] and the present data extend this knowledge with our comprehensive quantitative analysis using conditions for biological questions. In the presence of monovalent salt, GUVs were only obtained from PVA and Pt wire formation. This was not unexpected, as we used an electrode distance below 2 mm in our ITO coated glass slides that was previously shown to be insufficient for GUV formation at high salt concentrations.[257] Overall, PVA assisted GUV formation in the presence of salt tended to decrease the concentration of vesicles, and is in agreement with other reports for polymer assisted swelling methods with increasing ionic strength or osmolarity of solution,[237,269] although few polymer substrates showed increasing GUV concentrations.[272] Thus, concentration of GUVs in the presence of salt might depend on the substrate which is used. Only slight decrease in vesicle concentration was observed in Pt-wire electroformation experiments, mostly due to an increase in vesicle diameter, as was previously observed for electroformation using up to 100 mM NaCl.[256] We have used the same protocol as in the experiment without salt and the different sizes and concentration are likely a result of the changed electrical properties of the different formation conditions.[260] No influence of salt on the size was observed for PVA assisted swelling, although a study using agarose had also observed an increase in GUV diameter with increasing ionic strength.[237]

The immobilization behavior of PVA and Pt wire GUVs was investigated using the widely used biotin-streptavidin system in presence and absence of salt. It has been shown that strong adhesion of vesicles to a slide surface results in the formation of a spherical adhesion cap.[372,401] Vesicle attachment to the slide surface is determined by the competition between the adhesive strength (that is the membrane-

substrate interaction) and the bending rigidity of the vesicle membrane, the former one being sufficiently large or the latter one sufficiently small.[235] During this process, leakage through water permeation or through the formation of pores might occur to adjust for the shape changes induced by strong adhesion.[397,401] In agreement, strong adhesion has been shown to increase the membrane tension in GUVs[377,403] with tension being a potential driving force for the formation of transient pores.[404] Careful control of vesicle adhesion guarantees immobilization of GUVs while not compromising the membrane integrity. Modulation of the adhesion cap size was demonstrated by adjusting the $MgCl_2$ concentration in the medium,[377] which is also likely for other ions.[398] Here, we found that the formation of a spherical adhesion cap greatly depends on salinity of the buffer as well as the amount of streptavidin used for immobilization. Immobilization was strictly dependent on streptavidin, as no unspecific binding was observed on BSA coated slides. Generally, the presence of salt increased the immobilization of vesicles and spherical cap size compared to the same conditions without salt. In our flow-based assay, we find that at the lowest tested streptavidin density of 6 ng mm^{-2}, 20 % and 100 % of GUVs were immobilized in the absence or presence of NaCl, respectively. We also found an influence of the counterion (KOH or BTP) of the buffer (MOPS) if no salt was used, and that a higher buffer concentration improved immobilization. We consider the following two factors to be responsible for our observations. First, the presence of salt or other charged molecules in the buffer might influence the membrane-surface interaction, e.g. by screening repulsive charges or by bridging charged species on the surface and in the lipid membrane. It has been shown that salt facilitates the formation of supported lipid bilayers which is mediated by vesicle adhesion.[398] Second, both buffers and ions can affect the bending rigidity of the membrane, [406,415] but effects depend on the membrane composition.[407]

Strong adhesion is known to trigger pore formation and thus GUV content leakage at least temporarily, which is incompatible while measuring MPs with vectorial transport functions. Temporary leakage also leads to inhomogeneous concentrations of encapsulated dyes used for detection of MP function and complicates quantitative comparison between different vesicles. A limited number of studies has dealt with this topic in detail in the past. Generally, polar and charged molecules seem to have low permeability compared to nonpolar molecules,[212] but increased permeability for certain low molecular weight compounds has been observed for GUVs compared to LUVs[211] as well as the co-existence of low and high permeability GUV populations.[212] Proton permeability is difficult to quantify and the order of magnitude varies greatly in the literature, relating to differences in experimental conditions.[416,417] The composition of the membrane and the presence of MP further seems to influence the proton permeabilty.[50,220,418] Using a microfluidic approach, Dimova and colleagues found a slightly lower proton permeability for GUVs compared to LUVs.[220] Here, we were focused on the leakiness of immobilized GUVs and if immobilization strength can induce leakage. Interestingly, increased leakage of HPTS for GUVs between 7 and 20 µm with strong adhesion was only observed for GUVs prepared by PVA

formation but not with Pt wire GUVs. The difference in behavior observed here for PVA and Pt wire GUVs is not obvious, but trace amounts of PVA in or on the membrane can alter membrane property as suggested by Dao *et al.*[266] The difference observed for Pt wire GUVs with and without NaCl is unclear, but could also be due to alteration of membrane properties, such as the bending rigidity, in the presence of salt.[405–407]

Proton permeability was tested using GUVs with encapsulated HPTS in the presence of a proton gradient. The results of the HPTS leakage experiments helped us to settle for immobilization conditions that showed immobilization and minimal HPTS leakage. The proton gradient was applied by exterior washing of the GUVs, thus mimicking standard procedures during a biochemical experiment. Only minimal increase in the HPTS ratio was observed during the presence of a proton gradient and most GUVs showed a response to the addition of the protonophore gramicidin, indicating a low level of proton leakage. Our data suggest that immobilization should and can be fine-tuned depending on the experimental set-up. Encouragingly for studies of vectorial proton transport experiments, GUVs between 5 and 20 µm that retain HPTS seem to be also tight against protons.

Different strategies have been described to reconstitute membrane proteins into GUVs. While partial dehydration of deposited membrane protein before lipid rehydration seems to work well for some proteins, a milder procedure might be suitable for large multisubunit complexes such as the members of respiratory chain or eukaryotic proteins. Since reconstitution of many membrane proteins into SUVs are established, transfer from SUVs to GUVs via membrane fusion seems an attractive strategy. We and others have successfully applied charge mediated fusion for the insertion of SUV embedded proteins into the GUV membrane, retaining their functionality, and it is currently the method of choice in our lab and was also applied here.[80,81] The effect of salt on the fusion of liposomes with oppositely charged lipids has not been conclusively discussed in the literature as some observed no or little influence[80,390] and others reported impeded fusion in presence of salt.[81] Using our protocols, we clearly observe rapid and efficient fusion of unlabeled GUVs with fluorescently labeled SUVs both in the presence and absence of salt. However, the fluorescence intensity observed in the GUV membrane is reduced to 50 % if fusion is performed in presence of 100 mM NaCl, although the fusion kinetics are similar under both conditions. In fusion experiments with non-immobilized GUVs, PVA GUVs still show a slightly decreased fusion behavior in presence of salt, but the difference was almost gone in PT wire GUVs. We speculate that this might result from different lipid composition of the GUV membrane, i.e. asymmetry of composition in the two leaflets after electroformation[261] or that trace amounts of PVA might influence the fusion behavior in presence of salt.[266]

Finally, we correlated fusion efficiency with incorporation yield of labelled bo_3 oxidase into PVA GUVs without salt. We observed a linear dependence between bo_3 oxidase signal and lipid-coupled dye if

fusion was performed using labelled proteoliposomes. We concluded that the intensity of lipid-coupled dye correlates well with the intensity of labeled *bo*$_3$ oxidase. This is an important finding as it allows to estimate protein incorporation without the need of protein labeling. Unfortunately, the method is unable to distinguish between full fusion and hemifusion or simple adhesion of the vesicles to the GUV membrane. While we did not observe a GUV signal increase if neutral SUVs were used, positively charged SUVs might still be able to adhere to vesicles in the presence of salt and undergo lipid mixing without fusion, as suggested by Ishmukhametov *et al.*[81] In our previous experiments, however, we were able to show that fusion of SUV and GUV yields functional GUVs and that the fusion behavior was similar to fusion events between oppositely charged SUVs.[80] A possible solution are content mixing assays in which fusion of both membrane leaflets is a prerequisite to trigger a signal change. However, aside from enzyme-mediated assays, content mixing assays are rather difficult due to unwanted interaction of the often negatively charged cargo with the positively charged lipids. Recently, Lira *et al.*[390] described a FRET based assay allowing them to distinguish between hemifusion and full fusion, opening new avenues for verification of complete membrane fusion.

Concluding Remarks

The application of GUVs in a variety of biochemical and biophysical disciplines is very attractive and a broad variety of fascinating results have been described. In this work, we want to contribute to a broader application of GUVs as a system of choice for the investigation of membrane proteins incorporated into the GUV membrane, elevating GUVs from their current main role as sealed lipid container or membrane mimicking system used for docking or membrane deformation studies. We therefore have somewhat systematically analyzed existing methods for GUV formation and immobilization that are accessible without specialized equipment or knowledge and tested relevant properties for membrane protein reconstitution and substrate transport. Although both PVA assisted and electroformation methods used here are based on solvent-free systems, they differ in some of the investigated properties. Electroformation has been the method of choice for many researchers as it is well established and produces clean GUVs. We find that polymer assisted swelling has several advantages, like its ease of use, versatility, scalability, and the production of high GUV numbers, but further research in other materials than PVA and agarose is needed to establish whether polymer assisted swelling can produce GUVs free of impurities.[264,266] Obviously, powerful alternatives not described here exist, such as microfluidic or oil-emulsion techniques for GUV generation or detergent-mediated reconstitution techniques. There are also efforts to replace natural lipids as used here by more robust synthetic polymers,[214,218–220,418] and while they surpass GUVs properties in terms of robustness towards mechanical and chemical stresses and life span, they are rather unlikely to match the properties of natural lipids to accommodate for membrane protein thickness and annular lipid layer. GUVs are thus designated to play a critical role also in the future, and robust and widely applicable methods for their generation and use is of importance for all researchers interested.

Acknowledgment

We thank Dr. Thomas Schick for establishing electroformation on ITO coated glass slides and the handling of GUVs after formation. We thank Stephan Berger for establishing PVA assisted swelling in our lab. We thank Sofia Hutter for purification and labeling of the cytochrome bo_3 ubiquinol oxidase. The project was supported from funds of the Swiss National Science Foundation (No. 176154).

Competing Interest Statement

The authors have declared no competing interest.

Experimental Procedures

Materials

1,2-dioleoyl-sn-glycero-3-phosphocholine (DOPC), 1,2-dioleoyl-sn-glycero-3-phospho-(1'-rac-glycerol) (sodium salt) (DOPG) 1,2-dioleoyl-3-trimethylammonium-propane (chloride salt) (DOTAP), 1,2-distearoyl-sn-glycero-3-phosphoethanolamine-N-[biotinyl(polyethylene glycol)-2000] (ammonium salt) (DSPE-PEG2000-Biotin) and 1,2-dioleoyl-sn-glycero-3-phosphoethanolamine-N-(lissamine rhodamine B sulfonyl) (ammonium salt) (Liss Rhod PE) were obtained from Avanti Polar Lipids (Alabaster, AL, USA), Streptavidin from IBA-Lifesciences (Göttingen, Germany), Invitrogen™ 8-Hydroxypyrene-1,3,6-Trisulfonic Acid, Trisodium Salt (HPTS) from Thermo Fisher Scientific (Waltham, Massachusetts, USA), DY-647P1 Maleimide from Dyomics (Jena, Germany) and Polyvinyl alcohol (PVA), fully hydrolyzed, molecular weight approximately 145'000 for synthesis from Merck (Darmstadt, Germany). Other chemicals were obtained from Sigma (St. Louis, Missouri, USA).

PVA assisted GUV formation

GUV formation with PVA was done as described[265] with a few modifications. 1 mL 5 % PVA (*w/v*) in 200 mM sucrose was incubated for 1 h at 90 °C in a thermal shaker lite (VWR international GmbH, Dietikon, Switzerland) at 1'000 rpm, vortexing every 15 – 20 min. A coverglass (25 mm Ø # 1.0, VWR international GmbH) was rinsed with 70 % ethanol and placed on an aluminum-foil-covered heat plate set to 50 °C. Rubber O-rings with 20 mm diameter and 1.4 mm thickness were placed centrally on top of the coverglass. 200 µL PVA solution was pipetted onto the coverglass area inside the rubber ring and the gel was left to dry for 1 h at 50 °C. 20 µL of lipids dissolved in chloroform at 1 mg mL^{-1} composed of 68.8 mol% DOPC, 30 mol% DOPG, 1 mol% Liss Rhod PE and 0.2 mol% DSPE-PEG2000-Biotin were evenly distributed onto the gels using a 10 µl syringe (MICROLITER™ #701, Hamilton, Bonaduz, Switzerland). Solvent was evaporated for 1.5 – 2 h under vacuum, after which lipids were rehydrated for 1 h using 500 µl formation buffer (5 mM MOPS-BTP pH 7.4, 200 mM sucrose and salt as indicated). The solution was removed from the wells and GUVs were stored for at least 1 h at 4 °C before performing further experiments.

Pt wire GUV electroformation

Electroformation of GUVs using platinum (Pt) wires was performed as described previously[310,257] with minor modifications. Pt wires were cleaned by hand using soap before incubation in 94 % EtOH for 10 min, followed by incubation in chloroform for 10 min, both performed in a sonication bath. Pt wires were dried at RT at 1 atm for 10 min before applying lipid solution to the wires. 10 µL of lipids dissolved in chloroform at 2 mg mL^{-1} with lipid mixture as described were evenly deposited on the wires using a 10µL Hamilton syringe. Lipids were dried on the wires for 1 h in a desiccator under vacuum. For every chamber a coverglass (25mm Ø) was coated in a 0.1 g mL^{-1} milk powder solution for 30 min at RT and

mild agitation. The coverglass was rinsed with dH_2O and glued to the formation chamber using Dublisil 22 plus silicone (Dreve Dentamid GmBH, Unna, Germany). Pt wires were connected to an AC electric filed generator (PCGU1000, Velleman Group, Gavere, Belgium) using JST XH2.54 cable with 2 pin female socket (Play-Zone GmbH, Steinhausen, Switzerland) connected to a BNC male to 2 pin terminal block cable (Delock, Berlin, Germany). The formation chamber was filled with 800 µL formation buffer. The following wave sequence protocol was applied: 5 min at 0.44 V_{PP}, 5 min at 0.88 V_{PP}, 15 min at 1.32 V_{PP}, 30 min at 1.76 V_{PP} and overnight at 2.2 V_{PP}. Every step was performed at 500 Hz.

ITO GUV electroformation

Electroformation using indium tin oxide (ITO) coated glass slides was performed as described previously[257,310] with minor modifications. ITO coated slides were cleaned by hand using soap and incubated in 94 % EtOH for 10 min in a sonication bath. 10 µL of lipids dissolved in chloroform at 1 mg mL^{-1} with lipid mixture as described were evenly distributed on two separate slides on the conductive surface. The slides were dried for 1 h in a desiccator under vacuum. The electroformation chamber was assembled in a custom 3D printed slide holder (Supplementary File S1) using a 1.00 mm rubber spacer and filled with 600 µL formation buffer. The slides were connected to an AC electric field generator (PCGU1000, Velleman Group, Gavere, Belgium) using crocodile clamps (JYE BNC, Play-Zone GmbH, Steinhausen, Switzerland). The same wave sequence protocol was applied as for Pt wire formation.

Imaging slide preparation

Imaging of GUVs was performed in an 8 well chambered glass slide (#1.5 high performance cover glass, Cellvis, Mountain View, California, USA). To immobilize GUVs, wells were coated using 200 µL T50-buffer (10 mM Tris-HCL pH 8, 50 mM NaCl) containing 50 µg mL^{-1} biotinylated BSA for 30 min at RT with mild agitation. The solution was replaced by 200 µL T50 buffer containing 10 µg mL^{-1} streptavidin unless stated otherwise and incubated as above. Wells were washed once using 200 µL imaging buffer (5mM MOPS-BTP pH 7.4, 200mM glucose and salt as indicated). A desired amount of GUVs (10 – 100 µL) was loaded into imaging buffer with a final volume of 400 µL and GUVs were left to settle for 1 h prior to imaging. For experiments where immobilization was not required, GUVs were imaged in wells coated using only 200 µL T50-buffer containing 50 µg mL^{-1} BSA for 30 min. Washing and GUV loading was performed as described.

Image acquisition

Microscopy slides were imaged using an inverted fluorescence microscope (Nikon Ti-2 Eclipse with Crest X-light V2 spinning disk module (disk unit 60 µm), Nikon Europe BV, Amsterdam, Netherlands) with a CFI Plan Fluor 40x oil immersion objective (CFI Plan Fluor 40x/1.30 W.D. 0.24, Nikon Europe BV). Brightfield and fluorescence images were recorded by an Andor Zyla 4.2 Plus USB3 camera in widefield and Spinning

Disk Confocal mode using LED light excitation. HPTS was imaged with excitation at 395 nm and 470 nm and emission at 515 nm using appropriate exciter, emitter, dichroic filter cubes. Liss Rhod PE was imaged with excitation at 550 nm and emission at 595 nm and DY-647P1 with excitation at 640 nm and emission at 698 nm using appropriate exciter, emitter, dichroic filter cubes. Z-stacks were recorded in confocal mode from top to bottom (below the slide surface) with a step size of 1 µm and 72 steps. Time series were recorded as indicated.

Automatic detection of GUVs

Images in the Liss Rhod PE channel were analyzed in FIJI.[419] For Z-stack acquisitions, two custom macros were used to extract the data. With the first macro a background subtraction is performed on all slices of the Z-stack with a rolling ball radius of 100.0 pixels, then an average projection of the stack is made and a bandpass filter is applied to improve separation of nearby vesicles by highlighting the contrast between the background and vesicles using the following settings: filter large set to 40 pixels, filter small set to 5 pixels, suppress stripes set to None, tolerance of direction set to 5 %, with autoscale after filtering and saturation of image when autoscaling enabled. Manual thresholding is performed to create a binary mask separating vesicles and background. The second macro cleans up the mask by performing the binary processes Fill Holes, Erode and Watershed and vesicles are identified using the Analyze Particles function with Size set to 0.75 µm^2 - Infinity, Circularity set to 0.70 - 1.00 and Display Results, Exclude on Edges and Add to ROI manager enabled. For single images, the use of the first macro was omitted and manual thresholding was directly performed on the image. The second macro was then used as described, with Size set to 19.6 - 314.1 µm^2 (corresponding to vesicles with diameters between 5 and 20 µm).

Characterization of GUV formation

For characterization of GUV formations, GUVs were formed as described and 10 µL PVA GUVs or 100 µL electroformed GUVs were loaded to imaging wells coated with BSA as described. 9 Z-stacks were recorded in each well using a 3 x 3 multi spot acquisition from the top left corner of a well to the bottom right corner. GUVs were automatically identified from the Z stack as described. Using the Measure function in FIJI, the Feret diameter of the identified particles is obtained. To estimate the concentration of GUVs with a diameter between 5 – 20 µm, the number of identified particles with the according Feret diameters were counted. Based on the image dimensions (332.8 µm x 332.8 µm), a total area of 0.9968 mm^2 for all 9 images was obtained which was used to calculate the amount of GUVs per mm^2. This value was then multiplied by the area of the well which was taken as 80.91 mm^2, according to the manufacturer, to estimate the amount of GUVs in the entire well chamber. This number was then divided by the volume of GUV solution which was added to the well to obtain the concentration of GUVs (5 – 20 µm) in solution. As a measure for the quality of the formation to produce vesicles with the

desired size, the number of particles (5 – 20 µm) was divided by the total number of particles detected as described.

Calculation of Lipid Yield

To estimate the lipid yield, the total surface area A_{GUV} of each vesicle was calculated using equation 1 based on the measured Feret diameter d_{GUV} and the bilayer thickness $d_{bilayer}$ which was assumed to be 5 nm.

$$A_{GUV} = \underbrace{4\pi\left(\frac{d_{GUV}[nm]}{2}\right)^2}_{Outer\ leaflet} + \underbrace{4\pi\left(\frac{d_{GUV}[nm]}{2} - d_{bilayer}[nm]\right)^2}_{Inner\ leaflet} \quad \text{(Equation 1)}$$

The lipid yield was calculated using equation 2.

$$Yield\ [\,\%] = 100 * \frac{M_l}{N_A\, m} * \frac{A_{Well}\, V_{Form}}{A_{Img}\, V_{Well}} \sum_{i=1}^{n} \frac{A(d_i)_{GUV}}{A_{hg}} \quad \text{(Equation 2)}$$

The total number of lipids in GUV i with a diameter of d_i was calculated by dividing the surface $A(d_i)_{GUV}$ calculated according to Eq 1 by the surface area of the lipid headgroup A_{hg} which was assumed to be 0.71 nm^2.[420,421] The total number of lipids from all GUVs was calculated by summation of the lipid number of each GUV i with n as the total number of particles detected in one formation condition. To estimate the total number of lipids in the formation solution after removal from the formation chamber, the sum was divided by the total imaged area A_{Img} of the 9 images (0.9968 mm^2) times the volume V_{Well} of GUV solution added to the well (for example 10 µL for PVA GUVs) and multiplied with the total well area A_{Well} (80.91 mm^2) times the volume V_{Form} of solution used for the formation of GUVs (for example 500 µL for PVA GUVs). The yield was then obtained by dividing the total number of lipids in the formation solution by the Avogadro constant N_A, multiplying with the average molecular weight M_l of the lipids which was assumed to be 790 g mol^{-1}, based on a lipid composition of roughly 70 mol% DOPC and 30 mol% DOPG, and finally divided by the lipid weight m used to coat the surface for GUV formation (20 µg). This was multiplied by 100 to obtain values in percentage.

Immobilization assay

Flow immobilization experiments were performed in channel slides (µ-Slide III 3D Perfusion uncoated, ibidi GmbH, Gräfelfing, Germany) connected to a syringe pump (Ossila, Sheffield, UK). All experiments were performed at a flow rate of 5 µL s^{-1}. The slide was coated as described using 30 µL 100 µg mL^{-1} biotinylated BSA followed by 30 µL 0, 10 or 100 µg mL^{-1} streptavidin in T50 buffer. 1 µL 0 mM NaCl and 5 µL 100 mM NaCl PVA GUVs were loaded into imaging buffer to a final volume of 30 µL and GUVs were left to settle for 1 h. Prior to imaging the slide was sealed and the channels were filled with imaging buffer according to the manufacturer protocol. Image acquisition was performed using the confocal Liss Rhod PE settings and a time series was recorded over 2 min with a 0.5 s interval and 100 ms exposure

at 50 % laser intensity. Flow was started after 15 s using the syringe pump. GUVs were automatically detected as described on the last image before visible flow. To detect non-immobilized vesicles, all images recorded during flow were transformed into an average Z-projection, resulting in smearing and a decreased intensity for non-immobilized GUVs. This allowed automatic detection of immobilized GUVs by thresholding as described. The percentage of immobilized GUVs was calculated as the ratio between the detected number of GUVs on the average projection and before flow.

Calculation of the streptavidin density

To achieve equal slide coating, the streptavidin amount per surface was calculated based on the microscopy well dimensions indicated by the slide manufacturers. For simplicity reasons, we will refer to this value as the streptavidin density. For 8 well chambered slides, well dimensions are 8.7 x 9.3 mm leading to a bottom surface of 80.91 mm^2. Based on the coating volume of 200 µL, the height of the coated wall was estimated to be 2.47 mm, giving a total wall surface of 88.92 mm^2 leading to approximately 169.83 mm^2 of surface that is coated. This gives a volume to surface ratio of 1.18 µL mm^{-2}. For ibidi slides, the well diameter is 5.5 mm with a well height including the channels of 1.7 mm. This gives a bottom surface of 23.75 mm^2 and a wall surface of 29.37 mm^2. The well is connected by two channels which have a width of 1 mm and a height of 0.5 mm, which takes approximately 1 mm^2 away from the wall surface. This gives a total surface of 52.12 mm^2 and a volume to surface ratio of 0.58 µL mm^{-2} with 30 µL coating volume which is approximately half of the ratio for the 8 well chambered slide. Thus, to get similar immobilization conditions for both slides, the concentration of streptavidin for the ibidi slides should be twice as high as for the 8 well chambered slide.

HPTS leakage

For PVA GUVs, HPTS leakage during immobilization was measured at streptavidin densities of 0, 6, 30 and 60 ng mm^{-2} streptavidin as calculated above. HPTS was either added to imaging buffer before GUV addition or after immobilization. Final HPTS concentrations in the well chamber were 43 - 50 µM. 8 well chambered slides were prepared as described and 390 µL or 350 µL appropriate imaging buffer containing HPTS and 10 µL or 50 µL 0 mM NaCl or 100 mM NaCl GUVs were loaded, respectively. For leakage after immobilization, 375 µL appropriate imaging buffer as well as 25 µL GUV solution was loaded, whereby 5 µL 0 mM NaCl GUVs were diluted with 20 µL formation buffer and 100 mM NaCl were used undiluted. GUVs were left to settle, after which 100 µL appropriate imaging buffer containing 230 µM HPTS was added and incubated for 1 h before imaging. For Pt wire GUVs, HPTS leakage during immobilization was measured at coating densities of 6 and 60 ng mm^{-2} streptavidin. 8 well chambered slides were prepared as described and 380 µL or 350 µL appropriate imaging buffer containing HPTS and 20 µL or 50 µL 0 mM NaCl or 100 mM NaCl GUVs were loaded, respectively. GUVs were imaged by recording Z-stacks using the Liss Rhod PE channel and the 470 nm excitation channel for HPTS.

HPTS leakage analysis

GUVs were automatically detected from Z-stacks as described. The number of GUVs considered for analysis was limited to 148 for each sample. 20 background regions of interest (bgROIs) were drawn in by hand in areas that did not contain GUVs. For leakage analysis, a background subtraction with a rolling ball radius of 200 pixels and light background enabled was first performed on each slice of the Z-stack in the HPTS channel. An intensity profile of the GUVs and bgROIs in the Z dimension was recorded using the Time Series Analyzer V3 plugin in FIJI with the average intensity setting. The profiles were normalized to the average of the first 20 steps of the Z-stack. The profiles of the bgROIs were averaged to create a mean background profile. This was then subtracted from each GUV profile which were then inverted by multiplying with -1 to obtain positive values for GUVs that did not leak. The maximum intensity of the profile was then measured, indicating the largest absence of HPTS signal for each GUV. Only GUVs in the desired size range (5 – 20 µm diameter) were used for analysis. Because small GUVs tended to move at low streptavidin concentrations and were only imaged by very few slices, vesicles with diameters below 7 µm were further discarded as well. We further limited the number of vesicles from each experiment to 85 due to limitations in GraphPad Prism 8.0 which resulted in 20 – 85 vesicles that were analyzed. The median of the maximum intensity distribution of the GUVs was calculated in Prism and used to define a threshold for leakage based on the average median at low streptavidin concentrations. Leaky GUVs were defined by having a maximum intensity below approximately 25 % of the average median. The percentage of leaky GUVs was calculated by dividing the number of GUVs below the threshold by the total number of GUVs.

Proton leakage

For proton leakage, formation buffers contained 10 mM MOPS-KOH pH 7.4, 200 mM sucrose and imaging buffers were 10 mM MOPS-KOH pH 7.4, 200 mM glucose and 10 mM MOPS-KOH pH 8.0, 200 mM glucose. Buffers for GUVs with salt contained 100 mM NaCl as well. 8 well chambered slides for immobilization were prepared as descried. For PVA GUVs, 400 µL imaging buffer and 20 µL 0 mM NaCl or 50 µL 100 mM NaCl GUVs were loaded, respectively. For Pt wire GUVs, 400 µL imaging buffer and 50 µL GUVs were loaded, both for 0 mM NaCl GUVs and 100 mM NaCl GUVs. Before imaging, a pH exchange in the exterior solution was performed by performing two 1 mL wash steps with imaging buffer at pH 7.4 followed by two 1 ml wash steps with buffer at pH 8.0. Washing was performed using two 1 mL pipettes with simultaneous addition and removal of solution in a well chamber. A single image was acquired in confocal mode using the Liss Rhod PE channel and GUVs were then recorded in confocal mode using both HPTS channels for 60 min at 5 min intervals. Approximately 1 min after the 60 min acquisition (61 min), another time series was recorded for 5 min and 5 s intervals with addition of 5 µL 1 mM gramicidin (final concentration 12.5 µM) after 1 min (62 min). The total acquisition time was 66 min.

Proton leakage analysis

GUVs were identified using the single Liss Rhod PE image as described. The HPTS intensity for both channels were extracted using the Time Series Analyzer V3 plugin in FIJI with the average intensity setting. The HPTS ratio was calculated by dividing the intensity at 470 nm excitation by the intensity at 395 nm excitation. To assess the amount of leakage after 20 min, the ratio at 0 min was subtracted from the ratio at 20 min. As we expect an increase in pH on the inside as GUVs leak, only vesicles with a ratio difference > 0 were considered for further analysis. The ratio at 66 min was then subtracted from the ratio at 0 min, indicating the total possible increase for a GUV. The ratio difference 20 min – 0 min was then divided by the total possible increase and multiplied with 100 to obtain a percentage of leakage.

Preparation of SUVs

Liposomes were formed with a lipid composition of 69 mol% DOPC, 30 mol% DOTAP and 1 mol% Liss Rhod PE or 99 mol% DOPC and 1 mol% Liss Rhod PE. Lipids dissolved in chloroform were mixed in a 25-mL round bottom flask and chloroform was evaporated under a constant stream of N_2 while rotating the flask. The film was further dried overnight in a desiccator under vacuum. Lipids were resuspended in formation buffer to a concentration of 5 mg mL^{-1} and unilamellar vesicles were obtained by performing seven freeze-thaw cycles and stored at -80 °C before further use. For fusion experiments, liposomes were thawed and diluted to 50 µg mL^{-1} using imaging buffer and size was adjusted by sonication on ice using a tip sonicator (Vibra Cell 75186, Thermo Fisher Scientific, Waltham USA) for 2 min with 30 s ON and 30 s OFF pulses and 40 % amplitude.

Cytochrome bo3 ubiquinol oxidase purification and labeling

Cytochrome *bo_3* ubiquinol oxidase mutant IIIA21C, encoded by a cysless pETcyoII plasmid, was expressed and purified as described.[422–424] The protein was cysteine-labeled with DY-647P1 maleimide as previously published[425] with minor modifications. The excess dye was removed by performing a CentriPure P50 (emp BIOTECH, Berlin, Germany) size exclusion chromatography followed by a Superdex 200 Increase 10/300 GL column (ÄKTA Pure system, GE Healthcare, Boston, Massachusetts, USA) purification at 4 °C. The labeled protein was concentrated to 20 µM.

Reconstitution of cytochrome bo3 ubiquinol oxidase

DOTAP liposomes were formed and sonicated at 5 mg mL^{-1} as described. 240 µL liposomes were destabilized using a final concentration of 0.4 % (*w/v*) sodium cholate, mixed with 12 µL purified *bo_3* oxidase (20 µM) and incubated on ice for 30 min to obtain proteoliposomes. Empty liposomes were prepared by addition of 12 µL buffer instead of protein. Liposomes were collected by gel filtration using a CentriPure P10 column (*emp* BIOTECH GmbH, Berlin, Germany) pre-equilibrated with formation buffer. The column was eluted using 1.2 mL formation buffer to obtain 1 mg mL^{-1} liposomes. Prior to measuring, the liposomes were diluted to 0.2 mg mL^{-1} using formation buffer and proteoliposomes and empty

liposomes were mixed in a 3/0, 2/1, 1/2 and 0/3 ratio.

Charge mediated fusion

Charge mediated fusion of negatively charged GUVs and positively charged SUVs was performed in 8 well chambered slides and in 1.5 mL Eppendorf tubes. GUVs were prepared as described and 10 – 50 µL GUV solution was diluted in formation buffer to a final volume of 50 µL to achieve similar vesicle concentrations. For fusion in an 8 well chambered slide, diluted GUVs were loaded into imaging buffer containing salt as indicated to a final volume of 400 µL and immobilized for 1 h. A time series was recorded for 5 min at 5 s intervals using confocal Liss Rhod PE settings for all experiments and additional DY-647P1 settings for experiments with proteoliposomes. Fusion was initiated by addition of 100 µL SUVs after 30 s. Final concentration of SUVs was 10 µg mL^{-1} for experiments with PVA and Pt wire GUVs and empty vesicles and 40 µg mL^{-1} for experiments with PVA GUVs and mixtures of empty and proteoliposomes. For fusion in Eppendorf tubes, diluted GUVs were mixed with 50 µl empty SUVs (20 µg mL^{-1}) and incubated for 15 min at RT. 100 µL of fused GUVs were transferred into 400 µL imaging buffer and GUVs were immobilized for 1 h. Z-stacks were recorded as described using confocal Liss Rhod PE settings.

Analysis of charge mediated fusion

For fusion of PVA and Pt wire GUVs with empty SUVs in 8 well chambered slides, 10 – 50 GUVs were detected as described using a single Liss Rhod PE image recorded after 300 s. A bgROI was manually drawn next to every vesicle. The Liss Rhod PE intensity was extracted for every GUV and corresponding bgROI using the Time Series Analyzer V3 plugin in FIJI with the average intensity setting. For each GUV, the background was removed by subtracting the intensity of the corresponding bgROI. The mean intensity increase of GUVs per experiment was calculated and average and standard deviation of mean intensity values from four replicates were plotted. To show end point signal distributions, the final Liss Rhod PE intensity of individual GUVs of the four replicates were combined and plotted. For experiments using proteoliposomes, 30 – 50 GUVs were detected as described after 180 s. On the same image, mean grey intensity for Liss Rhod PE and DY-647P1 of GUVs and corresponding bgROIs were extracted using the Measure function of FIJI. Background was subtracted as described. To show signal correlation, the Liss Rhod PE signal of every GUV was plotted on the X-axis against the DY-647P1 signal of every GUV on the Y-axis. For fusion experiments in Eppendorf tubes, GUVs were automatically identified from Z-stacks as described. An average Z-projection was performed and the background was subtracted using a rolling ball radius of 200 pixels. Using the Measure function in FIJI, the mean grey intensity of the Liss Rhod PE channel was extracted for every GUV and plotted as a signal distribution.

Supporting Information

Supplementary Results and Discussion

Lipid yield and average diameter

To estimate the molar yield (based on deposited lipid) and the average diameter of giant unilamellar vesicles (GUVs), we used the size distribution data and the GUV concentration obtained from each experiment as described in the Materials and Methods. The mean and standard deviation of the molar yield of free-standing GUVs and average diameter are presented in Table S1. Not surprisingly, the highest yield (~ 30 % of deposited lipid was incorporated into GUVs) was obtained for PVA formation in the absence of salt which is similar to what has recently been reported for polymer assisted swelling using cellulose.[238] In the presence of 100 mM monovalent salt, the yield decreased to 17 - 19 % for PVA formation. All electroformations produced similar yields with around 4 % under the experimental conditions used here. Unlike PVA formation, the yield was not affected by the presence of monovalent salt although a slight decrease in GUV number was observed (from ~ 6 x 10^5 GUVs mL^{-1} in absence to ~ 3-4 x 10^5 GUVs mL^{-1} in presence of salt in the requested size). This is explained by the larger average diameter of salt GUVs that require more lipids per GUV. Thus, the decreased concentration is balanced by the increase in frequency of large Pt wire GUVs in the presence of salt, resulting in similar yields for those formations. The increased average diameter reflects the increase in frequency of large GUVs (> 10 µm) for salt GUVs (Figure S3 and S4).

HPTS leakage

Soluble fluorescent dyes are frequently used to detected substrates translocated across the lipid bilayer by membrane proteins (MPs). These dyes are usually encapsulated in GUVs and need to remain inside the vesicle for the duration of the experiment. Therefore, leakage of the dye, for example due to strong vesicle adhesion, would be detrimental for measuring MP activity. Thus, we investigated whether GUVs become permeable to the dye HPTS due to immobilization. After vesicles were left to immobilize, they were imaged by recording a Z-stack using both the Liss Rhod PE and HPTS channels. The signal from the labeled lipid Liss Rhod PE was used to identify the GUV membrane while leakage was assessed using the HPTS signal. For each vesicle, an average signal for each Z-slice was obtained which was normalized and inverted to obtain values close to 0 for vesicles with HPTS leakage and positive values for vesicles without leakage. To distinguish between leaky and non-leaky GUVs (Figure S6A), the maximum intensity value from the whole Z-stack (max Z intensity) was used for each vesicle and a threshold using the average median value (0.006) from GUVs at weak adhesion was defined. GUVs were thus denominated as leaky if the max Z intensity was below 25 % of the median value (< 0.0015). As small vesicles (< 7 µm) were recorded by only few slices and tended to be less well immobilized, they were discarded from the analysis, as were large GUVs > 20 µm which are outside of our desired size range. Figure S6B shows the

distribution of max Z intensity values for PVA and Pt wire GUVs with and without 100 mM sodium chloride. Although slight shifts in the distribution are observed for all GUVs at high streptavidin densities, only PVA GUVs show a clear increase in the number of vesicles with values below the threshold at high streptavidin density, indicating increased leakage for PVA GUVs with strong immobilization. For Pt wire GUVs, only the number of fully leaky GUVs was slightly higher without salt compared to 100 mM NaCl and occasional HPTS leakage at strong adhesion was only observed in Pt wire GUVs larger than 20 µm. Percentage of leaky GUVs for each of the three replicates (Figure S6C) were calculated. An increase in leakage at high streptavidin density is again observed for PVA GUVs, although the error is quite large at high streptavidin density. Importantly, even at high streptavidin concentration, the percentage of leaky GUVs never exceeded 35 %. Interestingly, GUVs formed with the Pt wire method were less affected by the increased streptavidin concentration compared to PVA GUVs. Generally, the number of leaky GUVs at weak adhesion was low.

Because we observed large differences in the number of leaky GUVs for PVA assisted formation at 6 and 60 ng mm^{-2} streptavidin, we repeated the experiment with 0, 6, 30 and 60 ng mm^{-2} streptavidin (Figure S7A and B). Increased leakage of HPTS to the inside of GUVs was already observed at 30 ng mm^{-2} streptavidin. However, at 6 ng mm^{-2} where low leakage is still observed, PVA GUVs with 0 mM sodium chloride were poorly immobilized (20 % as opposed to 100 % with sodium chloride), thus a streptavidin density between 6 and 30 ng mm^{-2} should be used. In the previous experiment, we were not able to discriminate if leakage happens only during immobilization and tightness is restored or if the leakiness is permanent. This is critical, as substrates or other chemicals are added after the immobilization process. We focused on PVA GUVs due to the observed differences at various streptavidin densities and added solution containing HPTS to vesicles that were already immobilized on the slide (Figure S7C and D). Strikingly, while leakage remained low for PVA GUVs without salt (< 10 %), it was highly elevated for PVA GUVs with 100 mM NaCl at strong adhesion with more than half of the vesicles showing HPTS influx. Sample images from all these different conditions are depicted in Figure S8.

The two different experiments (leakage during and after immobilization) show a different behavior for PVA GUVs. While no difference was observed for GUVs with and without salt for leakage during immobilization, a large difference was seen when HPTS was added to GUVs that were already immobilized, indicating that PVA GUVs in the absence of salt mostly form pores during the immobilization process while PVA GUVs in the presence of salt remain leaky after immobilization. It is important to note that in the experiment with HTPS addition after immobilization, flow stress is exerted to the vesicles that could lead to increased HPTS permeability, especially if vesicles are unstable.

Proton leakage

One of the main interests in our group are MPs form the respiratory chain which translocate protons. Thus, GUVs should be able to maintain a proton gradient. To detect proton leakage, GUVs containing HPTS were prepared at pH 7.4, immobilized and washed with buffer at pH 8.0, resulting in an inside acidic gradient of 0.6. The HPTS signal was monitored for 1 h before the pH gradient was equilibrated by the addition of the protonophore gramicidin, leading to an alkalinization of the GUV lumen and an increase in HPTS ratio. The signal increase of all GUVs that were selected for analysis showed minimal increase of HPTS ratio during the 1 h incubation, which is an indication of GUV tightness towards protons (Figure S10). Some GUVs displayed very small or higher percentages. The latter might indicate high leakage, but we also observed some GUVs which showed only small increase after gramicidin addition, which would in turn result in a large percentage. We are not sure why these GUVs did not react to gramicidin, it is possible that they were multilamellar or that the concentration of gramicidin was not high enough to achieve efficient gramicidin incorporation in all GUVs. Further, some GUVs seem to even decrease in signal after gramicidin addition, potentially due to HPTS leakage, which might even result in negative percentages and most likely account for the outliers at very small values.

Charge-mediated fusion in an Eppendorf tube

The last step towards measurements of MPs in GUVs is the functional reconstitution of the protein. Here, we used charge-mediated fusion of positively charged small unilamellar vesicles (SUVs) to negatively charged GUVs as a method to incorporate MPs into GUVs. We started by performing experiments with empty liposomes, initiating fusion directly on the microscopy slide by addition of SUVs to immobilized GUVs. We observed a large distribution of signals, potentially due to effects of immobilization or mixing and pipetting artifacts. To avoid these artifacts, we repeated the experiments by incubation of free-floating GUVs (approximately 0.3 – 1.6 x 10^6 5 – 20 µm GUVs per mL) with SUVs for 15 min in an Eppendorf tube after which they were transferred into a microscopy well and left to immobilize. Z-stacks were recorded for all conditions and an average Z-projection was created for every stack. Average signal intensities for every GUV were then extracted and depicted as a signal distribution (Figure S13). Contrary to our expectations, fusion in an Eppendorf tube did not lead to a smaller signal distribution, highlighting that the fusion process is not homogenous. For PVA GUVs, we observe a decrease in signal in the presence of 100 mM NaCl both for fusion in the microscopy well and in the Eppendorf tube. Interestingly, this was not the case for Pt wire GUVs where this trend was not observed for fusion in the Eppendorf tube.

Supplementary Tables and Figures

Table S1: Lipid Yield and mean average diameter of GUVs prepared by PVA formation or electroformation. The lipid yield was calculated as described in Material and Methods and the mean and standard deviation of three experiments is shown. The average diameter was calculated from the diameter distributions recorded for each formation and the mean and standard deviation of the average diameters for the three experiments are shown. Values could not be determined for formations that produced insufficient GUV numbers and are labeled with ND.

	PVA		Pt wire		ITO	
	Yield [%]	Diameter [µm]	Yield [%]	Diameter [µm]	Yield [%]	Diameter [µm]
0 mM salt	31.96 ± 12.67	3.82 ± 0.16	3.69 ± 1.14	4.21 ± 0.39	4.29 ± 2.66	6.40 ± 1.36
100 mM NaCl	16.65 ± 1.86	3.81 ± 0.33	4.18 ± 0.89	7.49 ± 0.84	ND ND	ND ND
100 mM KCl	18.63 ± 9.10	3.94 ± 0.46	4.25 ± 0.46	6.48 ± 1.09	ND ND	ND ND

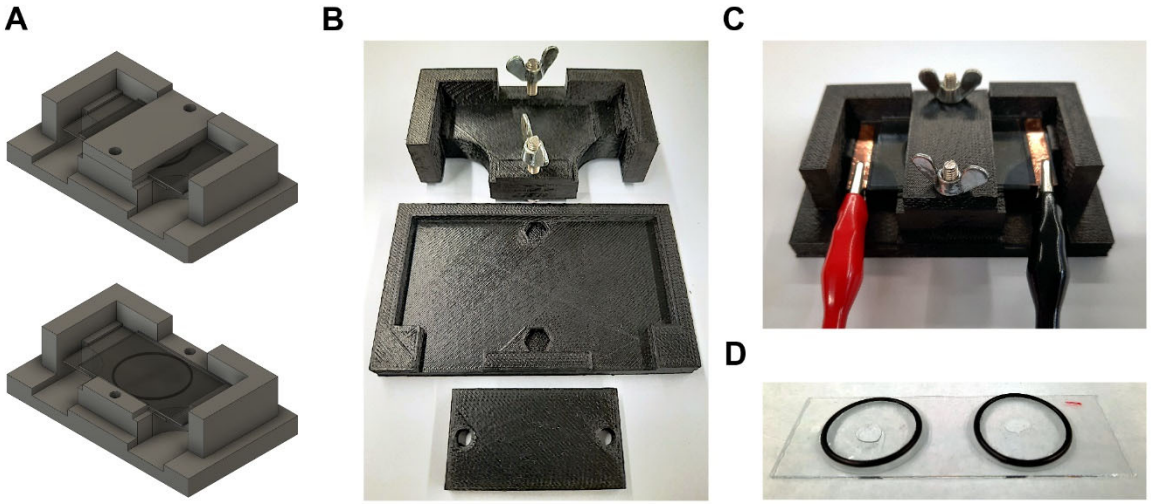

Figure S1: Assembly of the ITO electroformation and PVA formation chambers. A) 3D render of the custom ITO coated slide holder (Supplementary File S1) with (top) and without (bottom) lid to hold the slides in place. Slides are shown with rubber O-ring as spacer. B) 3D printed parts of the slide holder. Holes are designed to fit M4 hex bolts to screw on the lid using wing nuts (not 3D printed). The holder is composed of the main holder (top), a stand (middle) and a lid (bottom). C) Assembled ITO formation chamber. ITO coated slides are modified with adhesive copper tape and separated by a 1 mm rubber spacer. Crocodile claps are attached to the copper tape. D) PVA formation chamber. Two coverglasses (25 mm Ø) with PVA gel inside a rubber O-ring are glued to a microscopy slide for better transportation using grease for laboratories. The O-ring forms a barrier, allowing the addition of formation buffer to the gels. To protect the formation from dust, slides are covered by a lid (not shown).

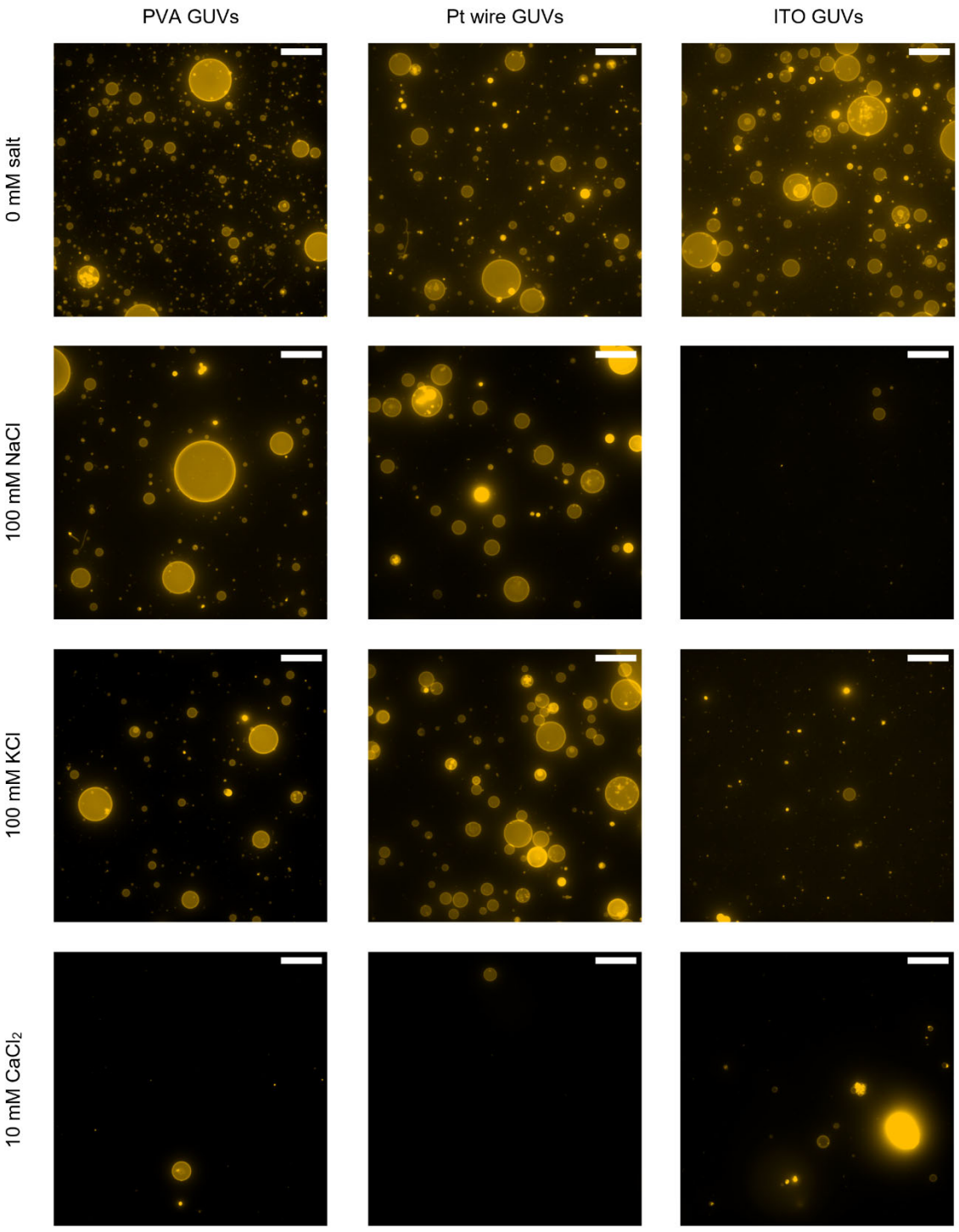

Figure S2: Representative GUV formations in the presence or absence of salt. Average Z-projections of confocal Z-stacks recorded in the Liss Rhod PE channel are shown. PVA GUV formations are shown in the first column, Pt wire formations in the second column and ITO formations in the third column. The first row depicts formations in the absence of salt, the second row with addition of 100 mM NaCl, the third row with addition of 100 mM KCl and the last row with addition of 10 mM $CaCl_2$ to the formation buffer. The scale bar is 50 µm.

Here we show the calculated histograms from the size distributions of each formation condition. A bin size of 1 µm was chosen to illustrate the size distribution in the relevant size range of 0 – 20 µm. A larger bin size of 5 µm was chosen to represent the entire size range of the formations (up to 100 µm) and the frequency is displayed in the logarithmic scale, due to the very small frequency of large GUVs.

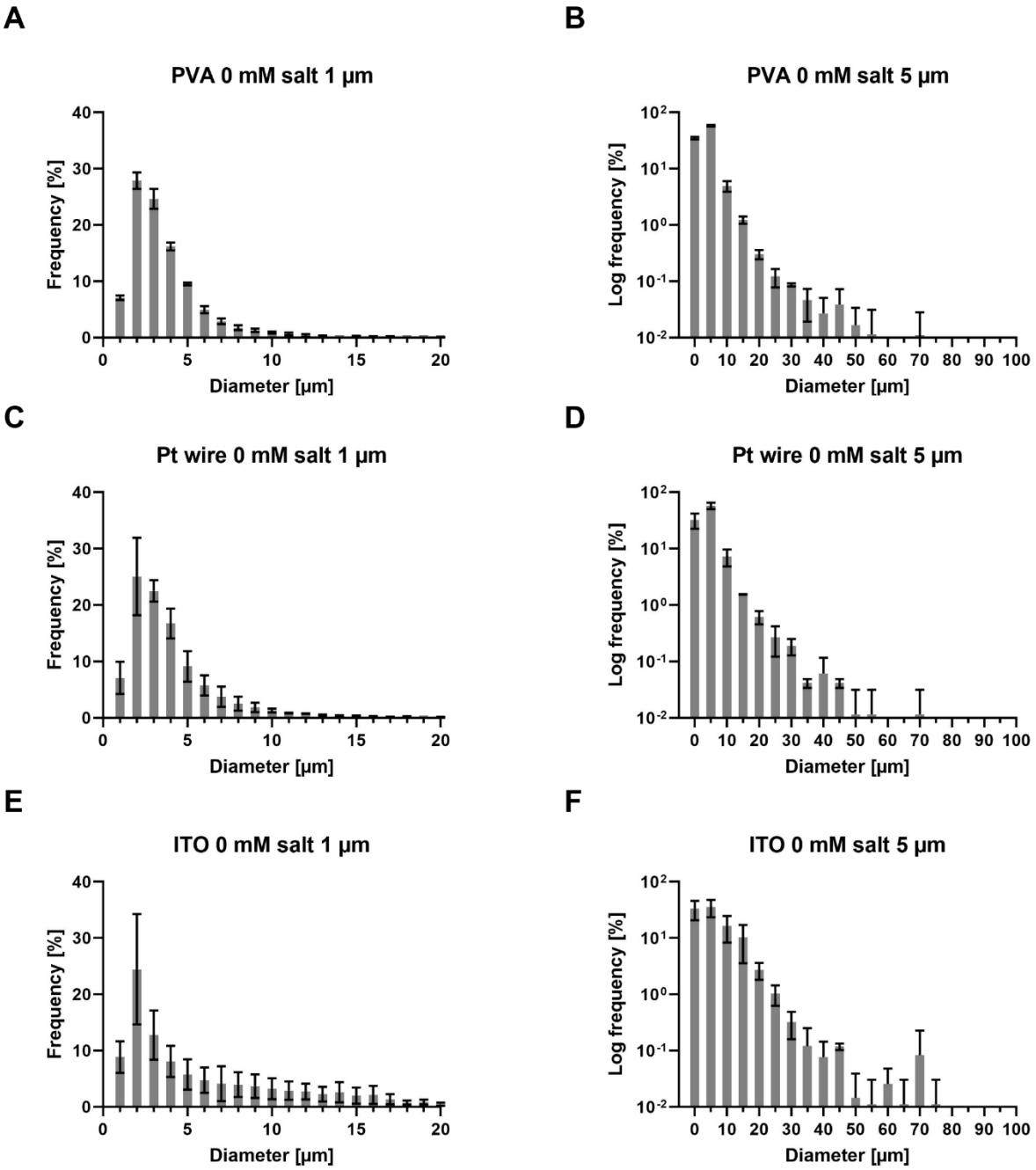

Figure S3: Histograms of GUV formations in the absence of salt. The bar height represents the average frequency and error bars the standard deviation from three experiments. A, C, E show histograms with a bin size of 1 µm cut off at 20 µm. B, D, F show histograms with a bin size of 5 µm cut off at 100 µm. The Y-axis is logarithmic as large GUVs tend to have small frequencies. A-B) Histograms from PVA formation. C-D) Histograms from Pt wire formation. E-F) Histograms from ITO formation.

A

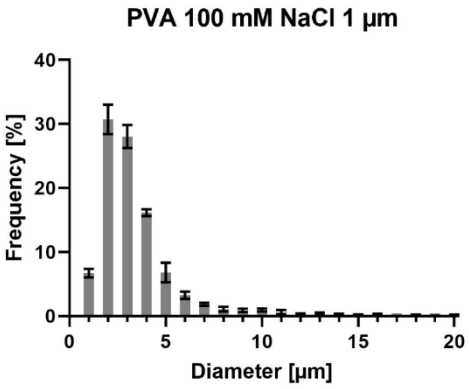
PVA 100 mM NaCl 1 µm
Frequency [%]
Diameter [µm]

B

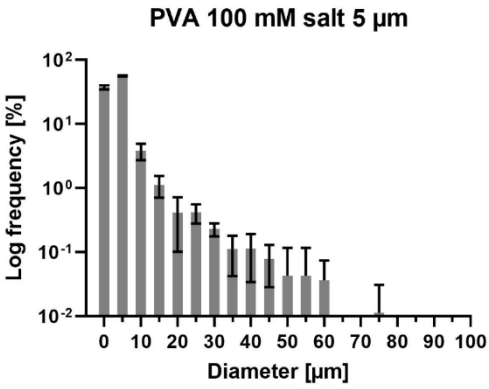
PVA 100 mM salt 5 µm
Log frequency [%]
Diameter [µm]

C

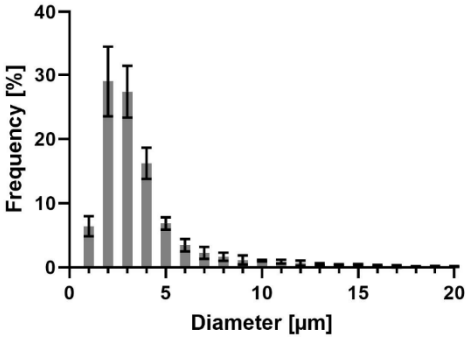
PVA 100 mM KCl 1 µm
Frequency [%]
Diameter [µm]

D

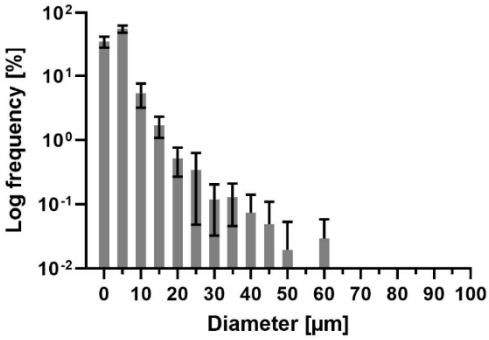
PVA 100 mM KCl 5 µm
Log frequency [%]
Diameter [µm]

E

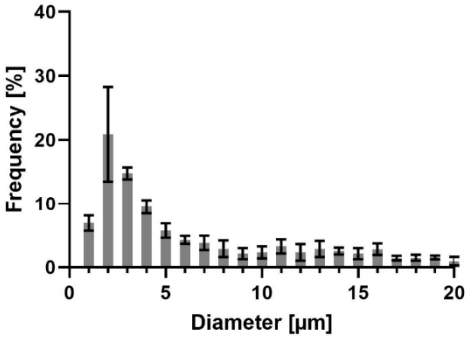
Pt wire 100 mM NaCl 1 µm
Frequency [%]
Diameter [µm]

F

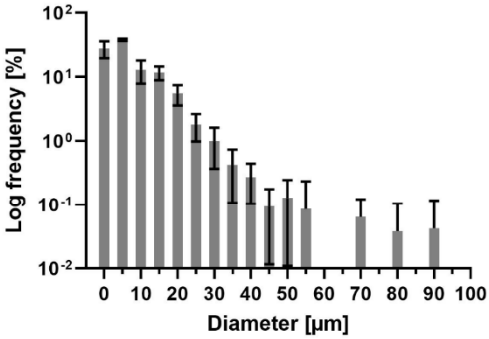
Pt wire 100 mM NaCl 5 µm
Log frequency [%]
Diameter [µm]

G

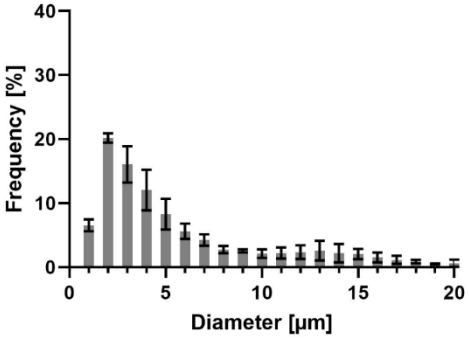
Pt wire 100 mM KCl 1 µm
Frequency [%]
Diameter [µm]

H

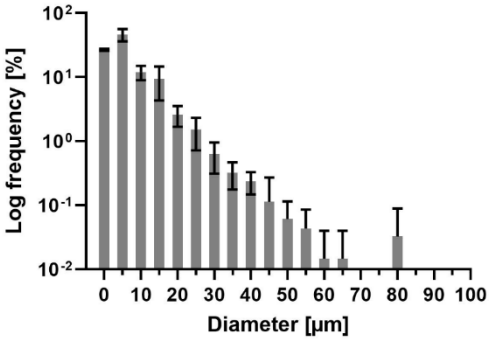
Pt wire 100 mM KCl 5 µm
Log frequency [%]
Diameter [µm]

Figure S4: Histograms of PVA and Pt wire GUV formation in the presence of salt. The bar height represents the average frequency and error bars the standard deviation from three experiments. A, C, E, G show histograms with a bin width of 1 µm cut off at 20 µm. B, D, F, H show histograms with a bin width of 5 µm cut off at 100 µm. The Y-axis is logarithmic as large GUVs tend to have small frequencies. A-B) Histograms from PVA formation with 100 mM NaCl. C-D) Histograms from PVA formation with 100 mM KCl. E-F) Histograms from Pt wire formation with 100 mM NaCl. G-H) Histograms from Pt wire formations with 100 mM KCl.

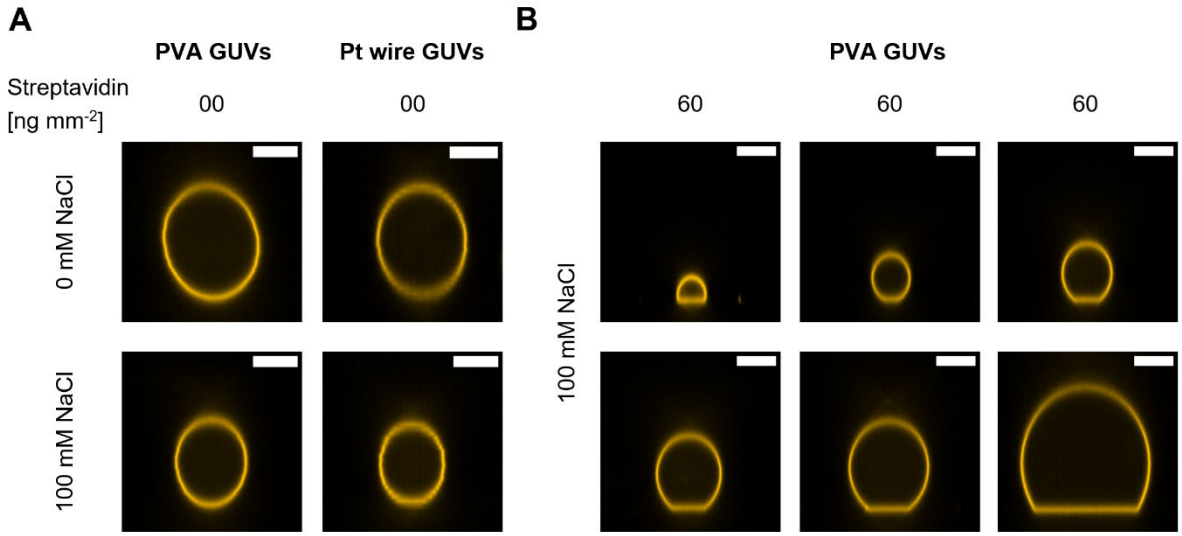

Figure S5: Spherical adhesion caps in the absence of streptavidin and heterogeneity of caps in a single well. Confocal Z-stacks were recorded and side-views of representative GUVs are shown. The scale bar is 10 µm. A) PVA and Pt wire GUVs in the presence and absence of 100 mM NaCl were immobilized at a streptavidin density of 0 ng mm^{-2} No Spherical caps are observed. B) Different PVA GUVs in the same well chamber with 100 mM NaCl immobilized at a streptavidin density of 60 ng mm^{-2} are shown.

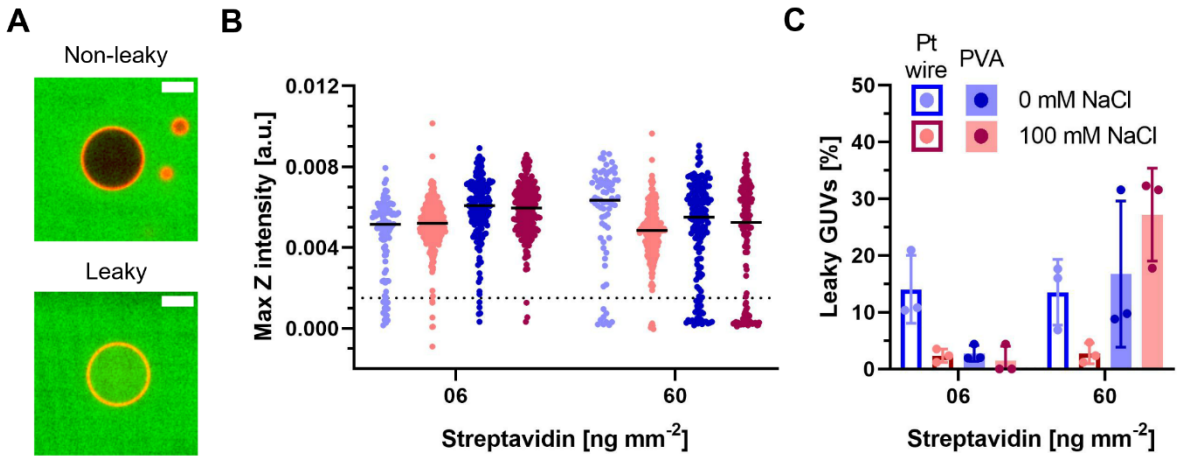

Figure S6: Immobilization-induced HPTS leakage of PVA and Pt wire GUVs (7 – 20 µm) in the presence (red) or absence (blue) of 100 mM NaCl at low and high streptavidin densities. A) Example GUV without (top) and with (bottom) HPTS leakage. Overlay of HPTS channel (green) and Liss Rhod PE channel (red). The scale bar is 10 µm. B) Combined distribution of the maximum Z intensity values from three experiments. Each dot represents a single GUV and vesicles from three replicates are combined. The median is indicated by a black line and the threshold is depicted by a dotted line. Maximum Z intensities were extracted

from Z stacks recorded in the HPTS channel according to Material and Methods. Values close to zero indicate HPTS leakage into GUVs and positive values indicate the absence of HPTS in the GUV lumen. The dotted line indicates the threshold (0.0015) used to calculate the percentage of leaky GUVs and is approximately 25 % of the average median (black lines) of GUVs immobilized at a low streptavidin density. GUVs below the threshold were classified as leaky. C) Percentage of leaky GUVs from B. The height of the bar indicates the average percentage of leaky GUVs with individual values from the three experiments shown as dots. Error bars indicate the standard deviation.

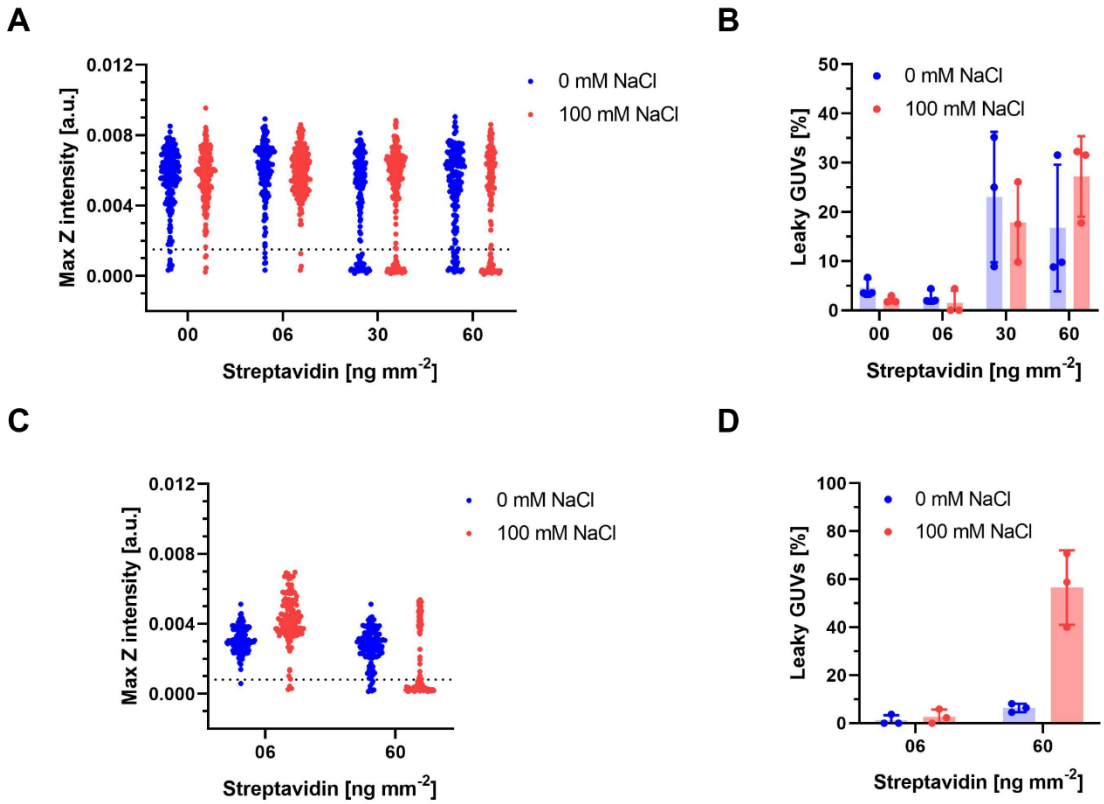

Figure S7: HPTS leakage of PVA GUVs (7 – 20 µm) in the presence (red) or absence (blue) of 100 mM NaCl at different streptavidin densities. A and B show immobilization-induced HPTS leakage at 00, 06, 30 and 60 ng mm^{-2} streptavidin. C and D show leakage of HPTS with addition of dye after immobilization at low and high streptavidin density. A and C show the combined distribution of the maximum Z intensity values from three experiments. Maximum Z intensities were extracted from Z stacks recorded in the HPTS channel according to Material and Methods. Values close to zero indicate HPTS leakage into GUVs and positive values indicate the absence of HPTS in the GUV lumen. The dotted line indicates the threshold used to calculate the percentage of leaky GUVs and is approximately 25 % of the average median of GUVs immobilized at a low streptavidin densities. GUVs below the threshold were classified as leaky. A) Maximum Z intensity distribution. The threshold (0.0015) was set based on the average median at streptavidin densities of 00 and 06 ng mm^{-2}. B) Percentage of leaky GUVs from A. The height of the bar indicates the average percentage of leaky GUVs with individual values from the three experiments shown as dots. Error bars indicate the standard deviation. C) Maximum Z intensity distribution. The threshold (0.0008) was set based on the average median at a streptavidin density of 06 ng mm^{-2}. D) Percentage of leaky GUVs from C. The height of the bar indicates the average percentage of leaky GUVs with individual values from the three experiments shown as dots. Error bars indicate the standard deviation.

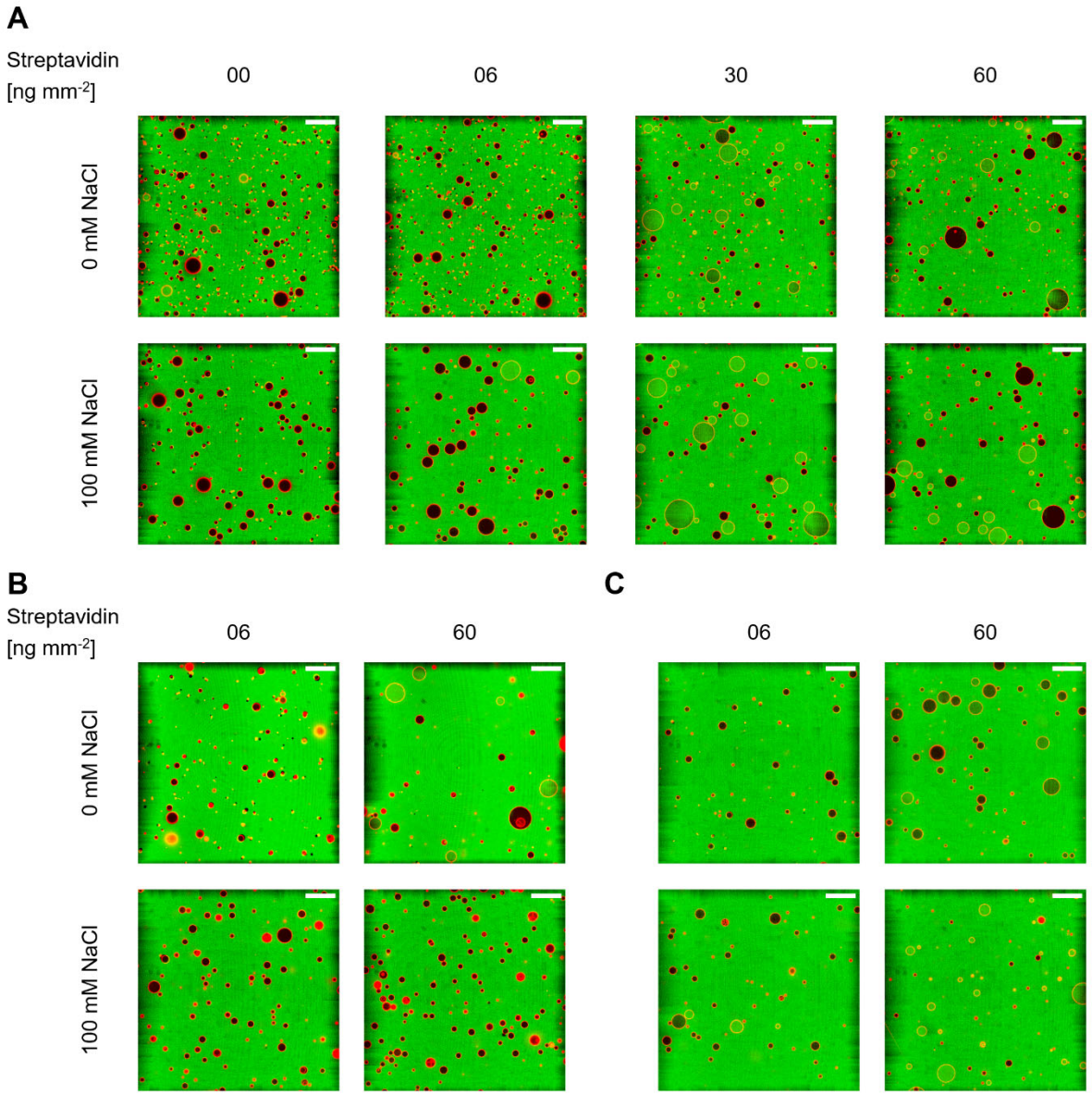

Figure S8: Confocal microscopy images of HPTS leakage in GUVs in the presence and absence of 100 mM NaCl. Overlay of HPTS channel (green) and Liss Rhod PE channel (red). Images were recorded approximately 5 µm above the slide surface. The scale bar is 50 µm. A) Images of immobilization-induced leakage of HPTS in PVA GUVs at different streptavidin densities. B) Images of immobilization-induced leakage of HPTS in Pt wire GUVs at low and high streptavidin density C) Images of leakage of HPTS in PVA GUVs with addition of dye after immobilization at low and high streptavidin density

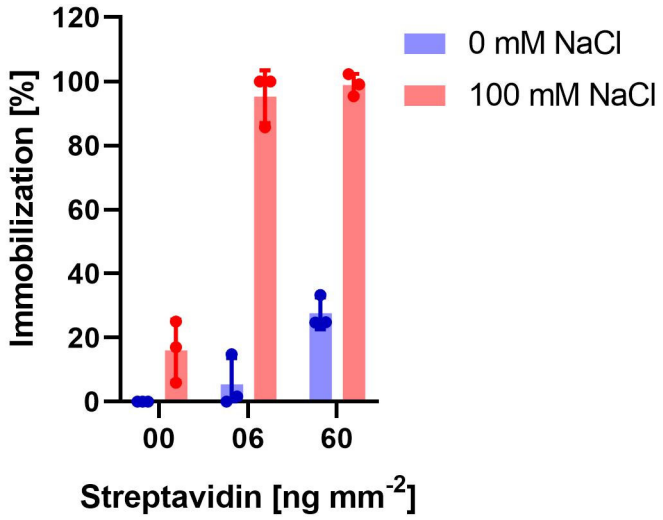

Figure S9 Immobilization assay using channel slides and PVA GUVs with 5 mM MOPS-KOH buffer. Percentage of immobilized PVA GUVs in the presence or absence of 100 mM NaCl at different streptavidin densities assessed by comparing the number of immobilized GUVs and the number of GUVs before application of flow. Data from three experiments are shown. GUVs were prepared in 5 mM MOPS-KOH pH 7.4, 200 mM sucrose with salt as indicated. The height of the bar indicates the average percentage of immobilization with individual values from the experiments shown as dots. Error bars indicate the standard deviation.

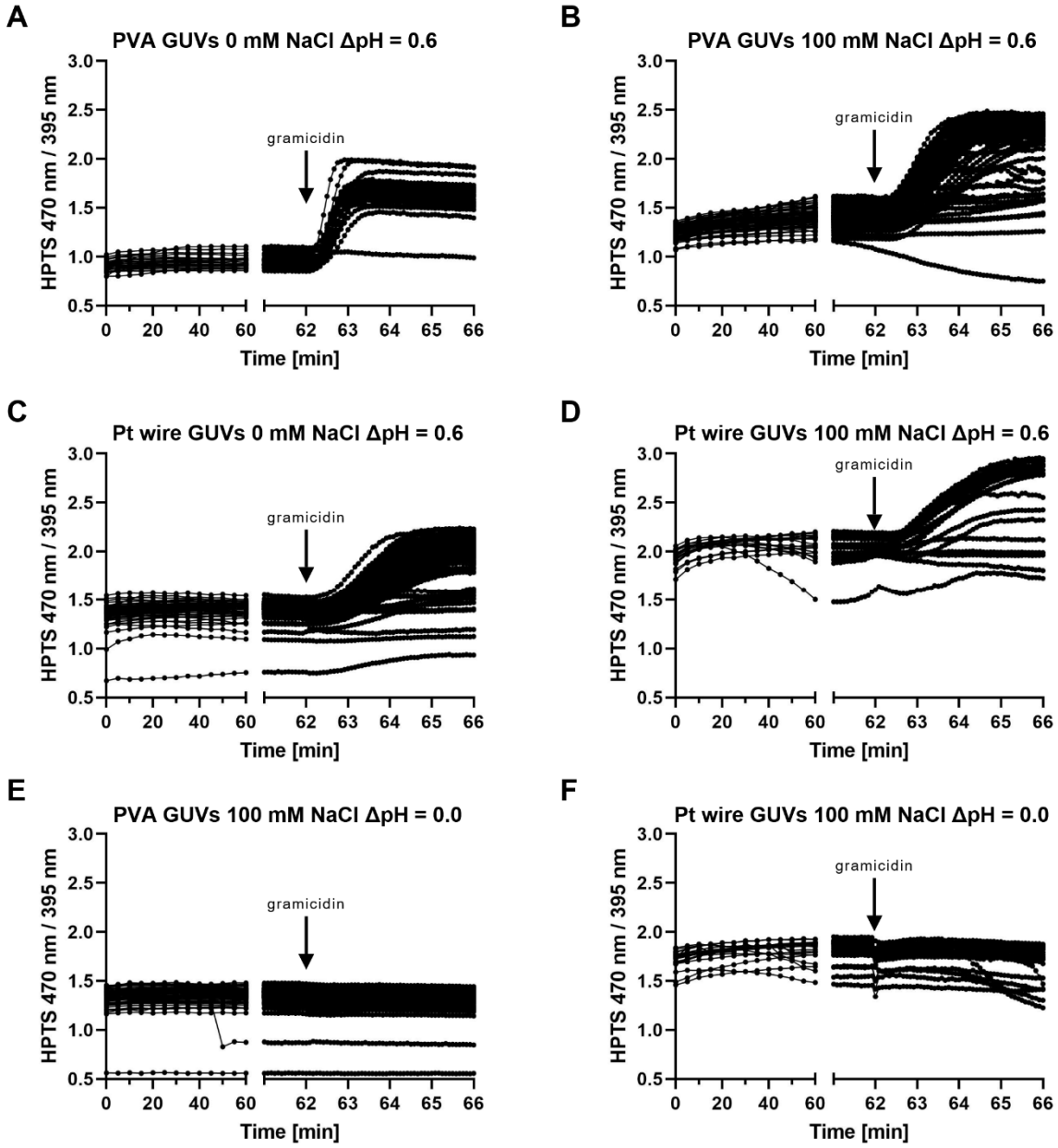

Figure S10: Proton leakage of immobilized PVA and Pt wire GUVs in the presence or absence of 100 mM NaCl. Analysis was limited to GUVs with diameters of 5 – 20 µm in the focal plane. Data are taken from a single time series for each condition. Each time point is represented by a dot. HPTS ratio of individual GUVs from one experiment are shown. Only GUVs with diameters of 5 – 20 µm in the focal plane were analyzed. A - D shows GUVs subjected to a pH gradient of 0.6 (pH inside = 7.4, pH outside = 8.0). E and F shows GUVs in the presence of 100 mM NaCl with no applied pH gradient. After 62 min, gramicidin was added to equilibrate the inner and outer pH. A) PVA GUVs in the absence and B) in the presence of 100 mM NaCl. C) Pt wire GUVs in the absence and D) in the presence of 100 mM NaCl. E) PVA GUVs and F) Pt wire GUVs without pH gradient.

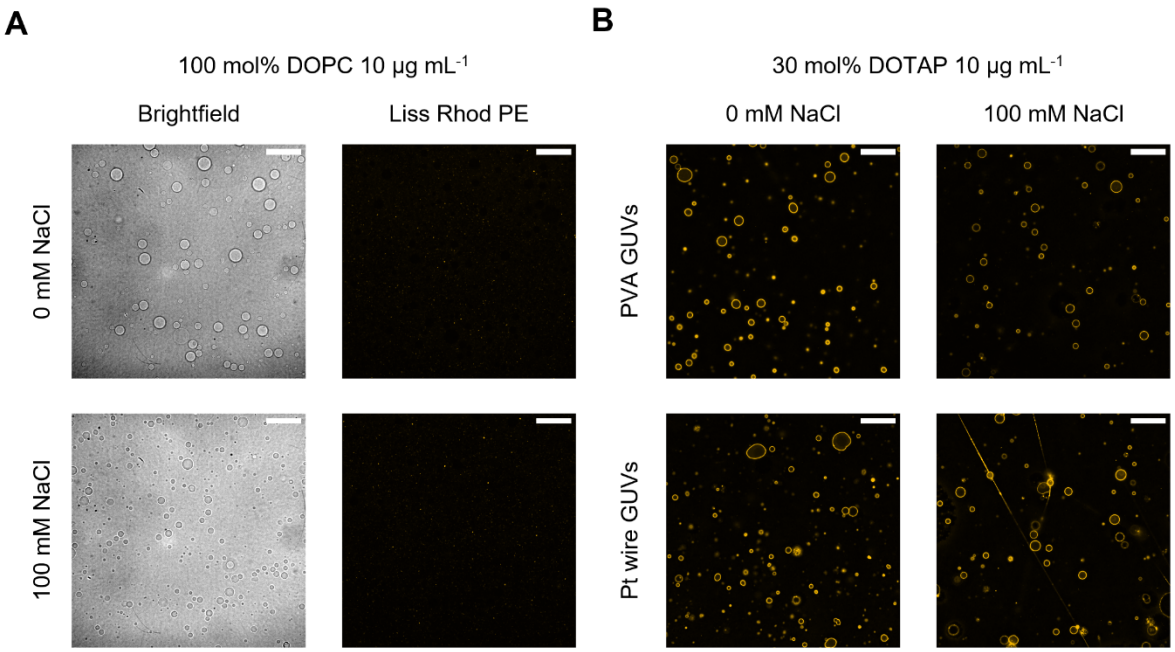

Figure S11: Representative confocal microscopy images of charge-mediated fusion performed in an 8 well chambered slide between negatively charged GUVs and neutral or positively charged SUV. The scale bar is 50 µm. All images from each channel were processed identically. A) Charge-mediated fusion with PVA GUVs and neutral SUVs (10 µg mL^{-1}) in the presence or absence of 100 mM NaCl. Brightfield and Liss Rhod PE images are shown. No fusion was observed, indicated by the absence of visible GUVs in the Liss Rhod PE channel. B) Charge-mediated fusion with PVA and Pt wire GUVs and positively charged SUVs (10 µg mL^{-1}) in the presence or absence of 100 mM NaCl.

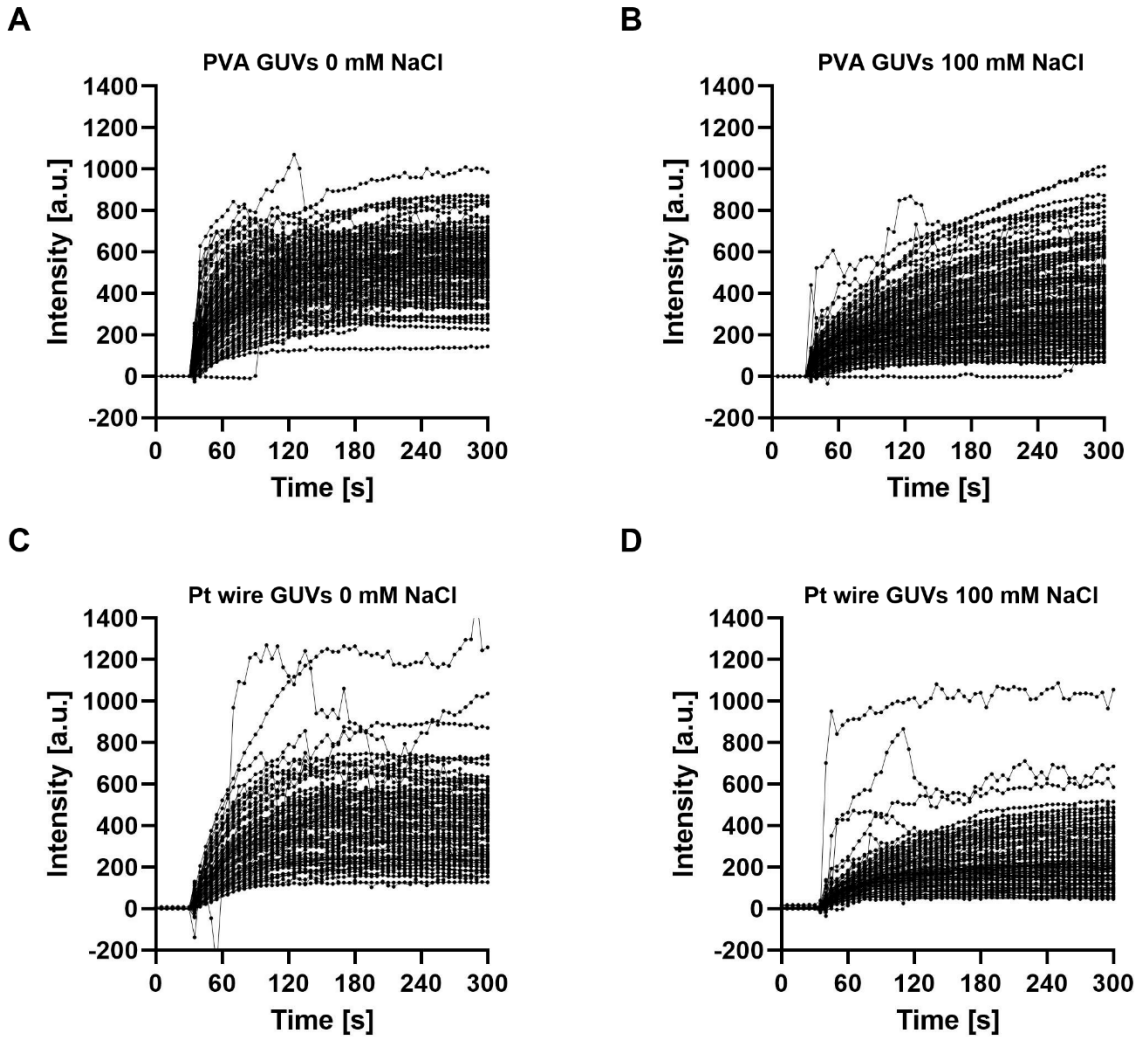

Figure S12: Charge-mediated fusion performed in an 8 well chambered slide between negatively charged GUVs and positively charged SUVs (10 µg mL^{-1}). Combined traces of GUVs from four experiments are shown. Only GUVs with diameters of 5 – 20 µm in the focal plane were analyzed (90 – 170 GUVs for all four experiments). Each recorded time point is represented as a dot. A) Fusion with PVA GUVs in the absence and B) in the presence of 100 mM NaCl. C) Fusion with Pt wire GUVs in the absence and D) in the presence of 100 mM NaCl.

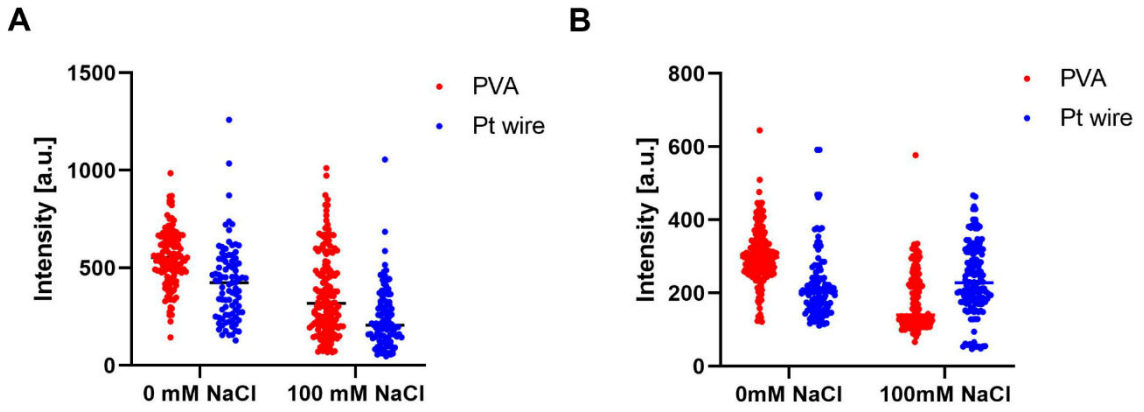

Figure S13: Charge-mediated fusion between negatively charged GUVs and positively charged SUVs. Combined distribution of Liss Rhod PE intensities from four experiments for PVA and Pt wire GUVs in the presence or absence of 100 mM NaCl. A) Intensity distribution from a single imaging plane after 270 s of fusion in an 8 well chambered slide. Concentration of SUVs in the slide was 10 µg mL^{-1}. B) Intensity distribution from an average projection of a Z-stack after fusion in an Eppendorf tube. Concentration of SUVs in the tube was 10 µg mL^{-1}. GUVs were fused for 15 min in the tube, added to an 8 well chambered slide coated with BSA and imaged after they were left to settle for 1 h.

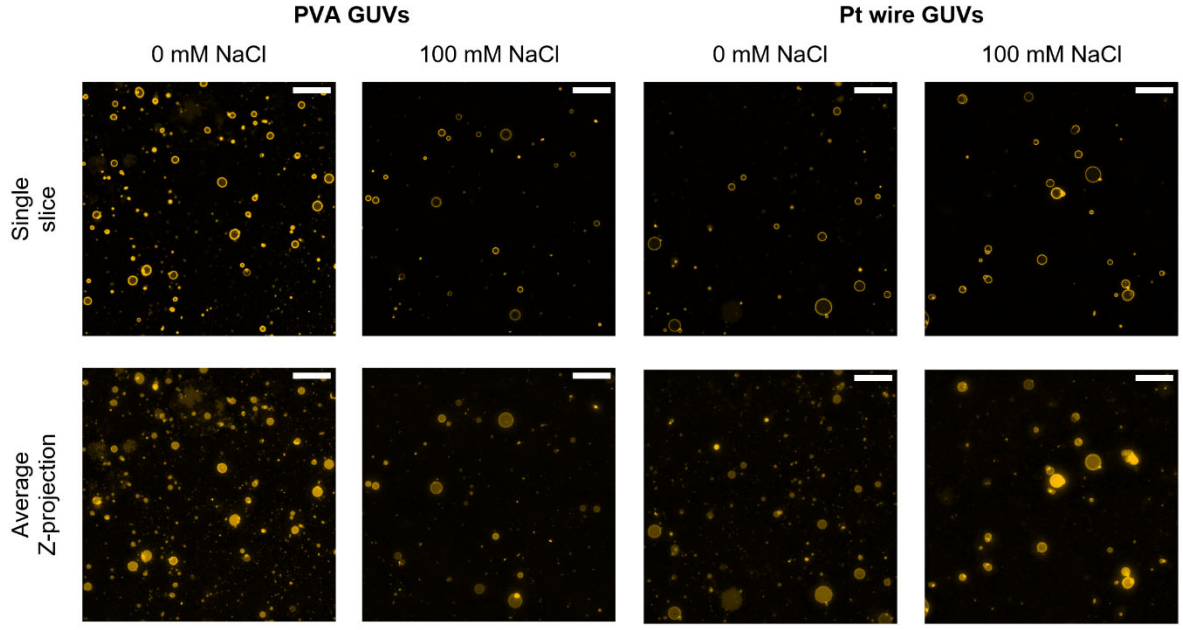

Figure S14: Representative confocal microscopy images of charge-mediated fusion between negatively charged GUVs and positively charged SUV performed in an Eppendorf tube. A single slice and the average Z-projection from a Z-stack image are shown for fusion with PVA and Pt wire GUVs and positively charged SUVs in the presence or absence of 100 mM NaCl. Concentration of SUVs in the tube was 10 µg mL^{-1}. GUVs were fused for 15 min in the tube, added to an 8 well chambered slide coated with BSA and imaged after they were left to settle for 1 h. The scale bar is 50 µm. All single slice images were processed identically. All average Z-projections were processed identically.

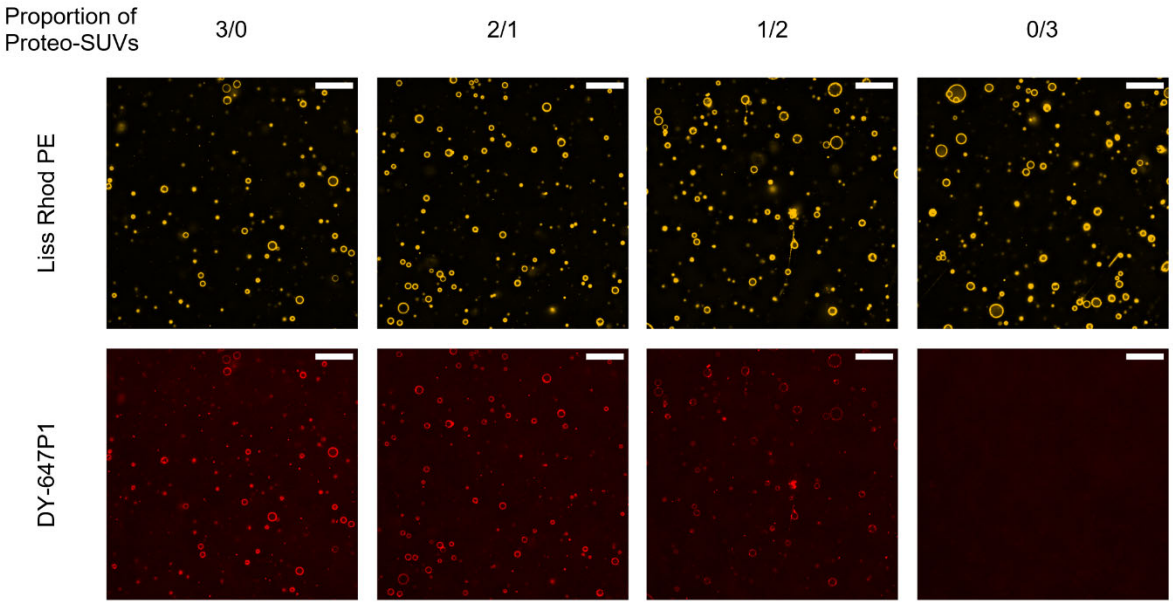

Figure S15: Confocal microscopy images of PVA GUVs at 0 mM NaCl fused with empty and proteo-SUVs (final concentration 40 µg mL^{-1}) containing DY-647P1-labeled cytochrome *bo$_3$* ubiquinol oxidase. Empty and proteo-SUVs were mixed at different ratios with proteo-SUV proportions of 3/0, 2/1, 1/2 and 0/3. Both the Liss Rhod PE and DY-647P1 channel are depicted. The scale bar is 50 µm. All images from each channel were processed identically.

Supplementary Movie S1: Charge-mediated fusion of rhodamine labeled positively charged empty SUVs with negatively charged GUVs in the microscopy well using 10 mM MOPS-BTP pH 7.4, 100 mM NaCl, and 200 mM glucose. A time series was recorded for 60 s with 1 s intervals using a 40x objective (scale bar 50 µm). The movie is displayed at a rate of 5 frames per second. SUVs were added after 6 seconds.

Supplementary File S1: The Autodesk Fusion 360 Archive File (*.f3d) of the slide holder used for ITO electroformation.

(Available online at https://doi.org/10.1101/2021.12.22.473796)

3.1.2. Functional Reconstitution of Cytochrome *c* Oxidase in Giant Unilamellar Vesicles

Title: Functional Reconstitution of Cytochrome *c* Oxidase in Giant Unilamellar Vesicles

Status: Experimental, Draft

Authors: Nicolas Dolder, Chao Song, Stavros Stavrakis, Andrew deMello, Christoph von Ballmoos

Contribution: Christoph von Ballmoos (CvB) supervised the study; Design of cytochrome *c* oxidase and GUV characterization experiments was a shared effort of CvB and Nicolas Dolder; Design, production, and optimization of a microfluidic device for GUV formation was carried out by Chao Song and supervised by Stavros Stavrakis and Andrew deMello; Nicolas Dolder performed experiments on GUVs and analyzed data; Nicolas Dolder wrote the draft; Chao Song provided figures of the microfluidic setup and GUV formation.

Abstract

In many bacteria and the mitochondria of eukaryotes, the final step in the breakdown of nutrients to enable the production of the cellular energy source adenosine triphosphate (ATP) is catalyzed by cytochrome *c* oxidases. They are thus part of the respiratory electron transfer chain (ETC) and work together with several other multisubunit proteins to build the proton motif force (*pmf*), which drives the production of ATP. Model membrane systems are needed to study the interplay between the proteins involved in the ETC. This bottom-up construction of a synthetic respiratory chain requires the coreconstitution of the individual ETC complexes, which has typically been done in small vesicles. The surface of these vesicles is much smaller than that of the energy-converting membranes where those proteins are found in nature. Giant unilamellar vesicles (GUV) are therefore more suitable to study synthetic respiratory chains, allowing for example to study the lateral diffusion of cytochrome *c* on the membrane surface and its interaction with the ETC proteins. As a first step in this direction, we need to be able to functionally reconstitute proteins of the ETC and be able to measure and characterize their function individually in GUVs. Here, we reconstitute cytochrome *c* oxidase from *R. sphaeroides* using the detergent free charge-mediated fusion method. Activity of the enzyme is followed using two different pH-sensitive fluorescent dyes. Carboxyfluorescein is first used where we observed strong bleaching and only small and not very clear signals of enzyme activity. Using the ratiometric pH-sensor HPTS, better signals could be obtained, and further characterization of the vesicles allowed comparing activities to different parameters such as the vesicle diameter and the relative amount of fusion. However, the large heterogeneity of the GUVs caused difficulties in the analysis of the data. Thus, to reduce the complexity, we turned to microfluidic production of GUVs to obtain vesicles with a monodisperse size and could show that these vesicles are fusogenic and could potentially be used to measure proton translocation.

Introduction

Cytochrome *c* oxidases are part of the respiratory electron transfer chain (ETC) in the energy-converting membranes of many bacteria and mitochondria of eukaryotes. They catalyze the final step in the breakdown of nutrients to enable the production of adenosine triphosphate (ATP) by transferring electrons from cytochrome *c* (cyt *c*) to the final electron acceptor oxygen to form water. Part of this highly exergonic electron transfer process is used for the translocation of protons across the membrane and thus contributes to the formation of the proton motive force (*pmf*), the driving force for ATP production by Complex V. In the aa_3 oxidase of *Rhodobacter sphaeroides*, the electron transfer is mediated by four redox centers. Reduced cyt *c* docks to its binding site and donates electrons to the dicopper Cu_A which is located slightly above the membrane surface. From there, electrons are transferred to heme *a* and finally to the binuclear site composed of Cu_B and heme a_3, where oxygen is reduced to water. For the reduction of one dioxygen molecule, eight protons are taken up from the N-side of the membrane. Four of them are translocated across the membrane to the P-side, while the other four are used for the conversion of oxygen to water.[426–428]

The bottom-up construction of a synthetic respiratory chain is an important endeavor to better understand the interplay between the different protein complexes of the ETC. By assembly of the individually purified complexes, one could have precise control over protein stoichiometries, lipid composition of the membrane, and substrate concentrations, to elucidate their influence on the production of ATP. Further, synthetic respiratory chains can be used to drive cellular processes such as protein synthesis[89,208] or actin polymerization[98] and thereby function as energy source for synthetic cells. The construction of a synthetic respiratory chain requires the coreconstitution of the individual ETC complexes. This has typically been done in small unilamellar vesicles (SUVs),[72,89,98,208] where the enzymes experience a high membrane curvature and might be generally close together which could have influence on the activity of the enzymes.[329] The membrane surface area of these small vesicles (diameters < 0.2 µm) is far below the surface area of the inner bacterial or mitochondrial membrane (diameters > 1 µm) where these enzymes are typically found. Thus, giant unilamellar vesicles (GUV) are an interesting model membrane system to study synthetic respiratory chains as they more closely mimic the natural environment of these respiratory enzymes in terms of size. As such, they have a large volume to surface ratio, reducing the dependency of substrate changes in the vesicle interior on the membrane surface and thus potentially allowing to follow transport process for longer periods of time compared to SUVs. Further, they might offer more room to play with protein stoichiometries to elucidate the importance of individual proteins and the relationship between the different enzymes.

As a first step in this direction, we must functionally characterize individual proteins of the ETC in the GUV membrane and compare their activities and kinetics with those observed in SUVs. Direct real-time

microscopy measurements in GUVs allows to follow transport process in individual vesicles where data on the size as well as the number of proteins reconstituted in a single vesicle can be obtained, allowing to better correlate transport rates to protein quantities compared to bulk experiments. In the literature, only few reports with functional reconstitution of respiratory enzymes in GUVs exist, often with a few single measurements under one condition[220,326] or using bulk assays.[80,81] Observed activities are also very slow or small and do not seem to hold up against measurements performed in SUVs, and critical controls are often missing, indicating that these are challenging experiments, including the reconstitution of membrane proteins (MPs) in GUVs, which is an ongoing field of research.[80,81,188,203] Second, an adequate imaging and data processing strategy is required to exploit the full potential of GUVs. This makes the functional characterization of MPs in GUVs not a trivial task.

Here, we reconstitute aa_3 oxidase from *Rhodobacter sphaeroides* into GUVs using the mild charge-mediated fusion strategy.[80,81] Outward directed proton translocation is initiated by the addition of ascorbate and cyt *c* to the outside of the GUVs. As cyt *c* is impermeable to the membrane, only proteins with their cyt *c*-binding site on the outside will be activated. Proton translocation is followed using two pH-sensitive dyes, carboxyfluorescein (CF) and 8-hydroxypyrene-1,3,6-Trisulfonic Acid (HPTS, pyranine), demonstrating the importance of an adequate detection system. Although MP activity is observed using both dyes, strong bleaching of CF complicated data analysis. By incorporation of a lipid-coupled dye in the SUV membrane that is fused to GUVs, relative MP concentration in different vesicles can be estimated. The diameter of fused GUVs was also determined and these parameters were related to the observed enzyme activities.

Experimental Procedures

Material

1,2-dioleoyl-sn-glycero-3-phosphocholine (DOPC), 1,2-dioleoyl-sn-glycero-3-phospho-(1'-rac-glycerol) (sodium salt) (DOPG) 1,2-dioleoyl-3-trimethylammonium-propane (chloride salt) (DOTAP), 1,2-distearoyl-sn-glycero-3-phosphoethanolamine-N-[biotinyl(polyethylene glycol)-2000] (ammonium salt) (DSPE-PEG2000-Biotin) and 1,2-dioleoyl-sn-glycero-3-phosphoethanolamine-N-(lissamine rhodamine B sulfonyl) (ammonium salt) (Liss Rhod PE) were obtained from Avanti Polar Lipids (Alabaster, AL, USA), Streptavidin from IBA-Lifesciences (Göttingen, Germany), Invitrogen™ 8-Hydroxypyrene-1,3,6-Trisulfonic Acid, Trisodium Salt (HPTS) from Thermo Fisher Scientific (Waltham, Massachusetts, USA), 5(6)-carboxyfluorescein (CF) from Molecular Probes (Eugene, Oregon, USA) and Polyvinyl alcohol (PVA), fully hydrolyzed, molecular weight approximately 145'000 for synthesis from Merck (Darmstadt, Germany). Other chemicals were obtained from Sigma (St. Louis, Missouri, USA).

Liposome formation

Lipids dissolved in chloroform were mixed in the desired ratio in a 25-mL round-bottom flask and chloroform was evaporated under a constant stream of N2 while rotating the flask. The thin lipid film was further dried for ≥ 2 h under high vacuum. Lipid mixtures contained 30 mol% DOTAP, 1-2 mol% Liss Rhod PE and 68-69 mol% DOPC The dried lipid film was resuspended at 5 mg mL^{-1}. Unilamellar liposomes were subsequently formed by seven freeze–thaw cycles and the size was adjusted either by extrusion through a Whatman polycarbonate membrane (Little Chalfont, UK) with a pore size of 100 nm or by sonication using a tip sonicator with 40 % intensity for 2 min using pulses of 30 s on and 30 s off. Liposomes were cooled on ice during sonication.

Reconstitution of cytochrome c oxidase

R. sphaeroides cytochrome *c* oxidase was purified according to published protocols[429] and reconstituted using detergent removal by gel filtration.[91] A desired amount of 5 mg mL^{-1} liposomes (50 – 70 µL) was mixed with 10 % Na-cholate to obtain a final concentration of 0.24 %, briefly incubated, and purified cytochrome *c* oxidase (44 µM) was added to obtain a final concentration of 0.84 µM. The sample was incubated for 30 min on ice with gentle shaking every 5 – 10 min. The sample was run on a CentriPure P2 column (emp Biotech GmbH, Berlin, Germany) according to the manufacturer's protocol resulting in liposome concentrations of 0.71 or 1.00 mg mL^{-1} and MP concentration of 0.12 and 0.17 µM after elution.

Reconstitution of cytochrome bo3 ubiquinol oxidase

Cytochrome bo_3 ubiquinol oxidase mutant IIIA21C, encoded by a cysless pETcyoII plasmid, was expressed and purified as described.[422–424] The purified protein was labeled with DY-647P1 maleimide and reconstituted into positively charged SUVs as described in Chapter 3.1.1. Experimental Procedures.[430]

PVA assisted GUV formation

GUV formation with PVA was done as described[265] with a few modifications. 1 mL 5 % PVA (*w/v*) in 280 mM sucrose was incubated for 1 h at 90 °C in a thermal shaker lite (VWR international GmbH, Dietikon, Switzerland) with 1'000 rpm shaking, and vortexing every 15 – 20 min. A coverglass (Ø 25 mm # 1.0, VWR international GmbH) was rinsed with 70 % ethanol and placed on an aluminum-foil-covered heat plate set to 50 °C. Rubber O-rings with 20 mm diameter and 1.4 mm thickness were placed centrally on top of the coverglass. 200 µL PVA solution was pipetted onto the coverglass area inside the rubber ring and the gel was left to dry for 1 h at 50 °C. 20 µL of lipids dissolved in chloroform at 0.75 mg mL^{-1} composed of 69.8 mol% DOPC, 30 mol% DOPG, and 0.2 mol% DSPE-PEG2000-Biotin were evenly distributed onto the gels using a Hamilton syringe. Solvent was evaporated for 1.5 – 2 h under vacuum, after which gels were rehydrated for 1 h using 500 µL buffer. The solution was removed from the wells and GUVs were stored for at least 1 h at 4 °C before performing further experiments.

Slide preparation and imaging

8 well chambered cover glass slides were coated for 30 min with approximately 50 µg mL^{-1} biotinylated BSA in 10 mM Tris-HCl, pH 8.0, 50 mM NaCl. Solution was removed and wells were coated as above with approximately 10 to 25 µg mL^{-1} streptavidin. Wells were washed once with appropriate imaging buffer, after which a desired amount of imaging buffer and GUV solution was added and GUVs were left to settle for 1 h. Slides were imaged using an inverted fluorescence microscope (Nikon Ti-2 Eclipse spinning disk confocal microscope, Nikon Europe BV, Amsterdam, Netherlands) with a 20x air objective (CFI Plan Apo 20x/0.75 W.D. 1.0, Nikon) or 40x oil-immersion objective (CFI Plan Fluor 40x/1.30 W.D. 0.24, Nikon). Fluorescent images were recorded in widefield and confocal mode using an Andor Zyla 4.2 Plus USB3 camera. CF was imaged using 470 nm excitation and 515 nm emission, HPTS using 395 nm excitation, 515 nm emission as well as 470 nm excitation and 515 nm emission, Liss Rhod PE using 555 nm excitation, 595 nm emission and DY-647P1 using 640 nm excitation and 698 nm emission with appropriate exciter, emitter and dichroic filter cubes.

Measurement of cytochrome c oxidase in GUVs with carboxyfluorescein

DOPG GUVs and DOTAP SUVs were formed in 10 mM MOPS pH 6.3, 50 mM KCl and 200 mM sucrose. Liposomes were prepared by extrusion. For GUVs, buffer contained 25 µM CF. 1 µL cytochrome *c* oxidase was reconstituted using 50 µL liposomes and 1.25 µL 10 % Na-cholate. Empty SUVs were produced as proteo-SUVs with addition of 1 µL buffer instead of cytochrome *c* oxidase. After elution from the P2 column, SUVs were diluted to 0.227 mg mL^{-1}. Microscopy slides were prepared as described with 25 µg mL^{-1} streptavidin. 400 µL imaging buffer (10 mM MOPS pH 6.3, 50 mM KCl, 200 mM glucose) and 10 µL GUV solution was loaded. GUVs were immobilized for 1 h. Non-encapsulated CF was removed by four 1 mL buffer exchanges in the microscopy well, adding fresh buffer while simultaneously removing

the same amount of solution from the well. Fusion was induced by addition of 5-10 µL SUVs and was stopped after 2 min by performing one 1 mL buffer exchange. Proteo-SUVs were fused at a final concentration of 5.4 µg mL^{-1} and empty SUVs at 2.7 µg mL^{-1}. Proton translocation was initiated by addition of 5 µL 1 mM cyt *c* followed by 2 µL 1 M sodium ascorbate and the proton gradient was dissipated by addition of 5 µL 1 mM gramicidin. The final concentrations were approximately 12 µM for both cyt *c* and gramicidin and approximately 4.7 mM for ascorbate. A time series was recorded with 3 s intervals for 7 min in widefield mode using the 20x objective and CF settings at 10 % intensity and 5 ms exposure time. Single Liss Rhod PE images were recorded using the Liss Rhod settings at 10 % intensity and 1 ms exposure time.

HPTS Calibration curve

GUVs were prepared as described with 68.8 mol% DOPC, 30 mol% DOPG, 1 mol% Liss Rhod PE and 0.2 mol% DSPE-PEG2000-Biotin in 10 mM MOPS pH 6.9, 7.3, 7.6 or 7.9, 50 mM KCl and 100 mM sucrose containing 50 µM HPTS. Microscopy slides were prepared as described and 400 µL imaging buffer (10 mM MOPS at corresponding pH, 50 mM KCl, 100 mM glucose) and 10 µL GUV solution was loaded. GUVs were immobilized for 1 h. GUVs at pH 6.9, 7.3 and 7.9 were imaged on a single focal plane in widefield mode using HPTS to record background signals (free HPTS). 18 % intensity and 10 ms exposure time were used for 395 nm excitation and 10 % intensity and 5 ms exposure time for 470 nm excitation. To remove non-encapsulated HPTS, four 1 mL buffer exchanges with imaging buffer were performed as described. GUVs at all pH values were imaged after washing in a single focal plane at multiple spots using settings as described.

Measurement of cytochrome c oxidase in GUVs with HPTS

DOPG GUVs and DOTAP SUVs were formed in 2 mM MOPS pH 7.4, 10 mM KCl and 100 mM sucrose. Liposomes were prepared by sonication. For GUVs, buffer contained 50 µM HPTS. 1.4 µL cytochrome *c* oxidase was reconstituted using 70 µL liposomes and 1.75 µL 10 % Na-cholate. Empty SUVs were produced as proteo-SUVs with addition of 1.4 µL buffer instead of cytochrome *c* oxidase. After elution from the P2 column, SUVs were diluted to 0.03 mg mL^{-1} using imaging buffer. Microscopy slides were prepared as described and 200 µL imaging buffer (2 mM MOPS pH 7.4, 10 mM KCl, 100 mM glucose) and 10 µL GUV solution was loaded. GUVs were immobilized for 1 h. To remove non-encapsulated HPTS two 1mL buffer exchanges were performed as described using 2 mM MOPS pH 7.4, 120 mM glucose. Fusion was induced by addition of 100 µL SUVs and was stopped after 5 min by performing two 1 mL buffer exchanges with 2 mM MOPS pH 7.4, 10 mM KCl and 100 mM sucrose. SUVs were fused at a final concentration of 10 µg mL^{-1}. Proton translocation was initiated by addition of 50 µL 40 mM sodium ascorbate followed by 50 µL 0.1 mM cyt *c* and the proton gradient was dissipated by addition of 50 µL 0.1 mM gramicidin. The final concentrations were approximately 11 µM for both cyt *c* and gramicidin

and approximately 4.3 mM for ascorbate. A time series was recorded with 5 s intervals for 10 min. Multiple positions in a well were imaged in widefield mode using both HPTS settings at 20 % intensity and 50 ms exposure time for HPTS. After the measurement, a Z-stack was recorded at every position using the Liss Rhod PE settings in confocal mode.

Characterization of OLA GUVs

OLA GUVs with 68.8 mol% DOPC, 30 mol% DOPG, 1 mol% Liss Rhod PE and 0.2 mol% DSPE-PEG2000-Biotin and 2 mM MOPS pH 7.4, 10 mM KCl and 100 mM sucrose were formed by our collaborators at ETH Zürich according to Dekker and colleagues[193,431] with modifications of the chip design and procedure based on Bao *et al.* (2021).[288] GUVs were collected by two different methods, either directly into a PCR tube after formation or first passing them through a serpentine module to aid separation of the octanol pocket. Collected GUVs were shipped to us for further characterization. Slides were prepared as described with 10 µg mL^{-1} used for fusion and size distribution measurements and 25 µg mL^{-1} used for gramicidin experiments. 380 µL imaging buffer (same as above with glucose instead of sucrose) and 20 µL GUVs were loaded for the latter two experiments, while fusion was performed with 50 µL GUVs loaded into 150 µL imaging buffer. Characterization of GUV size and number was done as described (Chapter 3.1.1. Experimental procedures)[430] recording 9 Z-stacks with 30 steps of 1 µm step size. Fusion with DOTAP SUVs containing labeled cytochrome bo_3 ubiquinol oxidase was done by addition of 200 µL 0.1 mg mL^{-1} SUVs to immobilized GUVs and imaging both 470 nm HPTS channel with 50 % intensity and 500 ms exposure time and DY-647P1 channel with 50 % intensity and 500 ms exposure time after fusion. Gramicidin experiment was performed by washing immobilized GUVs twice with imaging buffer at pH 7.4 and twice with imaging buffer at pH 8.0. Proton translocation was initiated by addition of 5 µL 1 mM gramicidin directly after washing. A time series was recorded with 5 s intervals for 5 min with addition of gramicidin after 1 min. HPTS signal was measured using both HPTS channels with 50 % intensity and 200 ms exposure time.

Image preparation

Image preparation and data extraction was performed using FIJI.[419] For fluorescent images, background was subtracted using the Background Subtract function with a rolling ball radius of 200.0 pixels and none of the options enabled. Brightness was adjusted to the desired values, a scale bar was added and images were exported as Tiff-files.

Data extraction and preparation

GUVs were detected by manual thresholding, creating a binary mask separating vesicles and background. For measurements involving pH-sensitive dye, thresholding was performed using the CF channel or the 470 nm excitation HPTS channel after background subtraction as described. GUVs are then identified using a macro which cleans up the binary mask by performing the processes Fill Holes,

Erode and Watershed and then uses the Analyze Particles function with Size = 0.75 µm^2 – Infinity, Circularity = 0.70 – 1.00 and Display Results, Exclude on Edges and Add to ROI manager enabled. Using the Measure function, the Feret diameter of the identified vesicles is obtained. The characterization of OLA GUVs from Liss Rhod PE Z-stacks was done as described. (Chapter 3.1.1. Experimental Procedures).[430] The same method was used to characterize cytochrome *c* oxidase GUVs from Z-stack Liss Rhod PE images. Adhesion was assessed by creating a profile view of GUVs using the reslice function in FIJI. The height of the sphere segment of attached vesicles was estimated using the line selection tool. All graphs from the extracted data were prepared using GraphPad Prism 8.3.0.

Analysis of cytochrome c oxidase activity in GUVs with carboxyfluorescein

For measurements with CF, approximately 30 GUVs were detected using the image at the start of the measurement for both GUVs fused with empty or proteo-SUVs. Background regions of interest (bgROIs) were drawn in by hand next to each GUV and intensity values were obtained using the Time Series Analyzer V3 plugin with the average intensity setting for both vesicles and bgROIs. GUVs with apparent diameters below 4 µm and vesicles which leaked all of the encapsulated CF were not considered for further analysis. For each trace, the corresponding bgROI signal was subtracted and traces were normalized to the starting value.

Analysis of cytochrome c oxidase activity in GUVs with HPTS

HPTS intensities form the calibration GUVs were extracted using the Measure function in FIJI. Mean grey intensities were obtained for single images and ratios were calculated by dividing the intensity at 470 nm excitation with the intensity at 395 nm excitation. No background subtraction was performed. A calibration was obtained by fitting the ratios obtained for GUVs above 10 µm apparent diameter with a linear regression. For GUVs fused with empty or proteo-SUVs, vesicles were identified using the last image of the time series. HPTS intensities for both excitations were obtained using the Time Series Analyzer V3 plugin with the average intensity setting. The ratio was formed as described and converted to pH values using the calibration curve (Ratio = 0.4272 x pH +2.637). ΔpH values were obtained as follows. First, the maximal pH value observed between 100 and 400 s (before addition of gramicidin) was extracted from the individual traces. Next, the time point before 90 % of the maximal pH was reached after addition of cyt *c* was determined. The time interval between addition of cyt *c* (120 s) and this time point was then calculated. The pH value was extracted from the traces at the time point where approximately 80 % of the calculated time interval had passed (pH_t). This pH value should be roughly at the end of the linear increase after cyt *c* addition. ΔpH was then calculated by subtracting the pH at 100 s (before addition of cyt *c*) from pH_t.

Comparison of cytochrome c oxidase activity and vesicle parameters in GUVs with HPTS

HPTS GUVs with cytochrome *c* oxidase activity were characterized as described using the Liss Rhod PE Z-stack images to obtain vesicle diameter and height of the sphere segment. This was used to calculate the volume and surface of the sphere segment. Mean grey intensities were obtained from an average Z-projection of the stack to obtain a measure for the relative fusion correlating to the relative protein density.

The relative protein amount was calculated by multiplication of the relative protein density with the GUV surface. The number of protons translocated to reach the observed pH difference was calculated according to equation 3.

$$\Delta H^+ = \left(\frac{c}{10^{pH_{100s}-pK_a+1}} - \frac{c}{10^{pH_t-pK_a+1}}\right) \times V_{GUV} \times N_A \quad \text{(Equation 3)}$$

The pH_{100s} corresponds to the pH before addition of cyt *c* and pH_t is the pH at the end of the linear increase after cyt *c* addition from a GUV with volume V_{GUV}. The concentration of buffer molecules (MOPS and HPTS) is given by c = 2.05 mM with a pK_a of 7.2. This gives the mols of protons which have to be translocated to reach pH_t. Multiplication with the Avogadro constant N_A gives the number of translocated protons. The activity in number of protons translocated per second is calculated by division of ΔH^+ with the time needed to reach pH_t after addition of cyt *c* at 120 s.

To check for correlation between two different values, they were first tested for normality using a Shapiro-Wilk test with α = 0.05 in GraphPad Prism 8.3.0. If both values were normally distributed, a Pearson correlation coefficient was calculated, otherwise Spearman correlation was used. All correlations were calculated in Prism with α = 0.05 and one-tailed correlation was used as a specific direction was expected for all comparisons, for example increasing activity with higher amount of MP.

Analysis of OLA GUV characterization

The Z-stacks recorded for the characterization of GUVs were analyzed as described in Chapter 3.1.1. Experimental Procedures[430] to obtain GUV size distributions and number of vesicles above 5 µm. Histograms were prepared in Prism with a bin size of 2 µm. For the gramicidin experiment, vesicles were identified using the last image of the time series. HPTS intensities for both excitations were obtained using the Time Series Analyzer V3 plugin with the average intensity setting. The ratio was formed and converted to pH values as described.

Results

Reconstitution of aa_3 oxidase in GUVs

Cytochrome *c* oxidase from *R. sphaeroides* was reconstituted into GUVs using the detergent-free charge-mediated fusion approach.[80,81] GUVs are prepared with a negative surface charge which mimics conditions found in biological membranes. Positively charged SUVs containing one or several MPs are then fused with the oppositely charged GUV membrane. Reconstitution of MPs in SUVs is well established, and fusion allows coreconstitution of MPs with incompatible reconstitution procedures and conserves the orientation of the proteins.[80] SUVs and GUVs were prepared containing 30 mol% charged lipids according to previously published results.[80] Negatively charged GUVs (DOPC/DOPG/DSPE-PEG2000-biotin 69.8/30/0.2 mol%) containing soluble pH-sensitive fluorophores were formed by the PVA assisted swelling method.[265] This GUV formation method is fast, simple and versatile and produces a large quantity of GUVs in a size range of 5 – 20 µm, which should be well suited for the investigation of MP function using light microscopy single vesicle measurements.[430] Biotinylated lipids were added to GUVs for immobilization on biotin-BSA/streptavidin coated glass slides, which is required to follow reactions in single vesicles under the microscope. Reconstitution of aa_3 oxidase into positively charged SUVs (DOPC/DOTAP/Liss Rhod PE 69/30/1 mol%) was done using the detergent-mediated reconstitution method as described in the Experimental Procedures. Fluorescent lipid (Liss Rhod PE) was included in the SUVs to follow fusion to unlabeled GUVs as previously described, allowing to estimate the relative protein concentrations of different vesicles.[430] For control experiments, empty SUVs without MP were prepared. After detergent removal and dilution to appropriate concentrations, SUVs were fused to immobilized and washed GUVs. The exact lipid-ratio of SUVs to GUVs was not determined, as washing of the GUVs prior to fusion, to remove non-encapsulated fluorophore, decreased the quantity of vesicles by an undetermined amount. Based on previously calculated yields for PVA formation[430] and the lipid amounts used here, the excess of SUV lipids is estimated to be at least 17 to 19-fold compared to GUV lipids and likely even higher. Fusion also resulted in the loss of encapsulated soluble dye in some of the vesicles which were disregarded for further analysis (Figure S16 and S17), decreasing the amount of usable GUVs.

Activity of aa_3 oxidase in GUVs containing carboxyfluorescein

Previously, we showed aa_3 oxidase activity in SUVs containing a bifunctional DNA duplex labeled with the pH-sensitive fluorophore carboxyfluorescein (CF). Thus, it made sense to measure aa_3 oxidase activity in GUVs using the same fluorophore to obtain comparable data. However, due to difficulties with incorporation of the bifunctional probe in GUVs (see chapter 3.2.2.), soluble CF was used instead, as encapsulation in GUVs and removal of non-encapsulated dye by washing of immobilized vesicles is simple, albeit not as efficient as incorporation of membrane-anchored dyes. The aa_3 oxidase was reconstituted in GUVs containing soluble CF using charge mediated fusion as described. Proton

translocation was triggered by addition of cyt *c* and sodium ascorbate to the exterior solution, activating only enzymes with the cytochrome *c*-binding site on the outside (orientation of aa_3 oxidase may be random), leading to outward proton translocation (Figure 11A). This should lead to an increase in CF intensity.[174] Addition of the protonophore gramicidin was used to dissipate the proton gradient. Data was extracted from GUVs containing CF after fusion using FIJI. Figure 11B shows the activity traces obtained from GUVs fused with either empty or aa_3 oxidase containing SUVs. For both empty and proteo-SUVs, approximately 30 GUVs were detected in a 20x field of view, but vesicles with apparent diameters below 4 µm were excluded from analysis due to very low signal-to-noise ratio. The exact diameter of the GUVs is not known as only a single focal plane was imaged. A fraction of these vesicles leaked most of the CF during the experiment (Figure S18) and was excluded from further analysis. This reduced the number of vesicles to nine for both empty and proteo-SUVs. Figure 11B shows the averaged kinetics including standard deviation of these nine GUVs. An increase in CF intensity for GUVs fused with proteo-SUVs is seen after both cyt *c* and ascorbate were added, while no increase is seen in the mean intensity of empty GUVs. The increase is only seen with a delay of some seconds after ascorbate addition. This might be due to mixing issues when adding substrates to the microscopy well, as mixing in the microscopy slide depends on factors such as the speed and the location of addition relative to the observed area. Addition of gramicidin also leads to a slight decrease of the CF signal in proteo-GUVs, indicating that the established pH gradient is dissipated. The described effects are easily visible in the mean traces, but they are less clear when looking at the individual traces (Figure 11C and D). Although for aa_3 oxidase GUVs, all traces follow the same behavior, there are also few traces in the empty GUVs that show an increase after addition of ascorbate. However, some traces also show a slight decrease which is not observed for any of the aa_3 oxidase GUVs which were analyzed. The data analysis in this experiment is further complicated by the fast bleaching of CF, despite using very low intensity for illumination and short exposure times. This further resulted in bad signal-to-noise ratio, especially in vesicles smaller than 4 µm. In our previous bulk measurements using a fluorescence spectrophotometer, no bleaching issues were observed for CF signal,[174] which demonstrates that bleaching is much more critical when performing microscopy experiments. This also does not allow direct comparison of the prior results in SUVs. However, based alone on the mean and standard deviation traces, one could assume that aa_3 oxidase is active in the GUVs.

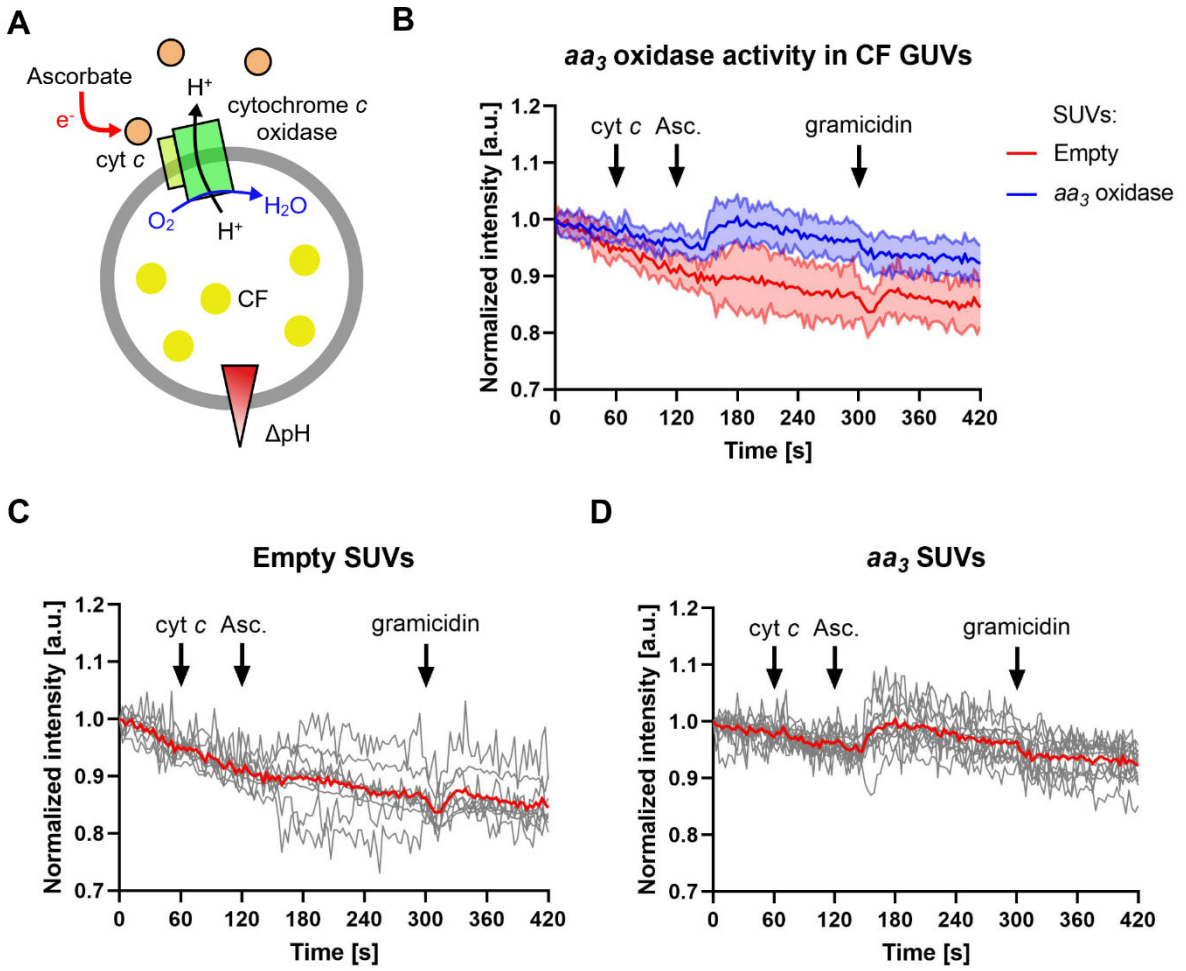

Figure 11: Proton pumping of cytochrome *c* oxidase in GUVs monitored using encapsulated CF. A) Cartoon representation of the experiment. GUVs with apparent diameter > 4 µm fused with SUVs containing *R. sphaeroides* aa_3 oxidase or as a negative control empty liposomes were measured. Proton pumping was initiated by addition of 12 µM cyt *c* followed by the addition of 4.7 mM Na-ascorbate (Asc.). The proton gradient is dissipated by the addition of 12 µM gramicidin. B) Mean and standard deviation of 9 GUVs from each experiment. C) Individual (grey) and mean (red) traces of GUVs fused with empty SUVs or D) with proteo-SUVs.

HPTS calibration

To circumvent the bleaching, we next decided to reconstitute aa_3 oxidase in GUVs containing HPTS. This pH-sensitive dye can be measured ratiometrically by excitation at two different wavelengths (395 nm and 470 nm) and emission at a single wavelength (515 nm).[412–414] The ratiometric measurement has several advantages over a single excitation and emission measurement. First, as bleaching is observed in both channels, the ratio of the two channels cancels the bleaching effect drastically and second, the ratio should be directly relatable to a corresponding pH value using a calibration curve. Thus, we formed GUVs containing HPTS at different pH values and measured the intensity at 515 nm with excitation using both 395 nm and 470 nm LED light in a single focal plane to obtain a calibration under similar conditions as for time series experiments. To measure only the ratio of encapsulated HPTS, immobilized GUVs were

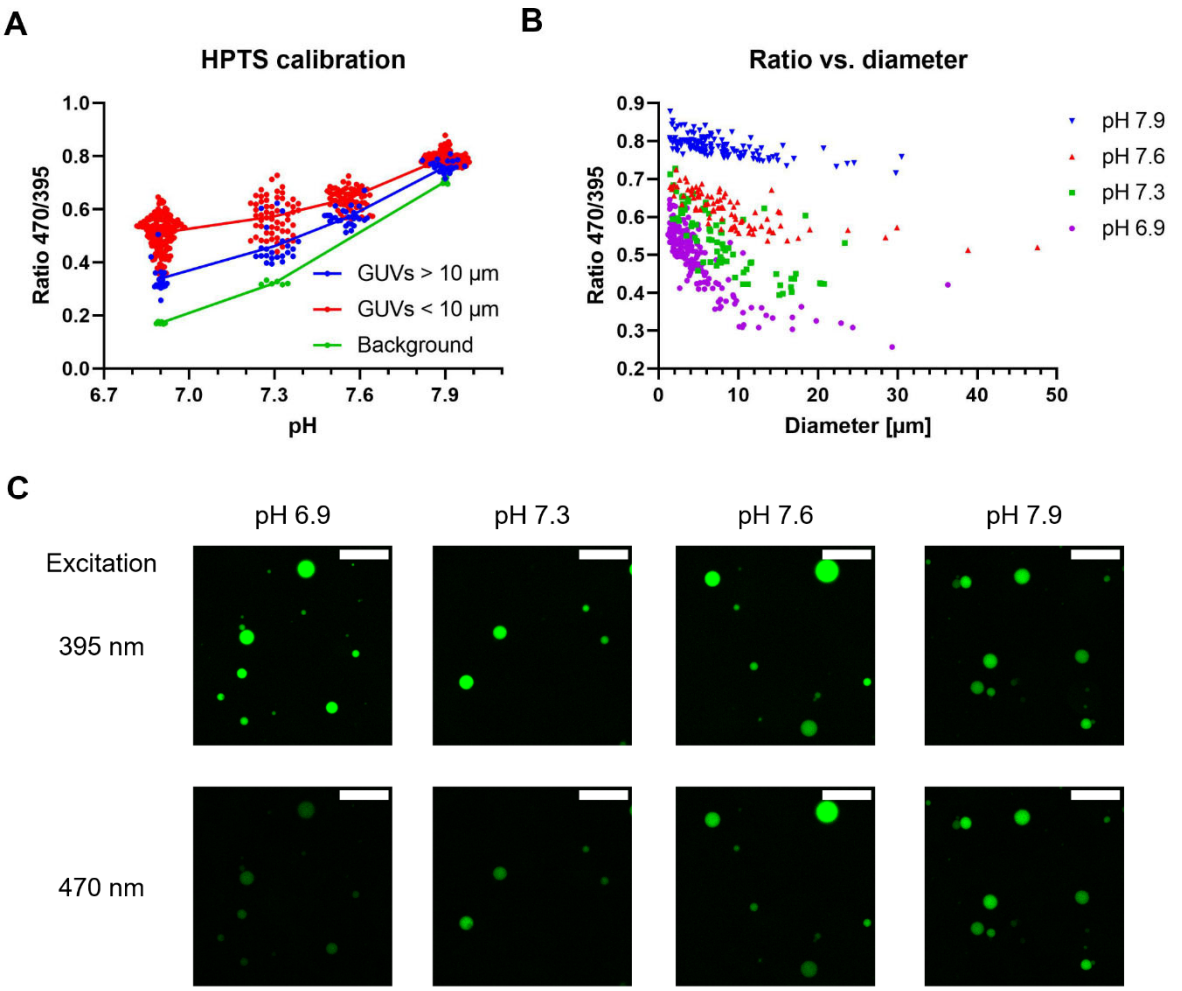

Figure 12: HPTS calibration in GUVs. A) HPTS ratios measured at different pH values in GUVs. Shown are traces for free HPTS measured in the surrounding solution of GUVs before washing (green), GUVs with apparent diameters > 10 µm (blue) and < 10 µm (red). Six background ROIs were recorded in areas outside of GUVs. Apparent diameter represents the diameter of a GUV in the focal plane. 60 – 160 GUVs with apparent diameters below 10 µm were detected and 20 – 30 GUVs with diameters above 10 µm. B) HPTS ratios measured at different apparent GUV diameters for pH 6.9 (violet circles), pH 7.3 (green squares), pH 7.6 (red triangles) and pH 7.9 (blue triangles). C) Representative microscopy images for both excitation wavelengths. All images were treated equally. The scale bar represents 50 µm.

washed before imaging. For three of the four tested pH values, images were also recorded before washing to measure HPTS in the surrounding solution, corresponding to free HPTS. Figure 12A shows the obtained HPTS ratios for the different pH values. GUVs are separated into two groups, vesicles with apparent diameters below and above 10 µm.

As depicted in Figure 12A, at pH 7.9, the HPTS ratio was similar for free HPTS as well as both GUV groups. However, towards lower pH values, the ratio is shifted upwards for GUVs and more so for the smaller vesicles, with a broadening of the ratio distribution. Thus, it seems that the HPTS ratio depends not only on the pH but also on the size of the vesicles under the experimental conditions used here. Plotting the ratio against the apparent vesicle diameter shows a clear dependence of the ratio on the size of the

vesicles (Figure 12B). At low pH values, small vesicles show a large shift towards higher ratios, with the shift decreasing with increasing pH. Based on absorption profiles of HPTS at different pH values, a decrease in the 395 nm channel is expected with increasing pH, while an increase should be observed in the 470 nm channel.[432] Figure 12C shows exemplary GUVs from the different pH values with the same processing and LUTs applied. For 470 nm excitation, a clear increase in signal is observed, while no large effect was observed in the 395 nm channel, with a slight decrease only observed at pH 7.9. Looking at the extracted intensities (Figure S19), similar distributions are obtained for small vesicles in the 395 nm channel with the mean only slightly shifted upwards for pH 7.3 and 7.6, while the large GUVs show the highest intensities for the lowest pH value as expected. For excitation at 470 nm, both small and large GUVs show the expected trend with higher intensities at higher pH values. Taken together, these results indicate that ratiometric measurements of pH in GUVs using HPTS are not without its challenges, especially when the size of the vesicles varies. Despite this, we decided to perform experiments using aa_3 oxidase with GUVs containing HPTS. The obtained ratios were converted to pH with the calibration data from large GUVs, as they correspond more closely to the free HPTS signal. However, a wide ratio distribution was observed for the calibration GUVs, and imaging conditions and buffer composition were slightly different for the aa_3 oxidase experiments, and we do not claim that the obtained pH values are highly accurate. HPTS is known to be sensitive to changes in buffer composition,[414] but the ratios obtained at the start of the aa_3 oxidase measurement corresponded well to the expected pH value of the solution, and the calibration was used for an approximate estimation of the pH changes due to proton translocation by the aa_3 oxidase.

Activity of aa_3 oxidase in GUVs containing HPTS

Reconstitution of aa_3 oxidase in GUVs containing HPTS by charge-mediated fusion was performed as described above. As a loss of dye due to fusion or immobilization was expected and images were recorded with a 40x objective, two to three spots in each well were imaged to reach > 10 GUVs for analysis. To gain more insight on the aa_3 oxidase activity for individual GUVs, fusion efficiency and GUV diameter were visualized recording Z-stacks using the Liss Rhod PE settings after performing the activity measurement. As GUVs were formed without lipid-coupled dye, the Liss Rhod PE intensity should indicate the relative amount of fusion and thus the relative amount of protein in each GUV.[430] Using the information from the Z-stacks allows to potentially investigate whether the observed activities in each vesicle depend on its morphology and the amount of MP incorporated. The size of the vesicles for analysis was limited to 5 – 20 µm as previously described.[430] Figure 13A shows an exemplary GUV microscopy image obtained with excitation at 470 nm for HPTS with GUVs after fusion. Four out of the ten GUVs detected in the desired size range are also shown in a profile view obtained from the Z-stack in the Liss Rhod PE channel. The HTPS traces corresponding to those four GUVs are shown next to the profile views. Variations in adhesion, size, Liss Rhod PE intensity and speed and magnitude of pH change

induced by aa_3 oxidase proton translocation are observed. The HPTS traces for all analyzed GUVs are depicted in Figure 13B. As controls, experiments were performed with GUVs fused with empty SUVs as well as addition of ascorbate to GUVs fused with aa_3 oxidase SUVs in the absence of cyt *c*. The experiments show that only GUVs with both aa_3 oxidase and addition of cyt *c* led to an increase in pH, indicating proton translocation from the inside to the outside of GUVs by aa_3 oxidase.

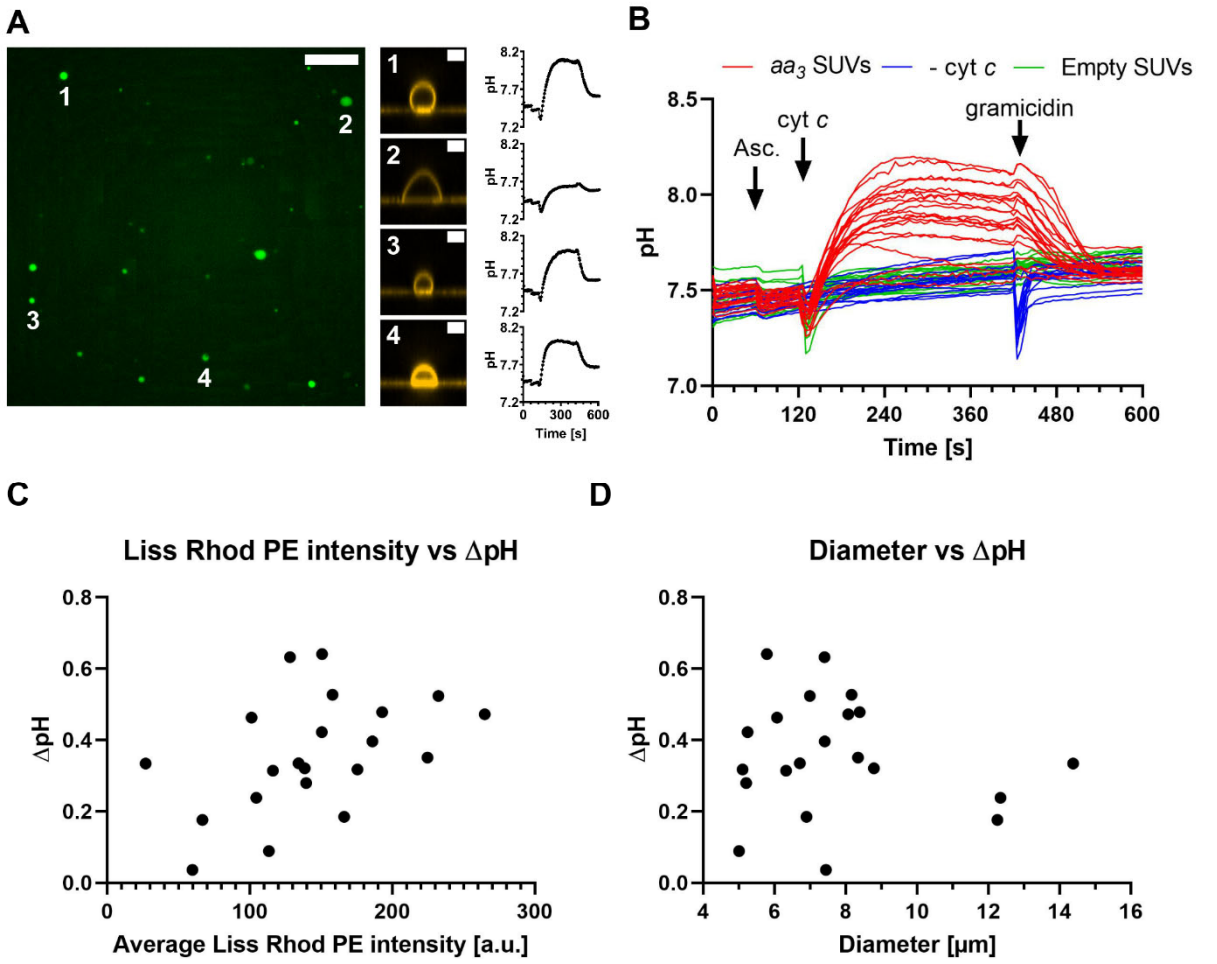

Figure 13: Proton pumping of cytochrome *c* oxidase in GUVs monitored using encapsulated HPTS. A) Microscopy images and traces of GUVs fused with proteo-SUVs depicting aa_3 oxidase activity. The HPTS emission with excitation at 470 nm at one of the recorded positions is shown (green) and GUVs which were used for analysis are labeled (1-4). The scale bar for the HPTS image is 50 µm. Profile views of the labeled GUVs from the Liss Rhod PE channel are shown (yellow) depicting differences in size, shape/adhesion and Liss Rhod PE signal. The scale bar is 5 µm. The traces corresponding to those vesicles are depicted next to them. The measured HPTS ratios were converted to pH values using the calibration obtained from the GUVs > 10 µm, showing differences in pH change and kinetics. B) All of the analyzed traces of GUVs fused with aa_3 oxidase SUVs (red, blue) and empty SUVs as negative control (green) Each condition corresponds to one microscopy well with two to three imaged spots. After 60 min, 4.3 mM ascorbate (Asc.) was added followed by the addition of 11 µM cytochrome *c* (cyt *c*) at 120 s. As a second negative control, buffer instead of cyt c was added to GUVs fused with aa_3 oxidase SUVs (blue). The proton gradient was dissipated by addition of 11 µM gramicidin at 420 s. Each trace represents a single GUV.C) Correlation of the average Liss Rhod PE intensity obtained form an average Z-projection of the Liss Rhod PE stack with the observed ΔpH values. (One-tailed Pearson r = 0.4543, n = 21, p = 0.0193). D) Correlation of the GUV diameter obtained form an average Z-projection of the Liss Rhod PE stack with the observed ΔpH values. (One-tailed Spearman r = 0.0091, n = 21, p = ~ 0.4844).

Comparison of aa_3 oxidase activity to relative protein density and GUV diameter

The aa_3 oxidase GUVs with addition of cyt *c* were further analyzed. From the Z-stack images in the Liss Rhod PE channel, the diameter and average Liss Rhod PE intensity were obtained by average Z-projection of the stack. According to previous results with labeled bo_3 oxidase, relative protein concentrations in GUVs can be estimated by comparing the intensity of lipid-coupled dye originating from SUVs.[430] Thus, the average Liss Rhod PE intensity obtained from the projection can be viewed as a relative protein density. Proton export from GUVs by the aa_3 oxidase leads to an increase of pH on the inside of GUVs and thus to a ΔpH across the GUV membrane. Using the traces from Figure 13B, ΔpH values from individual GUVs were obtained. Due to slightly different kinetics of the individual vesicles and to avoid being in the steady state between proton translocation and leakage, pH values at time points roughly at the end of the linear increase after cyt *c* addition were determined. First, the maximal pH reached between 100 s and 400 s (i.e. before addition of gramicidin) was obtained. Next, the time interval was calculated between cyt *c* addition (120 s) and the time point just before 90 % of the maximal pH was reached. The pH value pH_t was then determined at approximately 80 % of this time interval. On average pH_t values were obtained at around 200 s of the measurement, ranging from 165 s to 265 s. The ΔpH was then calculated by subtracting the pH value at 100 s from this pH_t value. ΔpH values were compared against the corresponding Liss Rhod PE intensity (Figure 13C) and diameter of the same GUVs (Figure 13D). First, all values were tested for normality using a Shapiro-Wilk test ($\alpha = 0.05$) in GraphPad Prism 8.3.0. Both the average Liss Rhod PE intensity ($p = 0.9932$) and the ΔpH ($p = 0.8927$) were found to be normally distributed while the diameter was not normally distributed ($p = 0.0040$). The Q-Q plots for the respective values are depicted in Figure S20B - D. Based on the hypothesis that a larger protein density (that is higher average Liss Rhod PE intensity or more MP per nm^2 GUV surface) should lead to a higher ΔpH and both values are normally distributed, one-tailed Pearson correlation was used. The results indicate that indeed the Liss Rhod PE intensity could be used to assess protein concentration in GUVs as a correlation with the ΔpH values was found ($r = 0.4543$, $n = 21$, $p = 0.0193$). With the diameter, one could expect that with increasing vesicles size, more protons need to be translocated to reach a certain pH so that ΔpH values might be smaller for large vesicles. As the diameter is not normally distributed, a one-tailed Spearman correlation was used. No correlation between the diameter and ΔpH was found ($r = 0.0091$, $n = 21$, $p = \sim 0.4844$). However, looking at the three largest GUVs, lower ΔpH was observed which would fit the hypothesis, but these vesicles also had lower Liss Rhod PE intensities (Figure S20A). GUVs with diameters < 10 µm showed rather random distribution of Liss Rhod PE intensities, possibly indicating different fusion efficiencies of these GUVs, so overall no significant correlation for Liss Rhod PE intensity and diameter was observed (one-tailed Spearman $r = -0.1130$, $n = 21$, $p = \sim 0.3129$). As evident by Figure 13C and D, there is still a large variation observed for the parameters directly obtained from the GUVs.

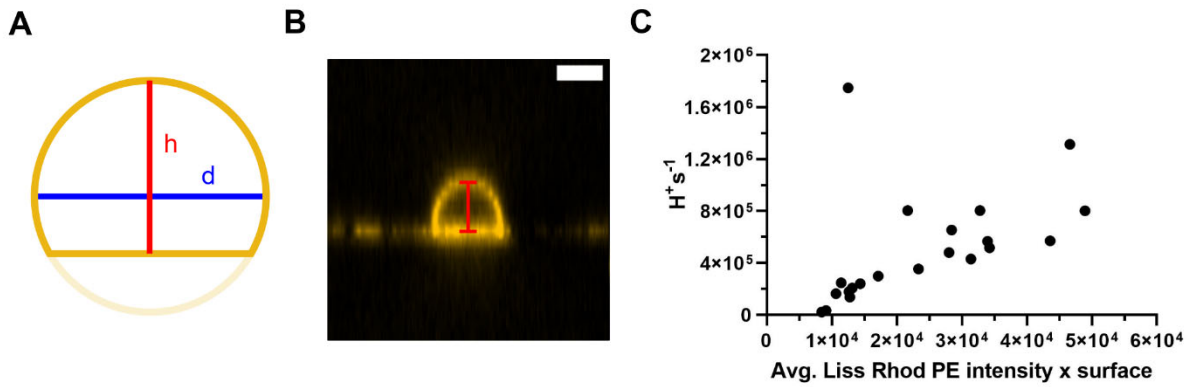

Figure 14: Characterization of the GUV shape and size to correlate relative protein number and activity. A) Cartoon representation of a GUV in the profile view. The GUV is modeled as a sphere segment with the cut-off part slightly faded. The diameter is indicated in blue which is obtained from the average Z-projection of the Liss Rhod PE Z-stack and the height of the sphere segment is indicated in red which is obtained by measurement using the line selection tool on the profile view of a GUV. B) Exemplary GUV profile view. The red line shows how the line selection tool was positioned to measure the height of the sphere segment. The scale bar is 5 µm. C) Correlation between the protons translocated per second as calculated from the pH values and volume of the GUV with the relative number of MPs as calculated by multiplication of the average Liss Rhod PE intensity with the surface of the GUV. (One-tailed Spearman r = 0.7026, n = 21, p = ~ 0.0002).

Calculation and comparison of translocated protons and relative number of proteins per vesicle

So far, a rather simplified picture was used to describe the system, as only parameters directly obtained from the measurements were compared. Looking at Figure 13A, it is apparent that vesicles with similar diameters can adhere to the surface with different strengths, which affects the available surface and volume. If these two parameters were considered precisely, a more accurate description of the relative number of proteins per vesicle as well as the number of translocated protons should be possible. When observing the GUVs in a profile view, the shape roughly corresponded to a segmented sphere which was used to model the GUV shape (Figure 14A and B). The GUV diameter d was already obtained from the average Z-projections of the Liss Rhod PE Z-stacks, and the height of the segment h was estimated from the profile views of the GUVs using the line selection tool in FIJI as depicted by the red line in Figure 14B. The obtained heights were smaller than the measured diameters (Table 3), corroborating the use of a segmented sphere as a model to calculate the surface and volume of the GUVs. Note that the estimation of the segment height is rather crude, as the start and end of the line are chosen by hand. Additionally, using a sphere assumes a perfectly circular diameter which is not the case for many of the GUVs (take for example GUV 2 in Figure 13A). The shape of some of the adhered vesicles also resembled more a segmented ellipsoid. Therefore, only a crude estimation of the volume and surface are possible with the obtained measurement but should be sufficient to estimate the number of translocated protons as well as the relative number of proteins per vesicle. More accurate parameters could be obtained by segmentation and 3D volume and surface estimation of individual GUVs. Based on the calculated ΔpH and the estimated GUV volume, the number of protons which need to be translocated was estimated.

To account for the buffering capacity of the solution, the Henderson-Hasselbalch equation was used and 2 mM MOPS and 50 µM HPTS were taken together as one buffering molecule due to the similar pK_a ($\sim$ 7.2)[412] and to simplify calculations. The contribution of the lipids to the buffering capacity was neglected due to the large volume to surface ratio in GUVs and because it may vary depending on the size of the vesicle. For more accurate calculations it should be determined experimentally. From the calculated number of translocated protons and time intervals, the protons translocated per second for each vesicle could be calculated. To estimate the relative number of MPs per vesicle, the average Liss Rhod PE intensity (corresponding to the relative protein density) was multiplied with the GUV surface. All of the measured and calculated parameters are summarized in Table 3. The relative number of proteins was compared to the protons translocated per second per vesicle (Figure 14C). Both parameters were not found to be normally distributed according to a Shapiro Wilk test (p = 0.0314 and 0.0074, respectively). The Q-Q plots are depicted in Figure S20E and F. If all oxidases are pumping with a similar activity, a higher proton translocation per second is expected for a higher relative number of MPs, and indeed a correlation was found for the two variables using one-tailed Spearman correlation (r = 0.7026, n = 21, p = $\sim$ 0.0002). This correlation also seems to be more significant with a lower p-value as the direct comparison of the average Liss Rhod PE intensity and ΔpH (Figure 13C).

Table 3: Measured and calculated parameters for each GUV with cytochrome *c* oxidase activity. Time ΔpH corresponds to the time after cytochrome *c* addition (120 s) until the pH_t was reached, corresponding roughly to the pH at the end of the linear increase after cyt *c* addition and used for calculation of the ΔpH.

Dimater [µm]	Height [µm]	Surface [µm²]	Volume [pL]	Avg. Liss Rhod PE [a.u.]	ΔpH	ΔH^+	Time ΔpH [s]	$H^+ s^{-1}$
5.006	3.8	74.16	0.056	113.467	0.09	3.13E+06	145	2.16E+04
5.103	3.4	72.70	0.052	175.523	0.32	8.79E+06	65	1.35E+05
5.203	3.5	75.94	0.055	139.666	0.28	8.98E+06	55	1.63E+05
5.246	4.3	83.65	0.069	150.648	0.42	1.50E+07	85	1.77E+05
5.786	4	95.15	0.078	150.684	0.64	2.39E+07	100	2.39E+05
6.067	5.1	112.70	0.109	101.191	0.46	2.71E+07	110	2.46E+05
6.321	4.3	112.69	0.100	116.273	0.31	1.75E+07	85	2.06E+05
6.712	4.6	127.52	0.121	134.223	0.33	2.23E+07	75	2.98E+05
6.896	5.2	140.36	0.146	166.18	0.19	1.59E+07	45	3.53E+05
6.989	5.6	147.39	0.160	232.472	0.52	4.39E+07	85	5.16E+05
7.400	6.4	168.89	0.202	128.172	0.63	6.42E+07	80	8.03E+05
7.411	6.3	168.67	0.200	186.127	0.40	4.30E+07	100	4.30E+05
7.443	4.8	152.09	0.154	59.802	0.04	3.52E+06	110	3.20E+04
8.068	4.5	164.50	0.161	264.868	0.47	3.99E+07	70	5.70E+05

Dimater [µm]	Height [µm]	Surface [µm^2]	Volume [pL]	Avg. Liss Rhod PE [a.u.]	ΔpH	ΔH$^+$	Time ΔpH [s]	H$^+$ s^{-1}
8.161	7.4	207.42	0.278	158.067	0.53	7.63E+07	95	8.03E+05
8.345	7.8	217.84	0.301	224.669	0.35	5.60E+07	70	8.00E+05
8.389	4.6	175.99	0.177	192.84	0.48	4.53E+07	80	5.66E+05
8.789	5.2	202.21	0.226	138.629	0.32	4.07E+07	85	4.79E+05
12.258	8.4	425.29	0.738	66.808	0.18	8.15E+07	125	6.52E+05
12.343	9.1	445.58	0.816	104.596	0.24	1.11E+08	85	1.31E+06
14.383	6.7	464.46	0.699	26.865	0.33	1.31E+08	75	1.75E+06

Microfluidic GUVs as a platform for membrane protein measurement

Based on the analysis performed above, it appears that the activity observed in any GUV depends on several factors, which makes it challenging to accurately quantify and compare activities. Based on the performed comparisons, the most important factor seems to be the number of MPs per vesicle which in our setup depends mostly on fusion efficiency of the individual GUVs. However, a rather broad distribution of Liss Rhod PE signals for individual GUVs was observed here as well as in previous experiments, indicating non-homogenous fusion.[430] While the shape and size did not show a direct influence on the ΔpH, it was necessary to calculate the relative number of proteins per vesicle. Certainly, a homogeneous size and lipid composition of the GUVs would be highly advantageous to minimize GUV to GUV variation and simplify calculations. As shown and discussed in the previous chapter, GUVs prepared with electroformation or PVA assisted swelling still show some variation. Highly homogenously looking GUVs have been obtained by microfluidic techniques in the past, but they are not free of problems.[193,239,288,295] So far, very few studies have been published for lipid vesicles produced by microfluidic techniques containing integral membrane proteins. One study shows incorporation of F_1F_0 ATP synthase and integrin in droplet stabilized GUVs produced using microfluidics,[295] while GUVs formed with octanol-based microfluidic techniques have thus far only incorporated α-hemolysin, which spontaneously inserts into the membrane, [239,290,433] to the best of our knowledge. Nevertheless, we were attracted by the system and started a collaboration with Chao Song and Dr. Stavros Stavrakis from the research group of Prof. Dr. Andrew deMello at the ETH Zürich. We decided to produce GUVs using the octanol-assisted liposome assembly (OLA) approach that has been recently developed by Dekker and colleagues[193,221,222,431] and allows the production of monodisperse vesicles. Three solutions are mixed at a six-way junction, an inner aqueous solution (IA), an outer aqueous solution (OA) and the organic phase (LO) which is the lipid-octanol solution (Figure 15). This results in the formation of a double emulsion, from which the octanol is removed by a de-wetting process resulting in solvent-free GUVs. The de-wetting takes place by separation of an octanol pocket, which is spontaneously formed on the GUV membrane. This spontaneous de-wetting process is the main advantage of this octanol-based

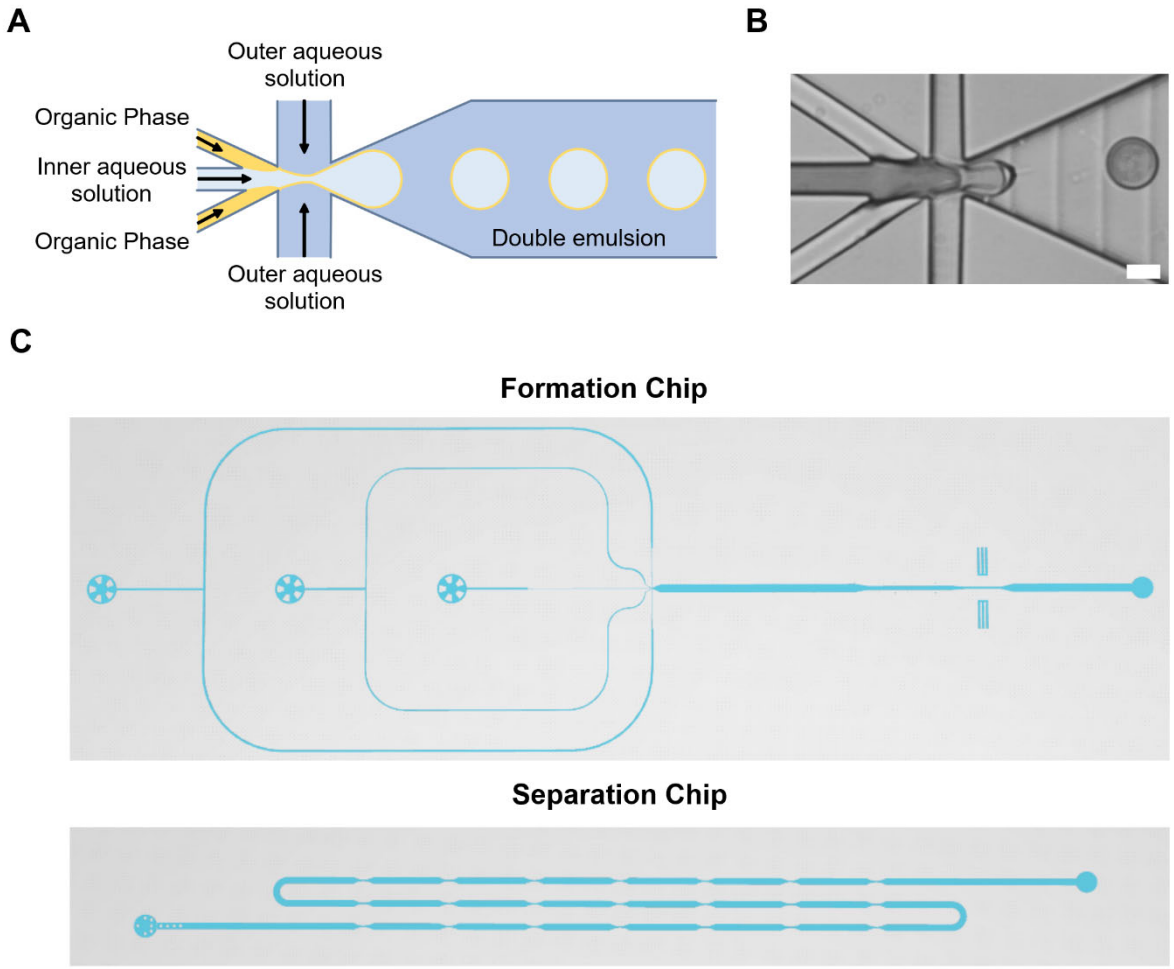

Figure 15: Design of the chips for microfluidic GUV formation. A) Schematic representation of GUV formation using the octanol-assisted liposome assembly approach. Double emulsion droplets are formed at a six-way junction, where an inner aqueous solution (IA), an organic phase which is the lipid-octanol mixture (LO) and the outer aqueous solution (OA) are combined. B) Brightfield view of the formation of the double emulsion droplets. The scale bar is 10 µm. C) Overview of the design of the formation chip, containing three inlets (from left to right OA, LO and IA) and one outlet, and the separation chip with one inlet and outlet and a snake-like path (serpentine module) to help de-wetting of the GUVs from the octanol pockets. The images on this figure were prepared by Chao Song.

system compared to other setups that use solvents different from octanol. The microfluidic chips are made from polydimethylsiloxane (PDMS), the most widely distributed material used in microfluidic research. A critical aspect of the method is the correct surface treatment of the outlet channel with PVA to render it hydrophilic, preventing wetting of the normally hydrophobic PDMS by the hydrophobic LO phase.[287,431] To aid the "on chip" de-wetting process, Dekker and colleagues use surfactants to adjust the interfacial tension, and shear and/or contact with the PDMS surface seem to be involved as well. The reliance on shear and/or contact could be responsible for the extremely low flow rates and precise manufacturing and pumping devices needed in the Dekker design.[288] Another challenge is the "on chip" separation of the freely floating octanol pockets from the GUVs which can be optimized with a few modifications of the chip design and protocol. It has been found that increasing the channel depth and

using higher lipid concentrations in the octanol solutions allows for "off-chip" de-wetting and omitting the use of surfactants.[288] Our collaborators at ETH initially designed the chip based on the original Dekker design for the production of 10 – 20 µm GUVs[193] and modified and optimized the design as well as the formation for "off-chip" de-wetting according to recommendations based on Bao *et al.* (2021).[288] Two forms of de-wetting were investigated. The first method simply involves the collection of GUVs after microfluidic production in PCR tubes, where de-wetting should spontaneously occur, leading to a phase separation of the aqueous solution containing GUVs and octanol (OLA direct). The second approach is based on a serpentine module (Figure 15C) where GUVs are passed through before collection to aid in the de-wetting process (OLA separation), similar to what has been used in a recent publication with a different chip design for octanol GUV formation.[239] The GUVs were then shipped by regular mail from Zurich to Bern for further analysis.

Using our standard GUV characterization approach,[430] the two de-wetting strategies were compared for GUVs from one formation (Figure 16A). Generally, fewer GUVs were obtained from the direct de-wetting approach and most GUVs still had not separated from the octanol pocket, which is visible as a bright spot on the GUVs (Figure 16A top). Analyzing the size distribution (Figure 16A bottom), GUVs that were collected directly after formation showed a narrow distribution with just two distinct populations of vesicles, one in the desired size range and smaller vesicles which might have resulted from bursting of vesicles during formation, transport or transfer to the imaging slide. The GUVs that passed through the serpentine module showed a broader size distribution compared to the directly collected vesicles, but only few octanol pockets were detected indicating an efficient separation process. Compared to a typical PVA formation, relative to the total amount of GUVs produced, many more GUVs are found in the desired size range for both de-wetting approaches. Similar trends were observed for formations performed on other dates. The concentration of GUVs with diameters above 5 µm were further calculated as previously described.[430] It reflects the number of the desired vesicles in the solutions obtained from Chao, created by collecting the outlet of the microfluidic chips into 100 µL outer solution in a PCR tube, after shipping of the GUV samples. Concentrations of 5.68×10^4 and 9.01×10^5 GUVs mL^{-1} were obtained for the OLA direct and OLA separation approach, respectively. The concentration of GUVs from the direct collection was slightly lower than typical concentrations obtained by film hydration methods in our lab while that of the separation approach was in the range of concentrations obtained by electroformation. However, GUV concentrations from microfluidic production depends on several factors such as GUV formation rate and device operation and could be further increased by adjusting these parameters. As depicted in Figure 16B, GUVs produced with the OLA method can be immobilized using the biotin-streptavidin system if biotin containing lipids are added to the LO phase. We also show that OLA produced negatively charged GUVs are competent for fusion with positively charged SUVs containing bo_3 oxidase (Figure 16C).

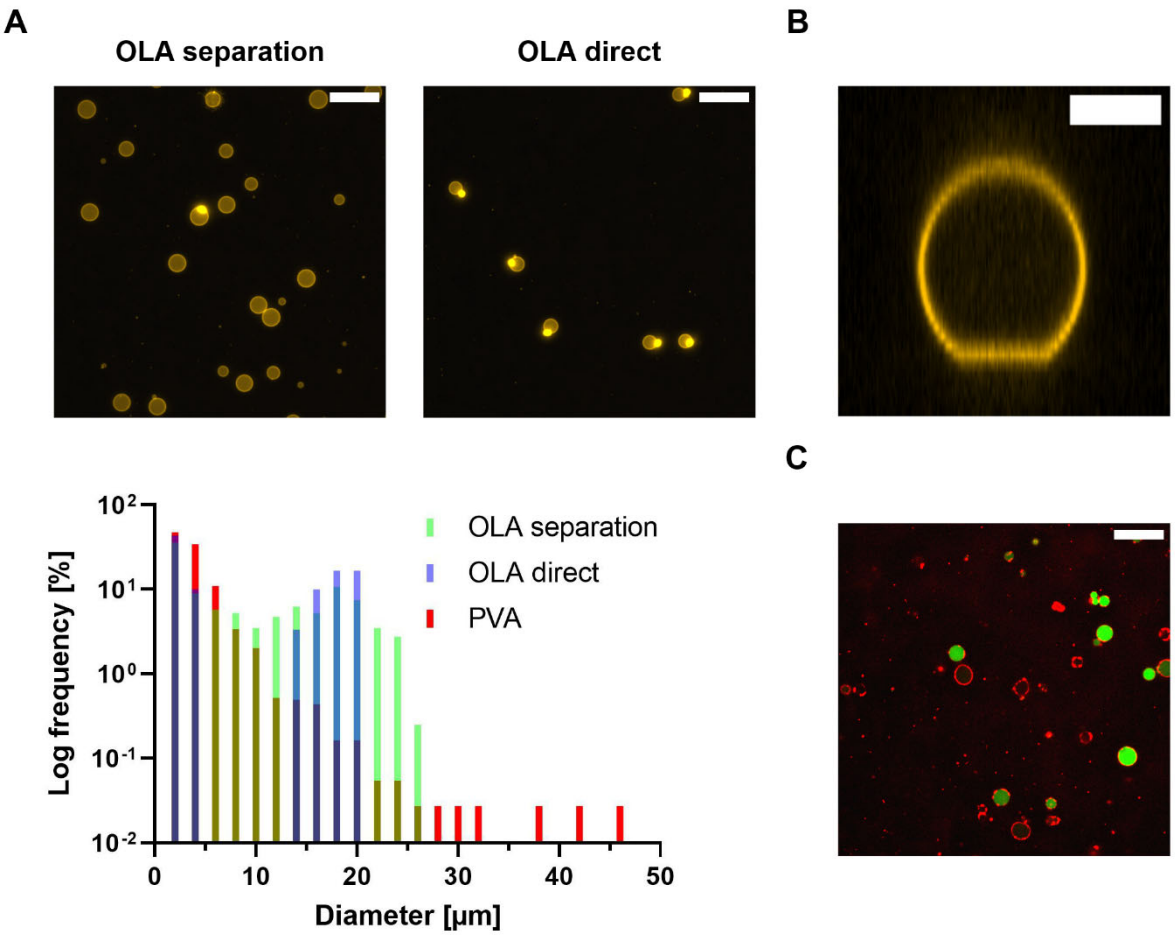

Figure 16: Characterization of GUVs formed by the octanol-assisted liposome assembly method. A) Average Z-projection (top) and histogram of the size distribution (bottom) of microfluidic GUVs containing Liss Rhod PE either collected after passing through a serpentine module for better octanol separation (OLA separation) or by direct collection after the formation (OLA direct). Octanol pockets are visible as bright spots attached to GUVs. The histogram of the diameters obtained from the Z-stack images was prepared with a bin size of 2 µm. The PVA formation data was taken from one of the formations in chapter 3.1.1.[430] The scale bar is 50 µm. B) Profile view of a GUV form the OLA separation formation in A, depicting surface adhesion due to immobilization with biotin-streptavidin. The scale bar is 10 µm. C) Overlay of the DY-647P1 image (red) and HPTS with 470 nm excitation image (green) of OLA separation GUVs fused with SUVs containing labeled bo_3 oxidase via charge-mediated fusion. The scale bar is 50 µm.

Finally, we assessed whether OLA GUVs could be used for measuring proton translocation if HPTS was encapsulated (Figure 17). In a first step, proton translocation was mediated by the ionophore gramicidin. To this end, in GUVs containing HPTS (Figure 17A) formed at pH 7.4, a proton gradient was applied by washing of immobilized vesicles with pH 8.0. After measuring a baseline, addition of gramicidin initiates proton translocation and the ΔpH is dissipated. The obtained ratios were transformed to pH values using the same calibration as for the aa_3 experiments. The obtained pH values do not fit exactly the expected values but are sufficiently close to use the calibration for better visualization. The results indicate that OLA GUVs are capable for proton translocation experiments, as many of the vesicles show an increase in pH after gramicidin addition (Figure 17B). However, the rates of proton translocation seem to vary

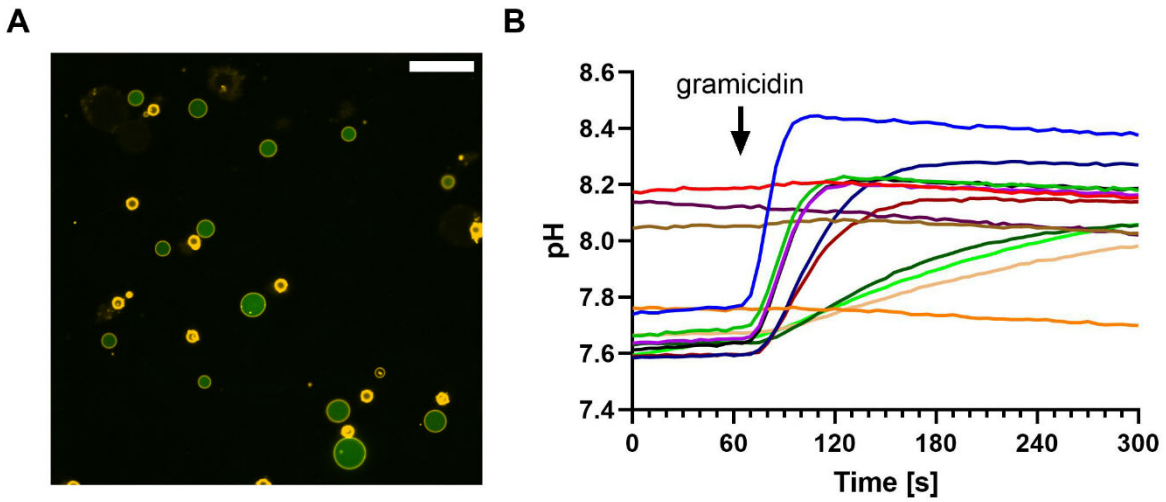

Figure 17: Gramicidin-induced proton translocation in OLA separation GUVs containing HPTS. A) Overlay of Liss Rhod PE (yellow) labeled OLA GUVs with encapsulated HPTS (green) used for the proton translocation measurement. The scale bar is 50 µm. B) GUVs were subjected to a proton gradient with a pH of 7.4 inside and pH 8.0 outside the GUVs. Gramicidin was added after 60 s. HPTS ratios were converted to pH values using the calibration data of GUVs > 10 µm.

rather extensively, and some vesicles seem to have leaked a considerable number of protons as they already show a high pH value before addition of gramicidin.

Discussion

Here, for the first time, we describe successful reconstitution and redox-driven proton translocation of bacterial cytochrome *c* oxidase in giant unilamellar vesicles. Using either carboxyfluorescein or HPTS as pH-sensitive fluorescent dye, successful transport was observed. However, several challenges were encountered during the process. In both cases, soluble dye was encapsulated in GUVs during PVA assisted swelling and GUVs were immobilized using biotin-streptavidin for observation of proton translocation. Charge-mediated fusion of positively charged SUVs containing MP with negatively charged GUVs was performed on the microscopy slide after immobilization. For both dyes, a considerable number of vesicles without encapsulated dye was observed after fusion which was likely the result of fusion-induced dye leakage as observed during live monitoring of the fusion process. This has been previously observed in our lab[434] and others,[435] while charge-mediated fusion of GUVs and SUVs without leakage has also been shown.[390] Loss of encapsulated dye makes it impossible to measure MP function and reduces the number of vesicles that can be analyzed. Even though we used streptavidin concentrations which should not lead to strong adhesion, some leakage of dye may also have occurred due to immobilization.[430]

As seen in experiments with carboxyfluorescein, the behavior of individual GUVs can be rather complex, complicating analysis if few (< 10) GUVs are evaluated. This was slightly improved for measurements with HPTS where about 15 – 20 GUVs were evaluated for each condition. Thus, the first challenge is obtaining a sufficiently large number of vesicles for measurements to be able to perform meaningful statistical analysis, ideally, we would suggest at least 20 or more vesicles should be observed. Based on the GUV concentration, the magnification and leakage of encapsulated dye, there are limitations in the number of usable GUVs that can be obtained in one field of view (FOV). High GUV concentrations are beneficial as a high density of GUVs can be obtained in the imaged area and the number of usable vesicles might be reduced during the experiment due to washing or leakage of encapsulated dye. Using a 20x magnification, more GUVs are visible in one FOV, but for accurate determination of the volume and surface of vesicles in the desired size range (5 – 20 µm),[430] a 40x magnification or even 60x magnification are more appropriate, reducing the imaged area and thus the number of GUVs per FOV. Multi-point acquisition is possible if a low frequency of time points is required, e.g., every five seconds as done in the activity measurements with HPTS, increasing the number of GUVs for analysis. The number of locations and the frequency of time points are limited by the exposure time as well as the number of wavelengths that need to be recorded, as adjustment of the filter cubes for different wavelengths and moving of the stage both requires some time, up to one or two seconds. Long exposure times might be needed if weak fluorescence signals are observed, which reduces the time window to change wavelength or move the stage. Another possibility of achieving high numbers of vesicles in the FOV would be microfluidic trapping where GUV are not immobilized by chemical bonds, but trapped

within specific structures on a microfluidic chip.[373,387–389] Next to a more complicated setup using microfluidic pumps, a major concern is a non-homogenous buffer/substrate exchange among the GUVs, as most trapping devices do not allow fast flow rates to prevent GUV deformation or removal from the traps.[389,391] However, more complicated setups with fast exchange rates have been described.[388,390] Immobilization with biotin-streptavidin thus remains a valuable alternative, but a high starting concentration of GUVs is important and multi-point acquisition may be necessary to obtain a good number of GUVs.

Measurements of proton translocation with CF showed low signal-to-noise ratios and illustrates that an adequate detection system is of importance for measuring MP function in GUVs. Although the observed traces do seem to suggest that some proton activity was measured, the resulting signal changes were rather small and sometimes not entirely clear, especially in the negative control using empty SUVs for fusion. CF was mainly chosen based on previous bulk experiments of aa_3 oxidase in SUVs using bifunctional DNA duplex probes, where CF is anchored to the membrane by a cholesterol-modified DNA.[174] This was done in the hope to achieve comparable results in GUVs and SUVs, but we were suspecting that CF might not be ideally suited for GUV experiments due to its known tendency for fast bleaching, which further complicated analysis. There are methods to correct for bleaching, but these might affect the data in undesired ways.[436,437] The use of ratiometric pH-sensitive dyes such as HPTS reduces the problems of bleaching or non-homogenous incorporation of dye, as measurements of the emission from two different excitation wavelengths delivers a ratiometric signal that is not affected by dye concentration or bleaching. Surprisingly, we found that the HPTS ratio was strongly affected by the GUV size when a calibration curve was recorded, especially at low pH values. GUVs with apparent diameters below 10 µm showed an increased 470/395 nm ratio. Inspecting the values from the individual excitation wavelengths, an unexpected trend was observed for those GUVs mainly at 395 nm excitation with almost no change in intensity, while GUVs > 10 µm showed the expected decrease at high pH values. The intensity at 470 nm excitation increased for high pH values for both small and large GUVs as expected. Combined with the overall heterogeneity of HPTS ratios observed, obtaining an accurate pH calibration seems thus challenging. Previous publications using HPTS to measure MP activity in GUVs have not performed ratiometric measurements, but focused on the excitation at 488 nm, likely due to limitations in the microscope setup.[204,326,351] Although Altamura *et al.* (2017) used confocal microscopy to record the calibration, only single values are shown for HPTS emission at different pH values and it is not clearly stated how these single points were obtained from the GUV images.[351] Almendro-Vedia *et al.* (2017) recorded HPTS calibration data at different concentrations of dye to adjust for the inefficient and inhomogeneous encapsulation during electroformation, which is a time-consuming and not a practical approach for general use.[326] Thus, ratiometric measurements might be the preferred strategy as it is fast and simple. Ratiometric pH calibration was shown by Lee *et al.* (2018)

using SNARF-1 that has two different emission peaks for the same excitation. However, no information is given on ratio heterogeneity between different GUVs. Interestingly, only GUVs with sizes from 15 – 30 µm were selected for calibration.[98] A further alternative are dyes that are less prone to bleaching, such as pHrodo™ or Oregon Green 488.[165,166]

Despite the difficulties with the HPTS calibration in GUVs and differences in buffer composition and imaging conditions, a linear regression was used to fit the calibration data for GUVs above 10 µm, as they displayed the expected behavior for both excitation wavelengths. The fit was then used to convert the signal ratios observed for proton translocation experiments using cytochrome *c* oxidase into pH values. Given the problems stated above, the absolute values of these numbers should be taken with some reservation, but they clearly visualize the potential for analysis approaches for proton translocation measurements by MPs in GUVs. The starting ratios from the proton translocation measurements matched well with the expected pH value and comparison of relative differences between vesicles are possible. To correlate proton translocation to protein activity, lipid-coupled dye in the SUVs was used to determine the relative extent of fusion between vesicles to estimate the relative protein density in the GUVs according to previous findings.[430] A significant correlation was found comparing directly the lipid-coupled dye signal with the observed ΔpH values. Such a correlation can be expected if GUVs have similar leakiness towards protons, which we recently demonstrated,[430] and if all of the incorporated MPs are equally active. It further depends on an equal co-insertion of MP and lipid-coupled dye for each fusion event, further supporting our previous hypothesis that the protein concentration in GUVs can be estimated by lipid-coupled dye incorporated in SUVs.[430] However, these direct comparisons still showed a rather large heterogeneity, showing that these parameters alone were not sufficient to describe our system. By further characterizing the shape of the individual vesicles to estimate volume and surface, the relative protein number and the number of translocated protons per second could be calculated, resulting in an even more significant correlation. From this, a stronger conclusion can be made that indeed, MPs have similar activities in GUVs, and vesicles are similar in terms of proton tightness. The calculated numbers were in the range of twenty thousand to almost two million protons per second. Theoretically, proteo-SUVs were reconstituted with approximately three proteins per vesicle for the activity measurements with HPTS. Further, a diameter of 50 nm was estimated for the SUVs as liposomes were prepared by sonication. Based on the calculated surfaces of the GUVs and SUVs as well as the charge of the vesicles (30 mol% charged lipids), the observed GUVs should be able to undergo $\sim 10^4$ - $\sim 6 \times 10^4$ rounds of fusion until the number of negatively and positively charged lipids are equal. With three proteins per vesicle and assuming described orientation (70 % outwards cyt *c*-binding site),[438] each SUV would on average introduce two proteins into the GUV with the cyt *c*-binding site on the outside. Using these values, an average activity of 1 to 20 protons translocated per second per enzyme is obtained, which is a reasonable, but rather low activity, as cytochrome *c*

oxidase has been shown to pump up to several hundreds of protons per second.[439,440] There are several reasons to explain this low activity. As discussed above, the pH calibration might not be very accurate leading to incorrect ΔpH values. Further, in our experiments following the lipid-coupled dye, we cannot distinguish between full fusion or hemifusion/adhesion, with the latter not contributing to proton pumping activity of the GUVs.[430] Thus, the concentration of functionally active MPs might be smaller than expected. Fusion might also not progress until all the opposite charges are equalized and stop earlier as attractive forces between the vesicles get too weak. This is likely, as charge mediated fusion was not observed below 10 % negatively charged lipids.[80] However, it is also possible that the enzyme activity is decreased in the GUV membrane, i.e. due to reduced binding of the positively charged cyt *c* to the GUVs containing positively charged lipids after fusion. Finally, the assumed buffer capacity is too low (e.g. buffering capacity for lipids was neglected) and more protons are pumped to obtain the observed pH change. This calculation could be improved by experimental determination of the buffer capacity. Until these issues are resolved, we believe that judging the quality of the activity measurements in GUVs and the relation to data observed in SUVs remains challenging. Unfortunately, a direct comparison to previously reported measurements of cytochrome *c* oxidase inside SUVs using a bifunctional DNA duplex probe labeled with carboxyfluorescein[174] is not possible as both measurements using CF and HPTS in GUVs were not performed under identical conditions as described for the SUV measurements, although it does appear that the signal plateau is reached much faster in SUVs (< 5 s) compared to GUVs containing CF (~ 30 s) or HPTS (> 100 s), indicating that the reaction in SUV stops earlier due to the smaller vesicle volume. However, these differences may also be explained by different buffer concentrations, pH values, and which substrate was used to start the reaction. Thus, for comparison of GUV and SUV data, it is crucial that the experiments are performed as identical as possible. Overall, our experiments indicate that a detailed characterization of the individual GUVs is beneficial to relate the observed activities of different vesicles.

Several of the observed difficulties in data analysis are related to the size of the vesicles. Thus, measuring MP function in vesicles with a controlled size will simplify data acquisition and analysis. An attractive method to control GUV size are microfluidic formation methods. Our collaborators at ETH Zürich were able to produce fusogenic GUVs with a narrow size distribution by modification of the octanol-assisted liposome assembly approach pioneered by Dekker and colleagues.[193,431] Removal of the octanol pocket was improved by passing the vesicles through a serpentine module after formation, although slightly broadening the size distribution. Compared to PVA formation, the frequency of GUVs obtained in the desired size range of 5 – 20 µm, corresponding to the size of many eukaryotic cells, is much higher for the OLA formation. The GUVs further seem to be suitable for measuring proton translocation. A next step will be to measure the function of cytochrome *c* oxidase in those GUVs. As detailed in the results, reports with integral MPs incorporated in GUVs produced by microfluidic formation methods are rare.

One of the main concerns is an incomplete de-wetting process, resulting in residual octanol that could negatively impact the integrity of the GUV membrane or the MP activity. At this time point in my PhD, I had to interrupt these experiments to write the PhD thesis, but I will continue them after the exam.

Conclusion and Outlook

Here we reconstituted cytochrome *c* oxidase from *Rhodobacter sphaeroides* into GUVs using charge-mediated fusion. Redox-driven proton translocation was measured using two different pH-sensitive fluorophores, carboxyfluorescein and HPTS. Although enzyme activity could be detected using both dyes, only small signals were observed with CF where bleaching and unclear single GUV traces in the negative control further complicated analysis. Thus, HPTS was selected for further experiments as it can be measured ratiometrically by excitation at two different wavelengths, which allows recording of a calibration curve independent of the dye concentration and simple removal of bleaching as the ratio should not be affected by it. While the latter was indeed the case, some challenges were observed with recording a calibration curve as the size of the GUVs affected the observed HPTS ratio. Despite that, measurements with cytochrome *c* oxidase in GUVs containing HPTS were performed. Even though the accuracy of the pH values is questionable, the data seems to indicate cytochrome *c* oxidase activity. By measuring a lipid-coupled dye introduced into the GUVs via fusion, we were able to infer relative protein concentrations which were correlated with the observed activities by considering the shape and size of the vesicles as well. As we found that several parameters seemed to be affected by the vesicle size, we turned to microfluidics for GUV formation in collaboration with members of the deMello group from the ETH Zürich. We could show that GUVs produced by the octanol-assisted liposome assembly method have a narrow size distribution, are fusogenic and could potentially be used for proton translocation measurements.

Several steps are required to improve the result obtained from proton translocation measurements by MPs in GUVs. First, determination of the number of protons translocated in each vesicle requires more accurate calibration data. Alternative fluorophores such as the ratiometric dye SNARF-1 should be tested to obtain a calibration curve that is independent of GUV size and buffer composition. Experimental determination of the contribution of the lipid membrane to the buffering capacity will further improve the calculation of the translocated number of protons. This contribution may vary depending on the size of the GUV as well as the lipid composition, which may be different in each vesicle due to varying fusion efficiencies (due to varying incorporation of positively charged lipids) or inhomogeneous lipid distribution during GUV formation. For a more accurate estimation of the amount of reconstituted MP in the GUV membrane, determination of the number of fusion events will be necessary. A calibration of the lipid-coupled dye signal in GUVs will allow to estimate the number of potential fusion events, but may not be able to distinguish between full fusion which is required for functional incorporation of MP.

This might be achieved using content mixing assays, although they are not trivial as the often negatively charged cargo can interact with the positively charged lipids. Recently, esterase's have been used to assess content mixing for fusion of cell-derived vesicles with GUVs.[441] Encapsulating enzymes in SUVs used for GUV fusion is thus a potential strategy to demonstrate content mixing, although it may still be inaccurate if a certain population of SUVs are empty for example. To limit the effect of size on the experiment and data analysis and decrease GUV to GUV variation, cytochrome *c* oxidase has to be reconstituted in GUVs with a more homogeneous size distribution, as obtained by microfluidic formation for example. While these GUVs appear to be suitable for proton translocation experiments, there is still room for improvement. De-wetting with the serpentine module reduced the number of octanol pockets, but also broadened the size distribution which is undesirable. If this broadening is caused by vesicles rupturing into smaller vesicles or by pore formation and vesicle shrinkage, this may also lead to a loss of encapsulated dye which is detrimental for MP measurements. Increasing the concentration of microfluidic GUVs will be beneficial for MP measurements, but it will be important to retain the quality and narrow size distribution as observed in the vesicles presented here. This may require further optimization of the devices and device handling, for example coating of the serpentine module with PVA or BSA may reduce negative interactions with PDMS to retain membrane integrity during the separation process.

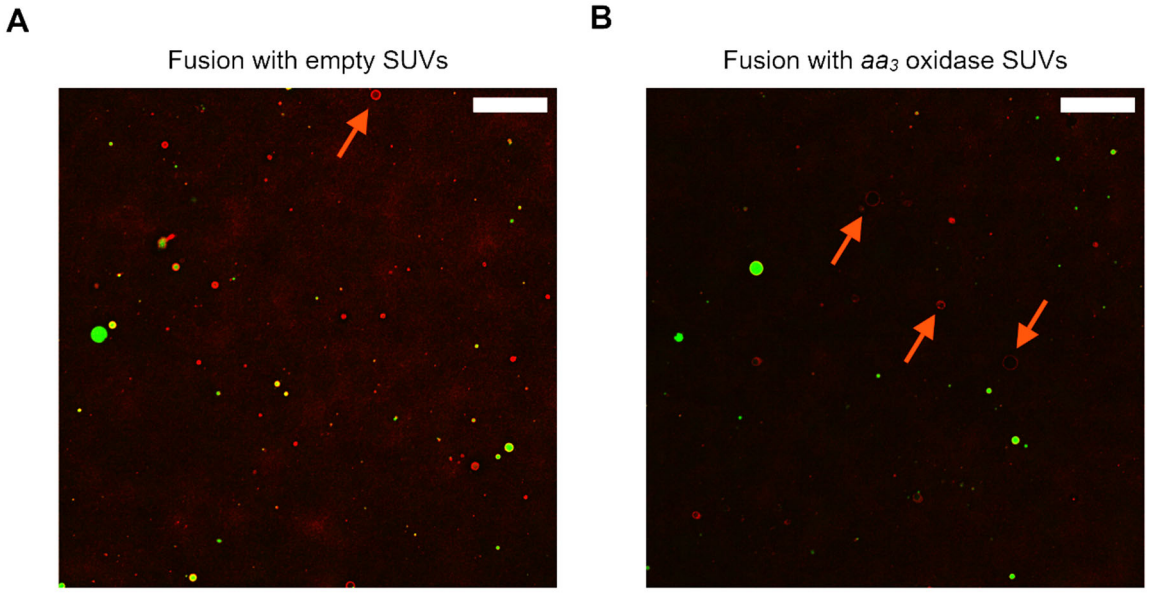

Figure S16: Fluorescence microscopy image overlay of GUVs fused with either SUVs containing *aa_3* oxidase or empty SUVs. Images were recorded in widefield mode. Liss Rhod PE signal is depicted in red (GUV membrane) and CF in green. Orange arrows indicate GUVs with leaked CF. The scale bar is 100 µm.

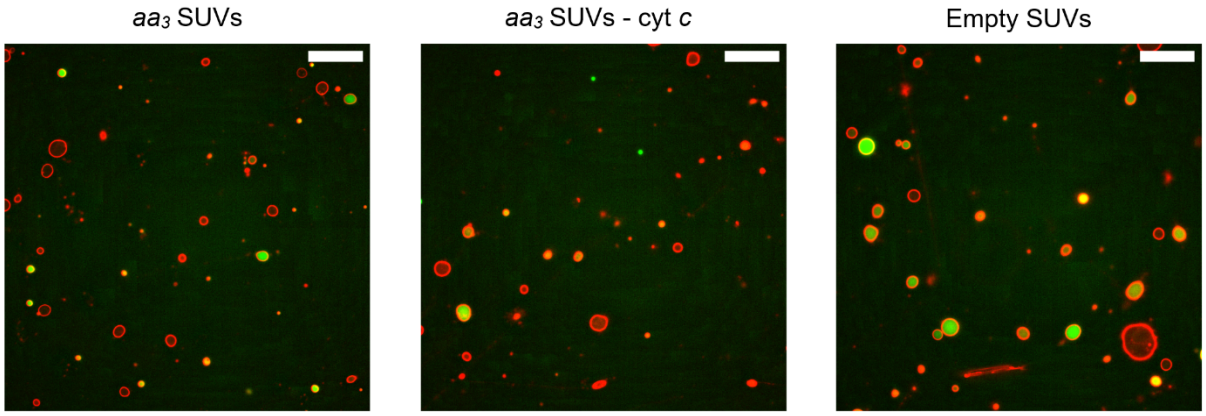

Figure S17: Fluorescence microscopy image overlay of GUVs fused with either SUVs containing *aa_3* oxidase or empty SUVs. HPTS images were recorded in widefield mode and Liss Rhod PE in confocal mode. Liss Rhod PE signal is depicted in red (GUV membrane) and HPTS in green using the 470 nm excitation image. The scale bar is 50 µm.

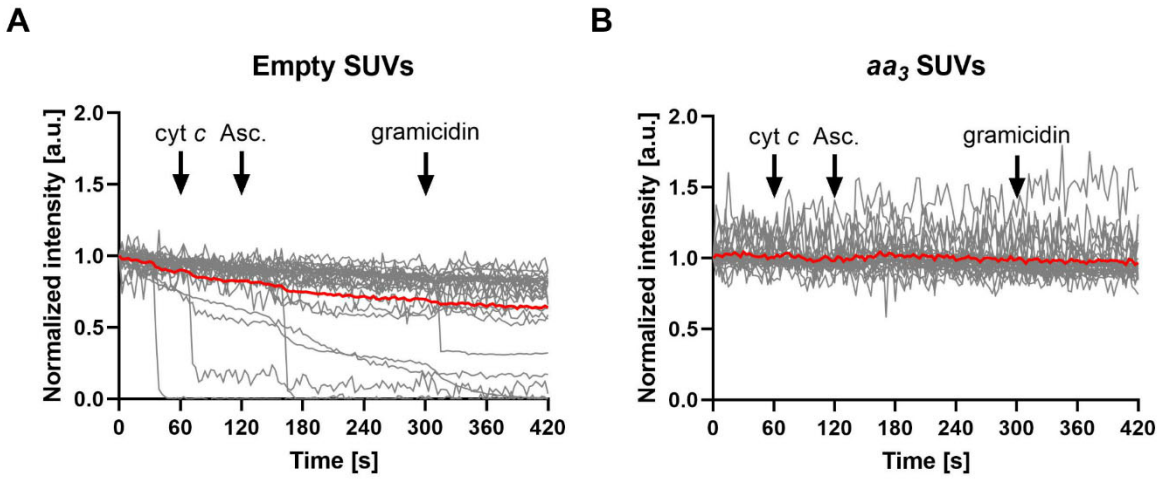

Figure S18: Proton pumping of cytochrome *c* oxidase in GUVs monitored using encapsulated CF. GUVs fused with SUVs containing aa_3 oxidase or as a negative control empty liposomes were measured. Proton pumping was initiated by addition of 12 µM cyt *c* followed by the addition of 4.7 mM Na-ascorbate (Asc.). The proton gradient is dissipated by the addition of 12 µM gramicidin. A) Individual (grey) and mean (red) traces of all detected GUVs fused with empty SUVs or B) with proteo-SUVs.

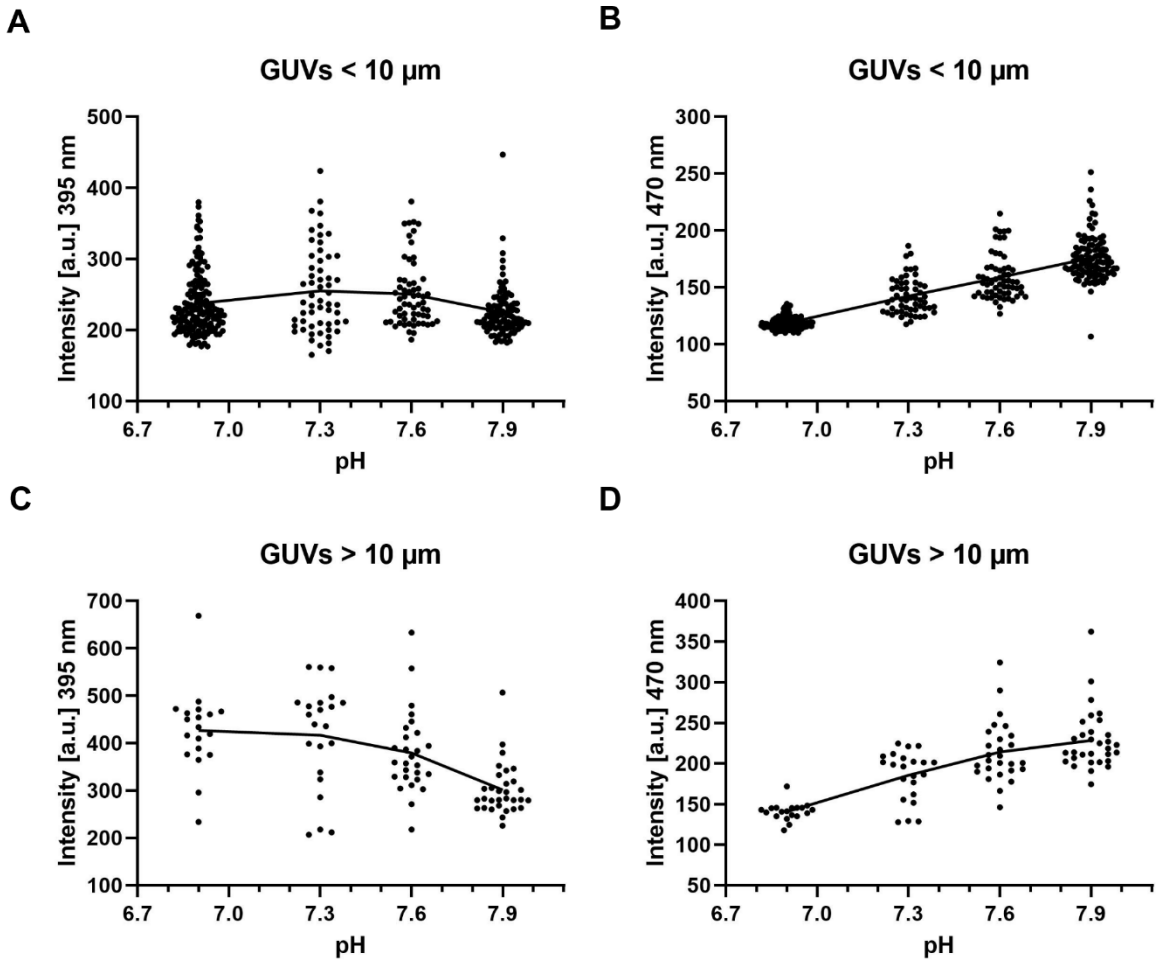

Figure S19: HPTS intensity distribution in GUVs. HPTS was measured at different pH values with 395 nm excitation (A, C) and 470 nm excitation (B, D). Each dot represents a single GUV and the line connects the mean intensities. A and B) Distribution of

intensities for 60 – 160 GUVs with apparent diameters below 10 µm. C and D) Distribution of intensities for 20 – 30 GUVs with apparent diameters below 10 µm. Apparent diameter represents the diameter of a GUV in the focal plane.

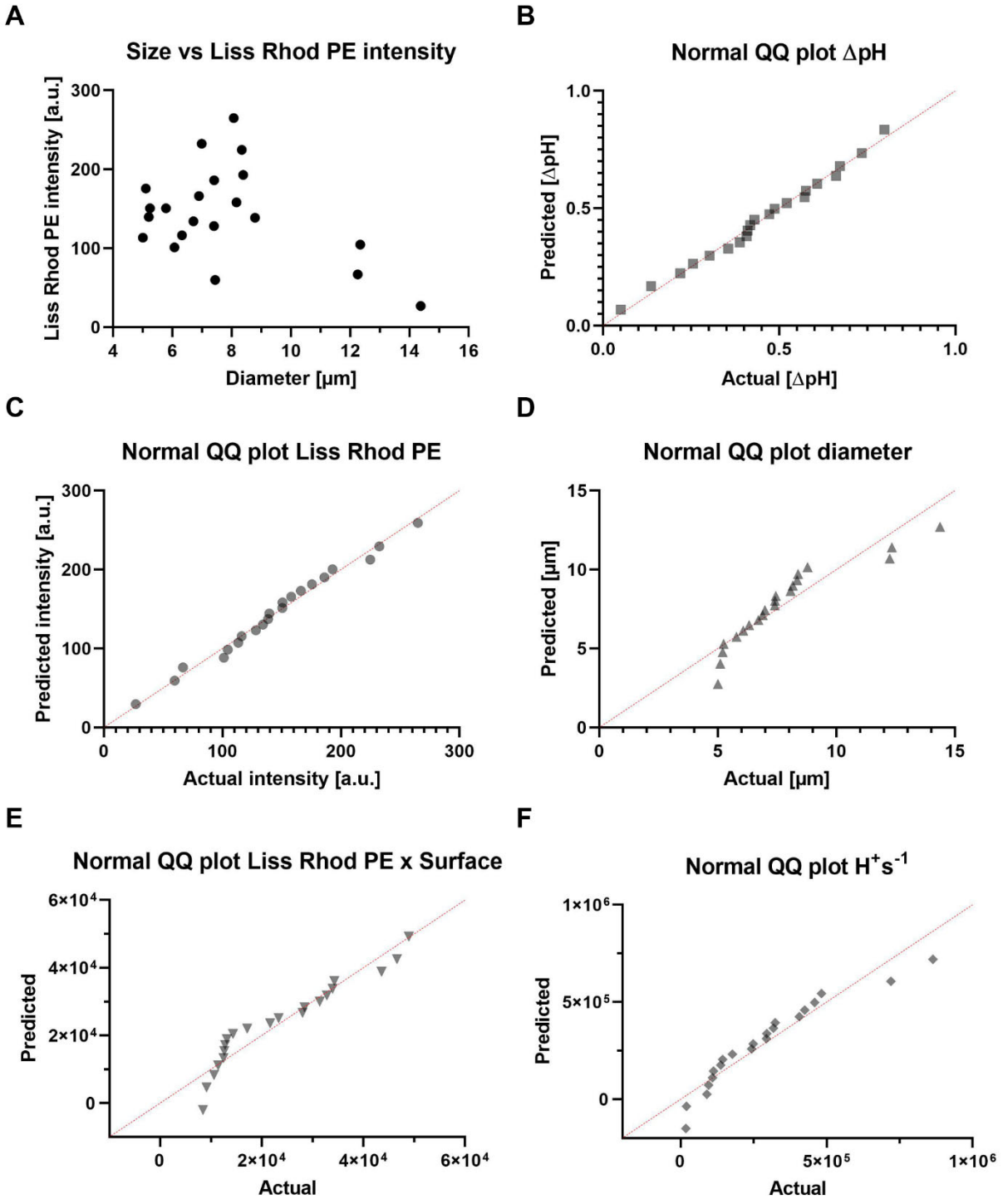

Figure S20: Correlation and QQ plots to assess normality of data. A) Correlation of GUV diameter with average Liss Rhod PE intensity (One-tailed Spearman r = -0.1130, n = 21, p = ~ 0.3129). B-F) Normal Q-Q plot of ΔpH (B), average Liss Rhod PE intensity (C), diameter (D), average Liss Rhod PE intensity multiplied by the surface (E) and protons translocated per second (F).

3.2. Bifunctional DNA Duplexes for the Measurement of Membrane Protein Function in Liposomes.

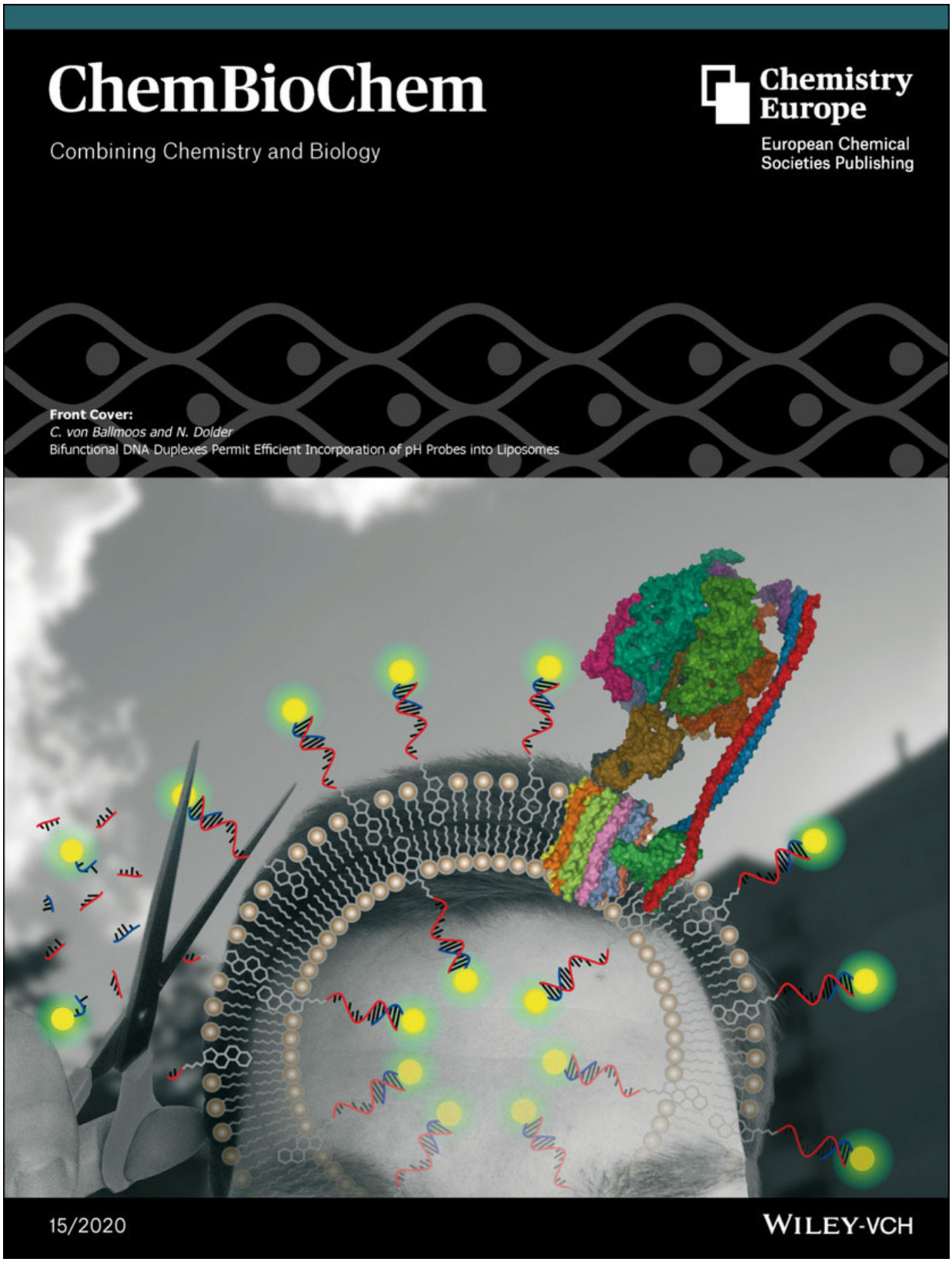

3.2.1. Bifunctional DNA Duplexes Permit Efficient Incorporation of pH Probes into Liposomes

Title: Bifunctional DNA Duplexes Permit Efficient Incorporation of pH Probes into Liposomes

Journal: ChemBioChem

Status: Published, March 2020

Authors: Nicolas Dolder, Christoph von Ballmoos

Contribution: Christoph von Ballmoos (CvB) conceived and supervised the study; CvB and Nicolas Dolder designed experiments; Nicolas Dolder performed the experiments and analyzed data, CvB and Nicolas Dolder wrote the manuscript and made manuscript revisions.

Abstract

Enzyme-mediated proton transport across biological membranes is critical for many vital cellular processes. pH-sensitive fluorescent dyes are an indispensable tool for investigating the molecular mechanism of proton-translocating enzymes. Here, we present a novel strategy to entrap pH-sensitive probes into the lumen of liposomes that has several advantages over soluble or lipid-coupled probes. In our approach, the pH sensor is linked to a DNA oligomer with a sequence complementary to a second oligomer modified with a lipophilic moiety that anchors the DNA conjugate to the inner and outer leaflet of the lipid bilayer. The use of DNA as a scaffold allows subsequent selective enzymatic removal of the probe in the outer bilayer. The method shows a high yield of insertion and is compatible with reconstitution of membrane proteins via different methods. The usefulness of the conjugate for time-resolved proton pumping measurements was demonstrated by using two large membrane protein complexes.

Introduction

Protons are the smallest chemical molecules, but they are highly relevant in various aspects of biological life. The concentration of free protons in an aqueous solution determines its pH and regulates the enzymatic activity and stability of all proteins. In addition, protons play important roles in transmembrane transport processes. Not only are proton pumps used to establish and maintain the essential electrochemical gradient, but protons also serve as coupling ions in secondary transporters that use the electrochemical gradient to, for example, enrich important substrates in biological compartments.[442,443] An impressive example of a proton coupled system are the members of the respiratory chain and the F_1F_0 ATP synthase found in the inner membrane of mitochondria or the cytoplasmic membrane of bacteria. These large multi-subunit complexes are responsible for the energy conversion of food-derived reduction equivalents (e.g., NADH) into the universal energy currency of the cell, adenosine triphosphate (ATP),[444] that energizes a wide variety of cellular reactions including nutrient uptake, nerve conduction and muscular motion. During this process termed oxidative phosphorylation, respiratory chain complexes I to IV transfer electrons from NADH and succinate to oxygen in a stepwise manner.[445] These exergonic processes are coupled to transmembrane proton pumping that establishes and maintains an electrochemical proton gradient (proton motive force, *pmf*) that is used by the rotating F_1F_0 ATP synthase to regenerate ATP from ADP and inorganic phosphate.[446]

Not surprisingly, measurement of these transmembrane proton movements are key experiments to understand the molecular mechanism of these and many other membrane proteins. Typically, after purification in detergent solution, membrane proteins are reconstituted into liposomes, imitating their native environment for functional analysis. Proton transport activities are measured with soluble pH-sensitive dyes that are incorporated into the liposomes and detected either via absorbance or fluorescence measurements.[87,91,151,447] After reconstitution, the non-incorporated dye has to be removed by gel filtration or ultracentrifugation or a combination of both. While convenient, the method suffers from poor incorporation yield (< 5 %) of the dye which is not desirable if precious dyes are used. Furthermore, many dyes (e.g. containing carboxylic acids) tend to cross the membrane over time,[165,166] rendering this technique somewhat inefficient. Recently, pH-sensitive fluorophores such as Oregon Green 488 or pHrodo coupled to a phosphatidylethanolamine lipid have been used to follow the activity of ATPases.[165,166,187] In contrast to freely soluble dyes, lipid-coupled dyes incorporate into the membrane of the liposome with very high yield. However, as lipid orientation is random during liposome formation, the dye will be evenly distributed in both membrane leaflets. As only the pH of the inside of the liposome changes during proton transport (the outside is buffered), the constant signal of the dye in the outer leaflet is expected to affect the overall signal-to-noise ratio of the proton transport signal.[166]

Here, we present a method using commercially available tools to circumvent this drawback. Using cholesterol modified DNA-oligomers and complementary DNA-carboxyfluorescein conjugates, the dye is incorporated in both leaflets during reconstitution. In a follow-up step, the DNA embedded in the outer leaflet is digested by DNase I and liposomes containing dye solely on the inner leaflet can be obtained by ultracentrifugation (Figure 18A). Using two large multi-subunit membrane protein complexes from bacterial respiratory chains, F_1F_0 ATP synthase and cytochrome *c* oxidase, we show that transmembrane proton pumping can be followed into either direction and that the signal-to-noise ratio is improved in the DNase I treated samples. Additionally, a probe with a different pH-sensitive dye, namely CypHer5E, was synthesized showing the versatility of the presented approach.

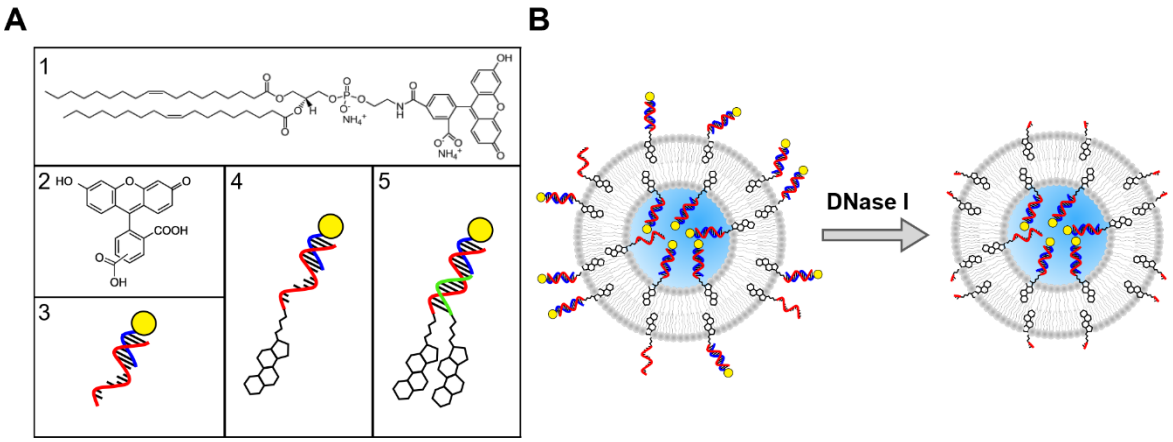

Figure 18: Scheme of the different CF variants and of the dye removal by DNase I. A) Schematic representations of the different CF variants added to the liposomes. 1 = 18:1 PE CF, 2 = CF, 3 = ON-CF, 4 = LON-CF, 5 = L_2ON-CF. For the LON probes, the DNA strands are shown in red, blue and green, CF is depicted as a yellow dot. B) Scheme of the dye removal by DNase I treatment of vesicle incorporated LON-CF.

Results and Discussion

In the past, lipophilic oligonucleotides (LON's) have been used in a variety of studies. Examples are immobilization of lipid vesicles to solid surfaces or supported bilayers, tethering of liposomes to induce membrane fusion or functionalizing of vesicles with different nanostructures.[448–451] LON's have also been used to immobilize biosensors for ions or small molecules.[160,177,452,453] Being commercially available, DNA modified with cholesterol has been used in many of these studies and the influence of using one or two cholesterol moieties for membrane-anchoring has been compared.[454]

Here, the following commercially available DNA oligomers have been used. A 30-nt-long oligo, either unmodified (ON*1*) or modified with cholesterol at the 3'-end (ON*2*) has been used as the scaffold for the lipophilic probe. The pH-sensitive dye 5(6)-carboxyfluorescein was coupled to the 3'-end of an 18-nt oligo (ON*3*) that is complementary in sequence to the 5'-end of oligos 1 and 2 (apparent melting temperature 37.8 °C of the pairing region). Additionally, a cholesterol modified oligo at the 5'-end (ON*4*) that is complementary to the 3' region of oligos ON*1* and ON*2* was used to build the lipophilic probe with two cholesterol moieties (apparent melting temperature of 40 °C). An overview of the different probes is given in Figure S21 in the Supporting Information. The respective complementary oligos were allowed to hybridize for 10 min at room temperature and hybridization was confirmed using TBE 20 % polyacrylamide gel electrophoresis (Figure S22).

In a first series of experiments, the incorporation efficiency of the different lipophilic probes into liposomes was compared to free and lipid anchored carboxyfluorescein (CF). The variants comprised of free CF, CF coupled to a lipid (18:1 PE CF), CF coupled to DNA without (ON-CF), with one (LON-CF) or with two cholesterol-moieties (L_2ON-CF) and were incorporated into unilamellar 1,2-dioleoyl-sn-glycero-3-phosphocholine (DOPC) vesicles. In addition, liposomes also contained 0.03 mol% TexasRed™-labeled lipids (TR-DHPE) that was used to normalize for lipid loss or dilutions during the procedure. Schematic representations of the different variants can be seen in Figure 18A. The lipid-coupled dyes (18:1 PE CF and TR-DHPE) were mixed with DOPC in chloroform prior to lipid drying, while all other variants were added in the rehydration buffer used to form the liposomes, as described in the Methods section. Addition of the DNA containing variants to the lipids prior to drying using an organic solvent mixture (chloroform: methanol: water = 6.25:6.25:1*, v/v/v*) was abandoned after initial trials, as no improvement over addition to the rehydration buffer was observed. However, we note that it is also possible to add the DNA conjugates at an earlier step prior to drying, which might be useful for other applications or LON probes. After rehydration, 100 nm unilamellar liposomes were produced using the freeze-thaw and extrusion method, split into two fractions to which either DNase I or water was added and incubated for 20 min at 37 °C (Figure 18B). Subsequently, free dye was removed by ultracentrifugation and pelleted liposomes were resuspended, mixed with measuring buffer and carboxyfluorescein and TexasRed™

fluorescence was measured. Relative recovery of CF was calculated as the intensity ratio of the sample after and before the centrifugation. The liposome recovery was calculated similarly using the TR-DHPE intensities after and before the centrifugation. Finally, incorporation yield of CF into liposomes was determined as the ratio of CF and liposome recovery (Table 4).

The results are shown in Table 4. Not surprisingly, lipid-coupled CF is fully incorporated into the vesicles while only very little free CF is incorporated (~ 3.5 %), and both values were unaffected by DNase I treatment. Surprisingly, ~ 17 % of fluorophore coupled to DNA (ON-CF) was found in the preparation without DNase I treatment, while only ~ 4.5 % was left after the nuclease treatment, indicating an unspecific interaction of the DNA with the zwitterionic membrane as observed earlier.[455] Finally, the assembled lipophilic probes (LON- and L_2ON-CF) were incorporated to > 80 % before and 40 % after DNase I treatment, respectively. These values represent good incorporation of the dye via the cholesterol moiety and successful DNA cleavage after treatment. The non-incorporated 15 - 20 % indicate that free DNA-fluorophore-conjugate is present or that some of the DNA-pair contains no cholesterol moiety (the DNA conjugates were used as obtained by the company). Alternatively, a small portion of the DNA-pair might have partitioned into the aqueous phase due to the hydrophilic nature of the DNA moiety.

Table 4: Incorporation yields of different CF variants into liposomes. The incorporation was calculated as detailed out in the text. Each sample (extruded liposomes, liposomes with DNase I treatment, liposomes without DNase I treatment) was measured three times and three separate experiments were performed.

No.	Dye variant	Without DNase I		With DNase I	
1	18:1 PE CF	103.5	± 11.5 %	102.0	± 10.8 %
2	CF	3.4	± 0.3 %	3.6	± 0.3 %
3	ON-CF	16.6	± 1.6 %	4.5	± 0.4 %
4	LON-CF	81.7	± 8.8 %	43.0	± 5.9 %
5	L_2ON-CF	84.7	± 11.8 %	37.8	± 4.3 %

In an earlier study[454] a DNA trimer containing two cholesterol moieties was found to yield a more stable incorporation of the DNA in the membrane than a single cholesterol conjugate, but in our experiments, no significant difference between the two corresponding constructs LON-CF and L_2ON-CF was observed. In the original article, incorporation into planar, supported lipid bilayers was investigated, while spherical vesicles were used here. As no significant difference was seen between the two conjugates, LON-CF was used in the remainder of the experiments.

It has been reported that pH-sensitive groups coupled to lipid headgroups change their apparent pK_a (up to several pH units) when incorporated into liposomes, likely due to the influence of the nearby

membrane surface.[165,166] In the worst case, this effect shifts the detectable pH range outside the experimental conditions. In our scenario, the dye is expected to be several nanometers away from the membrane surface and thus to be unaffected by it. Nevertheless, in the next series of experiments, the useful pH range of the reconstituted DNA-carboxyfluorescein dye was determined. To this end, we reproduced the elegant experiment with lipid-coupled Oregon Green reported by Schwamborn *et al.*[166] CF and Oregon Green have very similar characteristics, exhibiting high fluorescence at neutral to alkaliphilic pH and a low fluorescence at acidic pH. In this experiment, liposomes containing DNA coupled dye, either untreated or treated with DNase I, where incubated at different pH values ranging from 5.5 to 10.3 at 4 °C overnight, allowing to equilibrate the luminal pH value with the bulk pH. The next day, liposomes were diluted into buffer with a pH of 6.9 and fluorescence emission was measured. This situation mimics an experiment, where protons have either been pumped to the inside or to the outside of the liposome (luminal pH changes between pH 5.5 and 10.3), while the bulk pH remains constant at pH 6.9 (Figure 19A, red traces).

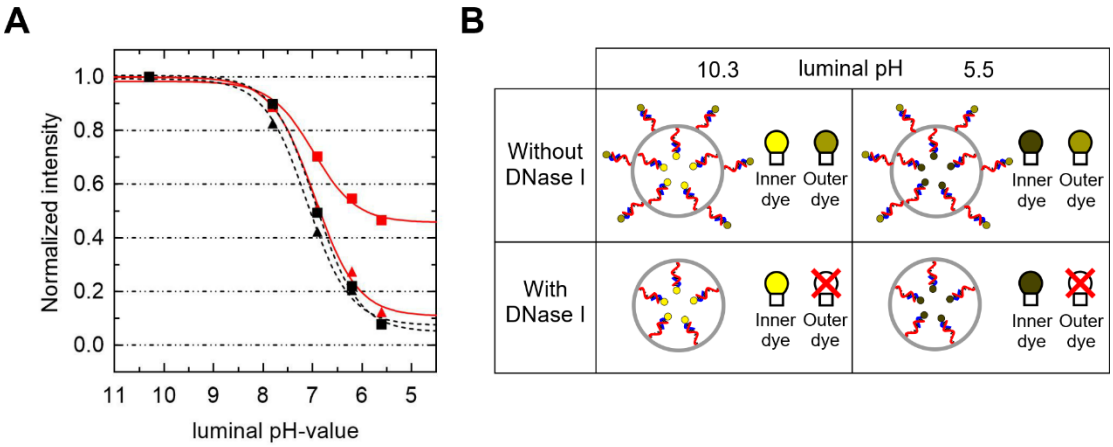

Figure 19: pK_a and signal range determination of vesicle incorporated LON-CF. A) Fluorescence intensity of LON-CF in liposomes measured at different pH values. Liposomes were either measured at the same luminal and bulk pH (black dotted traces) or at a constant bulk pH with varying luminal pH (red traces). A sigmoidal curve was used to fit the points. Data were normalized to the fluorescence at pH 10.3. B) Schematic representation of liposomes containing LON probe treated with or without DNase I at a constant bulk pH of 6.9 with a luminal pH of 10.3 (left) and 5.5 (right). Next to the liposomes, two light bulbs represent the inner and outer fluorophores, respectively. For both treated and untreated liposomes, fluorescence of the inner CF is strong at a luminal pH of 10.3 and weak at a luminal pH of 5.5. For the untreated liposomes, outer CF has a medium fluorescence both at luminal pH 10.3 and 5.5 due to the constant bulk pH of 6.9. For the treated liposomes, the additional medium fluorescence of the outer CF is removed.

As shown in Figure 19 for the DNase I treated sample (triangles), fluorescence was maximal at pH > 8, but decreased when the pH was lowered, and at pH 5.5, essentially no fluorescence was observed. In the untreated sample (squares), the fluorescence also decreased at higher pH values but remained at ~ 50 % at pH 5.5. The remaining fluorescence at low luminal pH values stems from the dye on the outside of the liposome, where the pH is unchanged (pH 6.9), similar to what has been observed with the lipid-

coupled Oregon 488 dye.[166] As a control, liposomes were also measured in the same buffer as incubated overnight (luminal pH = bulk pH, black dotted traces), yielding a very similar dependence to the DNase I treated sample. A sigmoidal dose-response curve was used as a fit and apparent pK_a values in the range of ~ 6.9 were obtained. The pK_a of the membrane embedded conjugate is thus slightly higher than free carboxyfluorescein with a reported pK_a of 6.5,[413] but a similar shift from free to DNA-conjugated fluorescein has been reported in the literature.[456] These data show that the apparent pK_a of the DNA-coupled dye is therefore not influenced by the membrane and is useful for pH measurements in the physiologically important range between pH 6 and pH 8. Furthermore, DNase I experiments show that removal of the dye from the outer leaflet increases the available signal range in these experiments.

Next, the conjugate was used to monitor ATP driven H^+-pumping by the ATP synthase of *Escherichia coli*. In this experiment, F_1F_0 ATP synthase was reconstituted into liposomes containing LON-CF using two different established methods. In the first, ATP synthase was mixed with liposomes in the presence of 0.8 % n-octyl-β-d-glucoside (OG), incubated on ice followed by detergent removal using SM-2 BioBeads (Figure 20). In the second reconstitution method, sodium cholate was used as a detergent that was subsequently removed by gel filtration chromatography (Figure S23). After reconstitution, half of the sample was treated with DNase I and liposomes from both samples were collected by ultracentrifugation and resuspended in buffer. The optimal amount of DNase I was determined by titrating the amount of DNase I using a liposome acidification assay to detect digestion of the DNA as described in the Supporting Information (Figure S24 and S25).

The experimental setup is shown in Figure 20A. Proton pumping into the vesicle is started by addition of ATP binding to the catalytic site of the F_1 part of the ATP synthase that is exposed to the outside of the liposomes.[91] The acidification of the liposome interior was then followed using time resolved fluorescence spectroscopy. As depicted in Figure 20B (raw data) and Figure 20C (normalized to initial fluorescence), addition of ATP lead to a rapid decrease of the CF signal in the DNase I treated (red) and untreated (blue) sample, indicating ATP driven proton influx. Addition of the protonophore carbonyl cyanide *m*-chlorophenyl hydrazine (CCCP) dissipated the proton gradient and the fluorescence returned to its initial value. As expected from the experiments described above, the removal of the outer dye led to an increased signal in the normalized data (Figure 20B). No change in fluorescence was observed in liposomes containing no ATP synthase (yellow).

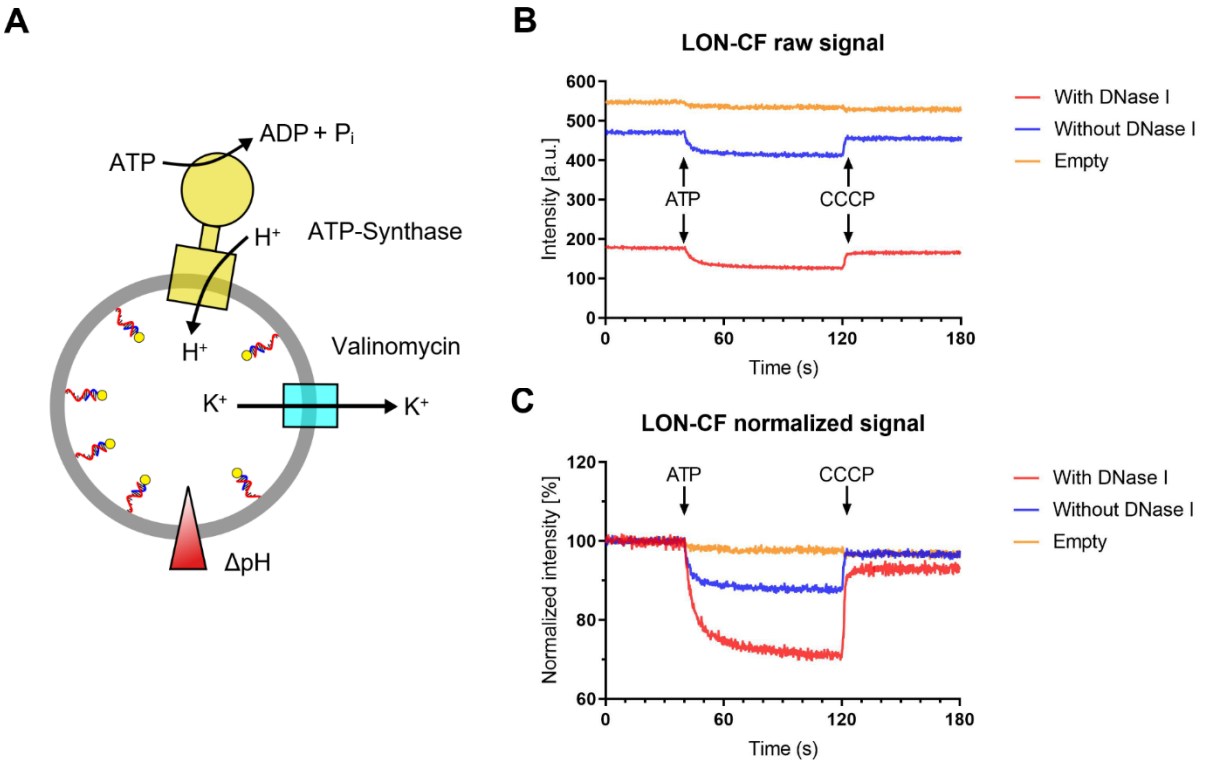

Figure 20: ATP-hydrolysis-driven proton pumping monitored by LON-CF fluorescence. A) Cartoon representation of the experiment. Proteoliposomes containing F_1F_0 ATP synthase were treated with (red trace) or without DNase I (blue trace). As a negative control, empty liposomes (yellow trace) were measured. Proton translocation is initiated by the addition of 1 mM ATP and the proton gradient is dissipated by addition of 5 µM CCCP. B) Raw data of the different proteoliposome preparations. C) as in (B), but traces were normalized to the averaged intensity before addition of ATP.

LON-CF was also used to follow proton transfer from the inside to the outside of the liposomes. To this end, purified bacterial cytochrome *c* oxidase from *Rhodobacter sphaeroides* was reconstituted into liposomes and redox-driven proton pumping was followed using the DNA conjugate. This enzyme catalyzes the final step of oxidative phosphorylation and uses the free energy released during oxygen reduction (to H_2O) to pump protons across the membrane and generate a proton motive force (Figure 21A). Cytochrome *c* oxidase of *R. sphaeroides* contains four redox centers, Cu_A, heme *a*, and the binuclear site consisting of heme a_3 and Cu_B that binds oxygen. Electron transport to the enzyme is mediated via reduced cytochrome *c* (cyt *c*), a small soluble protein that is unable to penetrate the membrane. If added to liposomes containing reconstituted cytochrome *c* oxidase, cyt *c* docks to its binding site and donates electrons via Cu_A and heme *a* to the binuclear site, where oxygen is reduced to water.[426,427] As a consequence, protons required for the reaction of O_2 to H_2O and those pumped across the membrane are taken up from the inside of the liposome, leading to an alkalization of the liposome lumen. Using CF as the probe, in contrast to the inwardly pumping ATP synthase, an increase in fluorescence signal should be observed. Proteoliposomes were mixed with oxidized cyt *c* and a baseline was recorded (Figure 21B) before 2 mM sodium ascorbate was added. Ascorbate is used as electron

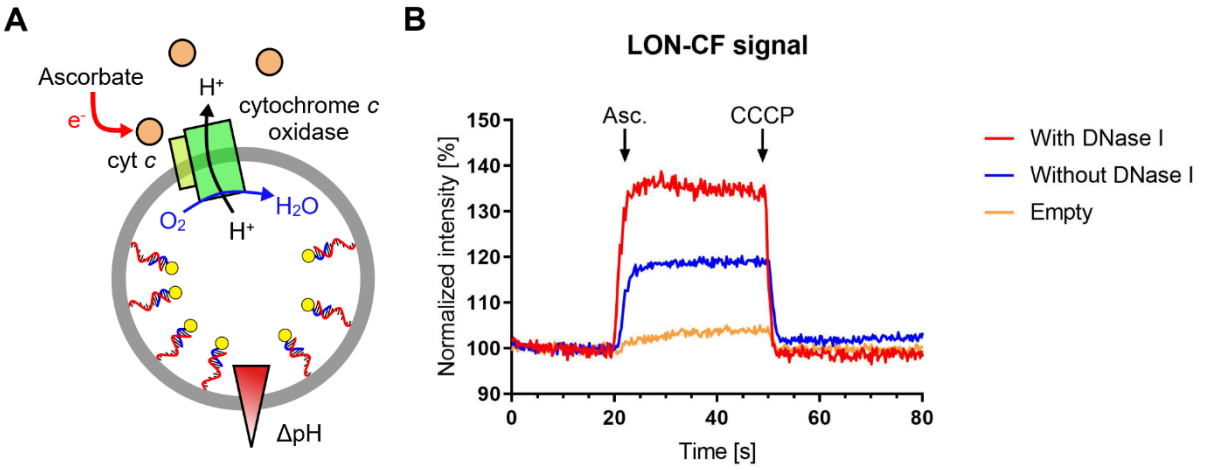

Figure 21: Redox-driven proton pumping in cytochrome *c* oxidase following LON-CF fluorescence. A) Cartoon representation of the experiment. Proteoliposomes containing *R. sphaeroides* cytochrome *c* oxidase were treated with (red trace) or without DNase I (blue trace). As a negative control, empty liposomes (yellow trace) were measured. A baseline was recorded after addition of 10 µM cyt *c* and proton translocation is initiated by the addition of 2 mM Na-ascorbate (Asc.). The proton gradient is dissipated by the addition of 5 µM CCCP. B) Proton translocation of proteoliposomes treated with and without DNase I and empty vesicles treated without DNase I normalized to the averaged intensity before addition of ascorbate.

source that reduces cyt *c* in solution within milliseconds. This ensures a continuous steady state reaction after cyt *c* has donated its electron to cytochrome *c* oxidase and is released from the enzyme in its oxidized form. Upon addition of ascorbate, a rapid increase in the fluorescence signal is observed, indicating proton efflux from the liposomes. As already observed for the ATP synthase in the experiment above, removal of the dye from the outer leaflet increased the relative signal increase substantially (red trace compared to blue trace). Addition of CCCP dissipated the proton gradient and signal returned to the value before ascorbate addition. Only a very small increase in signal was observed in liposomes containing no protein.

Conclusion

Here we present a novel tool to selectively incorporate DNA-coupled probes into the inner membrane leaflet of liposomes to follow the function of membrane proteins. An oligonucleotide with a lipophilic moiety, in this case cholesterol, was hybridized with a second oligonucleotide labeled with a pH-sensitive fluorophore and the conjugate was incorporated into the vesicle membrane during liposome formation. In contrast to earlier work, where lipophilic DNA conjugates have been used to sense the extracellular pH of live cells[159,180], our approach is suited for bottom-up assemblies of complex systems. In this article, we describe the sensitive detection of transmembrane proton transport by purified membrane proteins in synthetic vesicles, requiring a pH-sensitive probe located within the liposomal volume. In contrast to freely soluble probes, membrane-coupled probes allow for an almost quantitative incorporation of the dye into the liposomal membrane. Treatment with DNase I and subsequent ultracentrifugation led to a selective removal of the dye present in the outer leaflet of the vesicle, yielding a clean labeling of the inner leaflet. Thereby, the loss of the dye is limited to ~ 50 % compared to typical losses of > 95 % with soluble dyes, yielding an incorporation efficiency at least ten times higher. Previously, several methods that have been described to achieve selective labeling of the inner leaflet involved either chemical bleaching or photophysical quenching of the dye in the outer leaflet, for example by the addition of sodium dithionite, nitrobenzoxadiozole or iodide, or involved physical removal of the labeled lipids using either BSA, cyclodextrins or unlabeled acceptor vesicles.[173] Although the reagents needed for the first approach will likely interfere with the function of the MP, especially for proteins involved in redox reactions, the second approach is unspecific and might affect the stability and tightness of the liposomes that is crucial to ensure in proton transporting experiment. Here, we use the protein DNase I to selectively cleave the DNA linker located on the outside. Recently, DNase I mediated cleavage of DNA grafted on the outside of liposomes was used to release vesicles from DNA origami templates.[457] This enzyme-mediated method for the removal of the outer leaflet-embedded dye is specific and compatible with the presence of delicate multi-subunit protein complexes and redox reactions. The tight anchoring of the lipid dye will further suppress passive leakage of the dye across the membrane and the hydrophilic nature of the DNA backbone makes flipping from the inner to the outer leaflet highly unlikely. Taken together, we are convinced that our method is a valuable addition to the set of existing tools.

Our measurements with the respiratory enzymes F_1F_0 ATP synthase and cytochrome *c* oxidase show that the presence of the dye does not affect protein function, neither before nor after treatment with DNase I. The simple incorporation procedure during rehydration also ensures that the technique is compatible with a variety of reconstitution techniques. While not tested here, we envisage that the conjugates could also be added together with the enzyme during the reconstitution process, further simplifying the experimental process.

Certainly, the major advantage of the presented probe design is its versatility and flexibility based on the self-assembly of the complementary DNA strands. Here, we have chosen a commercially available carboxyfluorescein DNA modification to establish the principle. During the course of the experiment, an unlabeled version of oligo ON*3* was also customized with another pH-sensitive dye, CypHer5E, to yield ON*5*. The commercially available succinimidyl ester of Cypher5E was coupled unlabeled oligo ON*3* containing a C6-linker with a primary amine-group on the 3' end and HPLC purified (performed at Microsynth, Balgach, Switzerland). In contrast to CF, CypHer5E fluorescence increases with decreasing pH values,[458] making it an interesting complementary tool to CF-based sensors. We have used the dye in ATP synthase measurements and while not delivering an increased signal-to-noise ratio compared to the CF conjugate, the experiment shows that selective removal of the outer leaflet probe did strongly enhance the apparent sensitivity of the dye (Figure S26, blue and red trace). Given the simple coupling reaction, that is, NHS ester to primary amine on oligonucleotide, essentially any dye or probe can be selectively coupled to the inner leaflet. We also envisage that such probes have applications for microscopic approaches. Recently, efforts have been made to follow the function of membrane proteins in giant unilamellar vesicles,[166] which in terms of their size (1-100 μm) are very similar to eukaryotic cells and thus provide an interesting experimental model system. There, by the cleavage of the probe, unwanted background signals could be removed.

Finally, the use of DNA strands opens an interesting opportunity to control the distance of the dye to the surface of the membrane. In our experiments, the DNA linker ensured sufficient distance of the dye from the membrane to keep its protonation properties unchanged, a drawback that is encountered by direct coupling of, for example, pH-sensitive dyes to a lipid headgroup such as phosphatidyl-ethanolamine. Use of different linker lengths should allow to separate the inside of a giant vesicle into different zones, for example, to monitor membrane binding or release processes.

Acknowledgements

We thank Sandra Schär for the purification of ATP synthase and cytochrome *c* oxidase. The project was supported by the Swiss National Science Foundation SNFS (grant no. 176154).

Conflict of Interest

The authors declare no conflict of interest.

Supporting Information

Experimental Procedures

Material

1,2-dioleoyl-sn-glycero-3-phosphocholine (DOPC), 1,2-dioleoyl-sn-glycero-3-phosphoethanolamine-N-carboxyfluorescein (18:1 PE CF) were obtained from Avanti Polar Lipids (Alabaster, USA), Texas Red™ 1,2-Dihexadecanoyl-sn-Glycero-3-Phosphoethanolamine (TR-DHPE) from ThermoFisher Scientific (Waltham, Massachusetts, USA), DNase I from bovine pancreas, grade II from Roche (Basel, Switzerland), CypHer5E NHS Ester from Sigma (St. Louis, Missouri, USA) and 5(6)-carboxyfluorescein from Molecular Probes (Eugene, Oregon, USA). Oligonucleotides ON*1* to ON*5* 5'-TGG ACA TCA GAA ATA AGG CAC GAC GGA CCC-3' (ON*1*), 5'-TGG ACA TCA GAA ATA AGG CAC GAC GGA CCC-3'-cholesterol (ON*2*), 5'-TAT TTC TGA TGT CCA CCC-3'-carboxyfluorescein (ON*3*), cholesterol-5'-CCC TCC GTC GTG CCT-3' (ON*4*), 5'-TAT TTC TGA TGT CCA CCC-3'-C6-CypHer5E (ON*5*) were obtained from Microsynth (Balgach, Switzerland). Other chemicals were obtained from Sigma (St. Louis, Missouri, USA).

Hybridization of oligonucleotides

50 µL mixtures were prepared containing 4-8 µM ON*3* and different amounts of ON*2* and ON*4* (Table S3). The mixtures were prepared either in Milli-Q-water (MQW) or in 10 mM MOPS pH 7.4, 50 mM KCl and 2.5 mM $MgCl_2$. 20 µL of that was mixed with 4 µL 6x blue/orange loading dye (Promega, Madison, Wisconsin, USA) and loaded on a TBE 20 % polyacrylamide gel, which was prepared as follows. 5.2 mL 30 % acrylamide was mixed with 0.8 mL 10 x TBE (89.15 mM Tris, 88.95 mM boric acid, 20.00 mM ethylenediaminetetraacetic acid (EDTA)) and 2 mL (MQW). Polymerization was initiated with 40 µL 10 % ammonium persulfate and 8 µL N,N,N',N'-Tetramethylethylenediamine (TEMED). The gel was run for 90 min at 200 V and 8 °C of cooling in 1 x TBE. The gel was imaged using a G:BOX Chemi XX6 System using the appropriate settings, fluorescently labeled DNA was imaged before the gel was stained with GelGreen according to the manufacturers protocol to visualize non-fluorescently labeled DNA.

Liposome formation with LON probes

Lipids dissolved in chloroform were mixed in the desired ratio in a 25-mL round-bottom flask and chloroform was evaporated under a constant stream of N2 while rotating the flask. The thin lipid film was further dried for ≥ 2 h under high vacuum. Single stranded DNA (ssDNA) molecules were mixed in the desired amounts in rehydration buffer and self-hybridized to form the LON probes. The dried lipid film was resuspended at 5 mg mL^{-1} using the buffer containing the LON probe. Unilamellar liposomes were subsequently formed by seven freeze–thaw cycles and extruded through a Whatman polycarbonate membrane (Little Chalfont, UK) with a pore size of 100 nm.

Table S2: Final concentrations of oligonucleotides ON*1*-ON*4* used for the formation of liposomes.

	ON-CF	LON-CF	L_2ON-CF
ON*1*	10.2 µM	-	-
ON*2*	-	10.2 µM	10.2 µM
ON*3*	8.0 µM	8.0 µM	8.0 µM
ON*4*	-	-	12.0 µM

DNase I treatment

Lyophilized powder of DNase I was dissolved in MQW at 10 mg mL^{-1} and stored for maximally 1 week at 4 °C. Prior to experiments, the stock was diluted to 0.5 mg mL^{-1} and 5 µL was added per 100 µL of liposomes (final concentration 24 µg mL^{-1}). For untreated samples, 5 µL of MQW was added instead. The liposomes were next incubated at 37 °C and 500 rpm for 20 min, cooled on ice, diluted 5-fold and subsequently centrifuged at 200'000 x g for 90 min to remove the unbound or cleaved dye and DNase I. The supernatant was discarded, and the liposome pellets were carefully resuspended in the desired volume.

Titration of DNase I concentration

A dilution series of DNase I was prepared from stock solution at 10 mg mL^{-1} and DNase I treatment was performed as described above. The supernatant was discarded, and the liposome pellets were resuspended in the same volume of buffer as used during treatment. For measurements, 20 µL of the resuspended liposomes were mixed with 980 µL buffer containing 10 mM MOPS pH 7.4, 50 mM KCl, 2.5 mM $MgCl_2$ in a 1.5 mL cuvette, equipped with a magnetic stir bar and fluorescence was measured at room temperature using excitation and emission wavelengths of 495 nm and 520 nm, respectively. Acidification of the outside was obtained by addition of 40 µL 0.5 M HEPES, pH 5.3, with subsequent acidification of the inside of the vesicles by addition of 1 µL 10 mM gramicidin.

Incorporation of conjugates during rehydration

DOPC and TR-DHPE liposomes were formed as described above in rehydration buffer (10 mM MOPS pH 7.4, 50 mM KCl, 2.5 mM $MgCl_2$) containing different variations of carboxyfluorescein. The final concentration of the lipids in the liposomes was 6.7 mM for DOPC and 1.8 µM for TR-DHPE. The concentrations of ssDNA molecules in the rehydration buffer are shown in Table S2.

Free CF was used at 8.0 µM in the rehydration buffer. For the lipid-coupled CF, 18:1 PE CF was dissolved in chloroform and mixed with the lipids in the round-bottom flask to get a final concentration of 8.1 µM in liposomes. Therefore, all CF variants were added to yield 0.12 mol% CF in liposomes while TR-DHPE was used at 0.03 mol%. DNase I treatment was performed using 200 µL liposomes as described above

and 70 µL of liposomes before and after treatment were mixed with 700 µL measuring buffer (50 mM Tris-HCl, pH 8.0, 50 mM KCl, 2.5 mM $MgCl_2$ and 1 % (v/v) Triton). For measurements, 150 µL of diluted liposomes were added to a 150 µL quartz cuvette and fluorescence was measured using 589 nm and 615 nm as excitation and emission wavelengths respectively for TR-DHPE. For CF fluorescence, excitation and emission wavelengths of 495 nm and 520 nm were used. Each sample was measured three times and three separate experiments were performed. To calculate the incorporation of CF, the intensities of the three experiments were averaged and standard deviations of the measured CF and TR-DHPE fluorescence were calculated. Next, signals of both dyes were normalized to the liposomes before treatment to obtain the percentage of signal in the treated liposomes compared to the total signal for each dye. Finally, the normalized CF signal was divided by the normalized TR-DHPE signal to account for vesicle loss or dilution. The error was calculated by propagation of the standard deviation.

pH-dependency

Liposomes were formed as described with DOPC and TR-DHPE in rehydration buffer (5 mM MES, 5 mM Bis-Tris propane, 5 mM CAPS, adjusted to pH 6.9, 50 mM KCl, 2.5 mM $MgCl_2$) containing 10.2 µM ON*2* and 8.0 µM ON*3* for LON-CF. The final concentration of the lipids in the liposomes was 6.7 mM for DOPC and 1.4 µM for TR-DHPE. Therefore, LON-CF was added to yield 0.12 mol% CF in liposomes and TR-DHPE was used at 0.02 mol%. DNase I treatment was performed as described with the following modification. A suspension of 1.1 mL liposomes was treated with either water or DNase I and split to 5x 200 µL before ultracentrifugation. The pellets were resuspended in buffers (10 mM MES, 10 mM Bis-Tris propane, 10 mM CAPS, 50 mM KCl, 2.5 mM $MgCl_2$) with pH adjusted to 10.3, 7.8, 6.9, 6.2 and 5.5 and incubated overnight to equilibrate pH values on the inside and outside. Fluorescence was measured in a 150 µL quartz cuvette by mixing 20 µL liposomes and 200 µL buffer and emission spectra were recorded from 510 nm to 600 nm with 495 nm excitation for CF and from 615 nm to 670 nm using an excitation of 589 nm for TR-DHPE.

Purification of membrane proteins

F_1F_0 ATP synthase from *E. coli* and cytochrome *c* oxidase from *R. sphaeroides* were purified according to published protocols.[429,459]

Reconstitution of membrane proteins with BioBeads

Purified *E. coli* F_1F_0 ATP synthase was reconstituted using detergent removal by SM-2 BioBeads. 200 µL liposomes (5 mg mL^{-1}) containing LON probe in reconstitution buffer (10 mM MOPS pH 7.4, 50 mM KCl, 2.5 mM $MgCl_2$) were mixed with 7.5 µL 20 % n-octyl-β-d-glucoside before 10 µL 6.5 µM purified ATP synthase was added. The sample was incubated for 30 min with gentle shaking every 5 – 10 min. A total of 180 mg SM2 BioBeads, prewashed with isopropanol and water and equilibrated with reconstitution buffer, was added in three steps of 30 mg, 60 mg and 90 mg with incubation of 30 min at 4 °C for the

first two steps and 50 min after the last addition of beads. Beads were removed from the suspension prior to DNase I treatment as described.

Reconstitution of membrane proteins using gel filtration

R. sphaeroides cytochrome *c* oxidase and *E. coli* F_1F_0 ATP synthase were reconstituted using detergent removal by gel filtration.[91] 200 µL liposomes (5 mg mL^{-1}) containing LON-CF in reconstitution buffer were mixed with 5 µL 10 % Na-cholate, briefly incubated and 10 µL of either purified ATP synthase (6.5 µM) or 15µL cytochrome *c* oxidase (44 µM) was added. The sample was incubated for 30 min at room temperature with gentle shaking every 5 – 10 min. The sample was run on a P10 column equilibrated with 25 mL buffer. Briefly, sample and 750 µL buffer were loaded on the column and eluted with 1.2 mL buffer. The eluted sample was centrifuged at 200'000 x g for 90 min. The liposome pellet was resuspended in 200 µL reconstitution buffer and DNase I treatment was performed as described.

Proton translocation of ATP synthase and cytochrome c oxidase

Twenty µL proteoliposomes were mixed with 980 µL buffer containing 10 mM MOPS pH 7.4, 50 mM KCl, 2.5 mM $MgCl_2$ in a 1.5 mL quartz cuvette, equipped with a magnetic stir bar. CF fluorescence was followed at excitation and emission wavelengths of 495 nm and 520 nm, respectively while fluorescence of Cypher5E conjugate was followed at excitation and emission wavelengths of 650 nm and 670 nm, respectively. In all measurements, slit widths of 5 nm were used. All measurements were performed in the presence of 50 nM valinomycin. Proton translocation with the ATP synthase was started by addition of 5 µL of 200 mM ATP, and after a few minutes, 5 µL of 1 mM CCCP was added to dissipate the proton gradient. Proton translocation with the cytochrome *c*-oxidase was monitored in the presence of 10 µM oxidized cyt *c* and was started by addition of 2 µL 1 M ascorbate. After a few minutes, 5 µL of 1 mM CCCP was added to dissipate the proton gradient.

Proton translocation of ATP synthase with ACMA

Proton translocation of ATP synthase was followed with 9-Amino-6-Chloro-2-Methoxyacridine (ACMA) fluorescence to check for the activity of reconstituted protein after DNase I treatment.[149] Twenty µL proteoliposomes with or without LON-CF were mixed with 980 µL buffer containing 10 mM MOPS pH 7.4, 50 mM KCl, 2.5 mM $MgCl_2$ in a 1.5 mL quartz cuvette, equipped with a magnetic stir bar. Kinetic fluorescence measurements of liposomes were followed at excitation and emission wavelengths of 410 nm and 480 nm, respectively (slit widths of 5 nm). All measurements were performed in the presence of 50 nM valinomycin and 1 µM ACMA. Proton translocation with the ATP synthase was started by addition of 5 µL of 200 mM ATP, and after a few minutes, 40 µL of 1 M NH_4Cl was added to dissipate the proton gradient.

Results and Discussion

Hybridization of oligonucleotides at different molar ratios

The following oligonucleotides with modifications were used in this study:

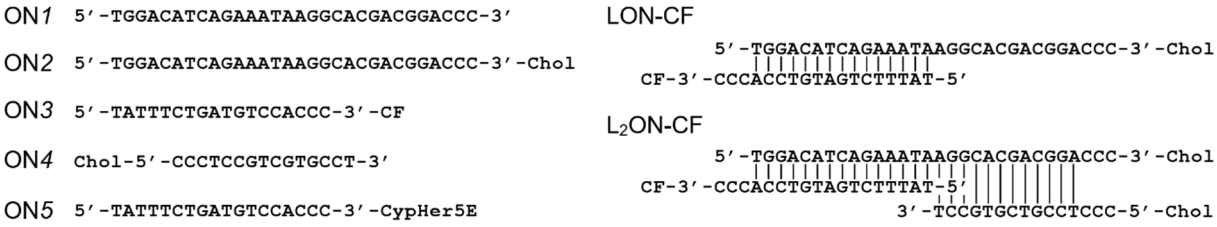

Figure S21: Sequence and modifications of oligonucleotides ON*1* – ON*5* and hybridization products LON-CF and L_2ON-CF. The modifications are noted at the appropriate end of the DNA strand. ON*1* does not contain a modification. ON*2* and ON*4* contain a cholesterol modification (Chol) at either the 3' end or the 5' end, respectively. ON*3* and ON*5* contain a fluorophore modification at the 3' end, once carboxyfluorescein (CF) and once CypHer5E. The dimer probe (LON-CF) is formed using ON*2* and ON*3*, the trimer probe (L_2ON-CF) is formed using ON*2*, ON*3* and ON*4*. Alternatively, ON*1* can be used instead of ON*2* as a negative control and ON*5* can be used instead of ON*3* as an alternative fluorophore.

Formation of the dimer and trimer from ssDNA oligonucleotides was checked by 20 % polyacrylamide TBE gel-electrophoresis (Figure S22). At an ON*3* concentration of 8 µM and a molar ratio of 1.275 for the cholesterol-modified DNAs, both the L_2ON-CF and LON-CF are formed when mixing the oligonucleotides and allowing hybridization for 10 min at room temperature (Lanes 1 and 2). However, a band of LON-CF is present in Lane 1 both in the CF channel and the GelGreen channel (Figure S22A and B), meaning that either not all of ON4 was hybridized to the dimer or that concentrations of ON4 were too low.

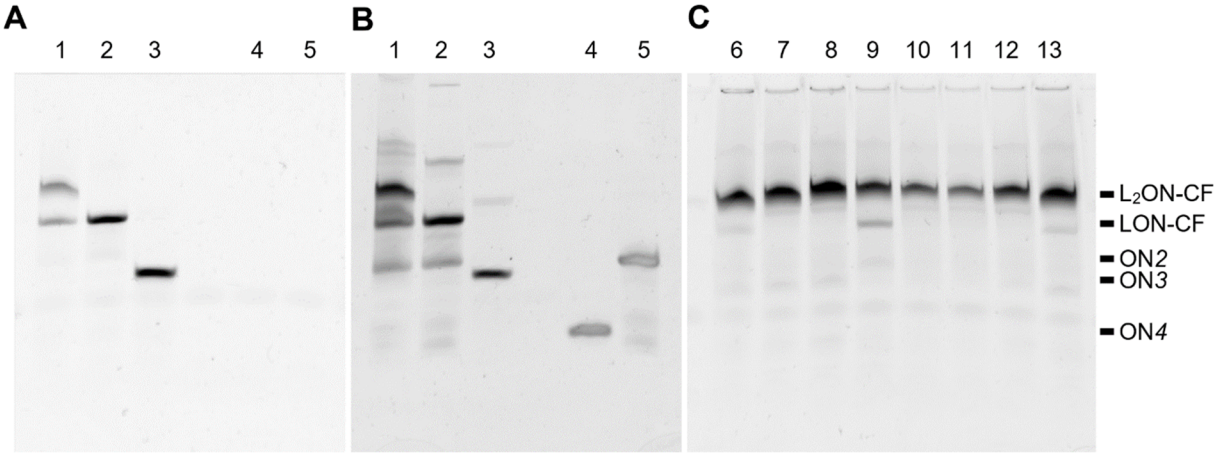

Figure S22: 20 % polyacrylamide TBE gel-electrophoresis analysis of different hybridization conditions. Gels were imaged with a G:BOX Chemi XX6 System using the appropriate settings to detect either fluorescence of CF or fluorescence of GelGreen to visualize unlabeled DNA.A) CF signal and B) GelGreen signal of the different ssDNA fragments and of LON-CF and L_2ON-CF. C) CF signal of L_2ON-CF using different ratios of oligonucleotides (Table S3).

Therefore, different molar ratios of cholesterol modified DNA and fluorophore-labeled DNA were tested in 5 mM MOPS pH 7.4, 50 mM KCl and 2.5 mM $MgCl_2$, mimicking the conditions used for ATP synthase reconstitution (Figure S22C). At the same ratios as used before, formation of both LON-CF and L_2ON-CF was again observed. Increasing the molar amount of ON*4* led to disappearance of the LON-CF band. Lowering the amount of ON*3* resulted in the disappearance of the LON-CF band only when ON*4* and ON*2* were added at more than double the molar amount of ON*3*. Based on these findings the molar ratio of 1: 1.275: 1.5 ON*3*: ON*2*: ON*4* was chosen for future experiments as it fully formed the trimer without using a high excess of ON*2* and ON*4*.

Table S3: Molar ratios of oligonucleotides used in the hybridization experiments. Lane number corresponds to the lanes on the gel in Figure S22. 8 µM ON*3* was used as reference and set to 1. Buffer indicates whether the hybridization was performed in Milli-Q-water (MQW) or in 10 mM MOPS pH 7.4, 50mM KCl and 2.5 mM $MgCl_2$ (MMK).

Lane	1	2	3	4	5	6	7	8	9	10	11	12	13
ON2	1.2	1.2	-	-	1.2	1.2	1.2	1.2	1.2	1.2	1.2	1.2	1.2
ON4	1.2	-	-	1.2	-	1.2	1.5	1.8	1.2	1.2	1.5	1.8	1.2
ON3	1	1	1	-	-	1	1	1	0.75	0.5	0.5	0.5	1
Buffer	MQW	MQW	MQW	MQW	MQW	MMK	MMK	MMK	MMK	MMK	MMK	MMK	MMK

Optimization of DNase I concentration for complete DNA cleavage after protein reconstitution

To test the successful reconstruction of the F_1F_0 ATP synthase, 9-Amino-6-Chloro-2-Methoxyacridine (ACMA) fluorescence was followed during addition of ATP. ACMA fluorescence can be used to detect proton translocation to the inside as fluorescence is quenched if the vesicle lumen is acidified.[149] Surprisingly after ultracentrifugation, all DNase I (476 µg mL^{-1}) treated samples showed a severely reduced (50 %) proton pumping activity, while non treated samples were not affected by centrifugation. The reduction in activity was even observed in the absence of LON-CF (Figure S23A). Thus, a DNase I titration experiment (described in the paragraph below) was performed to determine the minimal amount of DNase I necessary to obtain complete dye removal. Based on these findings, a ~ 20-fold lower concentration of DNase I (24 µg mL^{-1}) was used in following experiments, where the ACMA signal was unaffected after treatment (Figure S23B).

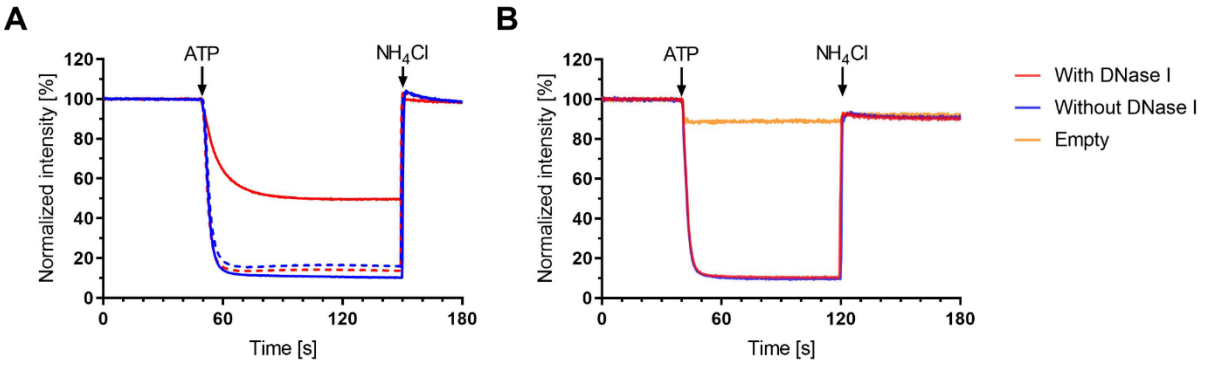

Figure S23: ATP hydrolysis driven proton pumping followed by ACMA fluorescence. Proteoliposomes containing F_1F_0 ATP synthase were treated with DNase I (red trace) or without DNase I (blue trace). As a negative control, empty liposomes (yellow trace) were measured. Proton translocation is initiated by the addition of 1 mM ATP and the proton gradient is dissipated by addition of 38.2 mM NH_4Cl. A) Data from liposomes without LON-CF normalized to the averaged intensity before addition of ATP. Liposomes were measured before (dotted lines) and after treatment (solid lines) with 476 µg mL^{-1} DNase I or water. B) Data from liposomes with LON-CF normalized to the averaged intensity before addition of ATP treated with a DNase I concentration of 24 µg mL^{-1}.

The DNase I titration was done using an acidification assay where buffer at pH 5.3 is added to liposomes in a 1 mL quartz-cuvette at pH 7.4. The outside of the liposomes is thus acidified first, while the vesicles are allowed to equilibrate after addition of gramicidin, a pore forming ionophore that allows the free diffusion of monovalent cations (such as protons) through the membrane.[460] In liposomes where LON-CF was not removed from the outside of the vesicles by DNase I treatment, the decrease after addition of HEPES made up 75 % of the total decrease after equilibration. (Figure S24A, blue trace). Liposomes where LON-CF was removed by DNase I from the outer leaflet of the membrane showed the opposite, with only a 25 % decrease after HEPES addition compared to the total decrease after equilibration (Figure S24A, red trace). Here, the decrease after addition of HEPES was surprising, as we expected to see no or just a slight decrease when LON-CF was only on the inside of the vesicle. However, a similar behavior has been previously observed in liposomes containing soluble Oregon Green 488 after they were acidified.[50] There are several possible explanations for this behavior in our case. One possibility is that the removal of CF from the outside is not complete, either due to incomplete DNA digestion or because a small percentage of soluble dye remains in the pellet after ultracentrifugation. Another possibility is that some of the vesicles are leaky and therefore equilibrate already after addition of HEPES. The observed effect can also be a combination of both of those things. Nevertheless, when looking at the ratio between the two decreases for different concentrations of DNase I the minimal ratio of ~ 1/3 is already reached at quite low concentrations of DNase I (Figure S24B). We therefore decreased the amount of DNase I in further experiments ~ 20-fold in order to be still well above the minimal amount needed for maximal digestion.

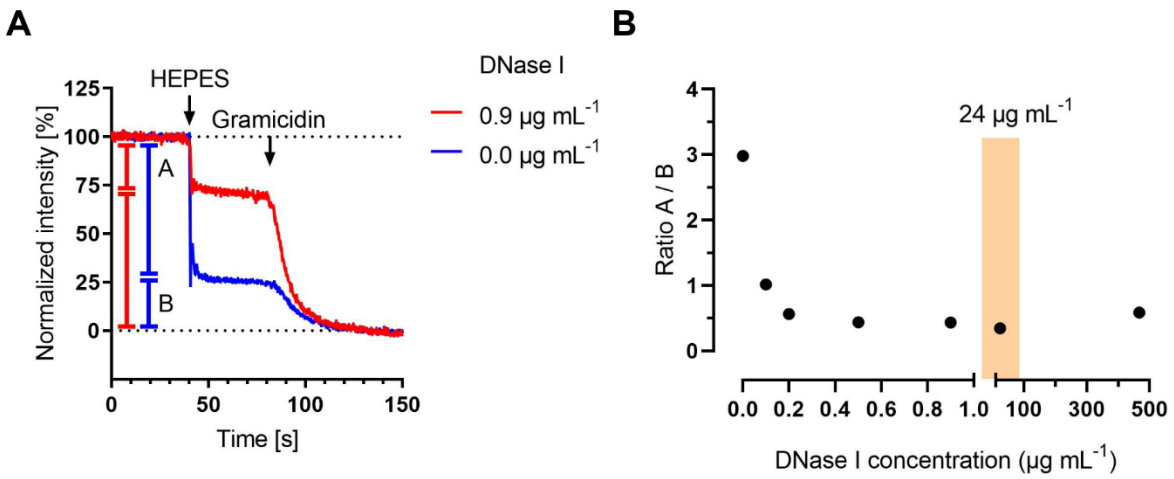

Figure S24: Titration of DNase I followed by a liposome acidification assay. Liposomes containing LON-CF were acidified on the outside with HEPES and gramicidin. 19.2 mM HEPES at pH 5.3 is added to a 1 mL quartz-cuvette containing 20 µL of liposomes in a total volume of 1 mL rehydration buffer at pH 7.4. Addition of 9.6 µM gramicidin allows for the influx of protons to the lumen of the liposomes, therefore leading to a further acidification of the inside of the vesicles and equilibrating the system. A) Exemplary traces of liposomes with (red trace) and without (blue trace) DNase I normalized to the averaged intensity before HEPES addition (=100 %) and after gramicidin addition (=0 %). The red and blue bar represent the relative signal decreases, with part A after addition of HEPES and part B after addition of gramicidin. B) Ratio of A/B at different DNase I concentration. Ratio of 3 represents undigested LON probe, ratio below 1 represents digested LON probe. The amount of DNase I used in further experiments is indicated by a yellow bar.

Reconstitution of ATP synthase into liposomes using Na-cholate and gel filtration

To test the versatility of the method, F_1F_0 ATP synthase was also reconstituted with an alternative method to BioBeads, using sodium cholate to destabilize preformed liposomes and subsequent detergent removal by gel filtration.[91] Similar to the reconstitution with BioBeads we observed an increased signal in the normalized data for the liposomes where the outer dye was removed (Figure S25B). Convincingly, no decrease in CF signal was observed when the ATP synthase inhibitor DCCD[461] was added prior to the measurement, that selectively blocks the ATP-driven rotation of F_1F_0 by binding to the proton binding site on the c-ring.

Use of CypHer5E coupled to oligonucleotide as an alternative pH sensor to carboxyfluorescein

Here, we used CypHer5E as an alternative pH-sensitive fluorophore. In contrast to carboxyfluorescein, CypHer5E has a cyanine scaffold and fluorescence increased with decreasing pH values, while both sharing a similar pK_a value. Typically, increase of fluorescence is preferred during a kinetic measurement, and CypHer5E might therefore be a valuable tool for acidification reactions. The commercially available succinimidyl ester of CypHer5E was coupled to ON3 containing a linker with a primary amine-group instead of the CF modification and HPLC purified (performed at Microsynth, Balgach, Switzerland). When the experiment with ATP synthase was repeated using CypHer5E coupled dye, the expected fluorescence increase was observed during ATP addition. Again, the signal range was greatly increased when the outer dye was removed by DNase I treatment and ultracentrifugation (Figure S26B).

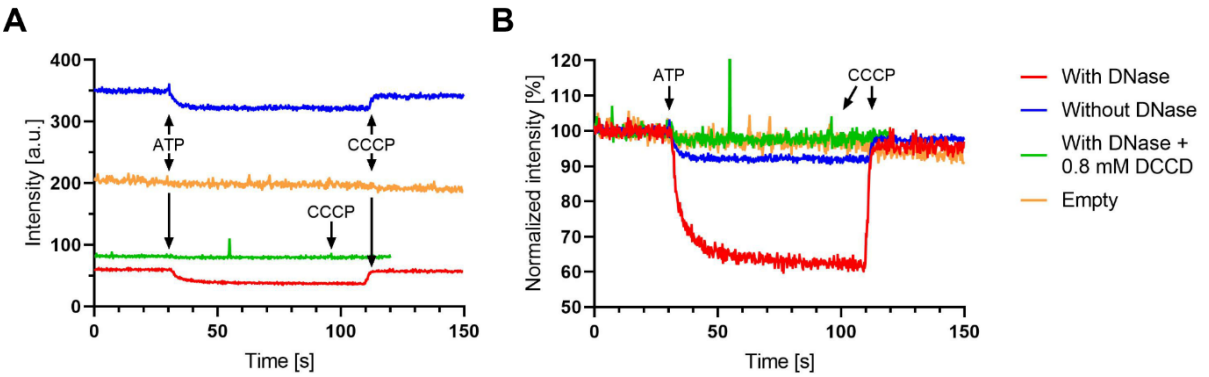

Figure S25: ATP hydrolysis driven proton pumping following LON-CF fluorescence. Proteoliposomes containing F_1F_0 ATP synthase were treated with DNase I (red trace) or without DNase I (blue trace). As a negative control, empty liposomes (yellow trace) were measured. Additionally, proteoliposomes were measured in the presence of 0.8 mM DCCD, a well know ATP synthase inhibitor (green trace). Proton translocation is initiated by the addition of 1 mM ATP and the proton gradient is dissipated by addition of 5 µM CCCP. B) Raw data of the different liposomes. C) Same as B but normalized to the averaged intensity before addition of ATP.

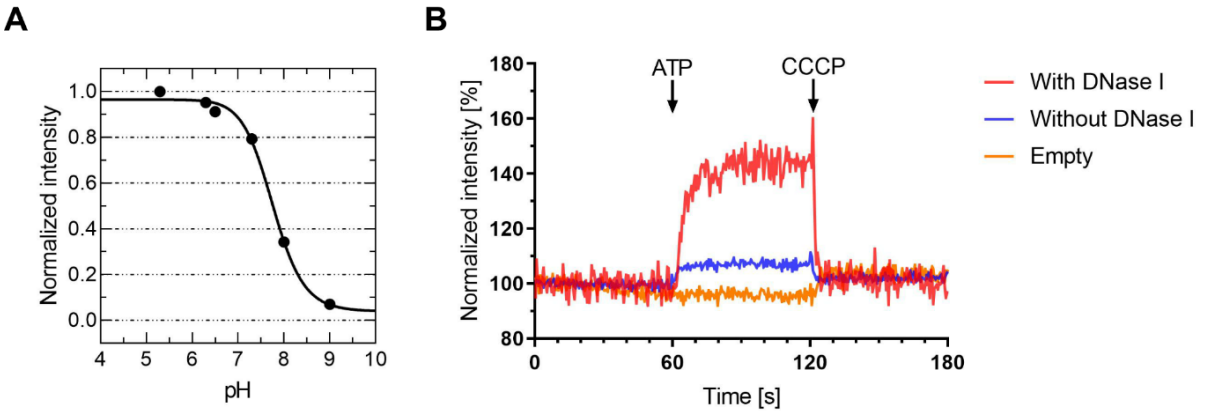

Figure S26: pH dependency of LON-CypHer5E and ATP hydrolysis driven proton pumping following LON-CypHer5E fluorescence. A) LON-CypHer5E fluorescence measured at different pH values. 4 µM LON-CypHer5E was measured in a 100 µL quartz cuvette in 50 mM HEPES buffer at pH 5.3, 6.3, 6.5 and 7.3 as well as in 50 mM Tris buffer at pH 8.0 and 9.0. B) Proteoliposomes containing F_1F_0 ATP synthase were treated with DNase I (red trace) or without DNase I (blue trace). As a negative control, empty liposomes (yellow trace) were measured. Proton translocation is initiated by the addition of 1 mM ATP and the proton gradient is dissipated by addition of 5 µM CCCP. The data is normalized to the averaged intensity before addition of ATP

3.2.2. Appendix to 3.2.1. Bifunctional DNA Duplex Incorporation into Giant Unilamellar Vesicles

Title: Bifunctional DNA Duplex Incorporation into Giant Unilamellar Vesicles

Status: Lab Data

Authors: Nicolas Dolder, Christoph von Ballmoos

Contribution: Christoph von Ballmoos (CvB) conceived and supervised the study; CvB and Nicolas Dolder designed experiments; Nicolas Dolder performed the experiments and analyzed data, Nicolas Dolder wrote the report.

Introduction

This chapter will show additional experiments that were performed with the bifunctional DNA duplex probes presented in the previous chapter. One of our goals was to use these probes not only in small unilamellar vesicles (SUVs), as demonstrated in the published results,[174] but to use them as well in giant unilamellar vesicles (GUVs). As we have seen throughout this thesis, GUVs have become increasingly popular in numerous fields of research, including drug delivery,[409] biosensing,[209,210] the construction of synthetic cells[8,203,462] and the study of membrane related phenomena.[235] Functionalization of the vesicles is required in many of these applications, e.g. to introduce fluorescent dyes for sensing of biomolecules. Lipophilic oligonucleotides (LONs) that are anchored in the membrane are one of the tools for such functionalization, as DNA offers many design possibilities, allowing the creation of nanostructures such as pores[463] or scaffolds,[450,464] new sensors, e.g. using aptamer technology,[159,160,465] and the mimicry of enzymes[466] and proteins such as the SNARE fusion machinery.[349,451,467,468] Establishing the incorporation of such LONs in the GUV membrane may open new avenues for the detection of MP function, e.g. by incorporating novel and improved sensors which, using aptamer technology, may be able to detect substrates that previously had to be followed using complicated enzymatic cascades[205] or by non-continuous methods such as detection of radioactive substrates.

MP protein function in GUVs has been mostly followed in the past using soluble dyes.[98,204,205,307,323,326,348,351] Encapsulation of these dyes in GUVs is extremely inefficient using film hydration methods for GUV formation[191], e.g. the internal vesicle volume for PVA GUVs removed from the formation chamber is < 2 % of the total volume of the solution.[430] Lipid-coupled dyes on the other hand incorporate nearly exclusively into vesicles, offering a more convenient and economical procedure, in which much smaller quantities of dye are required.[165,166,174] However, the use of lipid-coupled dyes in GUVs is limited, as they will be present in both leaflets of the membrane and thus would detect substrate also on the outside of vesicles. In the case of pH changes, the outer dye faces a buffered solution, yielding a stable fluorescence signal that does not contribute to the signal change, but nevertheless reduces the dynamic range of measurements. This issue is circumvented with our bifunctional DNA duplex probe which stably integrates into the membrane via a lipophilic anchor and allows convenient removal of the fluorescent pH-sensitive dye in the outer membrane leaflet via DNase I treatment.[174] Two different strategies for incorporation of the probe into GUVs will be explored based on previously established LON incorporation methods. The first strategy involves addition of the probe to the rehydration solution for GUV formation,[174,469] and the second strategy involves drying of the LON probe together with lipids on indium-tin-oxide (ITO) coated glass slides or on polyvinyl alcohol (PVA) hydrogels for GUV formation.[174,451,470–472] This project is not finished and only early data is presented. However, the results shed some light on questions that need to be addressed for using bifunctional DNA probes in GUVs.

Experimental Procedures

Material

1,2-dioleoyl-sn-glycero-3-phosphocholine (DOPC), 1,2-dioleoyl-sn-glycero-3-phosphoethanolamine (DOPE) 1-palmitoyl-2-oleoyl-glycero-3-phosphocholine (POPC) 1-palmitoyl-2-oleoyl-glycero-3-phosphoethanolamine (POPE) and cholesterol (chol) were obtained from Avanti Polar Lipids (Alabaster, USA), CypHer5E NHS Ester from Sigma (St. Louis, Missouri, USA). Oligonucleotides ON*2* to ON*5* 5'-TGG ACA TCA GAA ATA AGG CAC GAC GGA CCC-3'-cholesterol (ON*2*), 5'-TAT TTC TGA TGT CCA CCC-3'-carboxyfluorescein (ON*3*), cholesterol-5'-CCC TCC GTC GTG CCT-3' (ON*4*), 5'-TAT TTC TGA TGT CCA CCC-3'-C6-CypHer5E (ON*5*) were obtained from Microsynth (Balgach, Switzerland). Polyvinyl alcohol (PVA), fully hydrolyzed, molecular weight approximately 145'000 for synthesis was obtained from Merck (Darmstadt, Germany). Other chemicals were obtained from Sigma (St. Louis, Missouri, USA).

Preparation of lipid mixtures and rehydration buffer containing LON probe

Oligonucleotides ON*2*, ON*4* and ON*3* or ON*5* were mixed in the desired concentration in Milli Q water and hybridized by incubation for 10 min at room temperature (RT). Lipid mixture 1 was prepared by mixing 55 µL methanol, 35 µL chloroform, 20 µL 20 mg mL^{-1} lipids dissolved in chloroform (DOPC/DOPE/cholesterol or POPC/POPE/cholesterol, both 50/25/25 mol%) and 10 µL oligonucleotides (60 µM ON*3*/ON*5*, 93.5 µM ON*2*, 117 µM ON*4*). Lipid mixture 2 was prepared as lipid mixture 1 with a few modifications. Lipids were added at a concentration of 2 mg mL^{-1} and oligonucleotides were diluted to 30 µM ON*3*, 46.75 µM ON*2* and 58.5 µM ON*4*. ON rehydration solution containing oligonucleotides was prepared by mixing 570 µL formation buffer (10 mM MOPS-KOH pH 7.4, 400 mM sucrose) with 10 µL, 5 µL or 1 µL oligonucleotides (60 µM ON*3*, 93.5 µM ON*2*, 117 µM ON*4*) and filled up with Milli Q water to 620 µL total volume. Final concentrations of ON*3* in rehydration solution are approximately 1.0 µM, 0.5 µM and 0.1 µM respectively.

GUV electroformation with LON probe in rehydration buffer

Giant unilamellar vesicles were generated by electroformation as described[80] with the following modifications. DOPC was dissolved in chloroform containing 12.5 % methanol (v/v) at 0.25 mg mL^{-1}. Seven µL of lipid solution was spread on each indium-tin-oxide coated glass slide, dried for 1 h under vacuum and rehydrated using 620 µL ON rehydration solution. Electroformation chambers were assembled with a 1.0 mm rubber spacer and formation of GUVs was carried out with the Vesicle Prep Pro (NanION Technologies GmbH, Munich, Germany), applying an AC electric field with 1.1 V and 10 Hz for 80 min as well as two ramp phases, 5 min each at 37 °C. The GUVs were incubated for at least 2 h at 4 °C before performing further experiments.

GUV electroformation with LON probe in lipid mixture

GUV formation with lipid mixture 1 containing the oligonucleotides was performed as described above, using 10 µL of lipid mixture 1 to coat each ITO coated glass slide and using formation buffer. GUV formation with lipid mixture 2 was performed as described above with a few modifications. ITO coated slides modified with 5 mm adhesive copper tape on the conductive side (Play-Zone GmBH, Steinhausen, Switzerland) were coated with 10 µL of lipid mixture 2 and dried as described. Electroformation chamber was assembled in a custom 3D printed slide holder with a 1.0 mm rubber spacer and the chamber was connected to the function generator PCGU1000 (Velleman Group, Gavere, Belgium) using JYE BNC to crocodile clamps (Play-Zone GmBH, Steinhausen, Switzerland) attached to the copper tape. Formation of GUVs in formation buffer was carried out by applying an AC electric field with 2.2 Volt peak-to-peak (V_{pp}) and 10 Hz for 60 min as well as 2.2 V_{pp} and 3 Hz for 30 min at RT. The GUVs were incubated for at least 1 h at 4 °C before performing further experiments.

PVA assisted GUV formation with LON probe in lipid mixture

GUV formation with PVA was done as described[265] with a few modifications. 1 mL 5 % PVA (*w/v*) in 280 mM sucrose was incubated for 1 h at 90 °C in a thermal shaker lite (VWR international GmbH, Dietikon, Switzerland) with 1'000 rpm shaking, and vortexing every 15 – 20 min. Wells of an 8 well chambered cover glass slide (#1.5 high performance cover glass, Cellvis, Mountain View, California, USA) were treated for 1 h with 400 µL milk solution (0.5 g milk powder in 5 mL distilled water) and washed twice with 1 mL distilled water. 100 µL PVA solution was added to wells and the gel was left to dry for 1 h on at 50 °C on an aluminum-foil-covered heat plate. 10 µL of lipid mixture 2 was added dropwise onto the gel in each well and solvent was evaporated for 1 h at vacuum. Gels were rehydrated for 1 h using 300 µl 10 mM HEPES-KOH pH 7.4, 400 mM sucrose. The solution was removed from the wells and GUVs were stored for at least 1 h at 4 °C before performing further experiments.

Slide preparation and imaging

8 well chambered cover glass slides were coated for 30 min – 1 h with 0.05 mg mL^{-1} BSA in 10 mM Tris-HCl, pH 8.0, 50 mM NaCl. Wells were washed with appropriate imaging buffer, after which the desired amount of imaging buffer and GUV solution was added and GUVs were left to settle for 1 h. 200 µL imaging buffer (10 mM MOPS-KOH pH 7.4, 400 mM glucose) and 100 µL GUVs were used for vesicle prepared by electroformation while 400 µL imaging buffer (10 mM HEPES-KOH pH 7.4, 400 mM glucose) and 100 µL GUVs was used for vesicles prepared by PVA assisted formation. Slides were imaged using an inverted fluorescence microscope (Nikon Ti-2 Eclipse spinning disk confocal microscope, Nikon Europe BV, Amsterdam, Netherlands) with a 40x objective (CFI Plan Fluor 40x/1.30 W.D. 0.24, Nikon Europe BV). Images were recorded in Brightfield mode using a lamp intensity of 15.6 % and an exposure time of 50 ms. Fluorescent images were recorded in widefield and Spinning Disk

Confocal mode with 470 nm excitation and 515 nm emission, 5 – 10 % intensity and 100 – 200 ms emission for CF and 640 nm excitation and 698 nm emission, 2 – 3 % intensity and 200 – 300 ms emission for CypHer5E, with 2 x 2 binning if necessary. For estimation of vesicle concentration and diameter distribution, Z-stacks were recorded with 3 x 3 imaging positions in each well. For GUVs formed with LON probe in rehydration buffer, wells were washed 7 – 8 times with 200 µl buffer without LON probe, by simultaneous addition of new buffer and removal of 200 µL solution from the well, to remove non-incorporated LON probe.

Image preparation

Image preparation and data extraction was performed using FIJI.[419] For Brightfield images, the files were opened in FIJI, brightness was adjusted to the desired values, a scale bar was added and images were exported as Tiff-files. For fluorescent images, background was subtracted using the Background Subtract function with a rolling ball radius of 200.0 pixels and none of the options enabled. Brightness was adjusted to the desired values, a scale bar was added and images were exported as Tiff-files.

Data extraction and preparation

Profile plots of GUVs were made by drawing a line selection through a vesicle on the background subtracted images, using the Plot Profile function to extract the intensity data. As different imaging parameters were used, the intensities were normalized to their maximal value. Vesicle diameters were estimated from Z-stack recordings using two custom FIJI macros to extract the data. The first macro performs a background subtraction on all slices of the Z-stack with a rolling ball radius of 100.0 pixels, then makes an average projection of the stack and performs a bandpass filter to highlight the contrast between the background and vesicles with the following settings: filter large = 40 pixels, filter small = 5 pixels, suppress stripes = None, tolerance of direction = 5 %, with autoscale after filtering and saturation of image when autoscaling enabled. Manual thresholding is performed to create a binary mask separating vesicles and background. The second macro is performed which cleans up the binary mask by performing the binary processes Fill Holes, Erode and Watershed and vesicles are identified using the Analyze Particles function with Size = 0.75 µm^2 – Infinity, Circularity = 0.70 – 1.00 and Display Results, Exclude on Edges and Add to ROI manager enabled. Using the Measure function, the Feret diameter is obtained. GUVs with diameters of 5 – 20 µm are counted and their concentration is estimated based on the total imaged area, the area of the well and the volume of GUV solution added to the well. Profile plots and Diameter distributions are plotted using GraphPad Prism 8.3.0. Histograms were prepared using the frequency distribution analysis on the obtained vesicle diameters with a bin size of 2 µm.

Results and Discussion

GUV electroformation with bifunctional DNA probe in rehydration solution

As outlined in the previous chapter, we have used bifunctional DNA probes to detect proton translocation mediated by reconstituted MPs in SUVs.[174] These DNA probes were formed by hybridization of single-stranded DNA molecules, modified with either pH-sensitive fluorophores for detection of proton translocation or cholesterol moieties for membrane-anchoring. Two different probe designs were investigated, a DNA duplex containing the dye and one cholesterol moiety (LON-dye) as well as a trimer containing two cholesterol moieties (L_2ON-dye). For more details on the probe design and assembly, refer to the Results and Discussion of the Supporting Information in chapter 3.2.1. Removal of the dye from the outer leaflet via DNase I treatment enhanced the sensitivity of the probe and membrane-anchoring prevents leakage of the dye out of the vesicle interior,[174] both of which would be highly beneficial for MP measurements in GUVs. Various strategies have been established for incorporation of LONs into GUVs. A simple method is the addition of LONs to preformed vesicles, but this will result in an incorporation in the outer leaflet only,[349,467,473–475] which is not desired for measuring substrate changes in the GUV interior. For simple incorporation in both leaflets, LONs might be added to the rehydration solution during GUV formation, as performed with electroformation by Bunge *et al.* (2007).[469] Alternatively, LONs can be mixed with lipids, deposited on a surface and dried together, either by addition of a small volume of DNA in aqueous solution to a chloroform methanol lipid mixture[174,470] or by first drying followed by redissolving LONs in solvent (chloroform, methanol or a mixture thereof) containing the desired lipids.[451,471,472] GUVs are then formed from this lipid-LON film, for example by gentle hydration[451,471] or by electroformation.[470,472]

Contrary to previously published results,[454] we found stable incorporation of the probe into SUVs (~ 80 %) even with one cholesterol moiety and observed no difference between the probes with one or two cholesterols.[174] In our publication, we speculated that this might be due to our use of spherical vesicles compared to planar supported lipid bilayers as investigated by Pfeiffer & Höök (2004).[454] However, there is also a possibility that our experimental setup is not able to discern between stable or unstable incorporation. While the probe on the inside of the vesicles is trapped, the DNA molecules with just one cholesterol moiety may be able to exchange between the outer leaflets of different vesicles, as previously suggested.[454] Due to the relatively high lipid concentration (5 mg/mL), this effect is likely not detected in our case and overall, no difference is observed between the probes containing one or two cholesterol moieties, whereas for the latter, this exchange may not take place. The lipid concentrations of typical GUV solutions produced in our lab are over 100 times smaller compared to SUV solutions. In addition, the volume to surface ratio of a 10 µm GUV is 100 times bigger than that of a 100 nm SUV. Thus, a highly stable integration of the probe into the membrane may be much more important for GUVs

compared to SUVs. Based on this hypothesis, we decided to focus on the incorporation of the DNA trimer containing two cholesterol moieties.

As a first approach, we followed Bunge *et al.* (2007)[469] with addition of different concentrations of carboxyfluorescein-labeled trimer (L_2ON-CF) to the rehydration buffer for GUV electroformation on ITO coated glass slides using pure DOPC as lipid. The individual oligonucleotides were hybridized for 10 min before addition to the rehydration solution and concentrations of the CF-labeled oligonucleotide (ON) ranged from 0.1 to 1.0 µM, while the cholesterol-labeled oligonucleotides were present in slight excess as published.[174] In total, 4.4 nmol lipids and L_2ON containing 0.62, 0.31 and 0.06 nmol CF-ON were used for electroformation. GUVs were transferred to an 8 well chambered slide for imaging and despite not being immobilized, the wells were washed due to initial high background fluorescence, indicating the presence of non-incorporated dye. The GUVs that remained in the well after this careful washing were then imaged. Many of the observed GUVs showed CF signals both in the vesicle interior as well as in the membrane, with a slight enrichment of signal in the membrane (Figure 22d, e). CF fluorescence was readily observed at high concentration of probe with the used microscope settings, but no or very small fluorescence could be detected at the lowest concentration, with GUVs being clearly visible using Brightfield imaging (Figure 22c, f).

The presence of non-incorporated probe in the exterior solution and of CF signal in the vesicle interior both indicates that incorporation of L_2ON-CF into GUVs by addition to the rehydration buffer is inefficient. In SUVs, 15-20 % of the probes were not incorporated.[174] This is attributed to ONs which do not contain cholesterol-moieties, either because they are not fully hybridized or because of missing modifications in the anchoring strands, as ONs were used as supplied by the manufacturer without further purification. In the same manner, free CF may not be completely removed from the CF-labeled ON. During GUV formation, an alternating electrical current is applied and as DNA is highly charged, it is possible that the trimer is not stable during formation. It has also been shown that LONs can form aggregates or micelles in aqueous solutions, whereby the onset of aggregation or micelle formation depends on the hydrophobicity of the lipophilic moiety.[476–478] For cholesterol-labeled ONs, critical micellar concentrations in the µM range were previously reported.[476,477] Due to the bivalent cholesterol modification of the probe used here, it is possible that some aggregates or micelles were present in the rehydration solution, even though concentrations of the probe were not above 1 µM. It has been previously shown that the presence of liposomes reduces the abundance of aggregates[477] which is in line with the efficient incorporation in SUVs where the lipid concentration is high.[174] In contrast, these aggregates may be more frequent in GUVs due to the low lipid concentration and may be responsible for some of the non-incorporated dye signal.

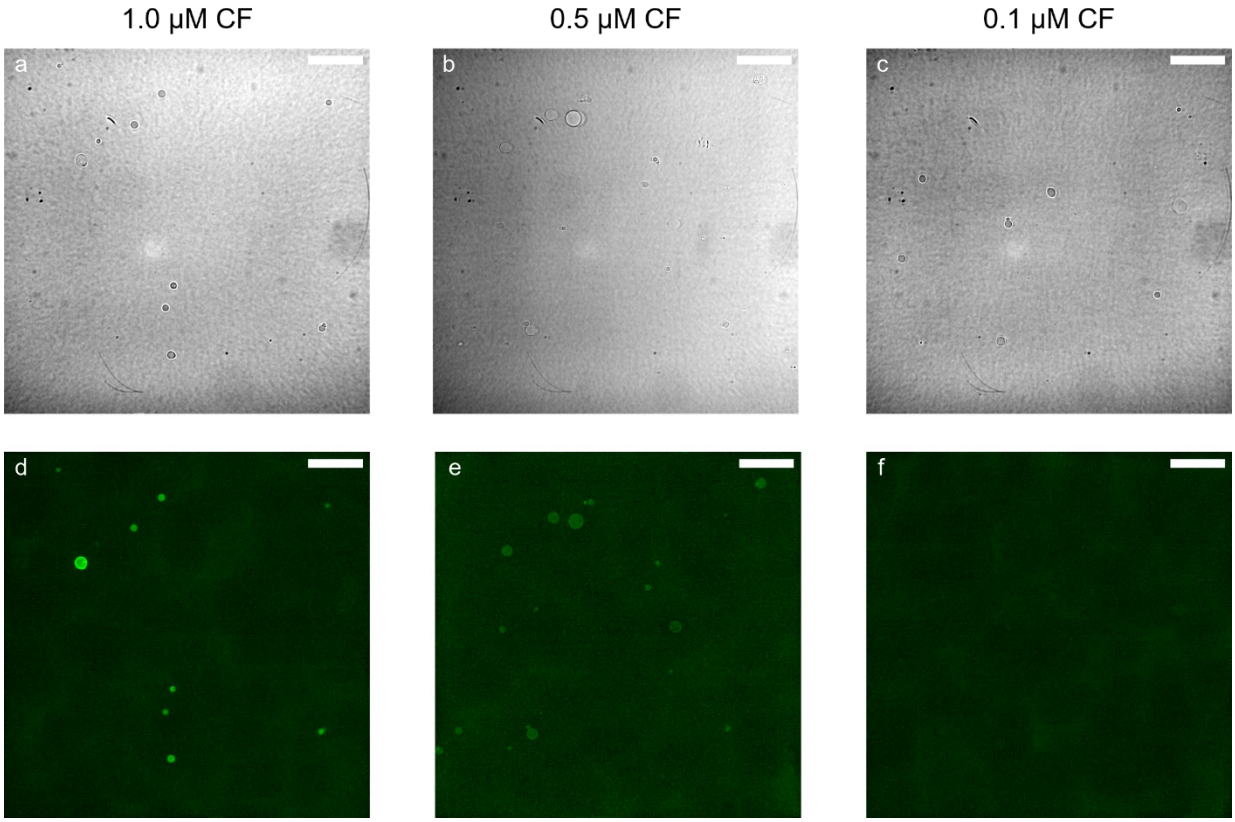

Figure 22: GUV electroformation with L_2ON-CF in the rehydration solution. Microscopy images of GUVs formed with three different concentrations of ON-CF in the rehydration buffer, namely 1.0 µM (a, d), 0.5 µM (b, e) and 0.1 µM (c, f). The scale bar is 50 µm in all figures. a-c) Brightfield images recorded in widefield mode. d-f) Confocal fluorescent microscopy images of CF-ON colored in green. Imaging settings and Look Up Tables are the same for all fluorescent images.

GUV electroformation from lipid deposits containing bifunctional DNA probe

To prevent the formation of micelles or aggregates in aqueous solution, we decided to mix lipids and L_2ON probes in solvent prior to deposition and drying on ITO coated glass slides for electroformation, as previously reported for other LONs.[470,472] Drying of the lipid-L_2ON mixture ensures a high lipid concentration which may allow integration of the probe into the lipid bilayers of the dried lipid patch. In our publication, mixing of LON probes and lipids prior to drying using an organic solvent mixture (chloroform: methanol: water = 6.25:6.25:1, *v/v/v*) showed no improvement compared to addition to the rehydration solution for SUV formation.[174] However, since formation of SUVs containing LON probe was successful from this mixture, it was decided to use this as a starting point for GUV formation. Occasionally, we observed some vesicles that showed membrane localization if GUVs had been stored at 4 °C overnight prior to imaging as opposed to when they were viewed directly after formation. Based on this, we hypothesized that the membrane order might play a role in efficient localization to the GUV membrane. Interestingly, several publications used a lipid mixture of 2/1/1 PC/PE/cholesterol for the formation of GUVs containing LONs.[451,467,471] While these publications do not state the reasoning for the choice of this mixture, sterols have been associated with the formation of the liquid ordered (L_o) phase,[479] and it has been reported that cholesterol-labeled DNA preferably partitions into the L_o phase

with enhanced partitioning for two cholesterol anchors.[473,475] Thus, we decided to investigate similar lipid compositions, namely DOPC/DOPE/cholesterol and POPC/POPE/cholesterol (50/25/25 mol% PC/PG/cholesterol). DOPC and DOPE both contain two oleic acid molecules (18 carbon chains with a cis double bond at the 9th position), with transition temperatures around -15 °C, while POPC and POPE contain one palmitic acid (16 carbon chain with no double bond) and one oleic acid, with transition temperatures of around 0 ° and 25 °C for POPC and POPE, respectively.[480] Thus, the membrane fluidity is expected to be higher for DOPC/DOPE/cholesterol than for POPC/POPE/cholesterol at room temperature, and based on our hypothesis, better localization for POPC/POPE/cholesterol is expected. We were also interested whether the pH-sensitive fluorophore had an influence on the localization of the probe, as we also had LON probes labeled with the pH-sensitive dye CypHer5E. The structural differences between this cyanine dye and carboxyfluorescein could influence the formation of aggregates or micelles.

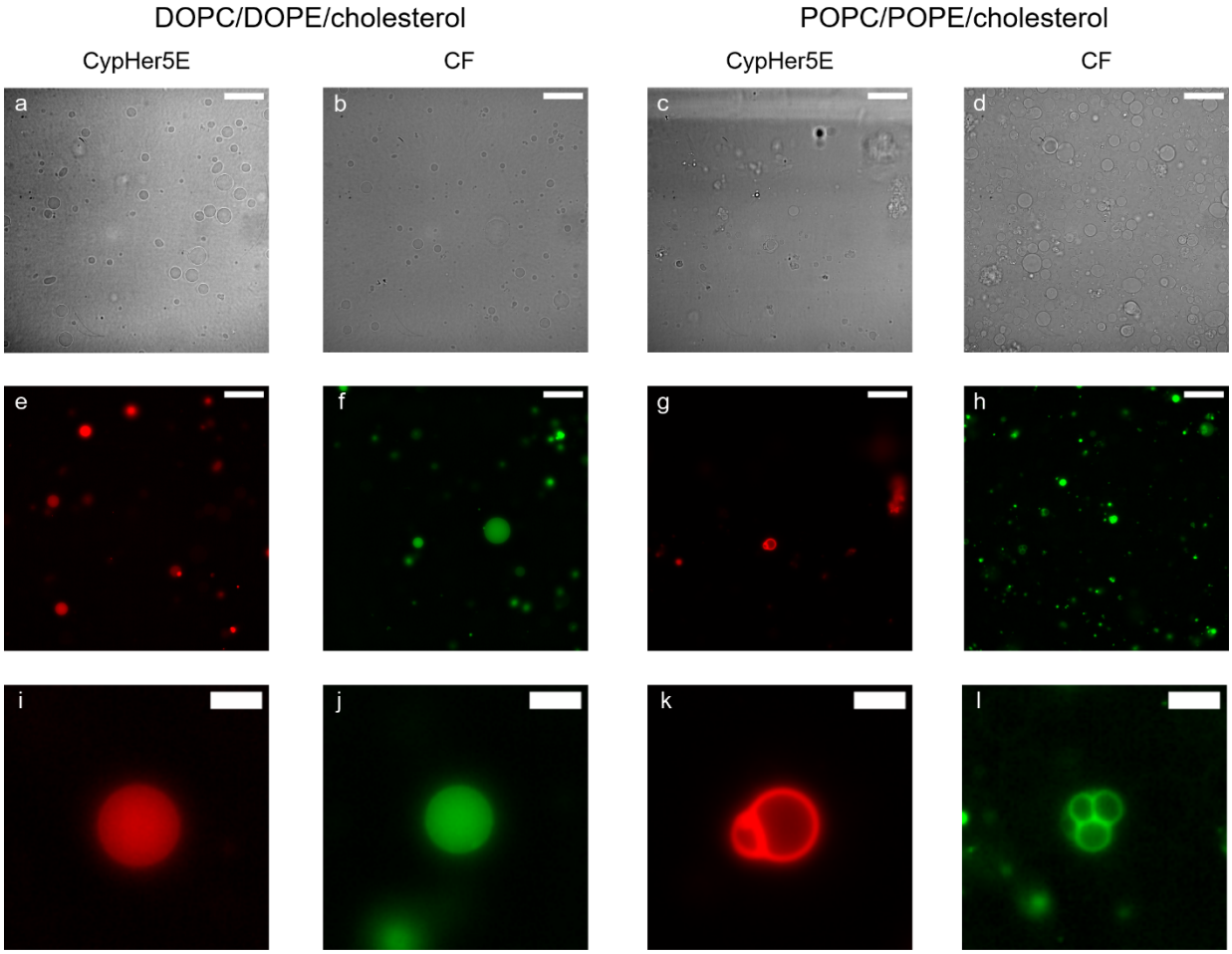

Figure 23: GUV electroformation of L_2ON probe mixed and dried with lipids. Microscopy images of GUVs formed with L_2ON-CypHer5E (a, e, i, c, g, k) and L_2ON-CF (b, f, j, d, h, l) and two different lipid mixtures were used, namely DOPC/DOPE/cholesterol (a, b, e, f, i, j) and POPC/POPE/cholesterol (e, f, g, h, k, l). a-d) Brightfield images recorded in widefield mode. e-l) Confocal fluorescent microscopy images of CypHer5E-ON colored in red and of CF-ON colored in green. Imaging settings and Look Up Tables are not the same for the fluorescent images to better visualize the GUVs from the different formations. a-h) The scale bar is 50 µm. i-l) Blow-up of a single GUV from e-f, the scale bar is 10 µm

GUV electroformations were carried out using both L_2ON-CF and L_2ON-CypHer5E, which were hybridized in water prior to mixing with the organic solvent mixture containing the lipids. ITO coated glass slides were coated with approximately 100 nmol lipids with L_2ON containing 0.1 nmol CF- or CypHer5E-ON, which should result in GUVs incorporating 0.1 mol% fluorescent dye. More details on the electroformation from dried lipid-L_2ON mixtures can be found in the Experimental Procedures. For GUV electroformation from dried lipid-L_2ON mixtures, less LON probe compared to lipid was used as in electroformation with probe in the rehydration solution. Results of the GUV formations are shown in Figure 23. Brightfield images are shown in panels a-d, indicating that GUVs were formed with both lipid mixtures and both pH-sensitive dyes. Panels e-l show that incorporation of L_2ON probe is observed in some of the GUVs. Interestingly, no washing was required as little background signal was observed in the surrounding solution. Despite the small concentration of L_2ON probe compared to the formation with probe in rehydration buffer, GUVs containing L_2ON probe showed intensities well above background levels. Strikingly, the probe incorporation was rather inhomogeneous, as many vesicles showed no detectable dye incorporation at all (Figure 23a-h). This indicates an inhomogeneous distribution of L_2ON probe in the dried lipid patch, likely due to the low amount of probe compared to lipids. The two lipid mixtures showed differences in terms of the localization of the probe, while the pH-sensitive dye did not influence the localization. For DOPC/DOPE/cholesterol, localization appeared to be exclusively in the GUV lumen (Figure 23e,f,i,j) while POPC/POPE/cholesterol showed at least some localization in the membrane, as a strong signal indicating the GUV outline was observed while the fluorescence intensity was lower in the vesicle interior. (Figure 23g,h,k,l). Even though localization in this lipid mixture was better, the quality of GUVs obtained was not as good as in the DOPC/DOPE/cholesterol mixture, with an increased number of multilamellar and aggregated vesicles (Figure 23c,d,g,h,k,l).

The concentration of probe inside the GUVs can be explained in two ways. First, if the L_2ON probe is anchored in the membrane, we would expect it to be present only in the GUVs and not in the surrounding solution. However, even if the probe is not anchored, a concentration in the vesicles is possible. During drying, the L_2ON-lipid mixture likely assembles into a stack or stacks of several lipid bilayers. For DNA molecules which are located in between lipid bilayers, it can be envisioned that diffusion to the inside of a forming GUV is easier than diffusing out of the bilayer stacks, although the latter may be possible if large bilayer defects are present near the DNA molecules. Further, we have shown that there is some interaction between the ONs and the zwitterionic membrane,[174] which would further contribute to a concentration in the vesicles. Assuming that the L_2ON probe is properly hybridized, the observed differences between the two lipid mixtures support our hypothesis that the membrane order influences the localization of the probe. Interestingly, Pfeiffer & Höök (2004)[454] used POPC in their incorporation studies of cholesterol modified ON, which has a stronger lipid packing than DOPC.[481] Simulations also found better packing of cholesterol with POPC than with DOPC,[482] thus

cholesterol anchors may integrate more easily into the membrane or may be more stably anchored. Cholesterol was added to the lipid mixtures to increase the order of the membrane. It was previously shown that cholesterol affects the bending rigidity only significantly for POPC and not for DOPC.[483–485] On the other hand, a recent report by Chakraborty *et al.* (2020) suggests that cholesterol stiffens the membrane even for mixtures containing DOPC.[486] However, in this case it may still not be enough to achieve stable anchoring of the probe. This would further mean that in the case of DOPC/DOPE/cholesterol, the L_2ON probe is dissolved in the vesicle interior, possibly in the form of micelles or aggregates. It is important to note that the ON which is labeled in these experiments does not contain a cholesterol modification. Thus, a definitive conclusion where the ONs with the cholesterol-anchors are located is not possible. It may also be the case that the L_2ON trimer is not properly hybridized or has dissociated in the organic solvent mixture or during electroformation. This would result in soluble dye-labeled ON that is separated from the cholesterol-labeled ONs, which may be anchored to the membrane in both lipid mixtures. The change in localization of soluble ON may be explained by lipid-phase dependent interaction of ON with the membrane, as previously suggested.[487] Further, it is not clear from the experiments performed here whether L_2ON probe is actually present in the outer leaflet of the membrane.

GUV electroformation from diluted lipid deposits and ON localization analysis method

Before tackling the question of ON localization, we wanted to achieve a more homogeneous distribution of L_2ON probe in the GUVs. As we suspect a non-homogeneous distribution of L_2ON probe in the dried lipid patch, formation with a reduced lipid to L_2ON probe ratio was performed, lowering both the lipid as well as L_2ON probe concentration to further avoid potential aggregation of the latter. Thus, a lipid mixture with a 10-fold reduction in lipid concentration and 2-fold reduction of L_2ON-CF concentration was used. Because no differences between the two pH-sensitive dyes were observed, only carboxyfluorescein was used for further experiments. GUVs were only formed from POPC/POPE/cholesterol as it showed the desired localization. ITO coated glass slides were coated with approximately 10 nmol lipids containing L_2ON with 0.05 nmol CF-ON, which should result in GUVs incorporating 0.5 mol% fluorescent dye. This total lipid concentration is also more in line with typical electroformations performed in our lab. The L_2ON probe showed again localization in the membrane, but far fewer GUVs were observed as in the previous formation (Figure 24A), as a decreased amount of lipids were used. The GUV concentration also appeared to be lower than expected, comparing to GUV electroformations without LON,[430] indicating that the probe negatively affects the formation.

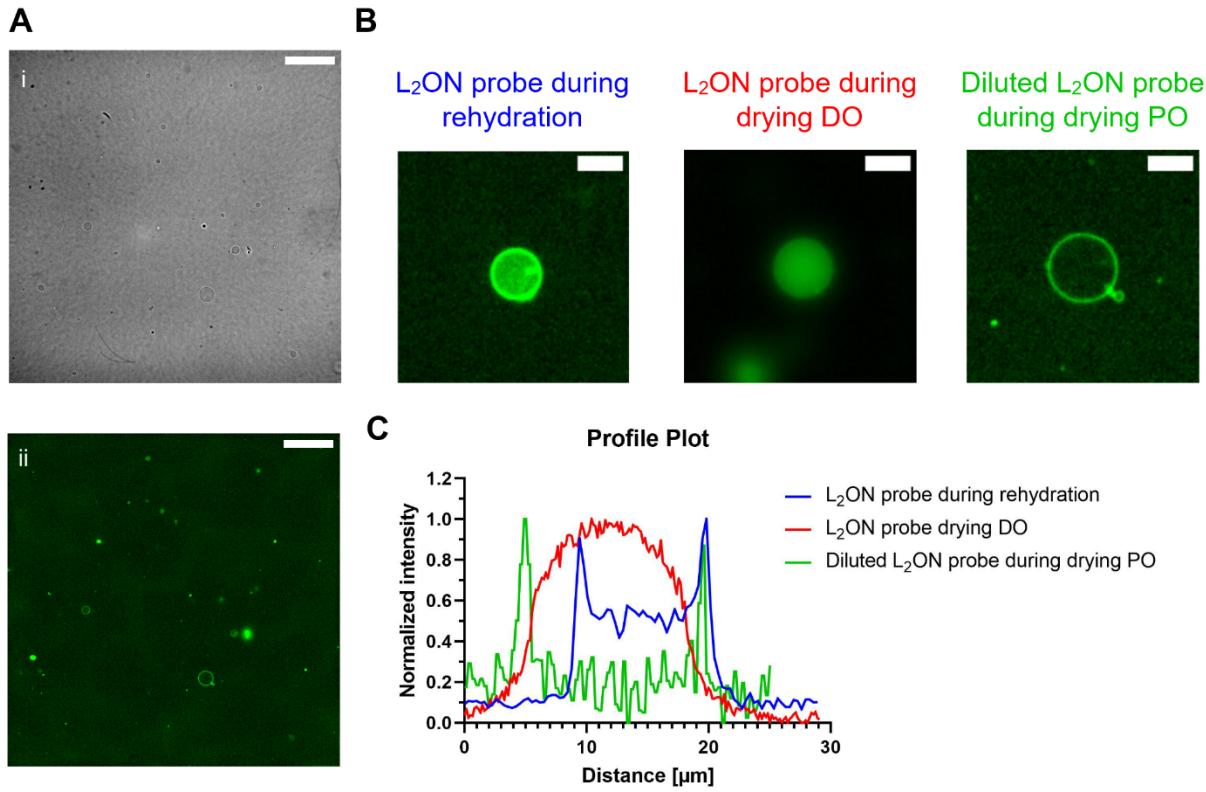

Figure 24: GUV electroformation of L_2ON-CF mixed and dried with lipids and overview of the different electroformation results. A). Microscopy images of GUV formed by electroformation using L_2ON-CF with reduced lipid and probe concentration. The scale bar is 50 µm. i) Brightfield images recorded in widefield mode. ii) Confocal fluorescent microscopy images of CF-ON colored in green. B) Confocal microscopy images of single exemplary GUVs from the different electroformation approaches. From left to right: GUV from the formation with L_2ON probe in the rehydration buffer, GUV from the formation with L_2ON probe mixed and dried with double unsaturated (DO) lipids, GUV from the formation with L_2ON probe mixed and dried with monounsaturated (PO) lipids with reduced concentrations of lipid and probe. Scale bar is 10 µm. Imaging settings and Look Up Tables are not the same for the fluorescent images. C) Profile plots of the exemplary GUVs. Profiles were obtained using FIJI by drawing a line selection over the GUV. Profiles were normalized to the maximal value as images were recorded using different settings and to highlight the differences of the profile depending on the localization of the probe.

In order to compare the efficiency of membrane localization for different formation methods and lipid mixtures, a quantitative measure is needed. Three exemplary GUVs were picked showing different dye localizations, one from GUV formation with L_2ON probe in rehydration buffer, one from formation with DOPC/DOPE/cholesterol and one form the formation with POPC/POPE/cholesterol and reduced lipid and dye concentrations (Figure 24B). Because only few GUVs were imaged for some conditions and different microscope settings were used in the different experiments, fluorescence intensities of the different lipid mixtures were not compared. Profile plots of these GUVs were extracted and normalized to the maximal intensity (Figure 24C). For a vesicle which shows L_2ON probe distributed in the vesicle interior, a bell-shaped curve is obtained, corresponding to the shape observed for soluble dyes encapsulated in GUVs.[488] For a vesicle where the probe is fully localized to the membrane, two peaks are expected representing the membrane, with signal going down to background levels in the vesicle

interior (as imaging is done in confocal mode). This is observed for a vesicle from the formation with diluted POPC/POPE/cholesterol lipids and probe. A GUV with a partial localization to the membrane shows peaks for the membrane, but signal in the vesicle interior does not go down to background levels, which is observed for a vesicle from the formation with probe in the rehydration buffer. Using such profile plots, the localization of the probe in different GUV preparations may be quantified by comparing the intensity at the membrane and in the middle of the vesicle. However, a second, lipid-coupled dye needs to be added to unambiguously identify the position of the membrane for all vesicles as well as to compare the relative amount of L_2ON incorporated. However, such a lipid-coupled dye was not used here, hence the method is only demonstrated on these three exemplary GUVs.

Polymer assisted GUV formation from lipid deposits containing bifunctional DNA probe

In all the experiments described above, electroformation was used to incorporate L_2ON probe into GUVs, resulting in either inhomogeneous incorporation or rather poor yield of GUVs. We have previously shown that PVA assisted formation of GUVs produces about 10-fold higher concentration of vesicles compared to electroformation.[430] To this end, 5 nmol lipids containing L_2ON with 0.025 nmol CF-ON, which should result in GUVs incorporating 0.5 mol% fluorescent dye, was added to PVA hydrogels using both double unsaturated and monounsaturated lipid mixtures for PVA formation. A much larger concentration of vesicles was obtained (Figure 25), as expected, allowing quantification of vesicle yield and size distribution. Incorporation of the probe was still inhomogeneous, but rather than two distinct populations (GUVs with dye and empty GUVs), the intensity of dye signal varied between GUVs (Figure 25c, d).

Using a previously described method,[430] GUV concentrations for vesicles with 5 - 20 µm diameters of 1.76 x 10^5 and 4.51 x 10^5 GUVs mL^{-1} were obtained for DOPC/DOPE/cholesterol and POPC/POPE/cholesterol, respectively. These concentrations are around 20 – 40 times lower than expected for PVA formations in buffer without salt and LON probes,[430] which indicates again that the L_2ON probe negatively affects formation. However, PVA formations were carried out using a different formation chamber setup. Typically, PVA gels are cast inside a rubber O-ring placed on top of a glass coverslip,[430] whereas formations here were carried out by casting the gel inside of 8 well chambered slides, which may be the reason for the decrease in vesicle concentration. Size distributions were comparable to other PVA formations,[430] with a large amount of very small vesicles and decreasing frequency with increasing GUV diameter (Figure 26). Interestingly, very few large GUVs (> 30 µm) were obtained, which is in contrast to previous results where a considerable amount of vesicles is observed in the range of 20 – 60 µm.[430] This might be another indication for the impeded formation in the presence of L_2ON probe, although an influence of the formation setup can't be excluded and data from only one formation is shown.

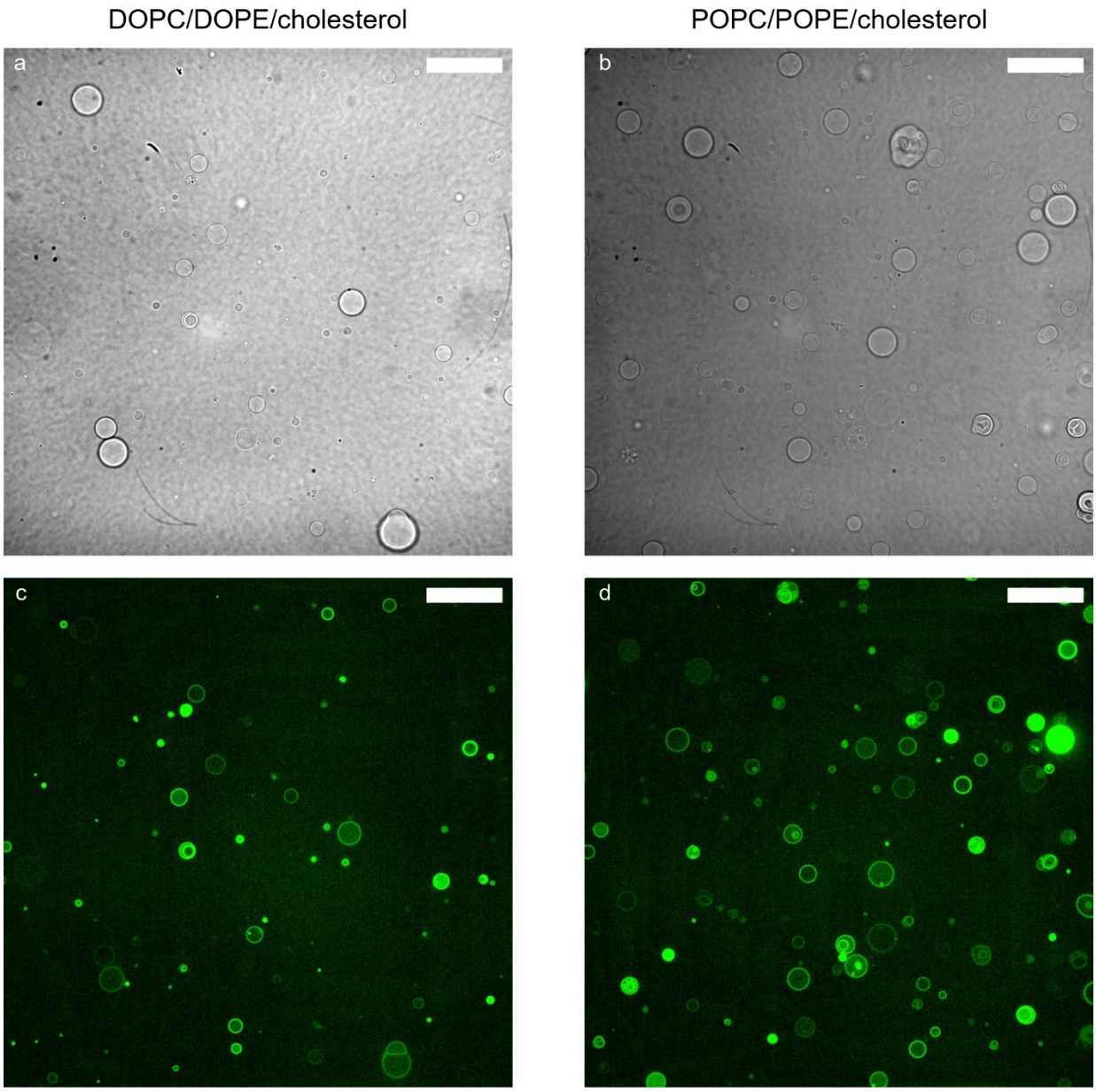

Figure 25: PVA assisted GUV formation of L_2ON-CF mixed and dried with lipids. Microscopy images of GUVs formed using PVA assisted swelling with lipid mixtures DOPC/DOPE/cholesterol (a, c) and POPC/POPE/cholesterol (b, d). The scale bar is 50 µm. a-b) Brightfield images recorded in widefield mode. c-d) Confocal fluorescent microscopy images of CF-ON colored in green. Imaging settings and Look Up Tables are the same for the fluorescent images.

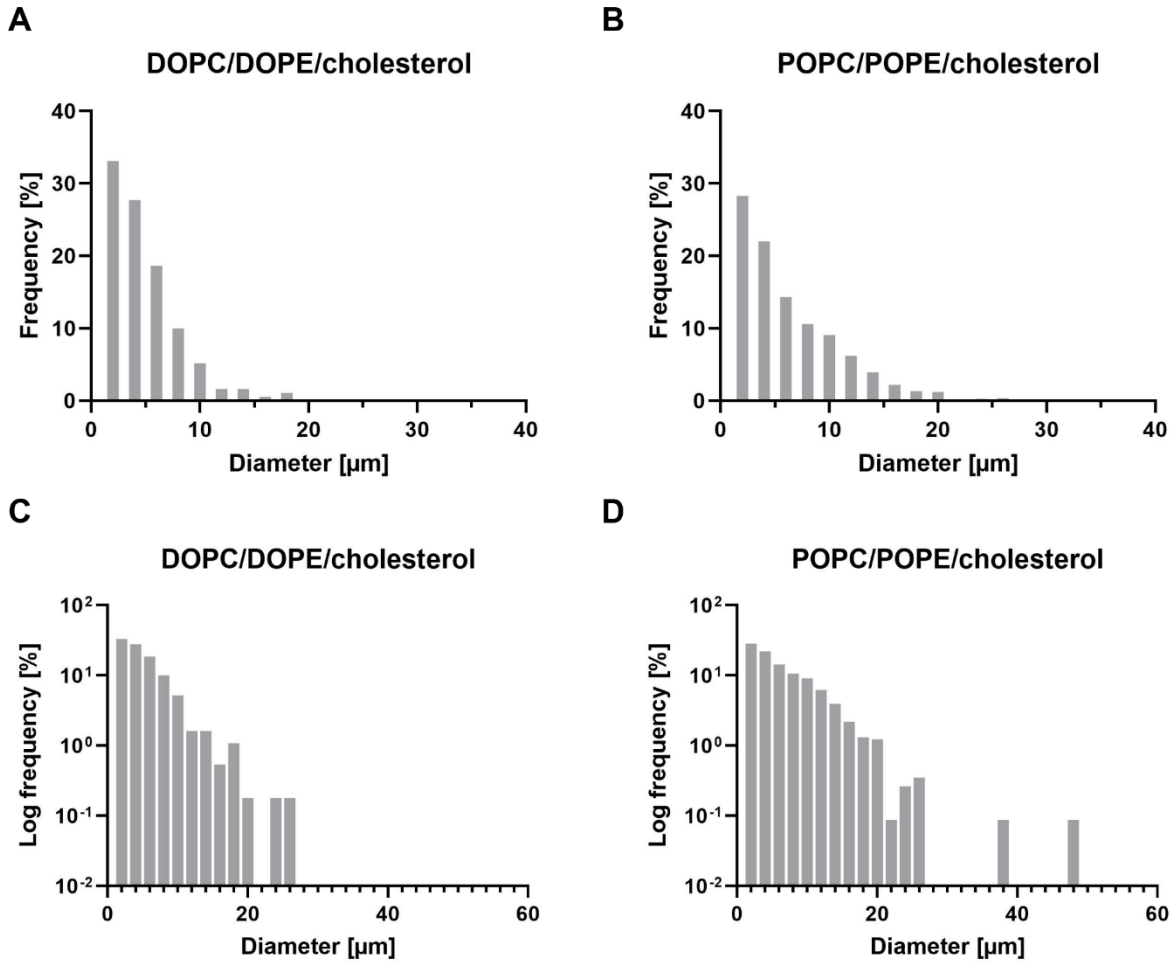

Figure 26: Size distribution of PVA assisted GUVs containing L_2ON-CF formed with PVA assisted swelling. Histograms made with a bin size of 2 µm showing the size distribution of GUVs measured using FIJI. A-B) Frequency distribution of GUVs with diameters between 1 – 40 µm using either DOPC/DOPE/cholesterol (A) or POPC/POPE/cholesterol (B) as lipid mixture. C-D) Logarithmic frequency distribution of GUVs with diameters between 1 – 60 µm using either DOPC/DOPE/cholesterol (C) or POPC/POPE/cholesterol (D) as lipid mixture.

Strikingly, in contrast to electroformation, the number of GUVs with dye localized primarily in the membrane has largely increased for DOPC/DOPE/cholesterol, while this was expected for POPC/POPE/cholesterol. The change of membrane localization for the DOPC/DOPE/cholesterol mixture is not trivial to explain. However, as previously discussed, the lipid order may influence both the anchoring of cholesterol-modified DNA in the membrane as well as interaction of soluble ON with the membrane. It has been shown that GUVs from PVA formation display altered membrane properties due to PVA contaminations.[266] This could influence the membrane order, or the contaminations themselves could influence the interaction of soluble ON with the membrane. Further, it has been shown that different buffers can affect the bending rigidity of the membrane, with MOPS buffer used in electroformation experiments leading to a decrease in bending rigidity while HEPES used for the PVA formation only slightly affected the bending rigidity.[415] A larger bending rigidity and better packing of the lipids might help anchorage of cholesterol-labeled ON or localization to the membrane of soluble

ON. The electric field used for electroformation could also have an influence on localization by interaction with the charged DNA or by lipid oxidation, which might also influence the membrane order. One or several of these effects could lead to an increased order of the DOPC/DOPE/cholesterol membrane for PVA GUVs compared to electroformed GUVs, leading to the change in probe localization. It is important to note that electroformation with the diluted lipid mixture was not performed using the DOPC/DOPE/cholesterol mixture. Thus, it can't be excluded that the concentration of lipids and L_2ON probe in the organic solvent mixture plays a role in the localization. The differences in localization observed using these different formation methods were very surprising, as efficient incorporation in SUVs was shown and was dependent on the presence of a cholesterol moiety on the DNA. Further, by DNase I digestion and pH calibration curves, we could show that half of the probe was located in the outer leaflet of the SUVs, further indicating that the probe is anchored in the membrane.[174] However, as discussed before, the lipid concentration is higher in SUV compared to GUV solutions, which may promote membrane-anchoring, and it is possible that our experiments in SUVs were not able to show unstable integration. Further, GUV formation differed in lipid and buffer composition, e.g. magnesium chloride was present in the buffer used for the formation of SUVs, which might influence the aggregation behavior of the probe or its membrane integration.

Conclusion and Outlook

Here, we investigated two different strategies for incorporation of LON probes into the membrane of GUVs, using two GUV formation methods. Incorporation by addition of probe to the rehydration buffer for electroformation was found to be inefficient as only partial localization to the membrane was observed as well as high background signals before washing, indicating the presence of non-encapsulated probe. Drying of L_2ON probe with lipids on ITO coated glass slides or PVA hydrogels resulted in concentration of dye in the GUVs, as probe signals were readily observed without washing of the wells before imaging. Different localizations of the probe were observed, ranging from localization in the GUV lumen only to partial membrane and lumen localization, to localization in the membrane only, depending on the lipid composition and GUV formation method. With electroformation, low yields of GUVs were obtained and localization to the membrane was observed primarily when using monounsaturated lipids. PVA formation resulted in higher GUV yields and localization to the membrane was observed with both monounsaturated and double unsaturated lipids. In both formation methods, vesicle yields were below expected concentrations, which might indicate that GUV formation is impeded by the presence of LON probe. However, GUV formations have not been performed using the organic solvent mixture with lipids but without LON probe, to show that the decreased GUV concentrations are indeed observed due to the presence of LON. Although the mol percentages of probe compared to lipids were low (< 0.5 %), DNA is highly charged and hydrophilic, and charged lipids have been known to affect GUV formation.[191,256] The probes used here hybridize to a 30-nt long double strand. If the DNA is responsible for the low GUV yields, better formations might be achieved by reducing the length of the probe, in other words lowering the charge and size of the hydrophilic moiety attached to the lipophilic anchor.

The difference in localization of the probe observed here, especially the presence of probe signal in the GUV lumen, was rather surprising in light of the 80 % incorporation observed in SUVs.[174] To assess the influence of lipid composition, lipid to probe ratio and concentration, as well as GUV formation method, on the localization of the probe, quantitative comparisons of the different conditions are required. By incorporating a different lipid-coupled dye, allowing the exact localization of the GUV membrane, the extent of LON probe localization could be quantified from intensity profile plots of GUVs. Further, the probe design used here does not allow to conclusively show whether the cholesterol-labeled ON is anchored in the membrane or in solution as micelles or aggregates, as the fluorescent label is present on the complementary soluble ON. For example, changes of membrane order may affect both integration of cholesterol-labeled ON in the membrane[473,475] or interaction of soluble ON with the membrane.[487] To show if localization is affected for the entire LON probe or just for the labeled ON, direct fluorescent labeling of the cholesterol-modified ON is necessary. ON without cholesterol modification should be used to assess whether probe concentration in GUVs during formation is possible

even in the absence of membrane-anchoring, and could be compared to free CF (i.e., dye not attached to DNA). As we can't conclude whether the trimer is stably integrated into the lipid bilayer of the GUV, we also don't know whether it is actually present in the outer leaflet of the GUV membrane. This question should be addressed before continuing with the addition of DNase I to remove the outer dye. Labeling of the LON probe with fluorophores such as NBD or DY-647P1, which can be quenched by membrane impermeable reagents,[261,425] could help to show the presence of LON probe in the outer membrane leaflet. Lastly, an improved localization of the probe could be achieved by changing of the anchoring moiety, in the case that the cholesterol-labeled ON is indeed not anchored in the membrane under certain conditions. For example, DNA coupling to a lipid instead of cholesterol may influence the stability of integration into the membrane, due to the increased hydrophobicity of the lipid compared to cholesterol. Different anchoring moieties have also been shown to possess different lipid phase preferences.[489] This could finally allow stable anchoring of LON probes in GUVs and replication of our functional measurements performed in SUVs.

4. General Discussion

The goal of this thesis project was to develop GUVs as a platform for the characterization of MPs and as a long-term aim the bottom-up creation of a synthetic cell (SC). To make full use of the potential of GUVs, we want to follow activity of MPs in real time under the microscope. By this, we can determine the behavior of individual vesicles which allows to observe empty vesicles and proteo-vesicles or different protein variants at the same time and under identical conditions, as was recently demonstrated for a glucose transporter.[205] This further allows about a 100-fold reduction of the protein amount needed to perform an experiment compared to bulk measurements, which is highly beneficial for MPs that are poorly expressed. Such a platform may serve for the development of new drugs by reconstituting for example human MPs. It is clear from the work in this project and the literature that this is not an easy task. There are many different options for the formation of GUVs, the reconstitution of MPs, how to investigate the vesicles microscopically and how to detect MP function as well as what kind of data to record and how to analyze it. The options that one should choose depend on the requirements that the researcher has on his experiments. This general discussion section will highlight how different requirements have opened different branches in the field of MP research in giant vesicles. Of course, these branches are not fully separated from each other and intertwine or overlap considerably. The first part of the discussion will focus on two such branches and highlight the requirements that have led to the emergence of polymer-based and cell-derived giant vesicles. In a second part, a critical analysis of the strategies investigated here will be presented and whether they are suitable for the requirements that we have on our platform. Lastly, we will take a glimpse into the future of giant SCs and how they may look like one day.

4.1. Use of Membrane Proteins in Giant Vesicles – Recent Developments

One aspect of using MPs in GUVs, besides their functional characterization, is the creation of synthetic cells. As in natural cells, MPs are crucial to provide many functionalities, such as substrate sensing, transport, or the delivery of energy for other processes to be carried out in the SC. Here, SC refers to an entity which mimics or replicates a biological function, e.g. that of the mitochondrion, or which combines a subset of cellular or artificial tools to carry out a specific task. These entities do not necessarily have to be autonomously self-sustaining and able to replicate, although this is of course an important aspect and considered to be the Holy Grail of SC research.[207] Before we take a look at approaches for the construction of SCs, I would briefly like to introduce two different motivations for SC research. Based on these two motivations, we can further formulate some requirements for these cells.

The first motivation is to understand all the biological components that are required to create a living cell. This is in its essence a basic scientific discipline, focusing on the identification and characterization of the minimal set of components required to create a SC that is able to replicate and sustain itself,

which may then be used to study the function of biological components not part of this minimal set to gain as much knowledge as possible about natural organisms.[490] Understanding the biology of life requires the use of naturally occurring parts (proteins, DNA, RNA, lipids and so on) with which one creates a cell containing the least number of unknown parts possible, ideally with no unknown parts. Using this cell, the interplay of the individual components can be studied in an environment that is as natural as possible.

The second motivation is more focused on the application of SCs in industrial or therapeutical processes and as such is more of an engineering discipline.[490] Here, the focus lies in the design of complex entities to carry out specific tasks, e.g. the synthesis of pharmaceutical or industrial products, either by combining a subset of cellular and artificial components or on a genome synthesis level, aided by computational modeling of metabolic networks.[490] With this idea in mind, SCs might harbor new functions that are so far not found in nature. One might thus use modified and improved natural parts and combine them with non-natural parts to create a cell that can carry out the desired task in a stable and reliable way. As long as the function of this cell can be carried out in a robust manner, it can also use components which contain unknown parts, in other words, the function of the entire component is known, but its composition or the functions of its individual parts are not fully characterized or well-described. Integration and combination of natural and non-natural components enables new functionalities and applications for these cells. Depending on the application, the use of unnatural or naturally occurring parts might be favored, for example to achieve stable and robust SCs for industrial purposes or to achieve a high biocompatibility for therapeutical purposes. Finally, it is clear that both motivations described here will contribute to the understanding of biological components, and each will benefit from the findings of the other. However, one motivation is clearly based on the goal to understand how living beings can exist while the other one is focused on creating entities for specific applications.

There are essentially two different strategies for the construction of a SC (Figure 27). The top-down approach takes an already existing organism and tries to reduce its complexity by step-wise removal of parts until a minimal set of components are identified that still shows the desired function of the organism, i.e. replication and self-sustainement.[491,492] One particularly popular effort using this strategy is carried out at the J. Craig Venter Institute where the genome of the bacterial parasite *Mycoplasma mycoides* is reduced to identify a minimal set of genes required for viability of the cell. Thus far, they have created a synthetic strain termed JCVI-syn3.0 with a set of only 473 genes, which is smaller than any other autonomously replicating organism.[493] JCVI-syn3.0 has served as a platform to identify further 19 genes which had been removed from the strain, but are required for normal morphological development of the cell and were thus reinserted to create JCVI-syn3.0A.[494] This strain is controlled by

a set of 452 proteins and 38 RNAs and was the basis for the creation of an *in silico* metabolic reconstruction that features 338 reactions using 304 metabolites categorized in nine subsystems based on approximately a third of the genome of JCVI-syn3.0A.[495] An important insight of this work is that rather than searching for a minimal genome, one should define the minimal set of functions that a SC needs (for example to help identifying redundant genes with similar functionalities), a task which is aided by the development of computer models such as developed for JCVI-syn3.0A.[490,495]

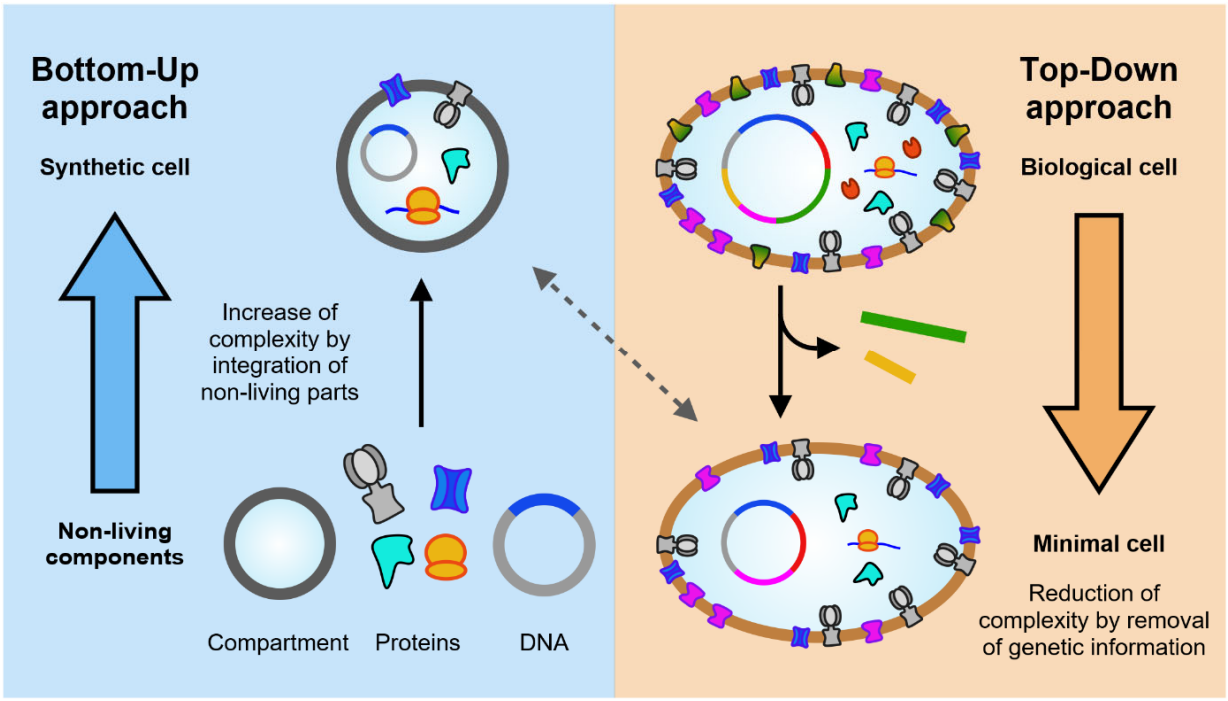

Figure 27: Schematic representations of the bottom-up and top-down construction of synthetic cells. For the bottom-up approach (left), non-living components such as DNA, proteins and a compartment formed from lipids or polymers are combined into a synthetic cell, increasing the overall complexity of the system, that mimics certain biological functions or is used for the synthesis of products for therapeutical or industrial purposes. For the top-down approach (right), genetic information is removed from a biological cell to create a minimal cell, a synthetic cell with a minimal set of components required for replication and self-sustaining, leading to a reduction of the complexity of biological cells. Further increase of complexity for bottom-up synthetic cells may lead to the production of "artificial" minimal cells from scratch, while reduction of complexity of minimal cells may produce systems without replication or autonomous self-sustaining more similar to bottom-up synthetic cells, as indicated by the grey dotted line.

The opposite of the top-down approach is the bottom-up strategy, where the construction of a SC is based on the assembly of individual non-living parts to create cells with defined functionalities. This task is inherently more challenging, and it remains unclear whether one day, perhaps, researchers will cross the line from the production of mere "machines", which may be sufficient for certain applications, to the creation of "living" organisms from scratch. However, recent advances have led to a rapid expansion of the research on bottom-up synthetic biology.[207,492,496] While the main focus here will not be on the bottom-up creation of a "living" artificial cell, it is still important to understand the basic elements

allowing replication and autonomous self-sustaining of SCs. These elements are molecules carrying information, ideally for the reproduction of the SC, molecules providing a metabolic system and a compartment that separates these molecules from the surrounding and creates the boundary of the living entity.[492,497,498] In this discussion, we will focus on the latter two as MPs are the machines which can provide metabolic functionality while giant vesicles form the compartments to contain the information and metabolic processes.

Polymer-Based Vesicles for Increased Stability in Industrial Applications

The potential use of SCs in therapeutical and industrial applications is an important driving force for the increased interest in this research field. Especially for industrial applications, SCs must be stable and robust, i.e., function under various temperatures and pH values as well as not degrade over time, and high-throughput production should be possible. In this regard, GUVs composed of lipid membranes might not be the most suitable vessel as they are generally not very stable and can be susceptible for leakage of certain compounds.[211,212] In recent years, polymer-based membrane vesicles have been developed using synthetic block copolymers (polymersomes)[214] (Figure 28) or protein-polymer nanoconjugates (proteinosomes).[499] These polymers offer an increased chemical stability compared to lipids and can be tailored to the specific needs of the application with a large diversity of polymers allowing direct engineering of physical and chemical membrane properties.[206,214,492,499,500] Pioneering work on the reconstitution of MPs into polymersomes was carried out by the group of Wolfgang Meier, where in 2001 the first MP (OmpF) was functionally reconstituted into the triblock copolymer PMOXA-PDMS-PMOXA.[501] In 2005, the group of Montemagno showed the first functional coreconstitution of ATP synthase and bacteriorhodopsin either as monomer or from purple membranes in PEtOz-PDMS-PEtOz vesicles.[502,503] These early experiments were performed in small vesicles as there were no methods at that time for the formation of giant polymersomes. This changed after the first giant polymer vesicles were reported,[504] leading to adaptation of a variety of GUV formation techniques such as electroformation, agarose assisted swelling and microfluidics to create giant polymersomes containing MPs.[505–508] However, direct comparison of protein performance in polymer and lipid-based vesicles revealed that activity of certain MPs can be decreased in polymer membranes.[218,219,418] One major concern is the thickness of the membrane which, depending on the polymer, ranges from 5 – 50 nm which is thicker than lipid membranes (3 - 5 nm).[213,214] As nature has tailored MPs to the thickness of lipid bilayers, this leads to a hydrophobic size mismatch, causing membrane perturbations when inserting MPs in polymer bilayers (Figure 28B).[505,509] On the other hand, polymer vesicles might offer an increased activity lifetime of the MP which is beneficial for industrial applications.[220,418]

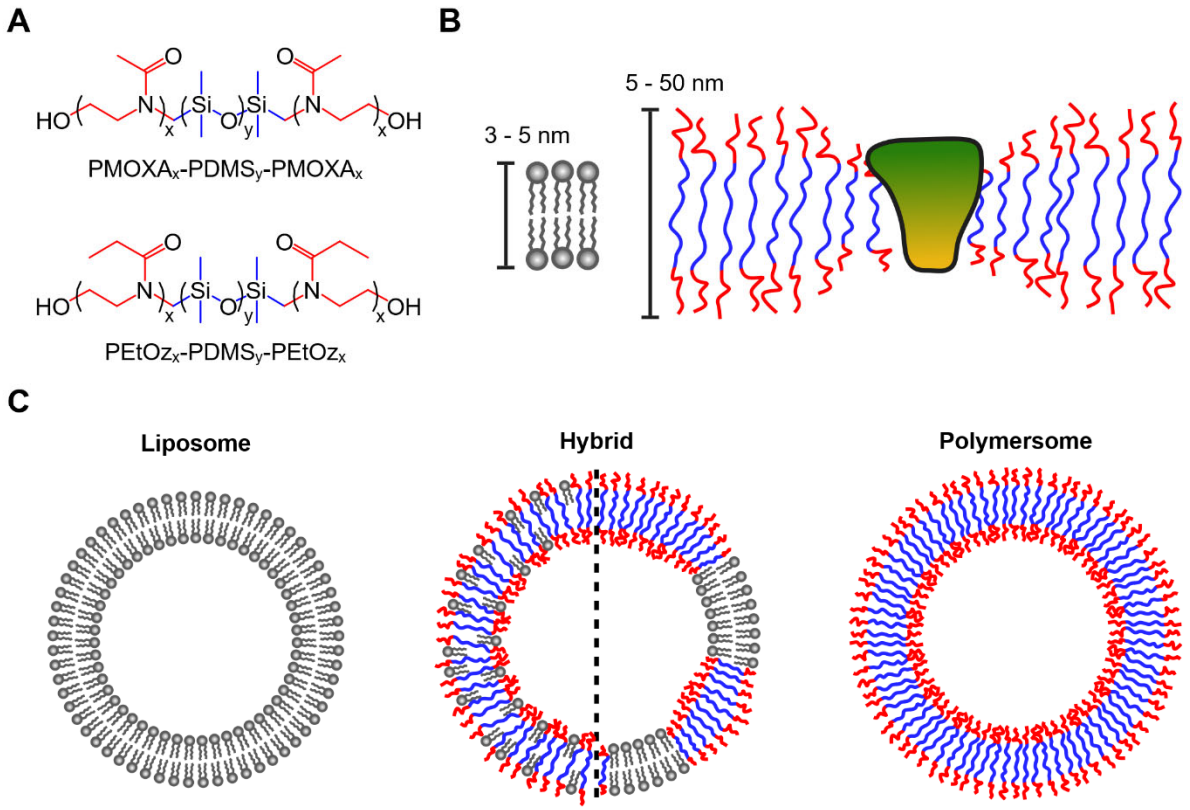

Figure 28: Overview of polymer membranes. A) Chemical structure of polymers used for the reconstitution of MPs.[501–503,510] The hydrophobic part is depicted in blue and the hydrophilic part in red. B) Bilayer thickness of lipid and polymer membranes. Insertion of a MP leads to membrane perturbations in the polymer membrane due to the hydrophobic size mismatch.[505,509] C) Liposome, Hybrid and Polymersome vesicles. Liposomes and polymersomes are purely composed of lipids and polymer, respectively, while hybrids contain a mixture of lipids and polymers. Hybrid lipopolymersomes are depicted with homogeneous lipid distribution (left) or with formation of micro or subdomains (right).[214]

Current research on MP-lipid interactions is making it increasingly clear that the lipids surrounding the MP do not simply provide an appropriate environment but also have essential roles in stabilizing the structure and maintaining the function of the MP.[511] Thus, one strategy to obtain higher activities while still retaining some of the benefits of polymer membranes is the creation of hybrid polymer-lipid vesicles (Figure 28C) using either pure lipids or lipid extracts.[219,220,512,513] Insertion of MPs in these hybrid vesicles can have pronounced effects,[512] which in some cases might even be beneficial. For example, a decrease in proton permeability was observed for hybrid vesicles after MP protein reconstitution while the opposite was observed for both pure lipid or polymer membranes.[220] When comparing activity measurements in pure polymersomes or liposomes to hybrid vesicles, it is important to determine the homogeneity of the hybrid vesicles in terms of polymer and lipid content. This is to ensure that differences in activity do not arise from subpopulations in the sample, for example pure lipid vesicles. Homogenous and well-mixed polymer-lipid hybrids have been reported in the literature and used for MP measurements.[218,514] The increased chemical stability and decreased membrane permeability of

polymer-membranes are ideal for industrial application, but fully synthetic polymersomes are considered to be less biocompatible and more toxic than liposomes which is important for therapeutic applications.[515,516] A recent trend which brings artificial cells into a more therapeutic direction are cell-derived vesicles which offer an excellent biocompatibility and low immunogenicity.[517–519]

Cell-Derived Vesicles for Increased Complexity and Biocompatibility

The reconstitution of purified MPs into artificial lipid vesicles produced from either natural lipid extracts or synthetic lipids has made a large contribution to our knowledge on the function of MPs and elucidating metabolic process such as energy transduction or membrane fusion. As outlined in *"Current Problems and Future Avenues in Proteoliposome Research"*,[8] increasing the complexity of these model membrane systems by coreconstitution of MPs with a defined orientation is still a challenging task, but necessary to advance our understanding on the interplay between several MPs and for the bottom-up creation of SCs. Additionally, the protein density and lipid complexity that is achieved in the synthetic systems still does not rival that of living cells[520,521] and as shown in this work, the challenge of achieving such complexity is even larger when using giant vesicles as model membranes. The mass percentage of proteins in biological membranes varies between 25 % to 75 %,[9–11], while liposomes are typically produced with only 0.5 % to 20 % proteins, although reconstitutions of bacteriorhodopsin or Ca^{2+} ATPase with a protein density of 50 % (*w/w*) have been described.[41,522] Cellular membranes have an asymmetric lipid composition in the two leaflets of the bilayer, which has been difficult to achieve in SUVs and GUVs and requires specialized protocols.[70,71,192,275] In addition, the occurrence of lateral inhomogeneity in the membrane with formation of distinct lipid domains, so called "rafts", has been proposed, based on lipid-lipid phase separation observed in biomimetic and isolated membranes. Sterols, sphingomyelin, and saturated lipids are thought to promote raft formation through preferential interactions, but the biological relevance of these rafts is highly debated due to the lack of their observation in cells, as discussed in a recent review by Levental *et al.* (2020).[234] The desire to gain more knowledge on the importance of these complex properties has brought upon the emergence of cell-derived vesicles in recent years, which serve as a platform to study MPs in a complex environment, especially in the context of liquid-liquid phase separation.[235] There is a variety of different cell-derived vesicles ranging from nanometer to micrometer-sized compartments, some of which are produced by cells themselves and used for cellular communication or tumor invasion,[523] while others are obtained through chemical treatment of cells.[301,523–527] These vesicles can originate both from bacterial and eukaryotic cells,[523,528] the latter of which will be the focus of this section. Applications of bacterial cell-derived vesicles are described in several excellent reviews.[523,529,530] A brief schematic overview of eukaryotic cell-derived vesicles is presented in Figure 29.

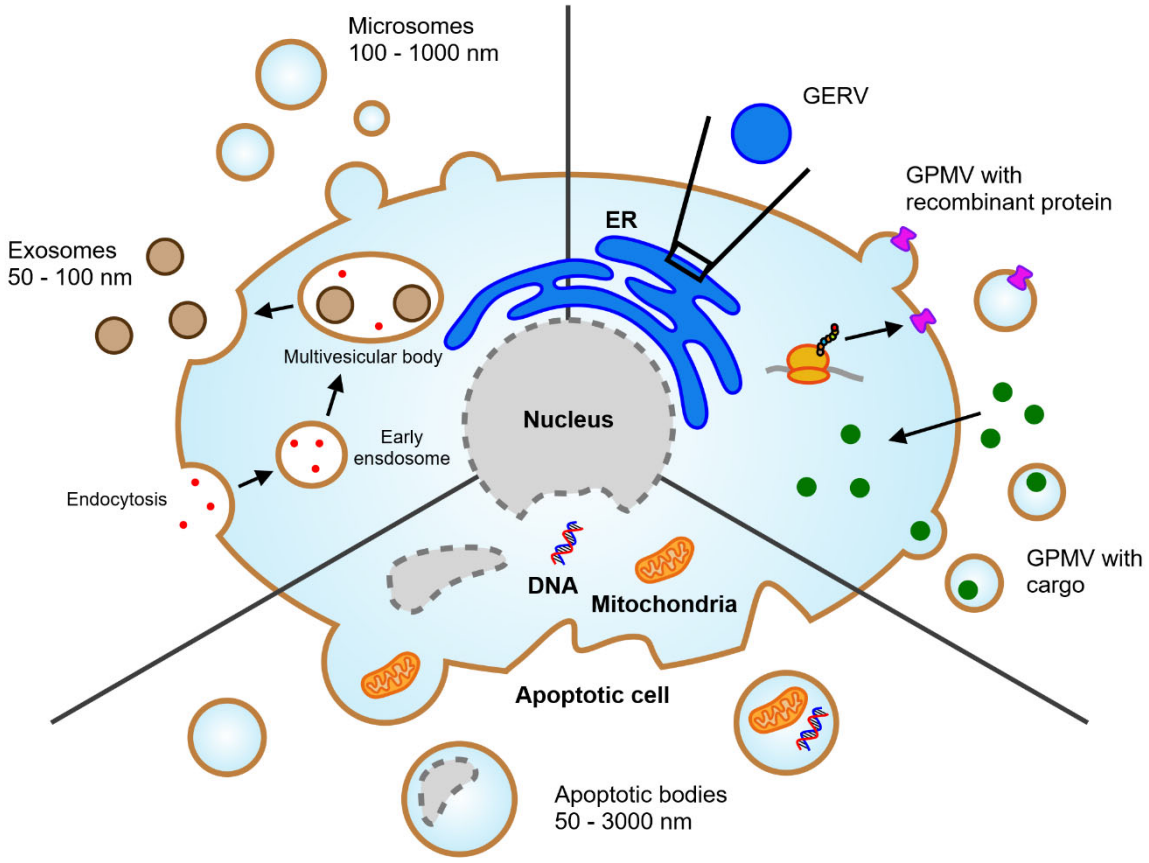

Figure 29: Schematic overview of eukaryotic extracellular and cell-derived vesicles.[523,531] On the top left, the formation of exosomes and microsomes is depicted. Exosomes are formed by the endocytic pathway in multivesicular bodies and have a size of 50 – 100 nm. Microsomes are formed by plasma membrane shedding and have a size of 100 – 1000 nm. On the bottom, the formation of apoptotic bodies from an apoptotic cell is depicted. Apoptotic bodies are large (50 -3000 nm) and can contain nuclear fragments, organelles, and DNA. On the top right, giant endoplasmatic reticulum vesicles (GERVs) and giant plasma membrane vesicles (GPMVs) are depicted. GPMVs can be formed with recombinant proteins (pink) expressed in genetically engineered cells or loaded with cargo such as polymersomes[519] (green) taken up by cells.

Extracellular vesicles (EVs) is a term which seems to be used in the literature to denote various forms of naturally produced vesicles. Classically, this term was used to describe exosomes, microsomes and apoptotic bodies, which have mainly gained interest in biosensing and drug delivery applications.[528–530,532] Exosomes originate from multivesicular bodies which are formed by the endocytic pathway and usually contain a specific set of proteins and a nucleic acid base cargo. Their membranes are enriched in cholesterol, diacylglycerols, sphingomyelin, and ceramides. Microsomes are formed by plasma membrane shedding and are enriched in phosphatidylserine. They contain cell adhesion molecules, cytosolic and membrane proteins as well as RNA. Apoptotic bodies are formed by outward blebbing or fragmentation of the membrane of apoptotic cells. Like microsomes, they are enriched in phosphatidylserine but in contrast to exosomes and microsomes, they can also carry DNA, nuclear fragments and organelles.[528,529] The molecular composition and size of EVs can be rather heterogeneous,

ranging from diameters of tens of nanometers to few micrometers. Thus, characterization of these vesicles is important to develop EV applications, and techniques for that have been reviewed elsewhere.[528] One application of EVs is their use as biomarkers for non-invasive diagnostics, as their composition, size and cargo depend on the origin and the stimulus leading to the production of the EV. Further, their excellent stability in body fluids and their natural role in cell to cell signaling makes EVs a promising tool for novel therapeutic applications, for example the delivery of therapeutic RNA agents or other drug molecules.[528–530,532] The cargos can be incorporated into EVs either by exogenous loading into or onto purified EVs or by endogenous loading where the cargo is produced in modified cells and taken up during formation of EVs.[530] The elaborate and error prone isolation and purification of these vesicles is still a major hurdle for their therapeutic application, but knowledge gained by the characterization of EVs might enable the production of fully synthetic EVs (fsEVs) as demonstrated in a recent report by Spatz and colleagues using the droplet-stabilized GUV formation method. They were able to show that fsEVs had similar therapeutic potential as natural EVs by assessing their ability to boost processes critical for wound healing.[533]

Giant plasma membrane vesicles (GPMVs), which are formed from cells by chemically induced plasma membrane blebbing, have been extensively used to study lipid phase separation and MP partitioning.[235,301,528,534,535] More recently, giant endoplasmatic reticulum vesicles (GERVs) were also developed which might shed light on processes related to the ER.[536] Although these vesicles have been typically used for the study of membrane organization, a recent report by Palivan and colleagues shows the potential of GPMVs to create artificial cells in a sort of hybrid bottom-up and top-down approach. By incubation of HepG2 cells with polymer-based vesicles containing reconstituted OmpF and encapsulating horse radish peroxidase (HRP) followed by GPMV formation, they were able to create cell-derived vesicles (top-down) containing artificial organelles (bottom-up) with preserved HRP functionality. These artificial organelles could potentially be used for product synthesis or biosensing as a sort of molecular factory inside GPMVs. The outstanding biocompatibility of molecular factories could promote the use of artificial cells in therapeutical applications.[519] Another potential hybrid top-down and bottom-up strategy was presented by Schmid *et al.* (2020), where transfer of cytosolic proteins and reconstitution of mammalian MPs from cell-derived vesicles to GUVs was achieved using calcium mediated liposome fusion.[441] While this presents on one hand a new reconstitution pathway for mammalian proteins into GUVs which does not require the use of detergent, it also contributes to achieving a high level of complexity while offering similar experimental accessibility as in fully synthetic vesicles. Another avenue for obtaining GUVs with reconstituted MPs without the use of detergent was recently pursued using red blood cell (RBC) membranes containing GLUT1. RBC membranes were mixed with lipids and used for agarose assisted swelling or electroformation, which resulted in the production of GUVs containing functionally active GLUT1.[537] Interestingly, similar approaches were used in the early

days of MP reconstitution into GUVs, mixing membrane fragments from cells with pure lipids or lipid extracts without MPs.[304,538] The three hybrid approaches presented here demonstrate a major challenge of mixing natural and synthetic materials, which is achieving homogeneous vesicle populations. For GUVs formed from RBC membrane and lipids, or which were fused with cell-derived vesicles, rather heterogeneous protein densities between individual vesicles were observed.[441,537] GPMVs containing artificial organelles displayed similar vesicle size distributions as GUVs prepared from film hydration methods and were loaded with different amounts of organelles.[519] Nonetheless, it becomes clear that cell-derived vesicles offer an opportunity to combine both top-down and bottom-up synthetic biology to create SCs for therapeutic applications, allowing for an increased complexity and providing knowledge to inform further design of fully-synthetic cells.

4.2. GUVs as a Tool for the Characterization of Membrane Proteins

The aims of this project are the development of GUVs as a platform for the characterization of MPs and as a long-term goal for the bottom-up creation of a SC. The latter involves also other projects from the group on establishing unidirectional orientation of MPs and optimizing coreconstitution of several MPs. In this part of the discussion, I would like to focus on the more immediate goal of using GUVs to characterize MPs and talk about the future of giant SCs in the last part of the general discussion.

As already mentioned earlier, only a handful of publications describe real-time single vesicle fluorescence measurements to detect MP function. I would like to highlight two key points based on the work in this thesis which I feel are frequently overlooked in those studies. First, measuring a sufficiently large number of vesicles is crucial as it allows performing better statistical analysis of the experiments, and may further help to reduce worries on selection bias (as to say that only GUVs with the desired behavior are shown) when reading publications, because no GUV behaves like the other. This was beautifully demonstrated in other publications as well which show single vesicle traces.[221,320] While this makes the data analysis a bit more challenging and time-consuming, the exploding expertise on big data analysis and customized software due to wide-spread programming skills will facilitate this process in the near future. Second, due to the general inhomogeneity of the vesicles, characterization of parameters like their shape and amount of reconstituted MP help to relate activities observed in individual GUVs and make them comparable with results obtained in other lipid bilayer systems. Although these characterizations are made in many publications, they are often done separately and not on the GUVs used for measurements.[204,220,326] For example, only average protein densities are determined with fluorescently-labeled MPs reconstituted in GUVs rather than indicating the protein density for each measured GUV individually. As observed here and by others,[309] depending on the reconstitution method, the protein density can vary considerable between different GUVs. There are of course some strategies that allow this simplification. For example, more homogenous protein

incorporation was previously obtained by using agarose assisted swelling compared to electroformation for the Dehydration-Rehydration reconstitution of KvAP.[309] One could also select GUVs with a specific size for analysis, however, many GUV formation methods produce GUVs which are polydisperse in size and thus the number of vesicles available for analysis would be reduced. Some GUV formations on the other hand allow the production of rather monodisperse vesicles, for example by swelling on micropatterned polymer surfaces[273] or using microfluidic techniques.[193,239,295,431] These methods are fairly recent and require considerable expertise and equipment, which limits their use by many labs. With further improvement of these methods and the development of "plug and play" style devices, the power of these techniques could be harnessed. At the moment, the most commonly used method for GUV formation seems to be electroformation based on the number of publications, likely as it was one of the first efficient techniques for giant vesicle formation and is regarded as a very clean method (no organic solvent or oil involved) unlike other methods that might lead to impurities in the membrane.[196] However, the chance of lipid oxidation and asymmetric distribution of charged lipids due to the electric field,[261] as well as the need to optimize formation conditions for different buffer compositions and the requirement of somewhat expensive equipment like treated glass slides, platinum wires and function generators makes this method costly and unattractive for scale-up or parallelization.[238] The more recent polymer assisted swelling method had a difficult start, as the early used substrates agarose and PVA led to impurities affecting membrane properties.[264,266] Since then, several different substrates have been successfully used for GUV formation, which in principle allow production of giant vesicles without impurities, although further studies in this regard are required. Together with existing literature data, the data obtained in this project clearly demonstrates the potential of polymer assisted swelling, as it requires minimal equipment and can thus be effectively scaled-up or parallelized,[238] with a remarkable versatility without much need for optimization, allowing the production of a large number of vesicles with diverse lipid and buffer compositions. Thus, polymer assisted swelling using a substrate that does not lead to membrane impurities seems to be the preferred GUV formation method for investigating MPs, as for example vesicles with different conditions to investigate optimal enzyme function can be obtained easily in parallel.

Regarding immobilization, the biotin-streptavidin system proved to be challenging under different conditions as the vesicle adhesion was affected by changes in the buffer composition, and strong adhesion could compromise the vesicle integrity. Other methods that avoid these issues like trapping in a gel-like matrix or microfluidic trapping might hinder or slow down addition of certain substrates or again require the use of sophisticated devices. We have ourselves spent over one hundred working hours on such trapping devices to happily return to biotin-streptavidin due to its ease of use. Finally, the method of substrate addition and especially mixing are also points to consider for GUVs immobilized in microscopy well chambers as used in this work, as these can considerably influence the results.

Here, charge-mediated fusion was used as a reconstitution method. Although this approach is very useful for the coreconstitution of several MPs, it is apparent from the literature and this work that this method of reconstituting MPs in GUVs is less well understood than other approaches. The challenge mainly lies in the quantification of reconstituted MP, which requires the distinction between adhesion or hemifusion and full fusion, as only the latter leads to functional incorporation of MP. Although Lira *et al.* (2019)[390] claim to be able to make this distinction using FRET, technical limitations to measure FRET on the microscope might hinder its broad applicability and we think there is a possibility that extensive lipid mixing by adhered or hemi-fused vesicles could lead to high FRET signals as well. Additionally, fusion-induced leakage was observed here which is of course not beneficial for measuring MP function. Thus, for the pure measurement of MP function, it might be worth investigating other reconstitution methods such as the frequently used Dehydration-Rehydration reconstitution. Even though there are concerns on protein stability, this method allows direct quantification of labeled MP in GUVs and has been demonstrated to work for some, but mainly monomeric MPs. Additionally, many substrates for polymer assisted swelling have not been explored yet in their ability to form GUVs from partially dehydrated SUVs, which might be an interesting avenue to explore. Fusion is still a valuable tool for the reconstitution of MPs, especially in regard to the bottom-up construction of SCs considering the coreconstitution capabilities and the fact that MPs are thought to keep their orientation during fusion. Complex systems could be created from a library of MPs reconstituted in cationic vesicles, by mixing the different vesicles in appropriate ratios and addition to negatively charged GUVs, allowing to test various combinations of proteins and different stoichiometries with ease compared to other coreconstitution methods.

A fantastic advantage of using light microscopy measurements with GUVs is the theoretically reduced MP amount needed to perform experiments. As demonstrated in this work, bulk cytochrome *c* oxidase measurements in small liposomes with bifunctional DNA duplexes required approximately 60 pmol of enzyme per measurement, while in the single vesicle experiment using GUVs, only approximately 0.6 pmol were needed. This is a 100-fold reduction of the required protein amount. However, the reconstitution method for both experiments was similar although scaled down for the GUV experiments. Still, liposomes that were prepared for fusion with GUVs would have been sufficient to perform 100 experiments, using only a tenth of a MP aliquot for reconstitution. This means that per MP aliquot that was thawed, 1000 experiments would be possible, and even with 5 minutes per experiment, it is not feasible to consume all the thawed aliquot in one day if using just one microscope. Thus, we ended up wasting a lot of MPs for now. There are two possible strategies to change this. One possibility would be to directly reconstitute MPs after purification and store these proteoliposomes in aliquots at -80 °C rather than the detergent-solubilized MPs. This way, a desired amount of liposomes containing MP can be thawed each time an experiment is performed. Another way would be to further scale down the

reconstitution method. However, the volumes used here were already quite small and at some point, the use of gel-filtration or BioBeads, which are frequently used for detergent removal, are not feasible anymore. For very small volumes, cyclodextrins could for example be used. Dilution of liposomes and MPs would be another possibility to decrease the amount of material used for reconstitution. However, it is clear that changing the reconstitution method will involve more optimization, as the reconstitution procedure might influence the efficiency of MP incorporation or orientation. For the first strategy, already established protocols can be used, if the storage of MP reconstituted in liposomes does not negatively affect its stability and activity over time. Disaccharides like sucrose have been shown to enhance protein stability during freeze-drying[539–541] and could be added as cryoprotective agents for storage of proteoliposomes. We have observed in our lab that addition of 100 g L^{-1} sucrose to liposomes containing bo_3 oxidase prolonged their activity from one day up to one month with storage at -80 °C. This could be further enhanced by storage of proteoliposomes in liquid nitrogen.

4.3. The Future of Giant Synthetic Cells

The research on the bottom-up creation of giant SCs is moving at a fast pace and recent publications have shown that this research field is finally heading towards industrial and therapeutical application.[210,217,496,533,542] One of the major hurdles in this regard is the scale-up of the fabrication of SCs, as the production of the individual components, such as for example MPs, is rather laborious and so far has been limited to smaller scales, alongside the production of giant vesicles. Even though recent advancements in microfluidic production[193,239,431,508] or polymer assisted swelling[238] of GUVs may lead to large-scale formation of these vesicles, the ultimate goal for SCs is of course self-reproduction which presently still seems to be far away from being easily achievable.[496] Nonetheless, I would like to highlight a few future directions in which SC systems might go despite that large-scale applications may still be far away.

As we have seen in previous sections of this general discussion, the combination of different techniques or hybrid approaches have gained interest in recent years, creating for example hybrid polymer-lipid vesicles with improved MP function over pure polymersomes while providing higher stability compared to pure liposomes,[219,220,418,513] or by combination of top-down and bottom-up synthetic biology strategies.[441,519,543–545] Similar to the endosymbiotic event that led to the creation of eukaryotic cells, Elani *et al.* (2018) encapsulated bacterial and eukaryotic cells, such as BE carcinoma colon cells, in POPG GUVs as organelle-like reactors that can be part of multi-step enzymatic cascades, involving the conversion of substrates by both biological cells and purified enzymes.[543] Göpfrich and colleagues genetically modified *E. coli* to express xenorhodopsin for the light-induced generation of proton gradients to control DNA assemblies on artificial vesicles. The bacteria are able to generate proton gradients which are larger and less laborious to obtain than those achieved with purified enzymes.[544] On

the opposite side, Ahmad *et al.* (2021) use artificial photosynthetic modules to fuel the function of isolated flagella, creating a light-induced self-sustaining motility system.[545] These approaches highlight the potential of combining bottom-up synthetic assemblies with top-down biological systems to create new functionalities. The large-scale production of some genetically engineered organisms is already possible and could thus contribute to the large-scale application of such semi-synthetic systems, until we are able to reach the high complexity of nature using fully bottom-up SCs.

While nature can provide us with a vast variety of "machines" (that is proteins, RNA, DNA and so on), they are often optimized for the environment of the organism where they originate from and therefore do not have the desired or optimal functionality in the context of a SC. Integrating chemically or biologically engineered machines will thus be another important step for the generation of functional SCs. Throughout this thesis, there have been glimpses of the capabilities of modified oligonucleotides. The established synthesis and the well understood properties and nature of the self-assembly of these molecules allows their structural sequence-based engineering for the creation of intricate designs that can even mimic the functionality of certain enzymes.[466,546–549] The lab of Hendrik Dietz for example has created a DNA-based rotary machine, similar to the rotary apparatus of the F_1F_0 ATP synthase, which could potentially be used as a generator of chemical energy, like its enzymatic counterpart, by applying mechanical forces to the device.[547,548] Recent advances in computational biology will facilitate even more the "*de novo*" design of proteins for specific functionalities, which has been more challenging due to the larger number of building blocks (amino acids) and the more complicated and hard to predict protein folding. For a long period, protein engineering was based on the modification of naturally occurring proteins using techniques such as directed evolution, involving cycles of mutation and selection of protein variants, or specific replacement of certain amino acids, for example in the catalytic site of the enzyme, using both natural and non-natural amino acids.[550–553] In recent years, a shift towards computational protein design has occurred made possible by our increased knowledge on different protein structures and tools to model and predict them more accurately.[551,554–556] For example, computational design was used to create α-helical membrane protein pores with selectivity for potassium over sodium ions.[557] Just very recently, two neural network based algorithms for the prediction of protein structures have been published, AlphaFold2.0 by Googles DeepMind project[558] and RoseTTAfold by David Baker and colleagues,[559] which for the first time achieved atomically accurate predictions of protein structures. In the future, such tools could allow the real-time *in silico* design of novel enzymes to equip SCs with new metabolic pathways, offering for example more efficient carbon fixation[560] or the production of renewable chemicals and biofuels.[561]

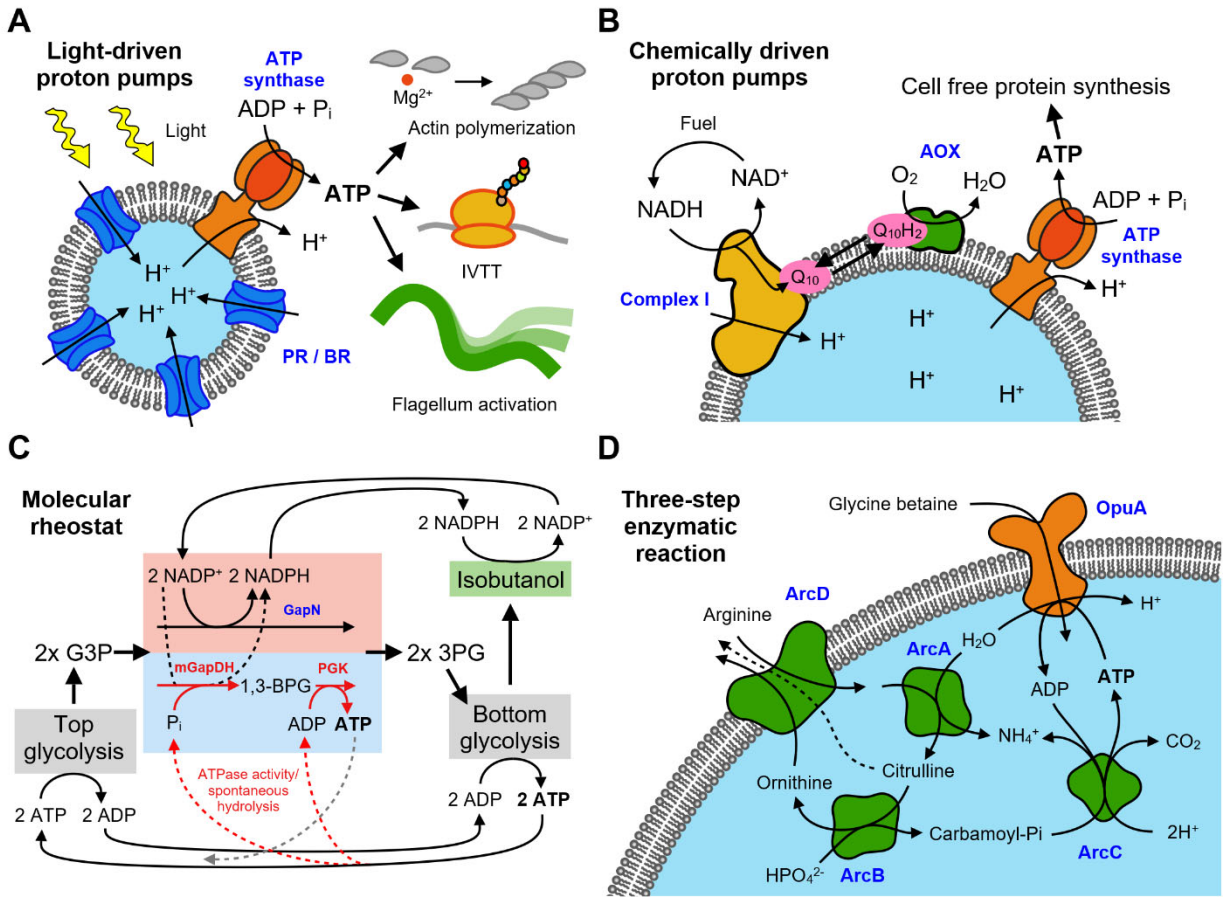

Figure 30: ATP generating modules for the creation of synthetic cells. ATP is written in bold for reaction steps that lead to its production. A) Light-driven proton pumps like proteorhodopsin (PR) or bacteriorhodopsin (BR) acidify the interior of a vesicle to enable the production of ATP from ADP and phosphate by the ATP synthase. The produced ATP is used to drive actin polymerization,[98] *in vitro* transcription and translation (IVTT) of membrane proteins[208] and to activate beating of isolated flagella.[545] B) Chemically driven ATP synthesis is achieved by coreconstitution of mammalian mitochondrial complex I, trypanosomal alternative oxidase and E. coli F_1F_0 ATP synthase. Metabolic processes fuel the reaction by production of NADH, which is used by complex I for the translocation of protons to the vesicle interior and the reduction of ubiquinone-10 (Q_{10}). This enables the production of ATP by the ATP synthase, while alternative oxidase recycles Q_{10} by reduction of oxygen to water. ATP is used to drive the cell free synthesis of proteins.[89] C) A molecular rheostat ensures efficient production of the biofuel isobutanol.[562] A top glycolysis pathway consumes two ATP molecules for the production of two glyceraldehyde-3 phosphates (G3P), which is converted by the molecular rheostat into two 3-phosphoglycerates (3PG), generating NADPH from $NADP^+$. In a bottom glycolysis pathway, two ATP molecules are regenerated from ADP and 3PG and isobutanol is produced, converting NADPH back to $NADP^+$. Both glycolysis pathways consume and produce equal amounts of ATP. In this situation, no free phosphate and ADP is available and G3P is converted in a one-step enzymatic reaction to 3PG by the non-phosphorylating glyceraldehyde phosphate dehydrogenase (GapN), generating NADPH using the red pathway. If the consumption of ATP is greater than its production by the bottom glycolysis pathway due to ATPase activity and spontaneous hydrolysis of ATP, the excess of free phosphate and ADP activates a second blue pathway (red dotted arrows) for the conversion of G3P to 3PG. This pathway involves a two-step enzymatic reaction, converting G3P first to 1,3-biphosphoglycerate (1,3-BPG) using $NADP^+$-specific, phosphorylating glyceraldehyde phosphate dehydrogenase (mGapDH), generating NADPH. In a second reaction, 1,3-BPG is converted to 3PG using phosphoglycerate kinase (PGK), generating ATP to flow back into the top glycolysis pathways (grey dotted arrow). Thus, both pathways lead to the production of NADPH, while the red pathway has a no net ATP production, and the blue pathway generates ATP, allowing the rheostat to react to the levels of free phosphate and ADP in the solution and

allowing prolonged synthesis of isobutanol. D) A three-step enzymatic reaction leads to the production of ATP from arginine.[76] ArcD imports arginine into the vesicle interior via arginine/ornithine antiport. Arginine is then converted to citrulline and ammonia by ArcA. ArcB uses phosphate and citrulline to generate ornithine and carbamoyl-P_i, and the latter is converted to ammonia and carbon dioxide by ArcC, generating ATP from ADP. ArcD exchanges both ornithine and citrulline for arginine, although citrulline exports occurs at a lower rate (indicated by the dotted arrows). OpuA acts as an ATP sink, establishing a basic physicochemical homeostasis and allowing to control the transmembrane fluxes of osmolytes by ionic-strength gated import of glycine betaine.

While we can use protein and oligonucleotide engineering to create more efficient "machines" with new functions for SCs, some of these "machines" may still require energy to carry out their desired functionality. In biological cells, the energy for many processes is of course provided in the form of adenosine triphosphate. Not surprisingly, the development of energy modules to produce ATP has been an important aspect of SC research to create potentially self-sustaining systems (Figure 30). One prominent energy module which has been integrated into several different processes in recent years involves the coreconstitution of ATP synthase with light-harvesting proton pumps. Such modules were used to drive actin polymerization,[98] *in vitro* MP synthesis[208] as well as the beating of isolated flagella[545] (Figure 30A). Using synthetic polymer-based membranes, the lifetime of these energy modules can be increased by several days.[418] Using chemically driven proton pumps, energy modules could be coupled to synthetic metabolic pathways. These modules essentially mimic the oxidative phosphorylation and are commonly described as synthetic mitochondria.[72,89,203,219,496] However, due to the requirement of constant reducing power,[496] integration of such modules into more complex assemblies remains challenging, although recent work by Biner *et al.* (2020) coupled ATP production fueled by complex I and alternative oxidase to cell-free protein synthesis (Figure 30B).[89] While these systems essentially mimic ATP production of natural cells, the expression and purification of these complex MPs can be rather laborious and unidirectional reconstitution to achieve efficient coupling of the individual MPs is still a challenge.[8] Further, modules mimicking oxidative phosphorylation may potentially lead to the production of reactive oxygen species, which cause damage to the energy modules or other components of the SC.[220,496] Thus, alternative methods for sustaining ATP levels in SCs are highly desirable. One such avenue would be to use electricity to convert ADP to ATP, however, no such synthetic system has been described so far to the best of our knowledge.[563,564] Potential routes in this direction could be the use of components of electrically active microorganisms[564] or oligonucleotide and protein engineering as discussed earlier. Another avenue is the design of metabolic pathways for the chemical production and recycling of ATP, as recently demonstrated by Opgenorth *et al.* (2017)[562] and Pols *et al.* (2019).[76] The former essentially designed an ATP rheostat that works using two different metabolic pathways, both converting glyceraldehyde 3-phosphate into 3-phosphoglycerate (Figure 30C). One of the two pathways generates no net ATP, using non-phosphorylating glyceraldehyde phosphate dehydrogenase, while the other pathway consumes one free phosphate and generates one additional ATP using $NADP^+$-specific,

phosphorylating glyceraldehyde phosphate dehydrogenase and phosphoglycerate kinase. This second pathway is only activated if free phosphate is present and thus reacts to the depletion of ATP, contributing to the restoration of ATP levels by additional ATP produced in this pathway. The ATP maintaining system was coupled to the production of the next generation biofuel isobutanol, extending the operational production lifetime together with protein engineering to improve the solvent stability of involved enzymes and continuous removal of the product from the enzymatic reactions, leading to efficient isobutanol production.[562,565] Pols *et al.* (2019) made use of Arc proteins, converting arginine imported into vesicles into ornithine, ammonia plus carbon dioxide, producing ATP in three enzymatic steps (Figure 30D). The ATP was then used to modulate osmolyte balance in the vesicles by activating the ATP-driven glycine betaine transporter OpuA.[76] Both of these systems demonstrate that by careful design of metabolic pathways and engineering of biological machines, sustainable energy can be generated for SCs without the need for artificial mitochondria.

5. Concluding Remarks

In this PhD thesis we have shown some of the challenges measuring MP function in GUVs. Unlike small vesicles that spontaneously form upon rehydration of a lipid film, the formation of giant vesicles must be promoted and a variety of methods have been established in the literature to guide the lipids into gigantic spheres. A first challenge is to choose the appropriate method which is best suited for the task that should be performed with the GUVs. Here, we have compared and characterized different methods to determine whether they can be used to establish a platform for the study of MP function in GUVs and in the long term for the bottom-up creation of a synthetic cell under physiologically relevant conditions. We have investigated whether the vesicles are able to retain soluble dyes for the measurement of MP function and maintain a proton gradient, which could be used as the driving force for the regeneration of energy in synthetic cells. Immobilization of the vesicles is required to follow MP function in real time. We have investigated how this affects the membrane integrity of the vesicles and how the immobilization itself can be affected by varying buffer compositions, which are be necessary to find optimal conditions for the measurement of enzymes or the operation of SCs.

The measurement of proton translocation by MPs in GUVs remains challenging. Several parameters can affect the observed MP activity such as the protein content and the size and shape of the vesicle. Accurate description of these parameters is necessary to relate the enzyme activities between different vesicles and potentially to other studies or lipid bilayer systems. An adequate detection system is of high importance to measure the pH changes. Fluorescent dyes might bleach more strongly under the microscope than they would in spectrophotometer-based assays. Further, encapsulation of pH-sensitive dyes during GUV formation by film hydration is inhomogeneous which needs to be considered when calibrating dyes using a single excitation and emission. Ratiometric pH-sensors such as HPTS allow the measurement of a ratio that should be independent of both bleaching and dye concentration. However, depending on the microscope setup, the use of such dyes is limited. Further, the measured HPTS ratios seemed to be affected by the vesicle size, which made calibration and accurate conversion to pH values difficult. To simplify the experimental setup, GUVs with monodisperse size might be beneficial which can be produced using microfluidics. While these GUVs appear to be fusogenic and can potentially be used to detect proton gradients, it remains to be seen whether they can be used to measure MP activity.

All of the experiments performed in this work have made it clear that no GUV is like the other. Essentially, every vesicle is its own experiment. Thus, a good imaging strategy and powerful analysis tools are necessary to gain the most information out of the experiments performed on the microscope. This large variability is another major challenge for the analysis and presentation of the data, and clear documentation of the imaging and data analysis process are necessary to judge the quality of the data.

6. Curriculum Vitae

Name: Nicolas Dolder

Date of Birth: 24th January 1994

Current address: Gesellschaftsstrasse 65, 3012 Bern, Switzerland, CH

Education

12.2017 - Today **PhD of Science** in Molecular Biology and Biochemistry at the Department of Chemistry, Biochemistry and Pharmaceutical Sciences, University of Bern.

Supervisor: Prof. Dr. Christoph von Ballmoos

Thesis: *"The Challenges of Measuring Membrane Protein Function in Giant Unilamellar Vesicles"*

09.2015 – 03.2017 **Master of Science** in Molecular Life Sciences with specialization in Biochemistry and Chemical Biology at the University of Bern.

Supervisor: Prof. Dr. Christoph von Ballmoos

Thesis: *"Monitoring transcription by FRET to investigate the membrane bound transcription regulator BcrR"*

Grade: summa cum laude

09.2012 – 07.2015 **Bachelor of Science** in Biochemistry at the University of Bern.
Supervisor: Prof. Dr. Christoph von Ballmoos

Thesis: *"Expression and Purification of different t-SNARE complexes from E. coli"*

Grade: magna cum laude

08.2009 – 05.2012	**Matura** with specialisation in Biology and Chemistry at the Gymnasium Neufeld, Bern, CH Average Grade: 5.2
08.2006 – 07.2009	**Secondary Education** at the Gyrisberg School in Jegenstorf, BE, CH
08.2000 – 07.2006	**Primary Education** at the Gyrisberg School in Jegenstorf, BE, CH

List of Publications

(I)	Bifunctional DNA Duplexes Permit Efficient Incorporation of pH Probes into Liposomes **Nicolas Dolder** & Christoph von Ballmoos *ChemBioChem*, 2020 doi.org/10.1002/cbic.202000146
(II)	Current problems and future avenues in proteoliposome research Andrea Amati, Simone Graf, Sabina Deutschmann, **Nicolas Dolder** and Christoph von Ballmoos Biochem Soc Trans, 2020 doi.org/10.1042/BST20190966

Teaching and supervision activities during the PhD studies

Teaching of biochemistry lab courses for bachelor students from 2018 until 2020
Supervision of one Bachelor theses and two Master theses, co-supervision of two Bachelor theses.

Prizes

Poster Prize at 85th Harden Conference: Dynamic Membrane Complexes: Respiration and Transport (2019)

7. Bibliography

1. Luckey, M. *Membrane Structural Biology: With Biochemical and Biophysical Foundations.* (Cambridge University Press, 2008). doi:10.1017/cbo9780511811098

2. Almeida, J. G., Preto, A. J., Koukos, P. I., Bonvin, A. M. J. J. & Moreira, I. S. Membrane proteins structures: A review on computational modeling tools. *Biochim. Biophys. Acta - Biomembr.* **1859**, 2021–2039 (2017).

3. Kobliakov, V. A. Role of proton pumps in tumorigenesis. *Biochem.* **82**, 401–412 (2017).

4. Licon-Munoz, Y., Fordyce, C. A., Hayek, S. R. & Parra, K. J. V-ATPase-dependent repression of androgen receptor in prostate cancer cells. *Oncotarget* **9**, 28921–28934 (2018).

5. Hwang, S. M., Lee, J. Y., Park, C. K. & Kim, Y. H. The Role of TRP Channels and PMCA in Brain Disorders: Intracellular Calcium and pH Homeostasis. *Front. Cell Dev. Biol.* **9**, 1–12 (2021).

6. Deisl, C., Albano, G. & Fuster, D. G. Role of Na/H exchange in insulin secretion by islet cells. *Curr. Opin. Nephrol. Hypertens.* **23**, 406–410 (2014).

7. Bull, S. C. & Doig, A. J. Properties of protein drug target classes. *PLoS One* **10**, e0117955 (2015).

8. Amati, A. M., Graf, S., Deutschmann, S., Dolder, N. & von Ballmoos, C. Current problems and future avenues in proteoliposome research. *Biochem. Soc. Trans.* **48**, 1473–1492 (2020).

9. Stillwell, W. Introduction to Biological Membranes. in *An Introduction to Biological Membranes* 3–15 (2016). doi:10.1016/b978-0-444-63772-7.00001-4

10. Alberts, B. *et al. Molecular Biology of the Cell*. (Garland Science, 2017).

11. Nelson, D. L., Lehninger, A. L. & Cox, M. M. *Lehninger Principles of Biochemistry*. (W. H. Freeman, 2008).

12. Shen, H. H., Lithgow, T. & Martin, L. L. Reconstitution of membrane proteins into model membranes: Seeking better ways to retain protein activities. *International Journal of Molecular Sciences* **14**, 1589–1607 (2013).

13. Mitchell, P. Chemiosmotic coupling in oxidative and photosynthetic phosphorylation. *Biochimica et Biophysica Acta - Bioenergetics* **1807**, 1507–1538 (2011).

14. Mitchell, P. Coupling of phosphorylation to electron and hydrogen transfer by a chemi-osmotic type of mechanism. *Nature* **191**, 144–148 (1961).

15. Prebble, J. Peter Mitchell and the ox phos wars. *Trends in Biochemical Sciences* **27**, 209–212 (2002).

16. Racker, E. & Stoeckenius, W. Reconstitution of purple membrane vesicles catalyzing light driven proton uptake and adenosine triphosphate formation. *J. Biol. Chem.* **249**, 662–663 (1974).

17. Hinkle, P. C., Kim, J. J. & Racker, E. Ion transport and respiratory control in vesicles formed from cytochrome oxidase and phospholipids. *J. Biol. Chem.* **247**, 1338–1339 (1972).

18. Racker, E. Reconstitution of a calcium pump with phospholipids and a purified Ca^{++}-adenosine triphosphatase from sarcoplasmic reticulum. *J. Biol. Chem.* **247**, 8198–8200 (1972).

19. Eytan, G. D., Persson, B., Ekebacke, A. & Rydström, J. Energy-linked nicotinamide-nucleotide transhydrogenase. Characterization of reconstituted ATP-driven transhydrogenase from beef heart mitochondria. *J. Biol. Chem.* **262**, 5008–5014 (1987).

20. Etemadi, A. H. Functional and orientational features of protein molecules in reconstituted lipid membranes. *Advances in lipid research* **21**, 281–428 (1985).

21. Drachev, L. A., Kaulen, A. D., Ostroumov, S. A. & Skulachev, V. P. Electrogenesis by bacteriorhodopsin incorporated in a planar phospholipid membrane. *FEBS Lett.* **39**, 43–45 (1974).

22. Drachev, L. A. *et al.* Direct measurement of electric current generation by cytochrome oxidase, H^+-ATPase and bacteriorhodopsin. *Nature* **249**, 321–324 (1974).

23. Bazzone, A., Barthmes, M. & Fendler, K. SSM-Based Electrophysiology for Transporter Research. in *Methods in Enzymology* **594**, 31–83 (2017).

24. Schulz, P., Garcia-Celma, J. J. & Fendler, K. SSM-based electrophysiology. *Methods* **46**, 97–103 (2008).

25. Früh, V., IJzerman, A. P. & Siegal, G. How to Catch a Membrane Protein in Action: A Review of Functional Membrane Protein Immobilization Strategies and Their Applications. *Chem. Rev.* **111**, 640–656 (2011).

26. Smit, J. M., Waarts, B. L., Bittman, R. & Wilschut, J. Liposomes as Target Membranes in the Study of Virus Receptor Interaction and Membrane Fusion. *Methods Enzymol.* **372**, 374–392 (2003).

27. Hoekstra, D. & Klappe, K. Fluorescence Assays to Monitor Fusion of Enveloped Viruses. *Methods Enzymol.* **220**, 261–276 (1993).

28. Tuthill, T. J., Bubeck, D., Rowlands, D. J. & Hogle, J. M. Characterization of Early Steps in the Poliovirus Infection Process : Receptor-Decorated Liposomes Induce Conversion of the Virus to Particles. *J. Virol.* **80**, 172–180 (2006).

29. Whitbeck, J. C., Zuo, Y., Milne, R. S. B., Cohen, G. H. & Eisenberg, R. J. Stable Association of Herpes Simplex Virus with Target Membranes Is Triggered by Low pH in the Presence of the gD Receptor, HVEM. *J. Virol.* **80**, 3773–3780 (2006).

30. Vallbracht, M. *et al.* Structure-Function Dissection of Pseudorabies Virus Glycoprotein B Fusion Loops. *J. Virol.* **92**, 1–26 (2017).

31. Zhukovsky, M. A. *et al.* Thermal stability of the human immunodeficiency virus type 1 (HIV-1) receptors, CD4 and CXCR4, reconstituted in proteoliposomes. *PLoS One* **5**, (2010).

32. Yeliseev, A. Expression and Preparation of a G-Protein-Coupled Cannabinoid Receptor CB2 for NMR Structural Studies. *Curr. Protoc. Protein Sci.* **96**, 1–21 (2019).

33. Shi, C. *et al.* Structure and Dynamics of the Rhomboid Protease GlpG in Liposomes Studied by Solid-State NMR. *J. Am. Chem. Soc.* **141**, 17314–17321 (2019).

34. Zhou, S. *et al.* Solution NMR structure of yeast Rcf1, a protein involved in respiratory supercomplex formation. *Proc. Natl. Acad. Sci. U. S. A.* **115**, 3048–3053 (2018).

35. Patel, M. M. & Patel, B. M. Crossing the Blood–Brain Barrier: Recent Advances in Drug Delivery to the Brain. *CNS Drugs* **31**, 109–133 (2017).

36. Li, X. *et al.* Nano carriers for drug transport across the blood–brain barrier. *Journal of Drug Targeting* **25**, 17–28 (2017).

37. Mittal, S., Chaudhary, A., Chaudhary, A. & Kumar, A. Proniosomes: The effective and efficient drug-carrier system. *Therapeutic Delivery* **11**, 125–137 (2020).

38. Zylberberg, C. & Matosevic, S. Pharmaceutical liposomal drug delivery: a review of new delivery systems and a look at the regulatory landscape. *Drug Delivery* **23**, 3319–3329 (2016).

39. Lila, A. S. A. & Ishida, T. Liposomal delivery systems: Design optimization and current applications. *Biological and Pharmaceutical Bulletin* **40**, 1–10 (2017).

40. Lee, Y. & Thompson, D. H. Stimuli-responsive liposomes for drug delivery. *Wiley Interdisciplinary Reviews: Nanomedicine and Nanobiotechnology* **9**, (2017).

41. Rigaud, J. L., Pitard, B. & Levy, D. Reconstitution of membrane proteins into liposomes: application to energy-transducing membrane proteins. *BBA - Bioenergetics* **1231**, 223–246 (1995).

42. Laubinger, W. & Dimroth, P. Characterization of the ATP Synthase of *Propionigenium modesturn* as a Primary Sodium Pump. *Biochemistry* **27**, 7531–7537 (1988).

43. Seddon, A. M., Curnow, P. & Booth, P. J. Membrane proteins, lipids and detergents: Not just a soap opera. *Biochimica et Biophysica Acta - Biomembranes* **1666**, 105–117 (2004).

44. Skrzypek, R., Iqbal, S. & Callaghan, R. Methods of reconstitution to investigate membrane protein function. *Methods* **147**, 126–141 (2018).

45. Rigaud, J. L. & Lévy, D. Reconstitution of Membrane Proteins into Liposomes. in *Methods in Molecular Biology* **1635**, 65–86 (2003).

46. Degrip, W. J., Vanoostrum, J. & Bovee-Geurts, P. H. M. Selective detergent-extraction from mixed detergent/lipid/protein micelles, using cyclodextrin inclusion compounds: A novel generic approach for the preparation of proteoliposomes. *Biochem. J.* **330**, 667–674 (1998).

47. Geertsma, E. R., Nik Mahmood, N. A. B., Schuurman-Wolters, G. K. & Poolman, B. Membrane reconstitution of ABC transporters and assays of translocator function. *Nat. Protoc.* **3**, 256–266 (2008).

48. Hatzi, P., Mourtas, S., G. Klepetsanis, P. & Antimisiaris, S. G. Integrity of liposomes in presence of

cyclodextrins: Effect of liposome type and lipid composition. *Int. J. Pharm.* **333**, 167–176 (2007).

49. Knol, J. *Membrane Reconstitution and Functional Analysis of a Sugar Transport System*. (1999).

50. Tsai, M. F. & Miller, C. Substrate selectivity in arginine-dependent acid resistance in enteric bacteria. *Proc. Natl. Acad. Sci. U. S. A.* **110**, 5893–5897 (2013).

51. van 't Klooster, J. S. *et al.* Membrane Lipid Requirements of the Lysine Transporter Lyp1 from *Saccharomyces cerevisiae*. *J. Mol. Biol.* **432**, 4023–4031 (2020).

52. Harris, N. J., Charalambous, K., Findlay, H. E. & Booth, P. J. Lipids modulate the insertion and folding of the nascent chains of alpha helical membrane proteins. *Biochemical Society Transactions* **46**, 1355–1366 (2018).

53. Martens, C. *et al.* Direct protein-lipid interactions shape the conformational landscape of secondary transporters. *Nat. Commun.* **9**, (2018).

54. Mirandela, G. Di., Tamburrino, G., Hoskisson, P. A., Zachariae, U. & Javelle, A. The lipid environment determines the activity of the *Escherichia coli* ammonium transporter AmtB. *FASEB J.* **33**, 1989–1999 (2019).

55. Vitrac, H., Mallampalli, V. K. P. S., Bogdanov, M. & Dowhan, W. The lipid-dependent structure and function of LacY can be recapitulated and analyzed in phospholipid-containing detergent micelles. *Sci. Rep.* **9**, (2019).

56. Dowhan, W., Vitrac, H. & Bogdanov, M. Lipid-Assisted Membrane Protein Folding and Topogenesis. *Protein Journal* **38**, 274–288 (2019).

57. Zhang, M., Mileykovskaya, E. & Dowhan, W. Cardiolipin Is Essential for Organization of Complexes III and IV into a Supercomplex in Intact Yeast Mitochondria. *J. Biol. Chem.* **280**, 29403–29408 (2005).

58. Paradies, G., Paradies, V., De Benedictis, V., Ruggiero, F. M. & Petrosillo, G. Functional role of cardiolipin in mitochondrial bioenergetics. *Biochim. Biophys. Acta - Bioenerg.* **1837**, 408–417 (2014).

59. Arnarez, C., Marrink, S. J. & Periole, X. Molecular mechanism of cardiolipin-mediated assembly of respiratory chain supercomplexes. *Chem. Sci.* **7**, 4435–4443 (2016).

60. De Lima Santos, H., Lopes, M. L., Maggio, B. & Ciancaglini, P. Na,K-ATPase reconstituted in liposomes: Effects of lipid composition on hydrolytic activity and enzyme orientation. *Colloids Surfaces B Biointerfaces* **41**, 239–248 (2005).

61. Mohraz, M. Reconstitution of detergent-solubilized Na,K-ATPase and formation of two-dimensional crystals. *J. Struct. Biol.* **125**, 76–85 (1999).

62. Cornelius, F. Modulation of Na,K-ATPase and Na-ATPase activity by phospholipids and cholesterol. I. Steady-state kinetics. *Biochemistry* **40**, 8842–8851 (2001).

63. Abeywardena, M. Y., Allen, T. M. & Charnock, J. S. Lipid-protein interactions of reconstituted membrane-associated adenosinetriphosphatases. Use of a gel-filtration procedure to examine phospholipid-activity relationships. *BBA - Biomembr.* **729**, 62–74 (1983).

64. Cornelius, F., Turner, N. & Christensen, H. R. Z. Modulation of Na,K-ATPase by phospholipids and cholesterol. II. Steady-state and presteady-state kinetics. *Biochemistry* **42**, 8541–8549 (2003).

65. Yeagle, P. L. *The Membranes of Cells*. (ACADEMIC PRESS, INC., 1993).

66. Lichtenberg, D., Ahyayauch, H. & Goñi, F. M. The mechanism of detergent solubilization of lipid bilayers. *Biophysical Journal* **105**, 289–299 (2013).

67. Marquardt, D., Geier, B. & Pabst, G. Asymmetric lipid membranes: towards more realistic model systems. *Membr.* **5**, 180–196 (2015).

68. Furse, S. & Scott, D. J. Three-Dimensional Distribution of Phospholipids in Gram Negative Bacteria. *Biochemistry* **55**, 4742–4747 (2016).

69. Bogdanov, M. *et al.* Phospholipid distribution in the cytoplasmic membrane of Gram-negative bacteria is highly asymmetric, dynamic, and cell shape-dependent. *Sci. Adv.* **6**, eaaz6333 (2020).

70. Doktorova, M. *et al.* Preparation of asymmetric phospholipid vesicles for use as cell membrane models. *Nat. Protoc.* **13**, 2086–2101 (2018).

71. Markones, M. *et al.* Stairway to Asymmetry: Five Steps to Lipid-Asymmetric Proteoliposomes. *Biophys. J.* **118**, 294–302 (2020).

72. Von Ballmoos, C., Biner, O., Nilsson, T. & Brzezinski, P. Mimicking respiratory phosphorylation using purified enzymes. *Biochim. Biophys. Acta - Bioenerg.* **1857**, 321–331 (2016).

73. Öjemyr, L. N., Von Ballmoos, C., Faxén, K., Svahn, E. & Brzezinski, P. The membrane modulates internal proton transfer in cytochrome *c* oxidase. *Biochemistry* **51**, 1092–1100 (2012).

74. Schadauer, F. *et al.* Silica nanoparticles for the oriented encapsulation of membrane proteins into artificial bilayer lipid membranes. *Langmuir* **31**, 2511–2516 (2015).

75. Geiss, A. F. *et al.* Proteo-lipobeads to encapsulate cytochrome *c* oxidase from Paracoccus denitrificans. *J. Colloid Interface Sci.* **500**, 119–125 (2017).

76. Pols, T. *et al.* A synthetic metabolic network for physicochemical homeostasis. *Nat. Commun.* **10**, (2019).

77. Seigneuret, M. & Rigaud, J. L. Partial separation of inwardly pumping and outwardly pumping bacteriorhodopsin reconstituted liposomes by gel filtration. *FEBS Lett.* **228**, 79–84 (1988).

78. Huang, H. *et al.* Using fluorescence quenching titration to determine the orientation of a model transmembrane protein in mimic membranes. *Materials (Basel).* **12**, (2019).

79. Young, H. S., Rigaud, J. L., Lacapère, J. J., Reddy, L. G. & Stokes, D. L. How to make tubular crystals by reconstitution of detergent-solubilized Ca^{2+}-ATPase. *Biophys. J.* **72**, 2545–2558 (1997).

80. Biner, O., Schick, T., Müller, Y. & von Ballmoos, C. Delivery of membrane proteins into small and giant unilamellar vesicles by charge-mediated fusion. *FEBS Lett.* **590**, 2051–2062 (2016).

81. Ishmukhametov, R. R., Russell, A. N. & Berry, R. M. A modular platform for one-step assembly of multi-component membrane systems by fusion of charged proteoliposomes. *Nat Commun* **7**, 13025 (2016).

82. Nordlund, G., Brzezinski, P. & Von Ballmoos, C. SNARE-fusion mediated insertion of membrane proteins into native and artificial membranes. *Nat. Commun.* **5**, 1–8 (2014).

83. Berg, J., Block, S., Höök, F. & Brzezinski, P. Single Proteoliposomes with *E. coli* Quinol Oxidase: Proton Pumping without Transmembrane Leaks. *Isr. J. Chem.* **57**, 437–445 (2017).

84. Li, M. *et al.* Single Enzyme Experiments Reveal a Long-Lifetime Proton Leak State in a Heme-Copper Oxidase. *J Am Chem Soc* **137**, 16055–16063 (2015).

85. Verkhovskaya, M. L. *et al.* Glutamic acid 286 in subunit I of cytochrome bo_3 is involved in proton translocation. *Proc. Natl. Acad. Sci. U. S. A.* **94**, 10128–10131 (1997).

86. Krenn, B. E., Koppenaal, F., Van Walraven, H. S., Krab, K. & Kraayenhof, R. Co-reconstitution of the H^+-ATP synthase and cytochrome b-563 c-554 complex from a thermophilic cyanobacterium. High ATP yield and mutual effects on the enzymatic activities. *BBA - Bioenerg.* **1140**, 271–281 (1993).

87. Lee, C. *et al.* A two-domain elevator mechanism for sodium/proton antiport. *Nature* **501**, 573–577 (2013).

88. Juge, N., Yoshida, Y., Yatsushiro, S., Omote, H. & Moriyama, Y. Vesicular glutamate transporter contains two independent transport machineries. *J. Biol. Chem.* **281**, 39499–39506 (2006).

89. Biner, O., Fedor, J. G., Yin, Z. & Hirst, J. Bottom-Up Construction of a Minimal System for Cellular Respiration and Energy Regeneration. *ACS Synth. Biol.* (2020). doi:10.1021/acssynbio.0c00110

90. Uzdavinys, P. *et al.* Dissecting the proton transport pathway in electrogenic Na^+/H^+ antiporters. *Proc. Natl. Acad. Sci. U. S. A.* **114**, E1101–E1110 (2017).

91. Wiedenmann, A., Dimroth, P. & von Ballmoos, C. Δψ and ΔpH are equivalent driving forces for proton transport through isolated F_0 complexes of ATP synthases. *Biochim. Biophys. Acta - Bioenerg.* **1777**, 1301–1310 (2008).

92. Knol, J., Sjollema, K. & Poolman, B. Detergent-mediated reconstitution of membrane proteins. *Biochemistry* **37**, 16410–16415 (1998).

93. Knol, J. *et al.* Unidirectional reconstitution into detergent-destabilized liposomes of the purified lactose transport system of *Streptococcus thermophilus*. *J. Biol. Chem.* **271**, 15358–15366 (1996).

94. Wang, L. & Sigworth, F. J. Structure of the BK potassium channel in a lipid membrane from electron

cryomicroscopy. *Nature* **461**, 292–295 (2009).

95. Nomura, T., Cox, C. D., Bavi, N., Sokabe, M. & Martinac, B. Unidirectional incorporation of a bacterial mechanosensitive channel into liposomal membranes. *FASEB J.* **29**, 4334–4345 (2015).

96. Dixon, J. F. & Hokin, L. E. The reconstituted (Na,K)-ATPase is electrogenic. *J. Biol. Chem.* **255**, 10681–10686 (1980).

97. Hokin, L. E. & Dixon, J. F. Reconstitution of the Na,K-Pump by Freeze—thaw Sonication: Estimation of Coupling Ratio and Electrogenicity. *Methods Enzymol.* **156**, 141–155 (1988).

98. Lee, K. Y. *et al.* Photosynthetic artificial organelles sustain and control ATP-dependent reactions in a protocellular system. *Nat. Biotechnol.* **36**, 530–535 (2018).

99. Happe, M., Teather, R. M., Overath, P., Knobling, A. & Oesterhelt, D. Direction of proton translocation in proteoliposomes formed from purple membrane and acidic lipids depends on the pH during reconstitution. *BBA - Biomembr.* **465**, 415–420 (1977).

100. Tunuguntla, R. *et al.* Lipid bilayer composition can influence the orientation of proteorhodopsin in artificial membranes. *Biophys. J.* **105**, 1388–1396 (2013).

101. Pfleger, N. *et al.* Solid-state NMR and functional studies on proteorhodopsin. *Biochim. Biophys. Acta - Bioenerg.* **1787**, 697–705 (2009).

102. Ritzmann, N. *et al.* Fusion Domains Guide the Oriented Insertion of Light-Driven Proton Pumps into Liposomes. *Biophys. J.* **113**, 1181–1186 (2017).

103. Rigaud, J. L., Paternostre, M. T. & Bluzat, A. Mechanisms of Membrane Protein Insertion into Liposomes during Reconstitution Procedures Involving the Use of Detergents. 2. Incorporation of the Light-Driven Proton Pump Bacteriorhodopsin. *Biochemistry* **27**, 2677–2688 (1988).

104. Richard, P., Rigaud, J. L. & Graber, P. Reconstitution of CF_0F_1 into liposomes using a new reconstitution procedure. *Eur. J. Biochem.* **193**, 921–925 (1990).

105. Lévy, D., Gulik, A., Bluzat, A. & Rigaud, J. L. Reconstitution of the sarcoplasmic reticulum Ca^{2+}-ATPase: mechanisms of membrane protein insertion into liposomes during reconstitution procedures involving the use of detergents. *BBA - Biomembr.* **1107**, 283–298 (1992).

106. Eytan, G. D. Use of liposomes for reconstitution of biological functions. *BBA - Reviews on Biomembranes* **694**, 185–202 (1982).

107. Zheng, H., Lee, S., Llaguno, M. C. & Jiang, Q. X. bSUM: A bead-supported unilamellar membrane system facilitating unidirectional insertion of membrane proteins into giant vesicles. *J. Gen. Physiol.* **147**, 77–93 (2016).

108. Serdiuk, T. *et al.* YidC assists the stepwise and stochastic folding of membrane proteins. *Nat. Chem. Biol.*

12, 911–917 (2016).

109. Serdiuk, T. *et al.* Insertion and folding pathways of single membrane proteins guided by translocases and insertases. *Sci. Adv.* **5**, 1–11 (2019).

110. Althoff, T., Davies, K. M., Schulze, S., Joos, F. & Kühlbrandt, W. GRecon: A method for the lipid reconstitution of membrane proteins. *Angew. Chemie - Int. Ed.* **51**, 8343–8347 (2012).

111. Blum, T. B., Hahn, A., Meier, T., Davies, K. M. & Kühlbrandt, W. Dimers of mitochondrial ATP synthase induce membrane curvature and self-assemble into rows. *Proc. Natl. Acad. Sci. U. S. A.* **116**, 4250–4255 (2019).

112. Denisov, I. G., Schuler, M. A. & Sligar, S. G. Nanodiscs as a New Tool to Examine Lipid–Protein Interactions. in *Methods in Molecular Biology* **2003**, 645–671 (2019).

113. Kariyazono, H. *et al.* Formation of stable nanodiscs by bihelical apolipoprotein A-I mimetic peptide. *J. Pept. Sci.* **22**, 116–122 (2016).

114. Carlson, M. L. *et al.* The Peptidisc, a simple method for stabilizing membrane proteins in detergent-free solution. *Elife* **7**, 1–23 (2018).

115. Angiulli, G. *et al.* New approach for membrane protein reconstitution into peptidiscs and basis for their adaptability to different proteins. *Elife* **9**, 1–20 (2020).

116. Smirnova, I. A. *et al.* Isolation of yeast complex IV in native lipid nanodiscs. *Biochim. Biophys. Acta - Biomembr.* **1858**, 2984–2992 (2016).

117. Dörr, J. M. *et al.* The styrene–maleic acid copolymer: a versatile tool in membrane research. *Eur. Biophys. J.* **45**, 3–21 (2016).

118. Dörr, J. M. *et al.* Detergent-free isolation, characterization, and functional reconstitution of a tetrameric K^+ channel: The power of native nanodiscs. *Proc. Natl. Acad. Sci. U. S. A.* **111**, 18607–18612 (2014).

119. Parmar, M. J., Lousa, C. D. M., Muench, S. P., Goldman, A. & Postis, V. L. G. Artificial membranes for membrane protein purification, functionality and structure studies. *Biochem. Soc. Trans.* **44**, 877–882 (2016).

120. Broecker, J., Eger, B. T. & Ernst, O. P. Crystallogenesis of Membrane Proteins Mediated by Polymer-Bounded Lipid Nanodiscs. *Structure* **25**, 384–392 (2017).

121. Smirnova, I. A., Ädelroth, P. & Brzezinski, P. Extraction and liposome reconstitution of membrane proteins with their native lipids without the use of detergents. *Sci. Rep.* **8**, 14950 (2018).

122. Dutta, D., Esmaili, M., Overduin, M. & Fliegel, L. Expression and detergent free purification and reconstitution of the plant plasma membrane Na^+/H^+ antiporter SOS1 overexpressed in *Pichia pastoris*. *Biochim. Biophys. Acta - Biomembr.* **1862**, 183111 (2020).

123. Scheidelaar, S. *et al.* Effect of Polymer Composition and pH on Membrane Solubilization by Styrene-Maleic Acid Copolymers. *Biophys. J.* **111**, 1974–1986 (2016).

124. Fluman, N., Tobiasson, V. & Von Heijne, G. Stable membrane orientations of small dual-topology membrane proteins. *Proc. Natl. Acad. Sci. U. S. A.* **114**, 7987–7992 (2017).

125. Hegde, R. S. & Keenan, R. J. Tail-anchored membrane protein insertion into the endoplasmic reticulum. *Nature Reviews Molecular Cell Biology* **12**, 787–798 (2011).

126. Dröse, S., Galkin, A. & Brandt, U. Proton pumping by complex I (NADH:ubiquinone oxidoreductase) from Yarrowia lipolytica reconstituted into proteoliposomes. *Biochim. Biophys. Acta - Bioenerg.* **1710**, 87–95 (2005).

127. Gerber, G. E., Gray, C. P., Wildenauer, D. & Khorana, H. G. Orientation of bacteriorhodopsin in *Halobacterium halobium* as studied by selective proteolysis. *Proc. Natl. Acad. Sci. U. S. A.* **74**, 5426–5430 (1977).

128. Kalmbach, R. *et al.* Functional Cell-free Synthesis of a Seven Helix Membrane Protein: In situ Insertion of Bacteriorhodopsin into Liposomes. *J. Mol. Biol.* **371**, 639–648 (2007).

129. Futai, M. Orientation of membrane vesicles from *Escherichia coli* prepared by different procedures. *J. Membr. Biol.* **15**, 15–28 (1974).

130. Raschle, T., Lin, C., Jungmann, R., Shih, W. M. & Wagner, G. Controlled Co-reconstitution of Multiple Membrane Proteins in Lipid Bilayer Nanodiscs Using DNA as a Scaffold. *ACS Chem Biol* **10**, 2448–2454 (2015).

131. Fang, G. *et al.* Manipulation of activity and orientation of membrane-reconstituted di-tripeptide transport protein DtpT of *Lactococcus lactis*. *Mol. Membr. Biol.* **16**, 297–304 (1999).

132. Geest, M. van & Lolkema Juke S. Membrane Topology and Insertion of Membrane Proteins: Search for Topogenic Signals. *Microbiol. Mol. Biol. Rev.* **64**, 13–33 (2000).

133. Pagano, A. & Spiess, M. Reconstitution of Rab4-dependent vesicle formation in vitro. *Methods in Enzymology* **403**, 81–92 (2005).

134. Bronder, A. M. *et al.* Oriented Membrane Protein Reconstitution into Tethered Lipid Membranes for AFM Force Spectroscopy. *Biophys. J.* **111**, 1925–1934 (2016).

135. Sumino, A., Uchihashi, T. & Oiki, S. Oriented Reconstitution of the Full-Length KcsA Potassium Channel in a Lipid Bilayer for AFM Imaging. *J. Phys. Chem. Lett.* **8**, 785–793 (2017).

136. Jang, S. & Javadov, S. Current challenges in elucidating respiratory supercomplexes in mitochondria: Methodological obstacles. *Frontiers in Physiology* **9**, 238 (2018).

137. Liu, F., Lössl, P., Rabbitts, B. M., Balaban, R. S. & Heck, A. J. R. The interactome of intact mitochondria by

cross-linking mass spectrometry provides evidence for coexisting respiratory supercomplexes. *Mol. Cell. Proteomics* **17**, 216–232 (2018).

138. Enríquez, J. A. Supramolecular Organization of Respiratory Complexes. *Annu. Rev. Physiol.* **78**, 533–561 (2016).

139. Brzezinski, P. New Structures Reveal Interaction Dynamics in Respiratory Supercomplexes. *Trends Biochem. Sci.* **45**, 3–5 (2020).

140. Rabe, M., Schwieger, C., Zope, H. R., Versluis, F. & Kros, A. Membrane interactions of fusogenic coiled-coil peptides: Implications for lipopeptide mediated vesicle fusion. *Langmuir* **30**, 7724–7735 (2014).

141. Stengel, G., Zahn, R. & Höök, F. DNA-induced programmable fusion of phospholipid vesicles. *J. Am. Chem. Soc.* **129**, 9584–9585 (2007).

142. Chan, Y. H., van Lengerich, B. & Boxer, S. G. Lipid-anchored DNA mediates vesicle fusion as observed by lipid and content mixing. *Biointerphases* **3**, FA17 (2008).

143. Marsden, H. R., Tomatsu, I. & Kros, A. Model systems for membrane fusion. *Chem. Soc. Rev.* **40**, 1572–1585 (2011).

144. Tsien, R. Y. New Calcium Indicators and Buffers with High Selectivity Against Magnesium and Protons: Design, Synthesis, and Properties of Prototype Structures. *Biochemistry* **19**, 2396–2404 (1980).

145. Minta, A. & Tsien, R. Y. Fluorescent indicators for cytosolic sodium. *J. Biol. Chem.* **264**, 19449–19457 (1989).

146. Verkman, A. S. Development and biological applications of chloride-sensitive fluorescent indicators. *Am. J. Physiol. - Cell Physiol.* **259**, (1990).

147. Berendes, R., Burger, A., Voges, D., Demange, P. & Huber, R. Calcium influx through annexin V ion channels into large unilamellar vesicles measured with fura-2. *FEBS Lett.* **317**, 131–134 (1993).

148. Rydström, J. Energy-linked nicotinamide nucleotide transhydrogenase. Properties of proton-translocating and ATP-driven transhydrogenase reconstituted from synthetic phospholipids and purified transhydrogenase from beef heart mitochondria. *J. Biol. Chem.* **254**, 8611–9 (1979).

149. Dufour, J. P., Goffeau, A. & Tsong, T. Y. Active proton uptake in lipid vesicles reconstituted with the purified yeast plasma membrane ATPase. Fluorescence quenching of 9-amino-6-chloro-2-methoxyacridine. *J. Biol. Chem.* **257**, 9365–9371 (1982).

150. Wielandt, A. G., Palmgren, M. G., Fuglsang, A. T., Günther-Pomorski, T. & Justesen, B. H. Measuring H^+ pumping and membrane potential formation in sealed membrane vesicle systems. in *Methods in Molecular Biology* **1377**, 171–180 (Humana Press, New York, NY, 2016).

151. Graf, S., Brzezinski, P. & von Ballmoos, C. The proton pumping *bo* oxidase from *Vitreoscilla*. *Sci. Rep.* **9**, 1–10 (2019).

152. Waggoner, A. S. Dye indicators of membrane potential. *Annu. Rev. Biophys. Bioeng.* **8**, 47–68 (1979).

153. Loew, L. M. Design and Use of Organic Voltage Sensitive Dyes. *Advances in experimental medicine and biology* **859**, 27–53 (2015).

154. Miller, E. W. Small molecule fluorescent voltage indicators for studying membrane potential. *Curr. Opin. Chem. Biol.* **33**, 74–80 (2016).

155. Liu, P. & Miller, E. W. Electrophysiology, Unplugged: Imaging Membrane Potential with Fluorescent Indicators. *Acc. Chem. Res.* **53**, 11–19 (2020).

156. Vetter, I. *et al.* High-Throughput Fluorescence Assays for Ion Channels and GPCRs. in *Advances in Experimental Medicine and Biology* **1131**, 27–72 (Springer, Cham, 2020).

157. Thelen, M., Petrone, G., O'Shea, P. S. & Azzi, A. The use of fluorescein-dipalmitoyl-phosphatidylethanolamine for measuring pH-changes in the internal compartment of phospholipid vesicles. *BBA - Bioenerg.* **766**, 161–168 (1984).

158. Etter, E. F., Minta, A., Poenie, M. & Fay, F. S. Near-membrane [Ca^{2+}] transients resolved using the Ca^{2+} indicator FFP18. *Proc. Natl. Acad. Sci. U. S. A.* **93**, 5368–5373 (1996).

159. Ke, G. *et al.* A cell-surface-anchored ratiometric fluorescent probe for extracellular pH sensing. *ACS Appl. Mater. Interfaces* **6**, 15329–15334 (2014).

160. Xiong, M. *et al.* A membrane-anchored fluorescent probe for detecting K^+ in the cell microenvironment. *Chem. Commun.* **52**, 4679–4682 (2016).

161. Yao, H. W., Zhu, X. Y., Guo, X. F. & Wang, H. An Amphiphilic Fluorescent Probe Designed for Extracellular Visualization of Nitric Oxide Released from Living Cells. *Anal. Chem.* **88**, 9014–9021 (2016).

162. Ohgaki, R. *et al.* Ratiometric fluorescence imaging of cell surface pH by poly(ethylene glycol)-phospholipid conjugated with fluorescein isothiocyanate. *Sci. Rep.* **7**, 1–9 (2017).

163. Świtalska, A., Dembska, A., Fedoruk-Wyszomirska, A. & Juskowiak, B. Cholesterol-bearing fluorescent g-quadruplex potassium probes for anchoring at the langmuir monolayer and cell membrane. *Sensors (Switzerland)* **18**, (2018).

164. Cebecauer, M. & Šachl, R. Lipophilic Fluorescent Probes: Guides to the Complexity of Lipid Membranes. in *Fluorescent Analogs of Biomolecular Building Blocks* 367–392 (John Wiley & Sons, Inc, 2016). doi:10.1002/9781119179320.ch16

165. Kemmer, G. C. *et al.* Lipid-conjugated fluorescent pH sensors for monitoring pH changes in reconstituted membrane systems. *Analyst* **140**, 6313–6320 (2015).

166. Schwamborn, M., Schumacher, J., Sibold, J., Teiwes, N. K. & Steinem, C. Monitoring ATPase induced pH changes in single proteoliposomes with the lipid-coupled fluorophore Oregon Green 488. *Analyst* **142**,

2670–2677 (2017).

167. Nichols, J. W. & Deamer, D. W. Catecholamine uptake and concentration by liposomes maintaining pH gradients. *BBA - Biomembr.* **455**, 269–271 (1976).

168. Bally, M. B., Hope, M. J., Van Echteld, C. J. A. & Cullis, P. R. Uptake of safranine and other lipophilic cations into model membrane systems in response to a membrane potential. *BBA - Biomembr.* **812**, 66–76 (1985).

169. Schubert, R., Wolburg, H., Schmidt, K. H. & Roth, H. J. Loading of preformed liposomes with high trapping efficiency by detergent-induced formation of transient membrane holes. *Chem. Phys. Lipids* **58**, 121–129 (1991).

170. Leiding, T. *et al.* Precise detection of pH inside large unilamellar vesicles using membrane-impermeable dendritic porphyrin-based nanoprobes. *Anal. Biochem.* **388**, 296–305 (2009).

171. Xu, X., Khan, M. A. & Burgess, D. J. Predicting hydrophilic drug encapsulation inside unilamellar liposomes. *Int. J. Pharm.* **423**, 410–418 (2012).

172. Eloy, J. O. *et al.* Liposomes as carriers of hydrophilic small molecule drugs: Strategies to enhance encapsulation and delivery. *Colloids Surfaces B Biointerfaces* **123**, 345–363 (2014).

173. Chiantia, S., Klymchenko, A. S. & London, E. A novel leaflet-selective fluorescence labeling technique reveals differences between inner and outer leaflets at high bilayer curvature. *Biochim Biophys Acta* **1818**, 1284–1290 (2012).

174. Dolder, N. & von Ballmoos, C. Bifunctional DNA duplexes permit efficient incorporation of pH probes into liposomes. *ChemBioChem* **21**, 2219–2224 (2020).

175. Ying, L. *et al.* A cell-surface-anchored ratiometric i-motif sensor for extracellular pH detection. *Chem. Commun.* **52**, 7818–7821 (2016).

176. Dembska, A., Bielecka, P. & Juskowiak, B. pH-Sensing fluorescence oligonucleotide probes based on an i-motif scaffold: a review. *Anal. Methods* **9**, 6092–6106 (2017).

177. Swiatkowska, A. & Juskowiak, B. Effect of Cholesterol Anchoring Group on the Properties of G-Quadruplex-Based FRET Probes for Potassium Ion. *Chemosensors* **2**, 267–286 (2014).

178. Feng, G. *et al.* Engineering of Nucleic Acids and Synthetic Cofactors as Holo Sensors for Probing Signaling Molecules in the Cellular Membrane Microenvironment. *Angew. Chemie - Int. Ed.* **58**, 6590–6594 (2019).

179. Qiu, L. *et al.* Cell membrane-anchored biosensors for real-time monitoring of the cellular microenvironment. *J. Am. Chem. Soc.* **136**, 13090–13093 (2014).

180. Liu, L. *et al.* Cell Surface-Anchored DNA Nanomachine for Dynamically Tunable Sensing and Imaging of Extracellular pH. *Anal. Chem.* **90**, 11198–11202 (2018).

181. Zeng, S. *et al.* Cell-Surface-Anchored Ratiometric DNA Tweezer for Real-Time Monitoring of Extracellular

and Apoplastic pH. *Anal. Chem.* **90**, 13459–13466 (2018).

182. Yuan, J. *et al.* Cell-Surface-Anchored Ratiometric DNA Nanoswitch for Extracellular ATP Imaging. *ACS Sensors* **4**, 1648–1653 (2019).

183. Zhao, Y. *et al.* Single-molecule dynamics of gating in a neurotransmitter transporter homologue. *Nature* **465**, 188–193 (2010).

184. Nishizaka, T., Hasimoto, Y. & Masaike, T. Single Molecule Enzymology. *Single Mol. Enzymol.* (2011).

185. English, B. P. *et al.* Ever-fluctuating single enzyme molecules: Michaelis-Menten equation revisited. *Nat. Chem. Biol.* **2**, 87–94 (2006).

186. Volkán-Kacso, S. & Marcus, R. A. What can be learned about the enzyme ATPase from single-molecule studies of its subunit F_1? *Quarterly reviews of biophysics* **50**, e14 (2017).

187. Veshaguri, S. *et al.* Direct observation of proton pumping by a eukaryotic P-type ATPase. *Science (80-.).* **351**, 1469–1473 (2016).

188. Jorgensen, I. L., Kemmer, G. C. & Pomorski, T. G. Membrane protein reconstitution into giant unilamellar vesicles: a review on current techniques. *Eur Biophys J* **46**, 103–119 (2017).

189. Pautot, S., Frisken, B. J. & Weitz, D. A. Production of unilamellar vesicles using an inverted emulsion. *Langmuir* **19**, 2870–2879 (2003).

190. Funakoshi, K., Suzuki, H. & Takeuchi, S. Formation of Giant Lipid Vesiclelike Compartments from a Planar Lipid Membrane by a Pulsed Jet Flow. *J. Am. Chem. Soc.* **129**, 12608–12609 (2007).

191. Walde, P., Cosentino, K., Engel, H. & Stano, P. Giant vesicles: preparations and applications. *Chembiochem* **11**, 848–865 (2010).

192. Matosevic, S. & Paegel, B. M. Layer-by-layer cell membrane assembly. *Nat. Chem.* **5**, 958–963 (2013).

193. Deshpande, S., Caspi, Y., Meijering, A. E. C. & Dekker, C. Octanol-assisted liposome assembly on chip. *Nat. Commun.* **7**, 10447 (2016).

194. Stein, H., Spindler, S., Bonakdar, N., Wang, C. & Sandoghdar, V. Production of Isolated Giant Unilamellar Vesicles under High Salt Concentrations. *Front. Physiol.* **8**, 63 (2017).

195. Bellon, J. A., Pino, M. J. & Wilke, N. Low-cost equipment for electroformation of Giant Unilamellar Vesicles. *HardwareX* **4**, e00037 (2018).

196. Rideau, E., Wurm, F. R. & Landfester, K. Self-Assembly of Giant Unilamellar Vesicles by Film Hydration Methodologies. *Advanced Biosystems* 1800324 (2019). doi:10.1002/adbi.201800324

197. Girish, V., Pazzi, J., Li, A. & Subramaniam, A. B. Fabrics of Diverse Chemistries Promote the Formation of Giant Vesicles from Phospholipids and Amphiphilic Block Copolymers. *Langmuir* **35**, 9264–9273 (2019).

198. Matsushita-Ishiodori, Y., Hanczyc, M. M., Wang, A., Szostak, J. W. & Yomo, T. Using imaging flow cytometry to quantify and optimize giant vesicle production by water-in-oil emulsion transfer methods. *Langmuir* **35**, 2375–2382 (2019).

199. Göpfrich, K. *et al.* One-Pot Assembly of Complex Giant Unilamellar Vesicle-Based Synthetic Cells. *ACS Synth. Biol.* **8**, 937–947 (2019).

200. Noireaux, V. & Libchaber, A. A vesicle bioreactor as a step toward an artificial cell assembly. *Proc. Natl. Acad. Sci.* **101**, 17669–17674 (2004).

201. Gessesse, B., Nagaike, T., Nagata, K., Shimizu, Y. & Ueda, T. G-protein coupled receptor protein synthesis on a lipid bilayer using a reconstituted cell-free protein synthesis system. *Life* **8**, (2018).

202. Ohta, N., Kato, Y., Watanabe, H., Mori, H. & Matsuura, T. In vitro membrane protein synthesis inside Sec translocon-reconstituted cell-sized liposomes. *Sci. Rep.* **6**, 1–9 (2016).

203. Biner, O., Schick, T., Ganguin, A. A. & von Ballmoos, C. Towards a Synthetic Mitochondrion. *Chim. Int. J. Chem.* **72**, 291–296 (2018).

204. Dezi, M., Di Cicco, A., Bassereau, P. & Levy, D. Detergent-mediated incorporation of transmembrane proteins in giant unilamellar vesicles with controlled physiological contents. *Proc Natl Acad Sci U S A* **110**, 7276–7281 (2013).

205. Hansen, J. S., Elbing, K., Thompson, J. R., Malmstadt, N. & Lindkvist-Petersson, K. Glucose transport machinery reconstituted in cell models. *Chem Commun* **51**, 2316–2319 (2015).

206. Spoelstra, W. K., Deshpande, S. & Dekker, C. Tailoring the appearance: what will synthetic cells look like? *Current Opinion in Biotechnology* **51**, 47–56 (2018).

207. Stano, P. Is Research on "Synthetic Cells" Moving to the Next Level? *Life* **9**, 3 (2018).

208. Berhanu, S., Ueda, T. & Kuruma, Y. Artificial photosynthetic cell producing energy for protein synthesis. *Nat. Commun.* **10**, 1325 (2019).

209. Hindley, J. W. *et al.* Building a synthetic mechanosensitive signaling pathway in compartmentalized artificial cells. *Proc. Natl. Acad. Sci. U. S. A.* **116**, 16711–16716 (2019).

210. Chen, Z. *et al.* Synthetic beta cells for fusion-mediated dynamic insulin secretion. *Nat. Chem. Biol.* **14**, 86–93 (2018).

211. Fischer, A., Oberholzer, T. & Luisi, P. L. Giant vesicles as models to study the interactions between membranes and proteins. *Biochim. Biophys. Acta - Biomembr.* **1467**, 177–188 (2000).

212. Nishimura, K. K. *et al.* Identification of giant unilamellar vesicles with permeability to small charged molecules. *RSC Adv.* **4**, 35224–35232 (2014).

213. Beales, P. A., Khan, S., Muench, S. P. & Jeuken, L. J. C. Durable vesicles for reconstitution of membrane

proteins in biotechnology. *Biochem. Soc. Trans.* **45**, 15–26 (2017).

214. Rideau, E., Dimova, R., Schwille, P., Wurm, F. R. & Landfester, K. Liposomes and polymersomes: a comparative review towards cell mimicking. *Chem. Soc. Rev.* **47**, 8572–8610 (2018).

215. Schmitt, C., Lippert, A. H., Bonakdar, N., Sandoghdar, V. & Voll, L. M. Compartmentalization and transport in synthetic vesicles. *Front. Bioeng. Biotechnol.* **4**, 1–12 (2016).

216. Klermund, L., Poschenrieder, S. T. & Castiglione, K. Biocatalysis in Polymersomes: Improving Multienzyme Cascades with Incompatible Reaction Steps by Compartmentalization. *ACS Catal.* **7**, 3900–3904 (2017).

217. Schwarzer, T. S., Klermund, L., Wang, G. & Castiglione, K. Membrane functionalization of polymersomes: Alleviating mass transport limitations by integrating multiple selective membrane transporters for the diffusion of chemically diverse molecules. *Nanotechnology* **29**, (2018).

218. Khan, S., Li, M., Muench, S. P., Jeuken, L. J. C. C. & Beales, P. A. Durable proteo-hybrid vesicles for the extended functional lifetime of membrane proteins in bionanotechnology. *Chem. Commun.* **52**, 11020–11023 (2016).

219. Otrin, L. *et al.* Toward Artificial Mitochondrion: Mimicking Oxidative Phosphorylation in Polymer and Hybrid Membranes. *Nano Lett.* **17**, 6816–6821 (2017).

220. Marušič, N. *et al.* Constructing artificial respiratory chain in polymer compartments: Insights into the interplay between bo_3 oxidase and the membrane. *Proc. Natl. Acad. Sci. U. S. A.* **117**, (2020).

221. Al Nahas, K. *et al.* A microfluidic platform for the characterisation of membrane active antimicrobials. *Lab Chip* **19**, 837–844 (2019).

222. Schaich, M. *et al.* An Integrated Microfluidic Platform for Quantifying Drug Permeation across Biomimetic Vesicle Membranes. *Mol. Pharm.* **16**, 2494–2501 (2019).

223. Cuevas, J. Structure and Function of Membranes. in *Reference Module in Biomedical Sciences* 1–5 (Elsevier, 2015). doi:10.1016/B978-0-12-801238-3.05320-4

224. Tanford, C. *The Hydrophobic Effect: Formation of Micelles and Biological Membranes (2nd Edition)*. **2**, (John Wiley & Sons, Inc, 1980).

225. Jouhet, J. Importance of the hexagonal lipid phase in biological membrane organization. *Front. Plant Sci.* **4**, 1–5 (2013).

226. Hishikawa, D., Hashidate, T., Shimizu, T. & Shindou, H. Diversity and function of membrane glycerophospholipids generated by the remodeling pathway in mammalian cells. *J. Lipid Res.* **55**, 799–807 (2014).

227. Blanco, A. & Blanco, G. Lipids. in *Medical Biochemistry* 99–119 (Elsevier, 2017). doi:10.1016/B978-0-12-803550-4.00005-7

228. Fadeel, B. & Xue, Di. The ins and outs of phospholipid asymmetry in the plasma membrane: roles in health and disease. *Crit. Rev. Biochem. Mol. Biol.* **44**, 264–277 (2009).

229. Ma, Y., Poole, K., Goyette, J. & Gaus, K. Introducing membrane charge and membrane potential to T cell signaling. *Front. Immunol.* **8**, 1–11 (2017).

230. Goñi, F. M. The basic structure and dynamics of cell membranes: An update of the Singer-Nicolson model. *Biochim. Biophys. Acta - Biomembr.* **1838**, 1467–1476 (2014).

231. Dowhan, W., Bogdanov, M. & Mileykovskaya, E. *Functional Roles of Lipids in Membranes*. *Biochemistry of Lipids, Lipoproteins and Membranes: Sixth Edition* (Elsevier, 2016). doi:10.1016/B978-0-444-63438-2.00001-8

232. Mouritsen, O. G. The liquid-ordered state comes of age. *Biochim. Biophys. Acta - Biomembr.* **1798**, 1286–1288 (2010).

233. Giocondi, M. C. *et al.* Surface topography of membrane domains. *Biochim. Biophys. Acta - Biomembr.* **1798**, 703–718 (2010).

234. Levental, I., Levental, K. R. & Heberle, F. A. Lipid Rafts: Controversies Resolved, Mysteries Remain. *Trends in Cell Biology* **30**, 341–353 (2020).

235. Dimova, R. & Marques, C. *The Giant Vesicle Book*. **53**, (CRC Press, 2019).

236. Reeves, J. P. & Dowben, R. M. Formation and properties of thin-walled phospholipid vesicles. *J. Cell. Physiol.* **73**, 49–60 (1969).

237. Peruzzi, J., Gutierrez, M. G., Mansfield, K. & Malmstadt, N. Dynamics of Hydrogel-Assisted Giant Unilamellar Vesicle Formation from Unsaturated Lipid Systems. *Langmuir* **32**, 12702–12709 (2016).

238. Pazzi, J. & Subramaniam, A. B. Nanoscale Curvature Promotes High Yield Spontaneous Formation of Cell-Mimetic Giant Vesicles on Nanocellulose Paper. *ACS Appl. Mater. Interfaces* **12**, 56549–56561 (2020).

239. Yandrapalli, N., Petit, J., Bäumchen, O. & Robinson, T. Surfactant-free production of biomimetic giant unilamellar vesicles using PDMS-based microfluidics. *Commun. Chem.* **4**, 100 (2021).

240. Van Swaay, D. & Demello, A. Microfluidic methods for forming liposomes. *Lab Chip* **13**, 752–767 (2013).

241. Dimova, R. Giant Vesicles and Their Use in Assays for Assessing Membrane Phase State, Curvature, Mechanics, and Electrical Properties. *Annu. Rev. Biophys.* **48**, 93–119 (2019).

242. Yuan, W., Piao, J. & Dong, Y. Advancements in the preparation methods of artificial cell membranes with lipids. *Mater. Chem. Front.* 5233–5246 (2021). doi:10.1039/d1qm00501d

243. Supramaniam, P., Ces, O. & Salehi-Reyhani, A. Microfluidics for artificial life: Techniques for bottom-up synthetic biology. *Micromachines* **10**, 1–27 (2019).

244. Robinson, T. Microfluidics and giant vesicles: creation, capture, and applications for biomembranes. in *Advances in Biomembranes and Lipid Self-Assembly* **30**, 271–315 (Elsevier Ltd, 2019).

245. Vaz, W. L. C., Stiimpel, J., Jovin, T. M., Kapitza, H. G. & Sackmann, E. Translational Mobility of Glycophorin in Bilayer Membranes of Dimyristoylphosphatidylcholine. *Biochemistry* **20**, 1392–1396 (1981).

246. Keller, B. U., Hedrich, R., Vaz, W. L. C. & Criado, M. Single channel recordings of reconstituted ion channel proteins: an improved technique. *Pflügers Arch. Eur. J. Physiol.* **411**, 94–100 (1988).

247. Bhatia, T. *et al.* Preparing giant unilamellar vesicles (GUVs) of complex lipid mixtures on demand: Mixing small unilamellar vesicles of compositionally heterogeneous mixtures. *Biochim. Biophys. Acta - Biomembr.* **1848**, 3175–3180 (2015).

248. Rodriguez, N., Pincet, F. & Cribier, S. Giant vesicles formed by gentle hydration and electroformation: A comparison by fluorescence microscopy. *Colloids Surfaces B Biointerfaces* **42**, 125–130 (2005).

249. Tsumoto, K., Matsuo, H., Tomita, M. & Yoshimura, T. Efficient formation of giant liposomes through the gentle hydration of phosphatidylcholine films doped with sugar. *Colloids Surfaces B Biointerfaces* **68**, 98–105 (2009).

250. Angelova, M. I. & Dimitrov, D. S. Liposome electroformation. *Faraday Discuss. Chem. Soc.* **81**, 303 (1986).

251. Angelova, M. I., Soléau, S., Méléard, P., Faucon, F. & Bothorel, P. Preparation of giant vesicles by external AC electric fields. Kinetics and applications. *Prog. Colloid Polym. Sci.* **89**, 127–131 (1992).

252. Niri, V. H., Flatt, B. K., Fakhraai, Z. & Forrest, J. A. Simultaneous monitoring of electroformation of phospholipid vesicles by quartz crystal microbalance and optical microscopy. *Chem. Phys. Lipids* **163**, 36–41 (2010).

253. Ayuyan, A. G. & Cohen, F. S. Lipid peroxides promote large rafts: Effects of excitation of probes in fluorescence microscopy and electrochemical reactions during vesicle formation. *Biophys. J.* **91**, 2172–2183 (2006).

254. Pereno, V. *et al.* Electroformation of Giant Unilamellar Vesicles on Stainless Steel Electrodes. *ACS Omega* **2**, 994–1002 (2017).

255. Pott, T., Bouvrais, H. & Méléard, P. Giant unilamellar vesicle formation under physiologically relevant conditions. *Chem. Phys. Lipids* **154**, 115–119 (2008).

256. Li, Q., Wang, X., Ma, S., Zhang, Y. & Han, X. Electroformation of giant unilamellar vesicles in saline solution. *Colloids Surfaces B Biointerfaces* **147**, 368–375 (2016).

257. Lefrançois, P., Goudeau, B. & Arbault, S. Electroformation of phospholipid giant unilamellar vesicles in physiological phosphate buffer. *Integr. Biol. (United Kingdom)* **10**, 429–434 (2018).

258. Herold, C., Chwastek, G., Schwille, P. & Petrov, E. P. Efficient Electroformation of Supergiant Unilamellar

Vesicles Containing Cationic Lipids on ITO-Coated Electrodes. *Langmuir* **28**, 5518–5521 (2012).

259. Politano, T. J., Froude, V. E., Jing, B. & Zhu, Y. AC-electric field dependent electroformation of giant lipid vesicles. *Colloids Surfaces B Biointerfaces* **79**, 75–82 (2010).

260. Ghellab, S. E., Mu, W., Li, Q. & Han, X. Prediction of the size of electroformed giant unilamellar vesicle using response surface methodology. *Biophys. Chem.* **253**, 106217 (2019).

261. Steinkühler, J., De Tillieux, P., Knorr, R. L., Lipowsky, R. & Dimova, R. Charged giant unilamellar vesicles prepared by electroformation exhibit nanotubes and transbilayer lipid asymmetry. *Sci. Rep.* **8**, 11838 (2018).

262. Breton, M., Amirkavei, M. & Mir, L. M. Optimization of the Electroformation of Giant Unilamellar Vesicles (GUVs) with Unsaturated Phospholipids. *J. Membr. Biol.* **248**, 827–835 (2015).

263. Horger, K. S., Estes, D. J., Capone, R. & Mayer, M. Films of Agarose Enable Rapid Formation of Giant Liposomes in Solutions of Physiologic Ionic Strength. *J. Am. Chem. Soc.* **131**, 1810–1819 (2009).

264. Lira, R. B., Dimova, R. & Riske, K. A. Giant unilamellar vesicles formed by hybrid films of agarose and lipids display altered mechanical properties. *Biophys. J.* **107**, 1609–1619 (2014).

265. Weinberger, A. *et al.* Gel-assisted formation of giant unilamellar vesicles. *Biophys. J.* **105**, 154–64 (2013).

266. Dao, T. P. T. *et al.* Membrane properties of giant polymer and lipid vesicles obtained by electroformation and pva gel-assisted hydration methods. *Colloids Surfaces A Physicochem. Eng. Asp.* **533**, 347–353 (2017).

267. Kresse, K. M., Xu, M., Pazzi, J., García-Ojeda, M. & Subramaniam, A. B. Novel Application of Cellulose Paper As a Platform for the Macromolecular Self-Assembly of Biomimetic Giant Liposomes. *ACS Appl. Mater. Interfaces* **8**, 32102–32107 (2016).

268. Pazzi, J., Xu, M. & Subramaniam, A. B. Size Distributions and Yields of Giant Vesicles Assembled on Cellulose Papers and Cotton Fabric. *Langmuir* acs.langmuir.8b03076 (2018). doi:10.1021/acs.langmuir.8b03076

269. Parigoris, E. *et al.* Facile generation of giant unilamellar vesicles using polyacrylamide gels. *Sci. Rep.* **10**, 1–10 (2020).

270. López Mora, N. *et al.* Preparation of size tunable giant vesicles from cross-linked dextran(ethylene glycol) hydrogels. *Chem. Commun.* **50**, 1953–1955 (2014).

271. Mora, N. L. *et al.* Evaluation of dextran(ethylene glycol) hydrogel films for giant unilamellar lipid vesicle production and their application for the encapsulation of polymersomes. *Soft Matter* **13**, 5580–5588 (2017).

272. Movsesian, N., Tittensor, M., Dianat, G., Gupta, M. & Malmstadt, N. Giant Lipid Vesicle Formation Using Vapor-Deposited Charged Porous Polymers. *Langmuir* **34**, 9025–9035 (2018).

273. Schultze, J. *et al.* Preparation of Monodisperse Giant Unilamellar Anchored Vesicles Using Micropatterned

Hydrogel Substrates. *ACS Omega* **4**, 9393–9399 (2019).

274. Teh, S. Y., Khnouf, R., Fan, H. & Lee, A. P. Stable, biocompatible lipid vesicle generation by solvent extraction-based droplet microfluidics. *Biomicrofluidics* **5**, 1–12 (2011).

275. Pautot, S., Frisken, B. J. & Weitz, D. A. Engineering asymmetric vesicles. *Proc. Natl. Acad. Sci. U. S. A.* **100**, 10718–10721 (2003).

276. Pagano, R. E., Martin, O. C., Schroit, A. J. & Struck, D. K. Formation of Asymmetric Phospholipid Membranes via Spontaneous Transfer of Fluorescent Lipid Analogues between Vesicle Populations. *Biochemistry* **20**, 4920–4927 (1981).

277. Chiantia, S., Schwille, P., Klymchenko, A. S. & London, E. Asymmetric GUVs prepared by MβCD-mediated lipid exchange: An FCS study. *Biophys. J.* **100**, L1–L3 (2011).

278. Cheng, H. T. & London, E. Preparation and properties of asymmetric large unilamellar vesicles: interleaflet coupling in asymmetric vesicles is dependent on temperature but not curvature. *Biophys J* **100**, 2671–2678 (2011).

279. Hamada, T. *et al.* Construction of asymmetric cell-sized lipid vesicles from lipid-coated water-in-oil microdroplets. *J. Phys. Chem. B* **112**, 14678–14681 (2008).

280. Moga, A., Yandrapalli, N., Dimova, R. & Robinson, T. Optimization of the Inverted Emulsion Method for High-Yield Production of Biomimetic Giant Unilamellar Vesicles. *ChemBioChem* **20**, 2674–2682 (2019).

281. Abkarian, M., Loiseau, E. & Massiera, G. Continuous droplet interface crossing encapsulation (cDICE) for high throughput monodisperse vesicle design. *Soft Matter* **7**, 4610–4614 (2011).

282. Van de Cauter, L. *et al.* Optimized cDICE for Efficient Reconstitution of Biological Systems in Giant Unilamellar Vesicles. *ACS Synth. Biol.* (2021). doi:10.1021/acssynbio.1c00068

283. Shum, H. C., Lee, D., Yoon, I., Kodger, T. & Weitz, D. A. Double emulsion templated monodisperse phospholipid vesicles. *Langmuir* **24**, 7651–7653 (2008).

284. Arriaga, L. R. *et al.* Ultrathin shell double emulsion templated giant unilamellar lipid vesicles with controlled microdomain formation. *Small* **10**, 950–956 (2014).

285. Ota, S., Yoshizawa, S. & Takeuchi, S. Microfluidic formation of monodisperse, cell-sized, and unilamellar vesicles. *Angew. Chemie - Int. Ed.* **48**, 6533–6537 (2009).

286. Matosevic, S. & Paegel, B. M. Stepwise synthesis of giant unilamellar vesicles on a microfluidic assembly line. *J. Am. Chem. Soc.* **133**, 2798–2800 (2011).

287. Schaich, M., Sobota, D., Sleath, H., Cama, J. & Keyser, U. F. Characterization of lipid composition and diffusivity in OLA generated vesicles. *Biochim. Biophys. Acta - Biomembr.* **1862**, 183359 (2020).

288. Bao, P. *et al.* Production of giant unilamellar vesicles and encapsulation of lyotropic nematic liquid crystals.

Soft Matter **17**, 2234–2241 (2021).

289. Petit, J., Polenz, I., Baret, J. C., Herminghaus, S. & Bäumchen, O. Vesicles-on-a-chip: A universal microfluidic platform for the assembly of liposomes and polymersomes. *Eur. Phys. J. E* **39**, (2016).

290. Cochereau, R., Renard, D., Noûs, C. & Boire, A. Semi-permeable vesicles produced by microfluidics to tune the phase behaviour of encapsulated macromolecules. *J. Colloid Interface Sci.* **580**, 709–719 (2020).

291. Stachowiak, J. C., Richmond, D. L., Li, T. H., Brochard-Wyart, F. & Fletcher, D. A. Inkjet formation of unilamellar lipid vesicles for cell-like encapsulation. *Lab Chip* **9**, 2003–2009 (2009).

292. Richmond, D. L. *et al.* Forming giant vesicles with controlled membrane composition, asymmetry, and contents. *Proc. Natl. Acad. Sci. U. S. A.* **108**, 9431–9436 (2011).

293. Coyne, C. W. *et al.* Lipid Bilayer Vesicle Generation Using Microfluidic Jetting. *J. Vis. Exp.* e51510 (2014). doi:10.3791/51510

294. Armstrong, M., Vahey, M. D., Hunt, T. P. & Fletcher, D. A. Forming and loading giant unilamellar vesicles with acoustic jetting. *Biomicrofluidics* **14**, (2020).

295. Weiss, M. *et al.* Sequential bottom-up assembly of mechanically stabilized synthetic cells by microfluidics. *Nat. Mater.* **17**, 89–96 (2017).

296. Haller, B. *et al.* Charge-controlled microfluidic formation of lipid-based single- and multicompartment systems. *Lab Chip* **18**, 2665–2674 (2018).

297. Allegretti, M. *et al.* Horizontal membrane-intrinsic α-helices in the stator a-subunit of an F-type ATP synthase. *Nature* **521**, 237–240 (2015).

298. Wardhan, R. & Mudgal, P. *Textbook of Membrane Biology*. (2017). doi:10.1007/978-981-10-7101-0

299. Liu, Y. J., Hansen, G. P. R., Venancio-Marques, A. & Baigl, D. Cell-free preparation of functional and triggerable giant proteoliposomes. *ChemBioChem* **14**, 2243–2247 (2013).

300. Eaglesfield, R., Madsen, M. A., Sanyal, S., Reboud, J. & Amtmann, A. Cotranslational recruitment of ribosomes in protocells recreates a translocon-independent mechanism of proteorhodopsin biogenesis. *iScience* **24**, 102429 (2021).

301. Baumgart, T. *et al.* Large-scale fluid/fluid phase separation of proteins and lipids in giant plasma membrane vesicles. *Proc. Natl. Acad. Sci. U. S. A.* **104**, 3165–3170 (2007).

302. Zartner, L., Garni, M., Craciun, I., Einfalt, T. & Palivan, C. G. How Can Giant Plasma Membrane Vesicles Serve as a Cellular Model for Controlled Transfer of Nanoparticles? *Biomacromolecules* **22**, 106–115 (2021).

303. Litschel, T. & Schwille, P. Protein Reconstitution Inside Giant Unilamellar Vesicles. *Annu. Rev. Biophys.* **50**, 525–548 (2021).

304. Darszon, A. *et al.* Reassembly of protein-lipid complexes into large bilayer vesicles: perspectives for membrane reconstitution. *Proc. Natl. Acad. Sci. U. S. A.* **77**, 239–243 (1980).

305. Manneville, J. B., Bassereau, P., Lévy, D. & Prost, J. Activity of transmembrane proteins induces magnification of shape fluctuations of lipid membranes. *Phys. Rev. Lett.* **82**, 4356–4359 (1999).

306. Manneville, J. B., Bassereau, P., Ramaswamy, S. & Prost, J. Active membrane fluctuations studied by micropipet aspiration. *Phys. Rev. E - Stat. Physics, Plasmas, Fluids, Relat. Interdiscip. Top.* **64**, 10 (2001).

307. Girard, P. *et al.* A new method for the reconstitution of membrane proteins into giant unilamellar vesicles. *Biophys. J.* **87**, 419–429 (2004).

308. Aimon, S. *et al.* Functional reconstitution of a voltage-gated potassium channel in giant unilamellar vesicles. *PLoS One* **6**, (2011).

309. Garten, M., Aimon, S., Bassereau, P. & Toombes, G. E. S. Reconstitution of a transmembrane protein, the voltage-gated ion channel, KvAP, into giant unilamellar vesicles for microscopy and patch clamp studies. *J. Vis. Exp.* 1–16 (2015). doi:10.3791/52281

310. Witkowska, A., Jablonski, L. & Jahn, R. A convenient protocol for generating giant unilamellar vesicles containing SNARE proteins using electroformation. *Sci. Rep.* **8**, 9422 (2018).

311. Doeven, M. K. *et al.* Distribution, lateral mobility and function of membrane proteins incorporated into giant unilamellar vesicles. *Biophys J* **88**, 1134–1142 (2005).

312. Kahya, N., Brown, D. A. & Schwille, P. Raft partitioning and dynamic behavior of human placental alkaline phosphatase in giant unilamellar vesicles. *Biochemistry* **44**, 7479–7489 (2005).

313. Streicher, P. *et al.* Integrin reconstituted in GUVs: A biomimetic system to study initial steps of cell spreading. *Biochim. Biophys. Acta - Biomembr.* **1788**, 2291–2300 (2009).

314. Collins, M. D. & Gordon, S. E. Giant liposome preparation for imaging and patch-clamp electrophysiology. *J. Vis. Exp.* 1–9 (2013). doi:10.3791/50227

315. Ramadurai, S. *et al.* Lateral diffusion of membrane proteins. *J. Am. Chem. Soc.* **131**, 12650–12656 (2009).

316. Nikolaus, J. *et al.* Hemagglutinin of influenza virus partitions into the nonraft domain of model membranes. *Biophys. J.* **99**, 489–498 (2010).

317. Betaneli, V., Petrov, E. P. & Schwille, P. The role of lipids in VDAC oligomerization. *Biophys. J.* **102**, 523–531 (2012).

318. Lorenz, M. *et al.* A single herpesvirus protein can mediate vesicle formation in the nuclear envelope. *J. Biol. Chem.* **290**, 6962–6974 (2015).

319. Hansen, J. S., Thompson, J. R., Hélix-Nielsen, C. & Malmstadt, N. Lipid directed intrinsic membrane protein segregation. *J. Am. Chem. Soc.* **135**, 17294–17297 (2013).

320. Horger, K. S. *et al.* Hydrogel-assisted functional reconstitution of human P-glycoprotein (ABCB1) in giant liposomes. *Biochim. Biophys. Acta - Biomembr.* **1848**, 643–653 (2015).

321. Zhemkov, V. *et al.* The role of sigma 1 receptor in organization of endoplasmic reticulum signaling microdomains. *Elife* **10**, 1–34 (2021).

322. Souissi, M. *et al.* Integrin-functionalised giant unilamellar vesicles via gel-assisted formation: Good practices and pitfalls. *Int. J. Mol. Sci.* **22**, (2021).

323. Diederichs, T. & Tampé, R. Single Cell-like Systems Reveal Active Unidirectional and Light-Controlled Transport by Nanomachineries. *ACS Nano* **15**, 6747–6755 (2021).

324. Lopez Mora, N. *et al.* The membrane transporter lactose permease increases lipid bilayer bending rigidity. *Biophys. J.* **120**, 3787–3794 (2021).

325. Kreir, M., Farre, C., Beckler, M., George, M. & Fertig, N. Rapid screening of membrane protein activity: Electrophysiological analysis of OmpF reconstituted in proteoliposomes. *Lab Chip* **8**, 587–595 (2008).

326. Almendro-Vedia, V. G. *et al.* Nonequilibrium fluctuations of lipid membranes by the rotating motor protein F_1F_0-ATP synthase. *Proc. Natl. Acad. Sci. U. S. A.* **114**, 11291–11296 (2017).

327. Battle, A. R., Petrov, E., Pal, P. & Martinac, B. Rapid and improved reconstitution of bacterial mechanosensitive ion channel proteins MscS and MscL into liposomes using a modified sucrose method. *FEBS Lett.* **583**, 407–412 (2009).

328. Wijekoon, C. J. K. *et al.* Copper ATPase CopA from Escherichia coli: Quantitative Correlation between ATPase Activity and Vectorial Copper Transport. *J. Am. Chem. Soc.* **139**, 4266–4269 (2017).

329. Sjöholm, J. *et al.* The lateral distance between a proton pump and ATP synthase determines the ATP-synthesis rate. *Sci. Rep.* **7**, 1–12 (2017).

330. Mahendran, K. R., Kreir, M., Weingart, H., Fertig, N. & Winterhalter, M. Permeation of antibiotics through *Escherichia coli* OmpF and OmpC porins: Screening for influx on a single-molecule level. *J. Biomol. Screen.* **15**, 302–307 (2010).

331. Gornall, J. L. *et al.* Simple reconstitution of protein pores in nano lipid bilayers. *Nano Lett.* **11**, 3334–3340 (2011).

332. Weichbrodt, C. *et al.* Antibiotic translocation through porins studied in planar lipid bilayers using parallel platforms. *Analyst* **140**, 4874–4881 (2015).

333. Cama, J. *et al.* Quantification of Fluoroquinolone Uptake through the Outer Membrane Channel OmpF of *Escherichia coli*. *J. Am. Chem. Soc.* **137**, 13836–13843 (2015).

334. Wang, J., Benier, L. & Winterhalter, M. Quantifying Permeation of Small Charged Molecules across Channels: Electrophysiology in Small Volumes. *ACS Omega* **3**, 17481–17486 (2018).

335. Guzel, F. D. & Citak, F. Development of an On-Chip Antibiotic Permeability Assay With Single Molecule Detection Capability. *IEEE Trans. Nanobioscience* **17**, 155–160 (2018).

336. Survery, S. *et al.* The N-terminal Ankyrin Repeat domain is not required for electrophile and heat activation of the purified mosquito TRPA1 receptor. *J. Biol. Chem.* **291**, 26899–26912 (2016).

337. Clausen, M. V., Jarerattanachat, V., Carpenter, E. P., Sansom, M. S. P. & Tucker, S. J. Asymmetric mechanosensitivity in a eukaryotic ion channel. *Proc. Natl. Acad. Sci. U. S. A.* **114**, E8343–E8351 (2017).

338. Kahya, N., Pécheur, E. I., De Boeij, W. P., Wiersma, D. A. & Hoekstra, D. Reconstitution of membrane proteins into giant unilamellar vesicles via peptide-induced fusion. *Biophys. J.* **81**, 1464–1474 (2001).

339. Tsumoto, K., Yamazaki, Y., Kamiya, K. & Yoshimura, T. Reconstitution and Microscopic Observation of G Protein Subunits on Giant Liposomes: Attempt to Construct a Cell Model with Functional Membrane Protein Components. in *2008 International Symposium on Micro-NanoMechatronics and Human Science* 145–150 (IEEE, 2008). doi:10.1109/MHS.2008.4752439

340. Tsumoto, K. & Yoshimura, T. Recombinant Proteoliposomes Prepared Using Baculovirus Expression Systems. in *Methods in Enzymology* **465**, 95–109 (Elsevier Inc., 2009).

341. Nishigami, M., Mori, T., Tomita, M., Takiguchi, K. & Tsumoto, K. Membrane fusion between baculovirus budded virus-enveloped particles and giant liposomes generated using a droplet-transfer method for the incorporation of recombinant membrane proteins. *Colloids Surfaces B Biointerfaces* **155**, 248–256 (2017).

342. Varnier, A. *et al.* A simple method for the reconstitution of membrane proteins into giant unilamellar vesicles. *J. Membr. Biol.* **233**, 85–92 (2010).

343. Mnatsakanyan, N. *et al.* A mitochondrial megachannel resides in monomeric F_1F_O ATP synthase. *Nat. Commun.* **10**, (2019).

344. Carnarius, C. *et al.* Green fluorescent protein changes the conductance of connexin 43 (Cx43) hemichannels reconstituted in planar lipid bilayers. *J. Biol. Chem.* **287**, 2877–2886 (2012).

345. Belardi, B. *et al.* Claudin-4 reconstituted in unilamellar vesicles is sufficient to form tight interfaces that partition membrane proteins. *J. Cell Sci.* **132**, (2019).

346. Galkin, M. A., Russell, A. N., Vik, S. B., Berry, R. M. & Ishmukhametov, R. R. Detergent-free ultrafast reconstitution of membrane proteins into lipid bilayers using fusogenic complementary-charged proteoliposomes. *J. Vis. Exp.* **2018**, 1–13 (2018).

347. Han, W. B., Kang, D. H., Na, J. H., Yu, Y. G. & Kim, T. S. Enhancement of membrane protein reconstitution on 3D free-standing lipid bilayer array in a microfluidic channel. *Biosens. Bioelectron.* **141**, 111404 (2019).

348. Bian, T. *et al.* Direct detection of SERCA calcium transport and small-molecule inhibition in giant unilamellar vesicles. *Biochem. Biophys. Res. Commun.* **481**, 206–211 (2016).

349. Peruzzi, J. A., Jacobs, M. L., Vu, T. Q., Wang, K. S. & Kamat, N. P. Barcoding Biological Reactions with DNA-Functionalized Vesicles. *Angew. Chemie - Int. Ed.* **58**, 18683–18690 (2019).

350. Yanagisawa, M., Iwamoto, M., Kato, A., Yoshikawa, K. & Oiki, S. Oriented reconstitution of a membrane protein in a giant unilamellar vesicle: experimental verification with the potassium channel KcsA. *J Am Chem Soc* **133**, 11774–11779 (2011).

351. Altamura, E. *et al.* Highly oriented photosynthetic reaction centers generate a proton gradient in synthetic protocells. *Proc. Natl. Acad. Sci.* **114**, 3837–3842 (2017).

352. Chiaruttini, N., Letellier, L. & Viasnoff, V. A novel method to couple electrophysiological measurements and fluorescence imaging of suspended lipid membranes: The example of T5 bacteriophage DNA ejection. *PLoS One* **8**, 1–11 (2013).

353. Gaßmann, O. *et al.* The M34A mutant of Connexin26 reveals active conductance states in pore-suspending membranes. *J. Struct. Biol.* **168**, 168–176 (2009).

354. Folgering, J. H. A., Kuiper, J. M., De Vies, A. H., Engberts, J. B. F. N. & Poolman, B. Lipid-mediated light activation of a mechanosensitive channel of large conductance. *Langmuir* **20**, 6985–6987 (2004).

355. Birkner, J. P., Poolman, B. & Koçer, A. Hydrophobic gating of mechanosensitive channel of large conductance evidenced by single-subunit resolution. *Proc. Natl. Acad. Sci. U. S. A.* **109**, 12944–12949 (2012).

356. Mukherjee, N. *et al.* The activation mode of the mechanosensitive ion channel, MscL, by lysophosphatidylcholine differs from tension-induced gating. *FASEB J.* **28**, 4292–4302 (2014).

357. Ou, X. *et al.* Ion- and water-binding sites inside an occluded hourglass pore of a trimeric intracellular cation (TRIC) channel. *BMC Biol.* **15**, 1–17 (2017).

358. Kapsalis, C. *et al.* Allosteric activation of an ion channel triggered by modification of mechanosensitive nano-pockets. *Nat. Commun.* **10**, (2019).

359. Carrara, G. *et al.* Golgi anti-apoptotic proteins are highly conserved ion channels that affect apoptosis and cell migration. *J. Biol. Chem.* **290**, 11785–11801 (2015).

360. Klaerke, D. A. *et al.* Reconstitution and Electrophysiological Characterization of Ion Channels in Lipid Bilayers. *Curr. Protoc. Pharmacol.* **81**, e37 (2018).

361. Agboh, K. *et al.* Powering the ABC multidrug exporter LmrA: How nucleotides embrace the ion-motive force. *Sci. Adv.* **4**, (2018).

362. Briones, R. *et al.* Voltage Dependence of Conformational Dynamics and Subconducting States of VDAC-1. *Biophys. J.* **111**, 1223–1234 (2016).

363. Molbaek, K. *et al.* Purification and initial characterization of *Plasmodium falciparum* K^+ channels, PfKch1

and PfKch2 produced in *Saccharomyces cerevisiae*. *Microb. Cell Fact.* **19**, 1–16 (2020).

364. Yang, H. *et al.* Pore architecture of TRIC channels and insights into their gating mechanism. *Nature* **538**, 537–541 (2016).

365. Papadopulos, A. *et al.* Flippase activity detected with unlabeled lipids by shape changes of giant unilamellar vesicles. *J. Biol. Chem.* **282**, 15559–15568 (2007).

366. Malsam, J. *et al.* Complexin arrests a pool of docked vesicles for fast Ca^{2+}-dependent release. *EMBO J.* **31**, 3270–3281 (2012).

367. Kedar, G. H. *et al.* A post-docking role of synaptotagmin 1-C2B domain bottom residues R398/399 in mouse chromaffin cells. *J. Neurosci.* **35**, 14172–14182 (2015).

368. Schupp, M. *et al.* Interactions between SNAP-25 and synaptotagmin-1 are involved in vesicle priming, clamping spontaneous and stimulating evoked neurotransmission. *J. Neurosci.* **36**, 11834–11836 (2016).

369. Heo, P., Park, J. B., Shin, Y. K. & Kweon, D. H. Visualization of SNARE-mediated hemifusion between giant unilamellar vesicles arrested by myricetin. *Front. Mol. Neurosci.* **10**, 1–8 (2017).

370. Christensen, S. M. & Stamou, D. Surface-based lipid vesicle reactor systems: Fabrication and applications. *Soft Matter* **3**, 828–836 (2007).

371. Ritz, S. *et al.* Cationized albumin-biocoatings for the immobilization of lipid vesicles. *Biointerphases* **5**, FA78–FA87 (2010).

372. Sarmento, M. J., Prieto, M. & Fernandes, F. Reorganization of lipid domain distribution in giant unilamellar vesicles upon immobilization with different membrane tethers. *Biochim. Biophys. Acta - Biomembr.* **1818**, 2605–2615 (2012).

373. Robinson, T. Microfluidic Handling and Analysis of Giant Vesicles for Use as Artificial Cells: A Review. *Adv. Biosyst.* **3**, 1800318 (2019).

374. Boukobza, E., Sonnenfeld, A. & Haran, G. Immobilization in surface-tethered lipid vesicles as a new tool for single biomolecule spectroscopy. *J. Phys. Chem. B* **105**, 12165–12170 (2001).

375. Stamou, D., Duschl, C., Delamarche, E. & Vogel, H. Self-Assembled Microarrays of Attoliter Molecular Vessels. *Angew. Chemie* **115**, 5738–5741 (2003).

376. Kuhn, P. *et al.* A facile protocol for the immobilisation of vesicles, virus particles, bacteria, and yeast cells. *Integr. Biol.* **4**, 1550 (2012).

377. Gleisner, M. *et al.* Epsin N-terminal Homology Domain (ENTH) Activity as a Function of Membrane Tension. *J. Biol. Chem.* **291**, 19953–19961 (2016).

378. Lira, R. B., Steinkühler, J., Knorr, R. L., Dimova, R. & Riske, K. A. Posing for a picture: Vesicle immobilization in agarose gel. *Sci. Rep.* **6**, 25254 (2016).

379. Tsumoto, K., Oohashi, M. & Tomita, M. Monitoring of membrane collapse and enzymatic reaction with single giant liposomes embedded in agarose gel. *Colloid Polym. Sci.* **289**, 1337–1346 (2011).

380. Kusters, I. *et al.* Taming membranes: Functional immobilization of biological membranes in hydrogels. *PLoS One* **6**, (2011).

381. Esquembre, R., Pinto, S. N., Poveda, J. A., Prieto, M. & Mateo, C. R. Immobilization and characterization of giant unilamellar vesicles (GUVs) within porous silica glasses. *Soft Matter* **8**, 408–417 (2012).

382. Bagatolli, L. A. & Needham, D. Quantitative optical microscopy and micromanipulation studies on the lipid bilayer membranes of giant unilamellar vesicles. *Chem. Phys. Lipids* **181**, 99–120 (2014).

383. Li, Q., Li, S., Zhang, X., Xu, W. & Han, X. Programmed magnetic manipulation of vesicles into spatially coded prototissue architectures arrays. *Nat. Commun.* **11**, 1–9 (2020).

384. Korlach, J., Reichle, C., Müller, T., Schnelle, T. & Webb, W. W. Trapping, deformation, and rotation of giant unilamellar vesicles in octode dielectrophoretic field cages. *Biophys. J.* **89**, 554–562 (2005).

385. Steinkühler, J., Agudo-Canalejo, J., Lipowsky, R. & Dimova, R. Modulating Vesicle Adhesion by Electric Fields. *Biophys. J.* **111**, 1454–1464 (2016).

386. Solmaz, M. E. *et al.* Optical stretching of giant unilamellar vesicles with an integrated dual-beam optical trap. *Biomed. Opt. Express* **3**, 2419 (2012).

387. Reccius, C. H. & Fromherz, P. Giant Lipid Vesicles Impaled with Glass Microelectrodes: GigaOhm Seal by Membrane Spreading. *Langmuir* **20**, 11175–11182 (2004).

388. Robinson, T., Kuhn, P., Eyer, K. & Dittrich, P. S. Microfluidic trapping of giant unilamellar vesicles to study transport through a membrane pore. *Biomicrofluidics* **7**, (2013).

389. Yandrapalli, N. & Robinson, T. Ultra-high capacity microfluidic trapping of giant vesicles for high-throughput membrane studies. *Lab Chip* **19**, 626–633 (2019).

390. Lira, R. B., Robinson, T., Dimova, R. & Riske, K. A. Highly Efficient Protein-free Membrane Fusion: A Giant Vesicle Study. *Biophys. J.* **116**, 79–91 (2019).

391. Kazayama, Y., Teshima, T., Osaki, T., Takeuchi, S. & Toyota, T. Integrated Microfluidic System for Size-Based Selection and Trapping of Giant Vesicles. *Anal. Chem.* **88**, 1111–1116 (2016).

392. Jain, A. & Cheng, K. The principles and applications of avidin-based nanoparticles in drug delivery and diagnosis. *J. Control. Release* **245**, 27–40 (2017).

393. Chiaruttini, N. *et al.* Relaxation of Loaded ESCRT-III Spiral Springs Drives Membrane Deformation. *Cell* **163**, 866–879 (2015).

394. Hisette, M. L., Haddad, P., Gisler, T., Marques, C. M. & Schröder, A. P. Spreading of bio-adhesive vesicles on DNA carpets. *Soft Matter* **4**, 828–832 (2008).

395. Ishizuka-Katsura, Y., Wazawa, T., Ban, T., Morigaki, K. & Aoyama, S. Biotin-containing phospholipid vesicle layer formed on self-assembled monolayer of a saccharide-terminated alkyl disulfide for surface plasmon resonance biosensing. *J. Biosci. Bioeng.* **105**, 527–535 (2008).

396. Köhler, M. *et al.* pH-dependent deformations of the energy landscape of avidin-like proteins investigated by single molecule force spectroscopy. *Molecules* **19**, 12531–12546 (2014).

397. Zhdanov, V. P. & Kasemo, B. Comments on rupture of adsorbed vesicles. *Langmuir* **17**, 3518–3521 (2002).

398. Seantier, B. & Kasemo, B. Influence of Mono- And Divalent Ions on the Formation of Supported Phospholipid Bilayers via Vesicle Adsorption. *Langmuir* **25**, 5767–5772 (2009).

399. Berthaud, A. *et al.* Spreading of porous vesicles subjected to osmotic shocks: the role of aquaporins. *Soft Matter* **12**, 1601–1609 (2016).

400. Amjad, O. A., Mognetti, B. M., Cicuta, P. & Di Michele, L. Membrane Adhesion through Bridging by Multimeric Ligands. *Langmuir* **33**, 1139–1146 (2017).

401. Bernard, A. L., Guedeau-Boudeville, M. A., Jullien, L. & Di Meglio, J. M. Strong adhesion of giant vesicles on surfaces: dynamics and permeability. *Langmuir* **16**, 6809–6820 (2000).

402. Cuvelier, D. & Nassoy, P. Hidden Dynamics of Vesicle Adhesion Induced by Specific Stickers. *Phys. Rev. Lett.* **93**, 228101 (2004).

403. Kliesch, T.-T. *et al.* Membrane tension increases fusion efficiency of model membranes in the presence of SNAREs. *Sci. Rep.* **7**, 12070 (2017).

404. Karatekin, E. *et al.* Cascades of transient pores in giant vesicles: Line tension and transport. *Biophys. J.* **84**, 1734–1749 (2003).

405. Hac, A., Heimburg, T., Grubmu, H. & Bo, R. A. Effect of Sodium Chloride on a Lipid Bilayer. *Biophys. J.* **85**, 1647–1655 (2003).

406. Faizi, H. A., Frey, S. L., Steinkühler, J., Dimova, R. & Vlahovska, P. M. Bending rigidity of charged lipid bilayer membranes. *Soft Matter* **15**, 6006–6013 (2019).

407. De Mel, J. U. *et al.* Influence of External NaCl Salt on Membrane Rigidity of Neutral DOPC Vesicles. *Langmuir* **36**, 9356–9367 (2020).

408. Wang, X., Du, H., Wang, Z., Mu, W. & Han, X. Versatile Phospholipid Assemblies for Functional Synthetic Cells and Artificial Tissues. *Adv. Mater.* **33**, 1–23 (2021).

409. Staufer, O. *et al.* Microfluidic production and characterization of biofunctionalized giant unilamellar vesicles for targeted intracellular cargo delivery. *Biomaterials* **264**, 120203 (2021).

410. Lundgren, C. A. K. *et al.* Scavenging of superoxide by a membrane-bound superoxide oxidase. *Nat. Chem. Biol.* **14**, 788–793 (2018).

411. Graf, S. S., Hong, S., Müller, P., Gennis, R. & von Ballmoos, C. Energy transfer between the nicotinamide nucleotide transhydrogenase and ATP synthase of Escherichia coli. *Sci. Rep.* **11**, 1–12 (2021).

412. Clement, N. R. & Gould, J. M. Pyranine (8-hydroxy-1,3,6-pyrenetrisulfonate) as a probe of internal aqueous hydrogen ion concentration in phospholipid vesicles. *Biochemistry* **20**, 1534–1538 (1981).

413. Han, J. & Burgess, K. Fluorescent indicators for intracellular pH. *Chem Rev* **110**, 2709–2728 (2010).

414. Avnir, Y. & Barenholz, Y. pH determination by pyranine: Medium-related artifacts and their correction. *Anal. Biochem.* **347**, 34–41 (2005).

415. Bouvrais, H., Duelund, L. & Ipsen, J. H. Buffers affect the bending rigidity of model lipid membranes. *Langmuir* **30**, 13–16 (2014).

416. Deamer, D. W. & Nichols, J. W. Proton-hydroxide permeability of liposomes. *Proc. Natl. Acad. Sci. U. S. A.* **80**, 165–168 (1983).

417. Paula, S., Volkov, A. G., Van Hoek, A. N., Haines, T. H. & Deamer, D. W. Permeation of protons, potassium ions, and small polar molecules through phospholipid bilayers as a function of membrane thickness. *Biophys. J.* **70**, 339–348 (1996).

418. Kleineberg, C. *et al.* Light-Driven ATP Regeneration in Diblock/Grafted Hybrid Vesicles. *ChemBioChem* **21**, 2149–2160 (2020).

419. Schindelin, J. *et al.* Fiji: An open-source platform for biological-image analysis. *Nat. Methods* **9**, 676–682 (2012).

420. Pan, J. *et al.* Molecular structures of fluid phase phosphatidylglycerol bilayers as determined by small angle neutron and X-ray scattering. *Biochim. Biophys. Acta - Biomembr.* **1818**, 2135–2148 (2012).

421. Lütgebaucks, C., Macias-Romero, C. & Roke, S. Characterization of the interface of binary mixed DOPC:DOPS liposomes in water: The impact of charge condensation. *J. Chem. Phys.* **146**, (2017).

422. Lai, L. Y., Samoilova, R. I., Gennis, R. B. & Dikanov, S. A. Characterization of the exchangeable protons in the immediate vicinity of the semiquinone radical at the QH site of the cytochrome bo_3 from *Escherichia coli*. *J. Biol. Chem.* **281**, 16879–16887 (2006).

423. Choi, S. K., Lin, M. T., Ouyang, H. & Gennis, R. B. Searching for the low affinity ubiquinone binding site in cytochrome bo_3 from *Escherichia coli*. *Biochim. Biophys. Acta - Bioenerg.* **1858**, 366–370 (2017).

424. Frericks, H. L., Zhou, D. H., Yap, L. L., Gennis, R. B. & Rienstra, C. M. Magic-angle spinning solid-state NMR of a 144 kDa membrane protein complex: *E. coli* cytochrome bo_3 oxidase. *J. Biomol. NMR* **36**, 55–71 (2006).

425. Deutschmann, S., Rimle, L. & von Ballmoos, C. Rapid Estimation of Membrane Protein Orientation in Liposomes. *ChemBioChem* 1–9 (2021). doi:10.1002/cbic.202100543

426. Svensson-Ek, M. *et al.* The X-ray crystal structures of wild-type and EQ(I-286) mutant cytochrome *c*

oxidases from *Rhodobacter sphaeroides*. *J. Mol. Biol.* **321**, 329–339 (2002).

427. Ferguson-Miller, S., Hiser, C. & Liu, J. Gating and regulation of the cytochrome *c* oxidase proton pump. *Biochimica et Biophysica Acta - Bioenergetics* **1817**, 489–494 (2012).

428. Michel, H. Cytochrome *c* oxidase: Catalytic cycle and mechanisms of proton pumping-A discussion. *Biochemistry* **38**, 15129–15140 (1999).

429. Mitchell, D. M. & Gennis, R. B. Rapid purification of wildtype and mutant cytochrome *c* oxidase from *Rhodobacter sphaeroides* by Ni^{2+}-NTA affinity chromatography. *FEBS Lett.* **368**, 148–150 (1995).

430. Dolder, N., Müller, P. & von Ballmoos, C. Experimental platform for the functional investigation of membrane proteins in giant unilamellar vesicles. *bioRxiv* (2021). doi:10.1101/2021.12.22.473796

431. Deshpande, S. & Dekker, C. On-chip microfluidic production of cell-sized liposomes. *Nat. Protoc.* **13**, 856–874 (2018).

432. Amali, A. J., Singh, S., Rangaraj, N., Patra, D. & Rana, R. K. Poly(l-Lysine)–pyranine-3 coacervate mediated nanoparticle-assembly: Fabrication of dynamic pH-responsive containers. *Chem. Commun.* **48**, 856–858 (2012).

433. Deshpande, S. *et al.* Spatiotemporal control of coacervate formation within liposomes. *Nat. Commun.* **10**, 1–11 (2019).

434. Schick, T. Incorporation of membrane proteins into giant unilamellar vesicles : Towards complex cell mimetic systems. (Dissertation, University of Bern, Faculty of Science of the University of Bern, 2019). doi:10.7892/boris.147166

435. Mora, N. L. *et al.* Controlled Peptide-Mediated Vesicle Fusion Assessed by Simultaneous Dual-Colour Time-Lapsed Fluorescence Microscopy. *Sci. Rep.* **10**, 1–13 (2020).

436. Sparrenberg, L. T., Greiner, B. & Mathis, H. P. Bleaching correction for DNA measurements in highly diluted solutions using confocal microscopy. *PLoS One* **15**, 1–17 (2020).

437. Miura, K. Bleach correction ImageJ plugin for compensating the photobleaching of time-lapse sequences. *F1000Research* **9**, 1–17 (2020).

438. Nordlund, G., Sing Ng, J. B., Bergström, L. & Brzezinski, P. A membrane-reconstituted multisubunit functional proton pump on mesoporous silica particles. *ACS Nano* **3**, 2639–2646 (2009).

439. Zhu, J., Han, H., Pawate, A. & Gennis, R. B. Decoupling Mutations in the D-Channel of the aa_3 -Type Cytochrome *c* Oxidase from *Rhodobacter sphaeroides* Suggest That a Continuous Hydrogen-Bonded Chain of Waters Is Essential for Proton Pumping. *Biochemistry* **49**, 4476–4482 (2010).

440. Hosler, J. P. *et al.* Cytochrome aa_3 of *Rhodobacter sphaeroides* as a model for mitochondrial cytochrome *c* oxidase. Purification, kinetics, proton pumping, and spectral analysis. *J. Biol. Chem.* **267**, 24264–24272

(1992).

441. Schmid, Y. R. F., Scheller, L., Buchmann, S. & Dittrich, P. S. Calcium-Mediated Liposome Fusion to Engineer Giant Lipid Vesicles with Cytosolic Proteins and Reconstituted Mammalian Proteins. *Adv. Biosyst.* **4**, (2020).

442. Krulwich, T. A., Sachs, G. & Padan, E. Molecular aspects of bacterial pH sensing and homeostasis. *Nature Reviews Microbiology* **9**, 330–343 (2011).

443. Guan, L. & Kaback, H. R. Lessons from lactose permease. *Annual Review of Biophysics and Biomolecular Structure* **35**, 67–91 (2006).

444. von Ballmoos, C., Wiedenmann, A. & Dimroth, P. Essentials for ATP Synthesis by F_1F_0 ATP Synthases. *Annu. Rev. Biochem.* **78**, 649–672 (2009).

445. Ohnishi, T., Ohnishi, S. T. & Salerno, J. C. Five decades of research on mitochondrial NADH-quinone oxidoreductase (complex I). *Biol. Chem.* **399**, 1249–1264 (2018).

446. Junge, W. & Nelson, N. ATP synthase. *Annual Review of Biochemistry* **84**, 631–657 (2015).

447. Kano, K. & Fendler, J. H. Pyranine as a sensitive pH probe for liposome interiors and surfaces. pH gradients across phospholipid vesicles. *BBA - Biomembr.* **509**, 289–299 (1978).

448. Benkoski, J. J. & Höök, F. Lateral Mobility of Tethered Vesicle−DNA Assemblies. *J. Phys. Chem. B* **109**, 9773–9779 (2005).

449. Achalkumar, A. S., Bushby, R. J. & Evans, S. D. Cholesterol-based anchors and tethers for phospholipid bilayers and for model biological membranes. *Soft Matter* **6**, 6036 (2010).

450. Czogalla, A., Franquelim, H. G. & Schwille, P. DNA Nanostructures on Membranes as Tools for Synthetic Biology. *Biophys. J.* **110**, 1698–1707 (2016).

451. Flavier, K. M. & Boxer, S. G. Vesicle Fusion Mediated by Solanesol-Anchored DNA. *Biophys. J.* **113**, 1260–1268 (2017).

452. Dave, N. & Liu, J. Biomimetic sensing based on chemically induced assembly of a signaling DNA aptamer on a fluid bilayer membrane. *Chem. Commun.* **48**, 3718 (2012).

453. Idili, A., Vallée-Bélisle, A. & Ricci, F. Programmable pH-triggered DNA nanoswitches. *J. Am. Chem. Soc.* **136**, 5836–5839 (2014).

454. Pfeiffer, I. & Höök, F. Bivalent cholesterol-based coupling of oligonucletides to lipid membrane assemblies. *J. Am. Chem. Soc.* **126**, 10224–10225 (2004).

455. Michanek, A., Kristen, N., Höök, F., Nylander, T. & Sparr, E. RNA and DNA interactions with zwitterionic and charged lipid membranes - A DSC and QCM-D study. *Biochim. Biophys. Acta - Biomembr.* **1798**, 829–838 (2010).

456. Sjöback, R., Nygren, J. & Kubista, M. Characterization of fluorescein–oligonucleotide conjugates and measurement of local electrostatic potential. *Biopolymers* **46**, 445–453 (1998).

457. Yang, Y. *et al.* Self-assembly of size-controlled liposomes on DNA nanotemplates. *Nat. Chem.* **8**, 476–483 (2016).

458. Cooper, M. E., Gregory, S., Adie, E. & Kalinka, S. pH-Sensitive Cyanine Dyes for Biological Applications. *J. Fluoresc.* **12**, 425–429 (2002).

459. Vorburger, T. *et al.* Arginine-induced conformational change in the c-ring/a-subunit interface of ATP synthase. *FEBS J.* **275**, 2137–2150 (2008).

460. David, J. M. & Rajasekaran, A. K. Gramicidin A: A New Mission for an Old Antibiotic. *J. Kidney Cancer VHL* **2**, 15 (2015).

461. Toei, M. & Noji, H. Single-molecule analysis of F_0F_1-ATP synthase inhibited by N,N-Dicyclohexylcarbodiimide. *J. Biol. Chem.* **288**, 25717–25726 (2013).

462. Jeong, S., Nguyen, H. T., Kim, C. H., Ly, M. N. & Shin, K. Toward Artificial Cells: Novel Advances in Energy Conversion and Cellular Motility. *Adv. Funct. Mater.* **30**, 1–26 (2020).

463. Thomsen, R. P. *et al.* A large size-selective DNA nanopore with sensing applications. *Nat. Commun.* **10**, 1–10 (2019).

464. Czogalla, A. *et al.* Amphipathic DNA Origami Nanoparticles to Scaffold and Deform Lipid Membrane Vesicles. *Angew. Chemie - Int. Ed.* **54**, 6501–6505 (2015).

465. Li, Y. & Liu, J. Aptamer-based strategies for recognizing adenine, adenosine, ATP and related compounds. *Analyst* **145**, 6753–6768 (2020).

466. Ohmann, A. *et al.* A synthetic enzyme built from DNA flips 107lipids per second in biological membranes. *Nat. Commun.* **9**, 2426 (2018).

467. Löffler, P. M. G. *et al.* A DNA-Programmed Liposome Fusion Cascade. *Angew. Chemie - Int. Ed.* **56**, 13228–13231 (2017).

468. Simonsson, L., Kurczy, M. E., Trouillon, R. L., Hook, F. & Cans, A. S. A functioning artificial secretory cell. *Sci. Rep.* **2**, 1–5 (2012).

469. Bunge, A. *et al.* Lipophilic oligonucleotides spontaneously insert into lipid membranes, bind complementary DNA strands, and sequester into lipid-disordered domains. *Langmuir* **23**, 4455–4464 (2007).

470. Chung, M., Lowe, R. D., Chan, Y. H. M., Ganesan, P. V & Boxer, S. G. DNA-tethered membranes formed by giant vesicle rupture. *J. Struct. Biol.* **168**, 190–199 (2009).

471. Rawle, R. J., Van Lengerich, B., Chung, M., Bendix, P. M. & Boxer, S. G. Vesicle fusion observed by content

transfer across a tethered lipid bilayer. *Biophys. J.* **101**, L37-9 (2011).

472. Chung, M., Koo, B. J. & Boxer, S. G. Formation and analysis of topographical domains between lipid membranes tethered by DNA hybrids of different lengths. *Faraday Discuss.* **161**, 333–345 (2013).

473. Beales, P. A. & Kyle Vanderlick, T. Partitioning of membrane-anchored DNA between coexisting lipid phases. *J. Phys. Chem. B* **113**, 13678–13686 (2009).

474. Parolini, L. *et al.* Volume and porosity thermal regulation in lipid mesophases by coupling mobile ligands to soft membranes. *Nat. Commun.* **6**, 5948 (2015).

475. Talbot, E. L., Parolini, L., Kotar, J., Di Michele, L. & Cicuta, P. Thermal-driven domain and cargo transport in lipid membranes. *Proc. Natl. Acad. Sci.* **114**, 846–851 (2017).

476. Gosse, C. *et al.* Micelles of lipid-oligonucleotide conjugates: implications for membrane anchoring and base pairing. *J. Phys. Chem. B* **108**, 6485–97 (2004).

477. Banchelli, M. *et al.* Phospholipid membranes decorated by cholesterol-based oligonucleotides as soft hybrid nanostructures. *J Phys Chem B* **112**, 10942–10952 (2008).

478. Schade, M., Berti, D., Huster, D., Herrmann, A. & Arbuzova, A. Lipophilic nucleic acids - A flexible construction kit for organization and functionalization of surfaces. *Advances in Colloid and Interface Science* **208**, 235–251 (2014).

479. Khmelinskaia, A. *et al.* Liquid-Ordered Phase Formation by Mammalian and Yeast Sterols: A Common Feature With Organizational Differences. *Front. Cell Dev. Biol.* **8**, 1–15 (2020).

480. Silvius, J. Thermotropic phase transitions of pure lipids in model membranes and their modifications by membrane proteins. *Lipid-protein Interact.* **2**, 239–281 (1982).

481. Ballweg, S. *et al.* Regulation of lipid saturation without sensing membrane fluidity. *Nat. Commun.* **11**, 1–13 (2020).

482. Pandit, S. A., Chiu, S.-W., Jakobsson, E., Grama, A. & Scott, H. L. Cholesterol Packing around Lipids with Saturated and Unsaturated Chains: A Simulation Study. *Langmuir* **24**, 6858–6865 (2008).

483. Pan, J., Mills, T. T., Tristram-Nagle, S. & Nagle, J. F. Cholesterol Perturbs Lipid Bilayers Nonuniversally. *Phys. Rev. Lett.* **100**, 198103 (2008).

484. Gracià, R. S., Bezlyepkina, N., Knorr, R. L., Lipowsky, R. & Dimova, R. Effect of cholesterol on the rigidity of saturated and unsaturated membranes: Fluctuation and electrodeformation analysis of giant vesicles. *Soft Matter* **6**, 1472–1482 (2010).

485. Steinkühler, J., Sezgin, E., Urbančič, I., Eggeling, C. & Dimova, R. Mechanical properties of plasma membrane vesicles correlate with lipid order, viscosity and cell density. *Commun. Biol.* **2**, 1–8 (2019).

486. Chakraborty, S. *et al.* How cholesterol stiffens unsaturated lipid membranes. *Proc. Natl. Acad. Sci. U. S. A.*

117, 21896–21905 (2020).

487. Lu, D. & Rhodes, D. G. Binding of phosphorothioate oligonucleotides to zwitterionic liposomes. *Biochim. Biophys. Acta - Biomembr.* **1563**, 45–52 (2002).

488. Mertins, O., Da Silveira, N. P., Pohlmann, A. R., Schröder, A. P. & Marques, C. M. Electroformation of giant vesicles from an inverse phase precursor. *Biophys. J.* **96**, 2719–2726 (2009).

489. Schade, M. *et al.* Remote control of lipophilic nucleic acids domain partitioning by DNA hybridization and enzymatic cleavage. *J. Am. Chem. Soc.* **134**, 20490–20497 (2012).

490. Lachance, J.-C., Rodrigue, S. & Palsson, B. O. Minimal cells, maximal knowledge. *Elife* **8**, 1–75 (2019).

491. Jewett, M. C. & Forster, A. C. Update on designing and building minimal cells. *Curr. Opin. Biotechnol.* **21**, 697–703 (2010).

492. Xu, C., Hu, S. & Chen, X. Artificial cells: from basic science to applications. *Mater. Today* **19**, 516–532 (2016).

493. Hutchison, C. A. *et al.* Design and synthesis of a minimal bacterial genome. *Science (80-.).* **351**, (2016).

494. Pelletier, J. F. *et al.* Genetic requirements for cell division in a genomically minimal cell. *Cell* **184**, 2430-2440.e16 (2021).

495. Breuer, M. *et al.* Essential metabolism for a minimal cell. *Elife* **8**, 1–75 (2019).

496. Ivanov, I. *et al.* Bottom-Up Synthesis of Artificial Cells: Recent Highlights and Future Challenges. *Annu. Rev. Chem. Biomol. Eng.* **12**, 287–308 (2021).

497. Solé, R. V. Evolution and self-assembly of protocells. *Int. J. Biochem. Cell Biol.* **41**, 274–284 (2009).

498. Noireaux, V., Maeda, Y. T. & Libchaber, A. Development of an artificial cell, from self-organization to computation and self-reproduction. *Proc. Natl. Acad. Sci. U. S. A.* **108**, 3473–3480 (2011).

499. Ugrinic, M. *et al.* Microfluidic formation of proteinosomes. *Chem. Commun.* **54**, 287–290 (2018).

500. Ugrinic, M., deMello, A. & Tang, T.-Y. D. Microfluidic Tools for Bottom-Up Synthetic Cellularity. *Chem* 1–16 (2019). doi:10.1016/j.chempr.2019.03.012

501. Nardin, C., Widmer, J., Winterhalter, M. & Meier, W. Amphiphilic block copolymer nanocontainers as bioreactors. *Eur. Phys. J. E* **4**, 403–410 (2001).

502. Choi, H. J. & Montemagno, C. D. Artificial organelle: ATP synthesis from cellular mimetic polymersomes. *Nano Lett.* **5**, 2538–2542 (2005).

503. Choi, H. J., Germain, J. & Montemagno, C. D. Effects of different reconstitution procedures on membrane protein activities in proteopolymersomes. *Nanotechnology* **17**, 1825–1830 (2006).

504. Howse, J. R. *et al.* Templated formation of giant polymer vesicles with controlled size distributions. *Nat. Mater.* **8**, 507–511 (2009).

505. Itel, F., Najer, A., Palivan, C. G. & Meier, W. Dynamics of Membrane Proteins within Synthetic Polymer Membranes with Large Hydrophobic Mismatch. *Nano Lett.* **15**, 3871–3878 (2015).

506. Gutierrez, M. G. *et al.* G Protein-Coupled Receptors Incorporated into Rehydrated Diblock Copolymer Vesicles Retain Functionality. *Small* **12**, 5256–5260 (2016).

507. Garni, M., Einfalt, T., Goers, R., Palivan, C. G. & Meier, W. Live Follow-Up of Enzymatic Reactions Inside the Cavities of Synthetic Giant Unilamellar Vesicles Equipped with Membrane Proteins Mimicking Cell Architecture. *ACS Synth. Biol.* **7**, 2116–2125 (2018).

508. dos Santos, E. C. *et al.* Combinatorial Strategy for Studying Biochemical Pathways in Double Emulsion Templated Cell-Sized Compartments. *Adv. Mater.* **32**, 1–13 (2020).

509. Pata, V. & Dan, N. The effect of chain length on protein solubilization in polymer-based vesicles (polymersomes). *Biophys. J.* **85**, 2111–2118 (2003).

510. Wang, G. & Castiglione, K. Light-driven biocatalysis in liposomes and polymersomes: Where are we now? *Catalysts* **9**, (2019).

511. Renard, K. & Byrne, B. Insights into the role of membrane lipids in the structure, function and regulation of integral membrane proteins. *Int. J. Mol. Sci.* **22**, (2021).

512. Rottet, S. *et al.* Characterisation of hybrid polymersome vesicles containing the eux pumps naatm1 or P-glycoprotein. *Polymers (Basel).* **12**, 1–22 (2020).

513. Otrin, L. *et al.* En route to dynamic life processes by SNARE-mediated fusion of polymer and hybrid membranes. *Nat. Commun.* **12**, 1–12 (2021).

514. Lim, S. K., de Hoog, H. P., Parikh, A. N., Nallani, M. & Liedberg, B. Hybrid, nanoscale phospholipid/block copolymer vesicles. *Polymers (Basel).* **5**, 1102–1114 (2013).

515. Sharma, A. K. *et al.* Emerging era of "somes": polymersomes as versatile drug delivery carrier for cancer diagnostics and therapy. *Drug Deliv. Transl. Res.* **10**, 1171–1190 (2020).

516. Mumtaz Virk, M. & Reimhult, E. Phospholipase A2-Induced Degradation and Release from Lipid-Containing Polymersomes. *Langmuir* **34**, 395–405 (2018).

517. Zhu, L., Xu, N., Zhang, Z. L. & Zhang, T. C. Cell derived extracellular vesicles: From isolation to functionalization and biomedical applications. *Biomater. Sci.* **7**, 3552–3565 (2019).

518. Snell, A. A. *et al.* Cell-derived vesicles for in vitro and in vivo targeted therapeutic delivery. *ACS Omega* **4**, 12657–12664 (2019).

519. Einfalt, T. *et al.* Bioinspired Molecular Factories with Architecture and In Vivo Functionalities as Cell Mimics. *Adv. Sci.* **7**, (2020).

520. Amy Yewdall, N., Mason, A. F. & Van Hest, J. C. M. The hallmarks of living systems: Towards creating

artificial cells. *Interface Focus* **8**, (2018).

521. Skinkle, A. D., Levental, K. R. & Levental, I. Cell-Derived Plasma Membrane Vesicles Are Permeable to Hydrophilic Macromolecules. *Biophys. J.* **118**, 1292–1300 (2020).

522. Accardi, A., Kolmakova-Partensky, L., Williams, C. & Miller, C. Ionic Currents Mediated by a Prokaryotic Homologue of CLC Cl- Channels. *J. Gen. Physiol.* **123**, 109–119 (2004).

523. Srivatsav, A. T. & Kapoor, S. The Emerging World of Membrane Vesicles: Functional Relevance, Theranostic Avenues and Tools for Investigating Membrane Function. *Front. Mol. Biosci.* **8**, 1–24 (2021).

524. Belkin, M. & Hardy, W. G. Relation between water permeability and integrity of sulfhydryl groups in malignant and normal cells. *J. Cell Biol.* **9**, 733–745 (1961).

525. Pick, H. *et al.* Investigating cellular signaling reactions in single attoliter vesicles. *J. Am. Chem. Soc.* **127**, 2908–2912 (2005).

526. Lederberg, J. Bacterial Protoplasts Induced by Penicillin. *Proc. Natl. Acad. Sci.* **42**, 574–577 (1956).

527. Kaback, H. R. & Stadtman, E. R. Proline uptake by an isolated cytoplasmic membrane preparation of *Escherichia coli. Proc. Natl. Acad. Sci. U. S. A.* **55**, 920–927 (1966).

528. Pick, H., Alves, A. C. & Vogel, H. Single-Vesicle Assays Using Liposomes and Cell-Derived Vesicles: From Modeling Complex Membrane Processes to Synthetic Biology and Biomedical Applications. *Chem. Rev.* **118**, 8598–8654 (2018).

529. Fuhrmann, G., Herrmann, I. K. & Stevens, M. M. Cell-derived vesicles for drug therapy and diagnostics: Opportunities and challenges. *Nano Today* **10**, 397–409 (2015).

530. Wiklander, O. P. B., Brennan, M., Lötvall, J., Breakefield, X. O. & Andaloussi, S. E. L. Advances in therapeutic applications of extracellular vesicles. *Sci. Transl. Med.* **11**, (2019).

531. Medeiros, T., Myette, R. L., Almeida, J. R., Silva, A. A. & Burger, D. Extracellular vesicles: Cell-derived biomarkers of glomerular and tubular injury. *Cell. Physiol. Biochem.* **54**, 88–109 (2020).

532. Xu, J. & Wang, C. Cell-derived vesicles for delivery of cancer immunotherapy. *Explor. Med.* 39–59 (2021). doi:10.37349/emed.2021.00031

533. Staufer, O. *et al.* Bottom-up assembly of biomedical relevant fully synthetic extracellular vesicles. *Sci. Adv.* **7**, 1–13 (2021).

534. Levental, K. R. & Levental, I. Giant Plasma Membrane Vesicles: Models for Understanding Membrane Organization. in *Current Topics in Membranes* **75**, 25–57 (Elsevier Ltd, 2015).

535. Fernandez-Trillo, F., Grover, L. M., Stephenson-Brown, A., Harrison, P. & Mendes, P. M. Vesicles in Nature and the Laboratory: Elucidation of Their Biological Properties and Synthesis of Increasingly Complex Synthetic Vesicles. *Angew. Chemie - Int. Ed.* **56**, 3142–3160 (2017).

536. Grimmer, M. & Bacia, K. Giant Endoplasmic Reticulum vesicles (GERVs), a novel model membrane tool. *Sci. Rep.* **10**, 1–8 (2020).

537. Jang, H. S., Cho, Y. K. & Granick, S. Biologically-active unilamellar vesicles from red blood cells. *Biomater. Sci.* **7**, 1393–1398 (2019).

538. Riquelme, G., Lopez, E., Garcia-Segura, L. M., Ferragut, J. A. & Gonzalez-Ros, J. M. Giant Liposomes: A Model System in Which To Obtain Patch-Clamp Recordings of Ionic Channels. *Biochemistry* **29**, 11215–11222 (1990).

539. Carpenter, J. F., Crowe, L. M. & Crowe, J. H. Stabilization of phosphofructokinase with sugars during freeze-drying: characterization of enhanced protection in the presence of divalent cations. *Biochim. Biophys. Acta - Gen. Subj.* **923**, 109–115 (1987).

540. Allison, S. D., Chang, B., Randolph, T. W. & Carpenter, J. F. Hydrogen bonding between sugar and protein is responsible for inhibition of dehydration-induced protein unfolding. *Arch. Biochem. Biophys.* **365**, 289–298 (1999).

541. Liao, Y. H., Brown, M. B., Quader, A. & Martin, G. P. Protective mechanism of stabilizing excipients against dehydration in the freeze-drying of proteins. *Pharm. Res.* **19**, 1854–1861 (2002).

542. Zhao, C. *et al.* Engineering proteinosomes with renewable predatory behaviour towards living organisms. *Mater. Horizons* **7**, 157–163 (2020).

543. Elani, Y. *et al.* Constructing vesicle-based artificial cells with embedded living cells as organelle-like modules. *Sci. Rep.* **8**, 4564 (2018).

544. Jahnke, K. *et al.* Proton gradients from light-harvesting E. coli control DNA assemblies for synthetic cells. *Nat. Commun.* **12**, 3967 (2021).

545. Ahmad, R. *et al.* Light-Powered Reactivation of Flagella and Contraction of Microtubule Networks: Toward Building an Artificial Cell. *ACS Synth. Biol.* **10**, 1490–1504 (2021).

546. Ramezani, H. & Dietz, H. Building machines with DNA molecules. *Nat. Rev. Genet.* **21**, 5–26 (2020).

547. Ketterer, P., Willner, E. M. & Dietz, H. Nanoscale rotary apparatus formed from tight-fitting 3D DNA components. *Sci. Adv.* **2**, 1–9 (2016).

548. Bertosin, E. *et al.* A nanoscale reciprocating rotary mechanism with coordinated mobility control Results Design of the rotary mechanism. *Bioarxiv* (2021).

549. Stömmer, P. *et al.* A synthetic tubular molecular transport system. *Nat. Commun.* **12**, 1–10 (2021).

550. Arnold, F. H. The nature of chemical innovation: New enzymes by evolution. *Q. Rev. Biophys.* **48**, 404–410 (2015).

551. Huang, P. S., Boyken, S. E. & Baker, D. The coming of age of de novo protein design. *Nature* **537**, 320–327

(2016).

552. Lutz, S. & Iamurri, S. M. Protein Engineering: Past, Present, and Future. in *Protein Engineering. Methods in Molecular Biology* (eds. Bornscheuer, U. T. & Höhne, M.) **1685**, 1–12 (Humana Press, New York, NY, 2018).

553. Jiang, N., Ma, L. & Lu, Y. Cell-free synthetic biology in the new era of enzyme engineering. *Chinese J. Chem. Eng.* **28**, 2810–2816 (2020).

554. Leaver-Fay, A. *et al.* Rosetta3: An object-oriented software suite for the simulation and design of macromolecules. in *Methods in Enzymology* **487**, 545–574 (2011).

555. Pan, X. & Kortemme, T. Recent advances in de novo protein design: Principles, methods, and applications. *J. Biol. Chem.* **296**, 100558 (2021).

556. Woolfson, D. N. A Brief History of De Novo Protein Design: Minimal, Rational, and Computational: De novo protein design. *J. Mol. Biol.* **433**, 167160 (2021).

557. Xu, C. *et al.* Computational design of transmembrane pores. *Nature* **585**, 129–134 (2020).

558. Jumper, J. *et al.* Highly accurate protein structure prediction with AlphaFold. *Nature* **596**, 583–589 (2021).

559. Baek, M. *et al.* Accurate prediction of protein structures and interactions using a three-track neural network. *Science (80-.).* **373**, 871–876 (2021).

560. Trudeau, D. L. *et al.* Design and in vitro realization of carbon-conserving photorespiration. *Proc. Natl. Acad. Sci. U. S. A.* **115**, E11455–E11464 (2018).

561. Scherer, M., Fleishman, S. J., Jones, P. R., Dandekar, T. & Bencurova, E. Computational Enzyme Engineering Pipelines for Optimized Production of Renewable Chemicals. *Front. Bioeng. Biotechnol.* **9**, 1–13 (2021).

562. Opgenorth, P. H., Korman, T. P., Iancu, L. & Bowie, J. U. A molecular rheostat maintains ATP levels to drive a synthetic biochemistry system. *Nat. Chem. Biol.* **13**, 938–942 (2017).

563. Bowie, J. U. *et al.* Synthetic Biochemistry: The Bio-inspired Cell-Free Approach to Commodity Chemical Production. *Trends Biotechnol.* **38**, 766–778 (2020).

564. Rasor, B. J. *et al.* Toward sustainable, cell-free biomanufacturing. *Curr. Opin. Biotechnol.* **69**, 136–144 (2021).

565. Sherkhanov, S. *et al.* Isobutanol production freed from biological limits using synthetic biochemistry. *Nat. Commun.* **11**, 1–10 (2020).

8. Declaration of Originality

Last name, first name: Dolder Nicolas

Matriculation number: 12-115-689

I hereby declare that this thesis represents my original work and that I have used no other sources except as noted by citations.

All data, tables, figures and text citations which have been reproduced from any other source, including the internet, have been explicitly acknowledged as such.

I am aware that in case of non-compliance, the Senate is entitled to withdraw the doctorate degree awarded to me on the basis of the present thesis, in accordance with the "Statut der Universität Bern (Universitätsstatut; UniSt)", Art. 69, of 7 June 2011.

Place, date

Bern, 26.01.2022

Signature